The Hashemite Kingdom of Jordan Scientific Research Support Fund The Hashemite University

JJEES

Jordan Journal of Earth and Environmental Sciences

Indexed by Scopus

ELSEVIER

Volume (12) Number (4)


Cover photo © Dr. Dr. Danill Moraitis

JJEES is an International Peer-Reviewed Research Journal

ISSN 1995-6681 jjees.hu.edu.jo December 2021

Jordan Journal of Earth and Environmental Sciences (JJEES)

JJEES is an International Peer-Reviewed Research Journal, Issued by Deanship of Scientific Research, The Hashemite University, in corporation with, the Jordanian Scientific Research Support Fund, the Ministry of Higher Education and Scientific Research.

Submission address:

Manuscripts should be submitted electronically to the following e-mail:

jjees@hu.edu.jo

For more information and previous issues:

www.jjees.hu.edu.jo

Hashemite Kingdom of Jordan

صندوق دعم البحث العلمي
Scientific Research Support Fund

Scientific Research Support Fund

Hashemite University

Jordan Journal of Earth and Environmental Sciences

JJEES

An International Peer-Reviewed Scientific Journal

Financed by the Scientific Research Support Fund

Volume 12 Number (4)

http:// jjees.hu.edu.jo/

ISSN 1995-6681

It is a reverse fault and a horizontal thrust In between (center of photo) we have a large block like a gigantic cataclasite
This is Thamama formation in wadi Rahbah in NE-UAE. The image rights is for Dr. Danill Moraitis, University of Sharjah.

In memorandum of
Prof. Abdulkader M. Abed (1943-2021)

JJEES

JJEES (2021) 12 (4): 275-284
ISSN 1995-6681

Jordan Journal of Earth and Environmental Sciences

Evaluation of the Use of Volcanic Tuff in concrete block production

Mohmd Sarireh[1*], Ayoub M. Ghrair[2], Sameh Alsaqoor[3], Ali Alahmer[4]

[1]Department of Civil Engineering, Tafila Technical University, Jordan.
[2]Faculty of Technological Agriculture, Applied Balqa University, Jordan
[3]Department of Mechanical Engineering, Tafila Technical University, Jordan.
[4]Department of Mechanical Engineering, Tafila Technical University, Jordan.

Received 31 January 2021; Accepted 16 March 2021

Abstract

Jordanian volcanic tuff has low specific gravity and density compared to ordinary limestone aggregate and sandstone used in concrete block production. The current study had considered volcanic tuff from Jabal Al Halain Tafila to be tested in concrete block production. Concrete mixes were designed by using volcanic tuff as the whole part of specific size gradation and in ratios of ordinary materials applying manual and vibration compaction. Volcanic tuff gives less density for concrete block compared to ordinary materials. Density reduction can reach 20-30% for all mixes on manual compaction, while it was increased by 20-30% when VEBE compaction was used. Compressive strength of volcanic tuff at 28-day age of concrete block can attain 40-50% of that for ordinary materials using manual compaction, and up to 50-60 of compressive strength using VEBE compaction. Regarding permeability, volcanic tuff has a noticed increase in permeability when compared with the permeability of ordinary materials. Increasing fine materials in concrete block mix and plastering of block walls' during construction can solve the problem of permeability. Therefore, it is recommended to use volcanic tuff in concrete block production in building construction widely.

Keywords: volcanic tuff, lightweight aggregate, compressive strength, concrete block production.

1. Introduction

In Jordan, the use of natural materials such as Tripoli, Basalt and Oil shale ashes in concrete and as cement replacing materials was studied by many (e.g. El-Hasan and Al-Hamaideh, 2012; Abdelhadi et al., 2014; El-Hasan et al., 2015, Al-Sekhaneh and El-Hasan, 2021). Also, the investigation and use of natural resources such as basaltic rocks that extend on 18% of Jordan area (Al Smadi et al., 2018; Ibrahim et al., 2014) required analysis, testing and employment in construction operations as materials that can add new properties for construction materials. Lime stone in Jordan was studied by Moh'd (2015) to investigate the skeleton structure of pores in lime stone and its different state and effect on stone structure, The use of natural lightweight aggregate in concrete production results in reducing the density and weight of concrete structure produced. This will influence the total dead load of the structure significantly. This allows structural designers to immensely reduce the size of load-bearing elements such as columns, walls and footings. The implementation of such natural resources will lead to lowering the cost in construction by reducing the load of structure and the required quantity of steel reinforcement (Fredrick, 2014) and Sarireh (2015).

Volcanic tuff is a natural reserve resource of aggregate that can be found in Jabal Al-Hala located in Tafila in the Southern part of Jordan (Sarireh, 2020). As the volcanic tuff is a volcanic rock containing natural mineral zeolite (aluminium silicate alkaline) with a mainly vitreous structure, the high reactive silica content determined by chemical analysis gives Măcicaş quarry tuff pozzolanic character and hydraulic properties (Bedelean et al., 2010). The advantages of volcanic tuff include its highly porous structure, high surface area, and low density that gives less weight for structures. It is available in different types, sizes, and colors, and can reduce concrete dead weight in structure when it is used. Similarly, to other volcanic tuff materials, such as silica fumes and fly ash, replacement with zeolite can help in improving the strength of concrete through the volcanic tuff reaction with $Ca(OH)_2$ compound with cement gel and its compounds of calcium, phosphate, and ferrous materials (Negis, 1999). A similar conclusion was reached by using the mixtures of oil ash with Red soil and phosphogypsum (El-Hasan et al., 2019). Also, depending on the mineralogical composition and physical-mechanical characteristics of zeolitic tuffs, they have many uses in other areas: wastewater treatment, as a lightweight aggregate for fertilizers in agriculture and horticulture, for the minimization of heavy elements in the soil, in animal husbandry, fisheries, for the separation of nitrogen from the air, elimination of radioactive elements (Cs and Sr) of nuclear waste, supplements in animal diets, deodorants (Dipayan, 2007).

Pozolana can be prepared in different sizes and gradations and can be used as a light aggregate that fits into all parts of aggregate production and for the production of cement as additives in the form of fine and ground pozolana.

* Corresponding author e-mail: m.sarireh@gmail.com

10% to 30% is added before incarnating of the weight to correct the mixture components in terms of iron content, as well as the proportion of added 30% to clinker, helps in increased strength of concrete. There is a very large reserve in North-Eastern part of Jordan estimated at 470 Millions of Tons. Featuring pozolanic cement by the resistance to the impact of fresh and salt water that is usually rich in sulfate, leads to dioxide interaction. Calcium surplus with article pozolanic reduces the permeability of concrete and absorb excess water in addition to mobilizing cracks resulting from hydration (Alnawafleh et al., 2013). Also, Abali et al. (2006) and Augenti and Parisi (2010) pointed that volcanic tuff has an important role in keeping an intermediate compressive strength of the concrete mix, and in decreasing the weight of the concrete structure. Volcanic tuff can be used to produce workable concrete, light-weight concrete with reasonable concrete strength.

Abdelhadi et al. (2009), had utilized the bituminous limestone ash in the production of lightweight concrete masonry block. This step was produced to reduce the environmental impact by the waste of production of oil shale treatment process. And the utilization process for the oil shale residuals after extraction will give and lead to the production of 52% by weight of original rock as solid waste (fly ash) material. The compressive strength of the ash-mixes has a range of 1.9 – 7.6 Mpa. And the compressive strength of ash-aggregate mixes has a range of 5.4 – 6.3 Mpa, all at 28 days. The ash-polyester gave 2.1 Mpa as compressive strength at 28 days. Furthermore, the compressive strength and permeability parameters were improved by adding the Red soil to the bituminous limestone ash (El-Hasan et al., 2019).

Semsettin (2011) indicates that the use of volcanic tuff in concrete mix preparation and constituents can help in improving the properties of fresh and hardened concrete. Workability is an important property of fresh concrete that will improve with the use of volcanic tuff. Bleeding and segregation can be less when volcanic tuff is used in concrete mix (Al-Zou'by and Al-Zboon, 2014). Permeability, compressive strength, and durability can be increased also with the increase of volcanic tuff constituents in concrete mix (Ababneh and Matalkah, 2018). Kan and Gul (2008) pointed that volcanic tuff can increase the adhesion of cement gel in the concrete mix, in addition to the increase of durability and strength of the concrete structure. Kilic et al. (2009) pointed that volcanic tuff aggregate can affect the properties of the concrete in unit weight and strength if used in the mix, which will lead to a decrease in unit weight, with a remarkable increase in compressive strength.

Haddad and Shannag (2008) in their study for masonry cement for construction purposes, identify the optimum mortar mixes best suited to different masonry applications. The study indicated that masonry mortar mixtures proposed in this investigation met the European and American standard needs for water retention and air content. The use of hydrated lime in these mixes causes reductions in compressive strength and flexural strengths without developing an increase in the workability of the mix. The compressive strength test also indicated that masonry mortars, prepared as an aggregate to cement ratio equal to or less than 4 on a loose volume basis, can be successfully used for different masonry applications in Jordan. Considering shrinkage and volume stability and also economic feasibility, it was found that to use an aggregate cement ratio not less than 3.

Al-Zou'by and Al-Zboon (2014) studied the effect of the use of fine volcanic tuff on the characteristics of cement mortar. Fine volcanic tuff was mixed at ratios of 0, 25. 50, 75, and 100% with ordinary fine sandstone to form the mix of mortar. The samples were tested for compressive strength, flexural strength, and unit weight at 3, 7, 28, and 56 days. The compressive and flexural strengths had increased up to 75% through the use of fine volcanic tuff in mortar mix, and unit weight, as usual, was decreased with the increase of mixing ratio of fine volcanic tuff.

Balog et al. (2014) in the valorization of volcanic tuff in construction materials andmanufacturing industry, introduced the use of zeolitic volcanic tuffs as a local source for construction in the building materials industry for rock embankment, aggregate, for the preparation of mortar for masonry, and the production of lightweight concrete or autoclaved aerated concrete. The study was based on using the zeolitic volcanic tuff as a substitute for cement or aggregate. The study aimed to obtain a new building material made from local resources that can be used to realize new masonry works and to rehabilitate the old structures. Tests included physical properties of aggregate and compressive strength of mortar. The results showed that strength can be improved by using the volcanic tuff as fine and coarse aggregate materials for mortar construction. In addition, volcanic tuff has no production waste through mining, sieving, preparation, and during transportation for concrete block production or any construction and structural work (Al-Tabal and Al-Zboon, 2019), so it has no environmental impact on the surrounding environment and species during its production operations(Al-Tabal and Al-Zboon, 2012).

The current study aims to introduce the use of volcanic tuff as a construction material in the industry of block production by employing volcanic tuff materials in the form of powder, sandstone, and aggregate gradation in the concrete mix for block production. The size variations aim to notice an adequate improvement in compressive strength and decrease in the weight of block that met the acceptable allowable limits.

2. Materials and Methods

2.1 Materials

A sufficient of grey-colored volcanic tuff material was obtained from Jabal-Alhala in Tafila governorate, south of Jordan.In addition to aggregate materials of screened crushed granular material consisting of well-graded gravel, crushed stone or crushed gravel for the use in concrete block production, and fine limestone powder materials. It is required to define the source area for the material sample and to describe the material by conducting physical tests (El-Hasan and Al-Tarawneh, 2019). Also, natural sources of materials can be helpful in the case of construction and concrete and mortar production, or rehabilitation of old and ancient sites. Abdelhadi et al. (2012) utilized El-Lajjun bituminous limestone ash in the rehabilitation works for the weathered and eroded mortar and plaster of Al-Shawbak castle in South of Jordan. The use of natural sources for construction materials adds sustainability, environmental, and cost effectiveness for construction process and operations.

2.1.1 Material characterization and description

Volcanic tuff from Jabal Al Halal1is highly found as grey colored material with a thickness of more than 50m. The volcanic tuff in Jabal Al Halal location is of Paleocene to Neogene age (Gradstein, 2012). Limestone was obtained from a local quarry in Tafila. X-ray diffraction (XRD) spectra were used to characterize the volcanic tuff materials. Figure 1 illustrates the XRD spectra for the volcanic tuff sample.

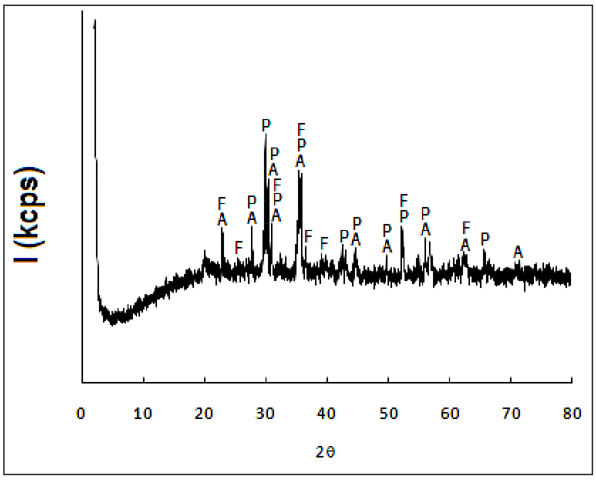

Figure 1. XRD spectra for Volcanic Tuff samples. Where A: Plagioclase feldspar (Anorthite), F: Olivine (Forsterite) and P: Pyroxene (Augite). Royal Society Laboratory, 2019.

2.2 Methodology

All materials were classified by sieve analysis using the sieve sizes that include sieve 3/8", and the sieves # 4, No. 6, No. 14, and No. 40). The volcanic material was tested for specific gravity, absorption, and density. Ordinary limestone aggregate that is used in block production was obtained from Tafila crusher query for limestone, the aggregate is called Adasyiah (3/8"-No. 4 sieves), sandstone (swaileh), and fine lime (boudrah). Ordinary materials were tested for specific gravity, absorption, and density. Mixes were prepared in concrete technology laboratory using Ordinary Portland Cement type I (OPC-1) and distilled water at the designed ratio of volcanic tuff materials including 10, 20, 30, 40, 60, and 80%. Concrete samples and specimens were prepared using wooden molds of cubes (15 cm and 20 cm cubes) and solid block (10 cm and 15 cm solid block) and tested at 7, 14, and 28 days for mass (Kg) and compressive strength (N/mm^2). Also, density was calculated considering their mass and dimensions of specimens. Results were compared for mass, density and compressive strength.

Trial Mix #1 constitutes of concrete mixes for solid block molds and concrete cubes were prepared from the original materials (Adasyiah, Boudrah, and Swaileh) at the volume ratios (9:4:1.5 in volume) as the control mix sample, then it was tested for mass, density, and compressive strength of concrete and block specimens. Samples of fresh concrete molds were prepared according to the ASTM C 192/C 192M -00 and ASTM C 31 / C 31 M. Specimens were prepared in the lab in dimensions of concrete cubes: (150x150x150 mm) and (200x200x200mm) (Sarireh and Al-Baijat, 2019a), and in solid block molds: (400x200x100mm and 400x200x150mm). In mix #2 original Adasyiah was replaced by pozolanic (volcanic tuff) of the same aggregate size. Similarly, in mix #3 swaileh was replaced by pozolanic (volcanic tuff) of the same aggregate size. Mix #4 fine boudrah was replaced by pozolanic (volcanic tuff) of the same aggregate size.

As expected the use of pozolanic materials reduced the mass of specimens, as volcanic tuff has less density and specific gravity. Using Adasyiah size from Pozolana (Volcanic Tuff Aggregate) cause a decrease in mass in all specimens, followed by swaileh size from Pozolana (Volcanic Tuff Aggregate) to a lesser extent. A recommendation was made based on the obtained results.

2.2.1 Volume relation and ratios

Table (1) shows the volume relation between components of concrete mix for the block using ordinary and volcanic tuff materials and water-related to (OPC-1). Ordinary materials were replaced by volcanic tuff at (10, 20, 30, 40, 60, and 80%) ratios in the mix for concrete block production.

Table 1. The volume of ordinary and volcanic tuff materials related to cement volume.

Material	Volume Ratio concerning cement volume
Ordinary Adasyiah (4-8 mm)	4.2
Tuff Adasyiah (4-8 mm)	Will be replaced on specific ratio (10, 20, 30, 40, 60, and 80 %)
Fine Tuff (4-0.075 µm)	Will be replaced on specific ratio (10, 20, 30, 40, 60, and 80 %)
Ordinary Swaileh	2.2
Ordinary Boudrah	0.7
Cement	1
Water	2.3

3. Results

3.1 Specific gravity, density and absorption of production materials

Specific gravity and absorption of coarse aggregate that used is called (Adasyiah) (4-8 mm particle diameter) were tested according to the AASHTO T 85. Specific gravity and absorption of fine aggregate (Boudrah, and Swaileh). (4-0.075 µm) were tested according to the AASHTO T 84-93 I and ASTM C 128-88. Table (2) presents the specific gravity and absorption of the tested materials. It is shown that volcanic tuff materials have less specific gravity than ordinary aggregate materials of Adasyiah and boudrah and swileh of the same size gradation.

The density of materials used in block production was determined for coarse aggregate according to ASTM C 127. Density for fine aggregate was determined according to ASTM C 128. Results of density showed that volcanic tuff materials have less density than ordinary material in the same size gradation, and the density decreases with the increase of aggregate size in both types of aggregates (Sarireh, 2017).

Table 2. Specific gravity, absorption, and density of materials in concrete and volcanic tuff block production.

Materials	Bulk Specific Gravity	SSD Specific Gravity	Density (g/cm^3)	Absorption%
Ordinary Adasyiah (4-8 mm)	2.453	2.587	1.29	5.48
Tuff Adasyiah (4-8 mm)	2.391	2.556	1.04	6.88
Fine Tuff (4-0.075 µm)	2.349	2.54	1.35	8.11
Ordinary Swaileh	2.615	2.653	1.68	1.42
Ordinary Boudrah	2.554	2.573	1.52	0.72

5 Mixes were prepared using ordinary and volcanic tuff materials as presented in Table (3) including the required mixes for block production to test mix and block properties.

Table 3. Concrete mix materials for block production

Mix Type		Components
Mix #1 control sample		Original or ordinary materials (Adasyiah and boudrah and swaileh)
Mix #2		Pozolanic addasiah with ordinary materials of (boudrah and swileh)
Mix #3		Pozolanic Swaileh with ordinary materials of (Adasyiah and boudrah)
Mix #4		Pozolanic boudrah with ordinary materials of (Adasyiah and swileh)
Mix #5 Trial Mix	1- rich cement-content	50 kg of cement with volcanic tuff mixed on 10, 20, 30, 40, 60, and 80% of ordinary original materials on manual compaction
	2- low cement-content with manual compaction	33 kg of cement with volcanic tuff mixed on 10, 20, 30, 40, 60, and 80% of ordinary original materials on manual compaction
	3- Low cement-content with VEBE compaction	33 kg of cement with volcanic tuff mixed on 10, 20, 30, 40, 60, and 80% of ordinary original materials on VEBE compaction

3.2 Results of concrete samples for block production

12 specimens were prepared for each mix (i.e. 12 molds and cubes). Then results were obtained at 28 days age of concrete samples to observe and test the concrete hardened properties.

3.2.1 Mass of solid concrete blocks and cubes

Figure (2) illustrates the results for the average mass of concrete and block specimens. Concrete block of mix #1 that was prepared using the ordinary aggregate materials (Adasyiah , swaileh, and fine boudrah at the volume ratios (9:4:1.5 in volume). In mix #2, ordinary addasyiah was replaced by volcanic tuff addasyiah, In mix #3, ordinary swaileh sand was replaced by fine volcanic tuff sand of similar size gradation, and in mix #4 ordinary fine boudrah was replaced by fine volcanic tuff of similar size gradation.

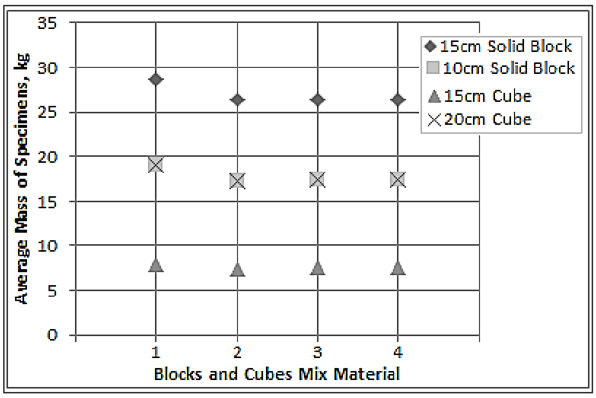

Figure 2. Mass of concrete cubes and solid block materials: Mix#1: Ordinary Materials, Mix #2: Pozolanic Addasiah, Mix #3: Pozolanic Swaileh, and Mix #4: Pozolanic Boudrah.

3.2.2 Density of solid concrete blocks and cubes

Concrete mixes were prepared in concrete cubes and solid block molds and cured until 28 days age (Al-Baijat and Sarireh, 2019a). Figure (3) illustrates the results of density (kg/m^3) for these samples. The results showed that pozzolanic or volcanic tuff can reduce the density of produced concrete block with lighter mass and weight. It is obvious the difference in results between original ordinary materials and volcanic tuff materials. But the use of Addasiah size volcanic tuff has the largest effect to give lighter material with lower density ranges between 2,150 to 2,200 kg/m^3 in mix #2. Then, mix #4 that used volcanic tuff boudrah instead of ordinary boudrah achieved an average density of 2250 kg/m^3. While the use of total swaileh as volcanic tuff in mix #3 achieved an average density of 2300 kg/m^3.While the average density for ordinary materials was 2350 kg/m^3.

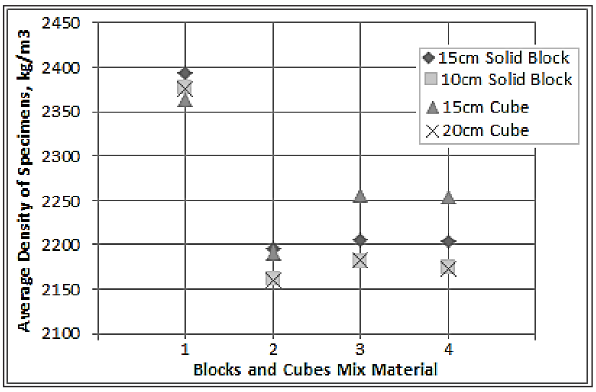

Figure 3. Density of block materials: Mix#1: Ordinary Materials, Mix#2: Pozolanic Addasiah, Mix#3: Pozolanic Swaileh, and Mix#4: Pozolanic Boudrah.

3.2.3 Compressive strength of concrete blocks and cubes

For compressive strength, specimens were prepared according to (BS EN 12390-2:2009) for making and curing specimens for compressive strength test, block specimens were prepared according to IS: 2185 (part-I) (1979-1987-1998) and IS : 2185 (part-II)- 1985 and tested according to (ASTM : C 140-03),and were tested according to (BS EN 12390-3:2009) for compressive strength of test specimens, and (BS EN 12390-4:2009) for compressive strength specification of test machines (Sarireh and Al-Baijat, 2019b). The results are presented in Figure (4). All specimens have achieved the required compressive strength of concrete block samples. It is showed that pozolanic of addasyah size and pozzolanic fine materials have the lowest compressive strength after 28-day. Pozolanic addasiah size has compressive strength in the range between 9 to 11 N/mm^2 in concrete block mix #2, and the pozolanic fine (boudrah size) material has the range of compressive strength of 9 to 12 N/mm^2 in concrete block mix #4. While the compressive strength of swaileh volcanic tuff has the range 10-14 Mpa in concrete block mix #3According to the term 603/2-Non-bearing block, the minimum compressive strength of block is 3.5 N/mm^2 (Technical Specifications for General Buildings, 1996).

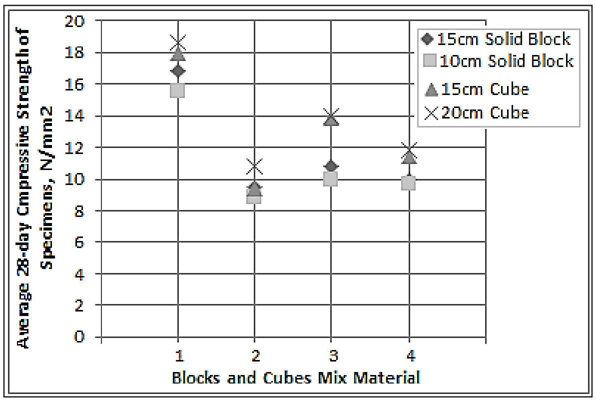

Figure 4. Compressive strength of block material: Mix #1: Ordinary Materials, Mix #2: Pozolanic Addasiah, Mix #3: Pozolanic Swailleh, and Mix #4: Pozolanic Boudrah.

3.3 Trial mix with rich cement content and replacement ratios of original materials

The mix was prepared by mixing (100) kg of block materials, with(20) Liter of water, and (50) kg of OPC-I. Pozolana (Volcanic Tuff) were mixed at 20, 30, 40, 60, and 80% replacing the original materials. And samples were formed in block molds of (400x200x100mm and 400x200x150mm), and in concrete cubes molds of (150x150x150 mm and 200x200x200 mm) (Al-Baijat and Sarireh, 2019b).

3.3.1 Mass of solid concrete block and cubes

As presented in Figure (5), the mass of the specimen was reduced by the increase of volcanic tuff (Pozolana) ratio in the concrete block mix. It is clear that the addition of volcanic tuff in replacing original materials, cause a decrease in the mass of specimens. But, the mass cannot be considered to judge the results because the specimens have different dimensions and shapes. So, in each mix or step the density will be considered for the judgement and compare with the control samples mix of ordinary materials that has 0-content of volcanic tuff. When volcanic tuff was used on 60-80%, the mass was decreased by 10-15% respectively compared to volcanic tuff of 10% replacement of ordinary.

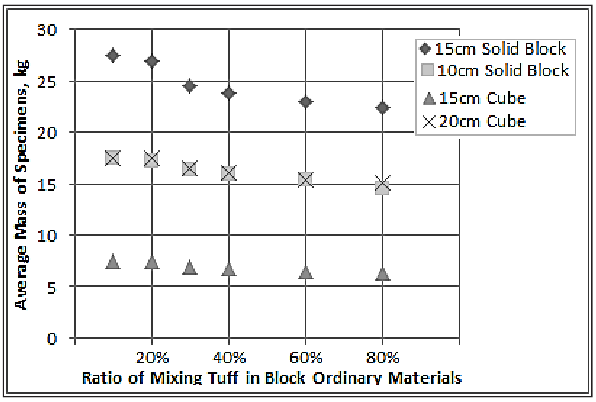

Figure 5. Mass reduction based on volcanic tuff ratios.

3.3.2 Density of block specimens and concrete cubes

Figure (6) presents the density (kg/m^3) of concrete specimens and block molds after pouring and casting in solid block molds. The addition of volcanic tuff to the concrete block mix will decrease the density, to reach the lowest density of 1857.7 kg/m^3 with the ratio of 80% of replacement. The reduction in density can reach 15.6% between 10% and 80% of volcanic tuff when used in material of concrete block production. Ordinary materials give an average density of 2,380 kg/m^3, compared to 1,900 kg/m^3 at 60%, and 1,800 kg/m^3 at 80%.

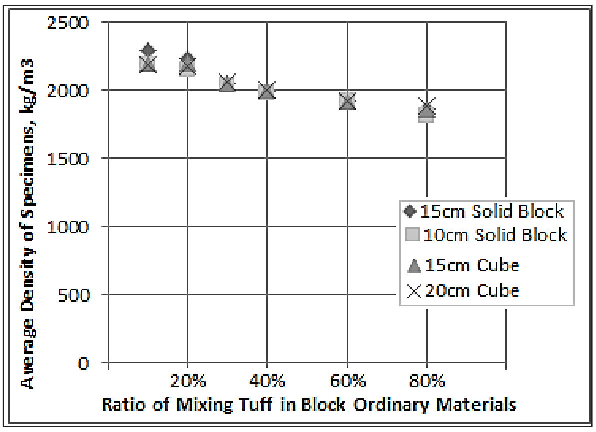

Figure 6. Density reduction based on volcanic tuff ratios.

3.3.3 Compressive strength of block specimens and concrete cubes

The specimens compressive strength of the mixes were prepared in block molds and cubes and tested after28-day age, results are presented in Figure (7). The addition of volcanic tuff decreases the compressive strength of concrete block mix at 28-day. The lowest value was obvious at an 80% replacement ratio, which can also be acceptable. 80% ratio can attain a compressive strength of range (6.5.5-8N/mm^2), and this result is acceptable for block production as the minimum value of compressive strength is 3.5 N/mm^2 for non-bearing block (Technical Specifications for General Buildings, 1996). Ordinary material gives an average compressive strength of 17.5 Mpa, while the compressive strength was reduced to 8.25 Mpa at 60%, and reduced to 7.5 Mpa at 80%, but still acceptable as discussed previously.

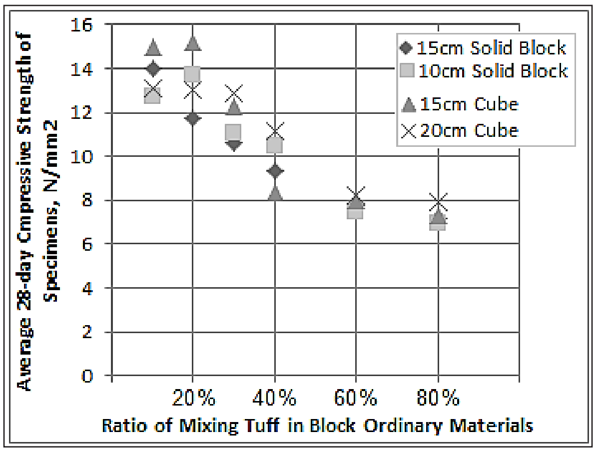

Figure 7. Compressive strength of block concrete specimens and cubes Mpa.

3.4 Trial mix with less cement content (Local Recipe) for local production plants

The 2nd trial for block mixes was prepared by mixing of block original materials(100) kg with Volcanic Tuff (Pozolana) in ratios including 20, 40, 60, 80, and 100% and 33 kg of cement.The concrete mix was poured into block molds andcubes, also cured for 28-day age.

3.4.1 Mass of concrete block and cubes

Figure (8) presents the results of specimens' mass on the designed mixing ratios of volcanic tuff. The results showed a decrease in the mass of specimens with an increase of volcanic tuff mixing ratio in mix. A 25% reduction in mass can be attained at 80%, while a reduction of 31.25% can be achieved when using volcanic tuff on 100%.

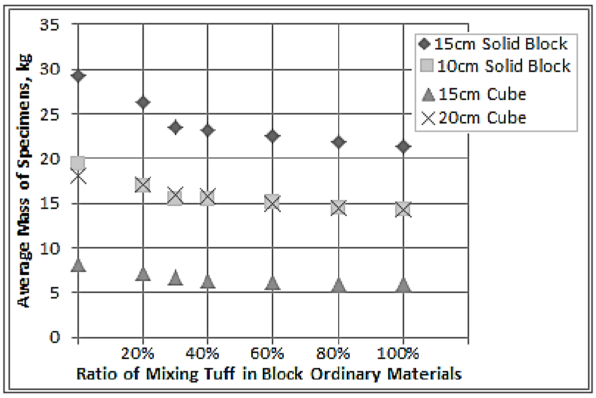

Figure 8. Mass of concrete block and cubes for volcanic tuff ratios.

3.4.2 Density of block and cube specimens

Figure (9) presents the values of density of concrete blocks and cubes using volcanic tuff materials in ratios for 10%-100% of production materials of blocks. The addition of volcanic tuff decreases the density of block density from 2400 kg/m^3 of original materials to 1800 kg/m^3 for 100% replacement. The ratio of 80% of volcanic tuff can reduce the density of block by 25% compared to original materials of zero content of volcanic tuff. While the use of 100% of materials from volcanic tuff can reduce the density of block by 29%. Ordinary materials give an average density of 2,380 kg/m^3, compared to 1,850 kg/m^3 at 60% and to 1,775 kg/m^3 at 80%. While the use of volcanic tuff materials by 100% reduced the density to 1,750 kg/m^3.

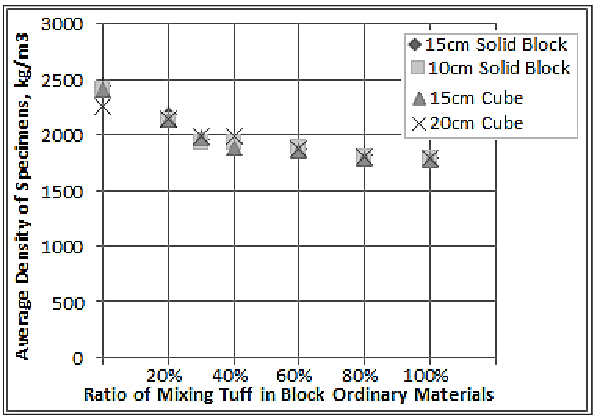

Figure 9. Density of concrete block and cubes for volcanic tuff ratios.

3.4.3 Compressive strength of block and cube specimens

Block and cube specimens were tested for compressive strength, the results are presented in Figure (10). The addition of volcanic tuff decreases the compressive strength of specimens. The least compressive strength of 100% replacement is equal to (5.5-7.25 N/mm2), although it is low it is still acceptable for a concrete block in construction (Technical Specifications for General Buildings, 1996). Ordinary materials give about 16 Mpa compressive strength, while the use of volcanic tuff materials by 60% reduced the compressive strength to7.35 Mpa, and to 7 Mpa at 80%. The use of volcanic tuff materials by 100% reduced the compressive strength to 6 Mpa, and this compressive strength is acceptable as discussed previously.

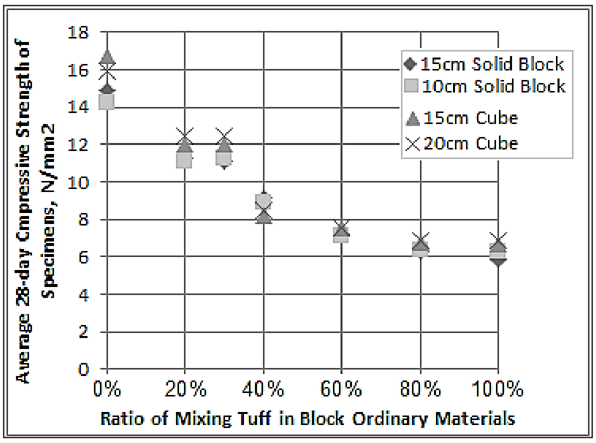

Figure 10. Compressive strength of concrete block and cubes for volcanic tuff ratios.

3.5 Preparation of block and cube specimens by VEBE-table for compaction

Block sand cube specimens were prepared using the VEBE-table for compaction instead of a 16 mm – diameter compaction rod.

3.5.1 Mass of concrete block and cube specimens

Figure (11) presents the results for a mass of concrete specimens, although there is a decrease in mass with increasing mixing ratios. But the compaction using VEBE-table can increase and maintain specific mass for specimens compared to the similar ratio and shape of the specimen. i.e. VEBE compaction has a moderate slope of decreasing in mass. VEBE- table compaction can increase the mass of concrete cubes and solid block specimens made of original material by 20%, while it increased the mass of these cubes and specimens by 10-15% when volcanic tuff was used.

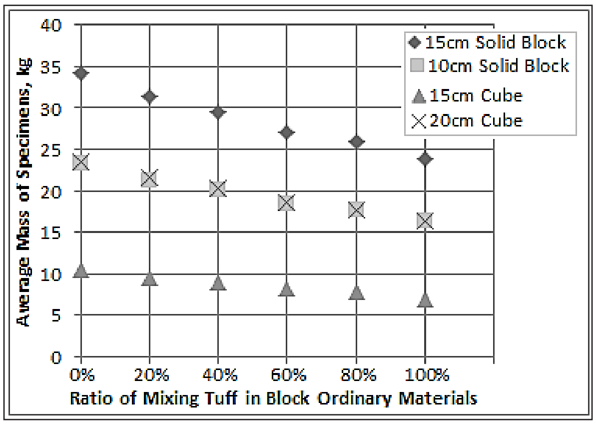

Figure 11. Mass of concrete block and cubes forvolcanic tuff ratios compacted by VEBE- table.

3.5.2 Density of concrete specimens using VEBE-table

Concrete block and cube specimens were prepared by compaction using VEBE-table to give more compaction for the density of specimens. Figure (12) presents the density test of concrete block and cube specimens compacted by VEBE-table. Results showed that the density of block materials can be smoothly decreased as the volcanic tuff is used and cause decreasing in density when mixed with original block materials. Using VEBE-table for compaction increased the density for original materials to 2,900 kg/m^3, while for 60% volcanic tuff the density was increased to 2,350 kg/m^3, and to 2,300 kg/m^3 at 80% volcanic tuff. While the use of volcanic tuff by 100% had increased the density to 2,000 kg/m^3.

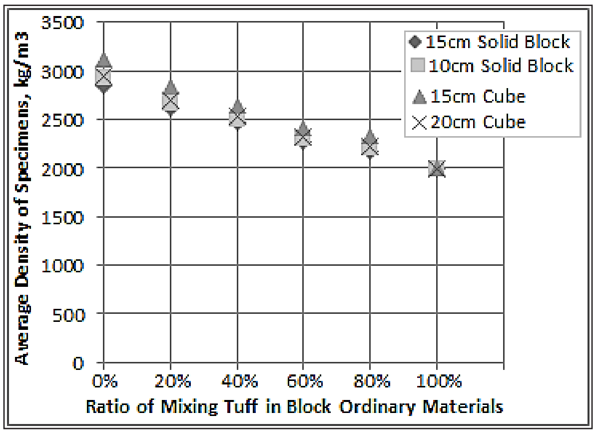

Figure 12. Density of concrete block and cubes for volcanic tuff ratios compacted by VEBE- table.

3.5.3 Compressive strength of VEBE-table compacted specimens

Figure (13) presents values of compressive strength for production materials of block compacted by VEBE-Table. The vibrated specimens by VEBE-table have cause an increase in compressive strength, even if volcanic tuff materials are used in 100% compared with compressive strength using original materials or any other ratio of volcanic tuff. The compaction effort by VEBE-table increases the compressive strength in a noticeable range. Ordinary materials increased the compressive strength to 22.5 Mpa when compacted by VEBE-table. Also, 60% as volcanic tuff increased compressive strength to 14 Mpa, and to 9.5 Mpa when used at 80%. The use of volcanic tuff by 100% increased the compressive strength to 8 Mpa. VEBE-table compaction can be effective in increasing compressive strength for block production.

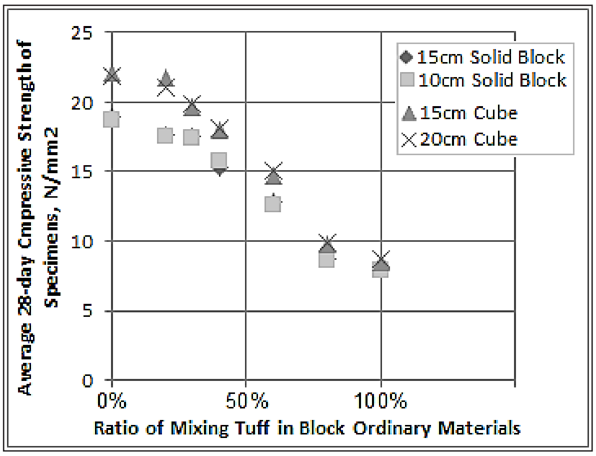

Figure 13. Compressive strength of concrete block and cubes for volcanic tuff ratios compacted by VEBE- table.

3.6 Permeability of block materials using volcanic tuff

Permeability of concrete block is another important test, Table (4) presents the values for permeability of waterfall for control specimens (ordinary block materials) and those of volcanic tuff based on designed mixing ratios with ordinary materials. Because of the higher porosity of volcanic tuff material, the block specimens of high mixing ratio have a noticeable and maximum waterfall and increase of seepage through volcanic tuff materials. Permeability increased when volcanic tuff used in concrete mix for block production, especially on 80-100%. While permeability seemed to be moderate when volcanic tuff was used on 60% in the concrete mix.

Table 4. Permeability of control sample and volcanic tuff samples

Mix Sample	Water height (cm)	Water Fall (cm)	Average Water Fall (cm)
Control (Ordinary Materials)	16.5	0.4, 1, 0.6	0.67
20% volcanic tuff	16.5	0.2, 0.3, 0.5	0.33
30% volcanic tuff	14.6	0.7, 0.5, 0.6	0.6
40% volcanic tuff	16.4	0.7, 0.9, 0.6	0.703
60% volcanic tuff	14.5	0.8, 1.2, 0.9	0.967
80% volcanic tuff	14.5	3.35, 5.55, 3.4	3.43
100% volcanic tuff	15.6	4.65, 5.75, 4.8	5.07

4. Discussion

In concrete and block production, the procedure of analysis implies comparing specimens based on mass, density, compressive strength, and permeability. Volcanic tuff materials were used as a total component of a specific size (Addesiah, Sweileh, and Boudrah) as prepared in mix #2, #3, #4 and compared to original materials in mix #1. Then, volcanic tuff was used on mixing ratios 10% to 80% and 100% of original materials. Also, cement was used on two contents; rich-cement content of 100 kg of cement, and low-cement content of 50 kg of cement with original and volcanic tuff materials at the specified mixing ratio. And finally, the low-cement content mix was prepared by VEBE-table compaction to study the effect of vibration on mass, density, and compressive strength.

The use of volcanic tuff in original material as whole or total part for specific size gradation such as (addasyiah, swaileh, and boudrah) in mix #2, #3, and #4 cause a decrease in mass and density of concrete blocks and cubes. The average density of samples of mix #2 was 2,175. For mix #3, the average density was 2,300. While the average density of mix #4 was 2,250. These values of density were compared to 2350-2400 kg/m^3 for ordinary materials.

Compressive strength had an average of 12 Mpa for mix#2, 10 Mpa for mix #3, and 11 Mpa for mix #4. While the concrete mix of ordinary materials had an average of 17.5 Mpa for compressive strength.

Then, volcanic tuff materials were used on mixing ratios consideringthe standard mix (rich-cement content), and the local mix considering(low-cement content). The rich-cement content mixes achieved density of 1,950 kg/m^3 at 60% and 1,900 kg/m^3 at 80%. While, the low-cement content mixes achieves less density of 1,900 kg/m^3 and 1,800 kg/m^3 at 60 and 80% respectively. Compared to ordinary materials that achieved 2,450 kg/m^3 and 2,380 kg/m^3 for rich-cement and low-cement contents for ordinary materials respectively. For compressive strength, rich-cement content mix achieves 8Mpa at 60%, and 7 Mpa at 80% compared to 17 Mpa for ordinary materials. The low-cement content mix achieves 7 Mpa at 60% and 6.5 Mpa at 80%, compared to 16 Mpa of ordinary materials.

Using VEBE-table for compaction, VEBE-table is used to measure the time and effort of compaction on concrete. Here it was used for compaction of specimens of low–cement content mix.VEBE-table raised the average density from 2,400 kg/m^{3}to 3,000 kg/m^3 for ordinary materials. While the average density of 60% volcanic tuff raised from 1,900 kg/m^{3}to 2,400 kg/m^3. For 80% volcanic tuff, the average density raised from 1,800 kg/m^3 to 2,300 kg/m^3.For 100% volcanic tuff, the average density raised from 1,750 kg/m^3 to 2000 kg/m^3.For compressive strength, VEBE-table increased strength from 16 to 21 Mpa of ordinary materials. For volcanic tuff, the compressive strength increased by VEBE compaction from 9.5 to 13.5Mpa, from 7 to 9 Mpa, and from 6 to 8 Mpa for 60, 80, and 100% respectively.

Based on the results of the current study; using volcanic tuff materials on specific mixing ratios in concrete block production can produce a lightweight concrete block that has an acceptable compressive strength. Also, volcanic tuff materials have less waste during miming and transporting, and has less cost for mining and production, which will save other resources such as limestone for other applications of concrete structures that require more density and compressive strength in its structural members such as columns, beams, and footings.

Conclusions

Based on the results of the current study, the following are the main points that can be concluded in deep:

1-Volcanic tuff has specific gravity and a density less than that for traditional ordinary materials of the same size gradation used for concrete block production, so volcanic tuff can produce less mass and density of concrete and block construction. Also, volcanic tuff has an acceptable concrete compressive strength, and permeability value when it is used when compared with these values of ordinary materials.

2-Volcanic tuff materials have preferable application within production traditional original materials that give less mass for handling, transporting, and loading in concrete structures when used for block work in building and project construction.

3- Volcanic tuff materials can attain 10% less in density when used as a whole part replacement (addaseyah, swieleh, or boudra), and can attain 20% less density when used by80% in rich-cement content mix, and 26% less density in the low-cement content mix at 80% mixing ratio. Compaction by VEBE-table can increase density by 20%.

4- Volcanic tuff when was mixed as a whole part of specific size gradation (such as addaseyah, swaileh, and boudrah), attained 52-57% of 28-day compressive strength of ordinary materials. Also, the compressive strength of 80% volcanic tuff in the low-cement content mix, has the range of 40-45% of compressive strength for ordinary materials.60 and 80% volcanic tuff using VEBE-table compaction, can attain 45-55% of 28-day compressive strength of that for ordinary materials.

5- It is noticed that permeability of specimens increases with the increase of volcanic tuff ratio, this problem can be treated by using more of fine materials and more compaction. Also, concrete block walls usually are coated by plastering (rough and smooth plaster layers) during the construction of buildings.

6- It is recommended to use volcanic tuff in concrete block production for buildings and projects construction in country widely, as the materials can achieve the required density and compressive strength.

References

Ababneh, A., and Matalkah, F. (2018). Potential use of Jordanian volcanic tuffs as supplementary cementitious materials. Construction Materials 8: 193-202.

Abali, Y., Bayca, S.U., Targan S. (2006). Evaluation of blends tincal waste, volcanic tuff, bentonite and fly ash for use as a cement admixture", Journal of Hazardous Materials 131(1-3):126-30. DOI: 10.1016/j.jhazmat.2005.09.031.

Abdelhadi, N., Khoury, H., Suleiman, H.M. (2009). Utilization of Bituminous Limestone Ash from EL-LAJJUN Area in production of lightweight Masonry block. Acta Geotechnica 4(3): 215-222.

Abdelhadi, N., Abdel Hadi, A., Monther, A. (2012). Rehabilitation of Al-Shawbak Castle Using El-Lajjun Bituminous Limestone Ash Mortars and Plasters. Jordan Journal of Earth and Environmental Sciences 4 (2): 1-6.

Abdelhadi, N., Abdelhadi, M., El-Hasan, T. (2014). The Characteristics of Cement Mortars Utilizes the Untreated Phosphogypsum Wastes Generated From Fertilizer Plant, Aqaba- Jordan. Jordan Journal of Earth and Environmental Sciences 6(2): 61-66.

Al-Baijat, H., and Sarireh, M. (2019a). The Use of Fine Blast Furnace Slag in Improvement of Properties of Concrete. Open Journal of Civil Engineering 9(2): 95-105.

Al-Baijat, H., and Sarireh, M. (2019b). Concrete Properties Using Tripoli." Electronic Journal of Geotechnical Engineering 24(2): 441-452.

Alnawafleh, H., Tarawneh, K., Alrawashdeh, R. (2013). Geologic and economic potentials of minerals and industrial rocks in Jordan. Natural Sciences. 5(06):756-769. DOI: 10.4236/ns.2013.56092.

Al Sekhaneh, W., and El-Hasan, T. (2021): Characterization of basaltic stone from cultural heritage site of Umm El-Jimal in northern. Iraqi Geological Journal. 54 (1B): 12-23.

Al Smadi, A., Al-Malabeh, A., Odat, S. (2019). Characterization and Origin of selected Basaltic Outcrops in Harrat Irbid (HI), Northern Jordan. Jordan Journal of Earth and Environmental Sciences 9(3): 185-196.

Al-Tabal, J., and Al-Zboon, K. (2012). Suitability assessment of groundwater for irrigation and drinking purpose in the northern region of Jordan, Journal of Environmental Science and Technology 5(5): 274-290.

Al-Tabal, J., and Al-Zboon, K. (2019). The Potential of the Application of Olive Cake and Stone Cutting Waste for Soil Amendment. Jordan Journal of Earth and Environmental Sciences 10 (1): 28-34.

Al-Zou'by, J., and Al-Zboon, K. (2014). Effect of volcanic tuff on the characteristics of cement mortar. Ceramica 60: 279-284.

ASTM C-128-88, Standard test method for specific gravity and absorption of fine aggregate, 1988.

ASTM C-127-88, Standard test method for specific gravity and absorption of coarse aggregate, 1988.

ASTM C 192/C 192M -00. Standards Practice for Making and Curing Concrete Test Specimens in the Laboratory.

ASTM C 31 / C 31 M. Practice for Making and Curing Concrete Test Specimens in the Field.

ASTM : C 140-03 Standard test methods for sampling and testing concrete masonry units and related units.

Augenti, N., and Parisi, F. (2010). Constitutive models for tuff masonry under uniaxial compression. Journal of Materials in Civil Engineering 22(11):1102-1111. DOI: 10.1061/(ASCE)MT.1943-5533.0000119.

Balog, A.A., Cobîrzana, N., Aciua, C., Iluțiu-Varvaraa, D. A. (2014). Valorification of volcanic tuff in constructions and materials manufacturing industry. The 7th International Conference Interdisciplinarity in Engineering (INTER-ENG 2013), Procedia Technology 12 (2014) 323 – 328.

Bedelean, H., Andrada, M., Silvia, B., Maria, S. (2010). Investigations on some zeolitic volcanic tuffs from Cluj County (Romania), used for zinc ions removal from aqueous solution, Studia Universitatis Babeș-Bolyai. Geologia 55 (1): 9 – 15.

BS EN 12390-3 (2009). Compression Strength of Test Specimens.

BS EN 12390-2 (2009). Making and Curing Specimens for Strength Test.

BS EN 12390-4 (2009). Compression Strength Specification of Test Machines.

Dipayan, J. (2007). A new look to an old pozzolan: clinoptilolite – a promising pozzolan in concrete, proceedings of the twenty-ninth conference on cement microscopy Quebec City, Canada.

El-Hasan, T., and Al-Hamaideh, H. (2012). Characterization and possible industrial applications of tripoli outcrops at Al-Karak province. Jordan Journal of Earth and Environmental Science 4 (2): 63-66.

El-Hasan, T., Mahasneh, B., Abdelhadi, N., Abdelhadi, M. (2015). High Calcium Ash Incorporating into Clay, Sand and Cement Mortars Used for Encapsulation of Some Heavy Metals. Jordan Journal For Earth and Environmental Sciences 6 (3): 23- 28.

El-Hasan, T., Abu-Jaber, N., Abdelhadi, N. (2019). Hazardous Toxic Elements Mobility in Burned Oil Shale Ash, and Attempts to Attain Short- and Long-Term Solidification. Oil Shale 36 (2S): 226-249.

El-Hasan, T., and Al-Tarawneh, A. (2019). Heavy-Metal Contamination and Distribution within the Urban Soil Cover in Mutah and Al-Mazar Municipal Area.

Jordan Journal For Earth and Environmental Sciences 11 (3): 202-210.

Fredrick, O. S. (2014). A Study Into The Performance of Volcanic Tuff as Partial Replacement of River Sand in Pre-cast Concrete. Project Report, University of Nairobi, 1-62.

Gradstein, F.M, Ogg, J.G., Schmitz, M.D., et al., (2012). The Geologic Time Scale 2012: Boston, USA, Elsevier. DOI: 10.1016/B978-0-444-59425-9.00004-4.

Haddad, R., and Shannag, M. J. (2008). Performance of Jordanian Masonry Cement for Construction Purposes. Jordan Journal of Civil Engineering 2(1): 20-31.

Ibrahim, K. M., Masri, B., Al-Taj, M. Musleh, S., Alzughoul, K. (2014). Volcanotectonic evolution of central Jordan: Evidence from the Shihan Volcano. Journal of African Earth Sciences 100: 541–553.

IS: 2185 (part-I) 1979-1987-1998. Specifications for concrete masonry. Units part- I. Hollow and Solid Concrete Blocks (Second Revision).

IS: 2185 (part-II)- (1985). Super seeding IS: 3590-1966 Specifications for concrete masonry units part-II Hollow and Solid light weight concrete blocks (First Revision).

Kan, A., and Gul, R. (2008). Properties of Volcanic Tuff Sands as a New Material for Masonry Mortar. International Journal of Natural and Engineering Sciences 2 (2): 69-73.

Kilic, A., Atis, C. D., Yasar, E., Ozcan, F. (2009). High strength lightweight concret Made with scoria aggregate containing mineral admixtures. Cement and Concrete Research 33(10): 1595-1599.

Moh'd, B. K. (2015). Deriving the Pore Structure of Selected Jordanian Building Limestones. Jordan Journal of Earth and Environmental Sciences 7 (2): 71-75.

NDR Standard Method T 85. Specific Gravity and Absorption of Fine Aggregate, AASHTO T 85.

NDR Standard Method T 84. Specific Gravity and Absorption of Fine Aggregate, AASHTO T 84-93 I.

Negis F. (1999). Zeolite based composites in energy storage. Master Thesis, Izmir Institute of Technology, Turkey.

Sarireh, M. (2015). The Use of Local Materials Crushed and Rounded Aggregate in Tafila and Karak Areasin Concrete Production. Dubai, 2015, Conference Poverty Alleviation Through Projects, American University, Dubai, United Arab Emirates, 25- 28/5/2015.

Sarireh, M.(2017). High Strength Concrete Using Basalt Aggregate in Concrete Mix Improvemnet. The International Academic Cluster Conference, Bangkok, Thailand, 5-6 October 2017.

Sarireh, M., and Al-Baijat, H. (2019a). Local Aggregate in Production of Concrete Mix in Jordan. Open Journal of Civil Engineering 9(2): 81-94.

Sarireh, M., and Al-Baijat, H. (2019b). Cement-Tripoli Admixture Replacement In Concrete Mix. Electronic Journal of Geotechnical Engineering 24(2): 387-394.

Sarireh, M. (2020). Testing the use of volcanic tuff in base and sub-base pavement construction in Jordan. International Journal of Construction Management. DOI: 10.1080/15623599.2020.1853007.

Semsettin, K. (2011). The effect of zeolite amount on the physical and mechanical properties of concrete. International Journal of Physical Sciences 6(13): 3041-3046.

Technical Specifications for General Buildings, Civil and Architectural Works. Volume (1), 2nd Edition. 1996.

JJEES

JJEES (2021) 12 (4): 285-294
ISSN 1995-6681

Jordan Journal of Earth and Environmental Sciences

Assessment of heavy metals contamination levels in surfaces soil in Baqa'a area, Jordan

Khaled Tarawneh, Issa Eleyan, Rakan Alalwan, Shoroq Sallam, Safa Hammad

Civil Engineering Department, Faculty of Engineering, Amman Arab University, Jordan.

Received 1 February 2021; Accepted 16 March 2021

Abstract

This study is focused to assest the heavy metals contamination levels in surface soil of Baqa'a area. Physicochemical tests have been carried out on thirteen samples from different localeties based on granulometric analysis (particle-size distribution), moisture content, pH, electrical conductivity (EC), total dissolved solids (TDS), Inductively coupled plasma (ICP) and X-Ray diffraction (XRD). Soil contamination was assessed using three indices including an index of geoaccumulation (I_{geo}), contamination factor (CF) and degree of contamination (C_{deg}). Regarding the granulometric analysis result, it can be noticed that most of the soil can be considered as sandy loam. The current study showed a moisture content of the study soil ranges from 16.2 to 18.3%, whereas the pH varies from 7.40 to 8.90. XRD results indicated that the major existing mineral is quartz, while calcite, dolomite and kaolin are minor minerals.The results of ICP showed that the soil contamination assessment allows for the arrangement of the metals from the higher to lower mean content as follows: Mn > Cr > V >Ni > Zn > Cu > Co > Pb > Cd, compared to the average soil. The I_{geo} values indicated that the results reported uncontaminated soil ($I_{geo} \leq 0$) for Cu, Pb, V and Cd, uncontaminated to moderately contaminated soil (0<Igeo<1) for Co and Mn, Zn, Ni. The results of the CF index of heavy metals of the studied samples indicated low contamination to considerable contamination, whereas the value of C_{deg} for most of the heavy metals in the studied samples indicated a moderate to a considerable degree of contamination. Exception of this conclusion can be noticed for some sites as indicated in site BR9, which shows a high degree of contamination (C_{deg}= 29.18). This site indicated also highly contaminated as approved by CF value. It can be concluded that most of reasons for high contamination in the study area are due to agricultural, industrial and dumping of waste materials that were observed in many localeties in Baqa'a area.

Keywords: Jordan, Baqa'a, soil, heavy metals, geoaccumulation, waste.

1. Introduction

Baqa'a is a residential area located in Ain Bal-Basha District, Balqa Governorate in northwest Jordan, which includes 16 districts area (Figure 1). This area is one of the hotspots affected by environmental pollution in Jordan. This due to many factors that are related to industrial, commercial, construction, agricultural activities and traffic load. This area included the largest refugee camps in Jordan with a high density of population. This in turn increases the pressure on infrastructure and soil uses in the region. In this context, the government is showing keen interest in the environment of the Baqa'a area to reduce pollution and thus the environmental risks that affect the population of the region through several practical and scientific measurement. The study area situated 640 m above sea level, on longitude 35° 48′ 30″ and 35° 53′ 00″ E and latitude 32° 03′ 00″ and 32° 03′ 00″ N. The study area embraces many types of small industries and farms producing various crops. The climate in the area is almost cold to moderate over a year (i.e. 7-33C°) with humidity of 50-70%, and average annual rainfall of 400 mm (Jordan Metrological Department, 2018). The area is located on a flat plain or as basin surrounding by high altitude area and it is considered as an aquifer for groundwater. Soil cover the topographical lows and pediment slopes, and together with calcrete obscures much of the bedrock. This study comes in the context of efforts to put the decision-maker in soil pollution by studying an assessment of the heavy metals in soil and their environmental impact. From geological point of view, the exposed rocks in the area are part of Jurassic- Cretaceous age. Structurally, the area covers the northeastern part of the Wadi Shu'ayb structure. Fluvial gravel, sand, silt and fine loess on hill slopes constitute Pleistocene sediments. Holocene to Recent alluvial and Wadi sediments consist of sorted clasts in a sand matrix and are being deposited and reworked by the present-day drainage. Soil cover the topographical lows and the pediment slopes and together with calcrete and carbonate obscures much of the bedrocks.

Heavy metals are extremely persistent in the environment and are non-biogradable and thus readily accumulate to toxic levels. When the toxic metals, trace elements and other organic substances are accumulated on the soil, the pollutants get deposited on the soil surface (Sharma and Raju, 2013). Determination of heavy metals in soil ecosystems has been noticed by many researchers, among them (Abrahim and Parker, 2008; Al Obaidy and Al Mashhadi, 2013; Asaah and Abimbola, 2006; Bambara et al., 2015; Stanley et al., 2014; Radojevic and Bashkin, 2006; Nada et al., 2019; Nowrouzi and Pourkhabbaz, 2014, Afrifa, et al., 2013). When the

* Corresponding author e-mail: khtarawneh62@yahoo.com

toxic metals, trace elements and other organic substances are accumulated on the soil, the pollutants get deposited on the soil surface (Sharma and Raju, 2013). Most of these pollutants can be carried by rain and wind from a pollution source to a great distance (Stanley et al., 2014).

This study is aimed to focus and to asset the heavy metals levels contamination in surfaces soil of Baqa'a area and to determine their concentration and interconnection released in urban areas. Physicochemical tests have been carried out to characterize the main properties of the soil based on granulometric analysis (particle-size distribution), moisture content, pH, electrical conductivity (EC), total dissolved solids (TDS), Inductively coupled plasma (ICP) and X-Ray diffraction (XRD). Soil contamination was assessed using three indices including an index of geoaccumulation (I_{geo}), contamination factor (CF) and degree of contamination (C_{deg}).

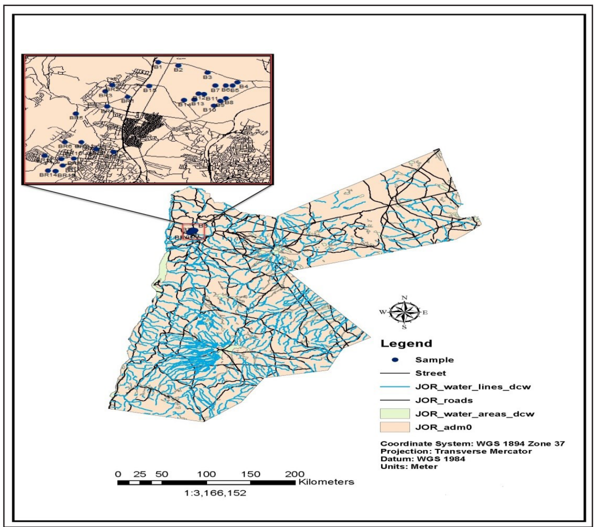

Figure 1. Location map of the study area.

2. Geology

The geology cropping out in the area is part of Jurassic - Cretaceous age (Sawariah and Barjous, 1993). The oldest exposed rocks in the area belong to the Azab Group (Jurassic) (Figure 2). The Azab group composed of mudstone, sandstone, dolomite and dolomitic limestone interbedded with silty dolomite and oolitic limestone. The lower cretaceous Kurnub Sandstone group (Aptian to early Cenomanian), rests unconformably on the Azab Group. Kurnub Sandstone overline by Ajlun Group, based marked by Na'ur Limestone Formation (Cenomanian) and consist of bituminous marly limestone, nodular in texture with fragments of gastropods and bivalves, intercalated with glauconitic marl. Na'ur Formation overlies by Fuhays Formation (Cenomanian) form gentle slopes. It consists of yellowish brown to olive-green marl intercalated with thin-bedded nodular limestone and marly limestone (Sawariah and Barjous, 1993).

The base of overlying Hummar Formation (Upper Cenomanian), is marked by a buff, massive marly limestone and micritic limestone, dolomitic limestone and dolomite intercalated with thin beds of marly limestone, marl and mudstone. The overlying Shu'ayb Formation (upper Cenomanian- Lower Turonian) consist of whitish-grey, thinly bedded chalky limestone and thinly bedded limestone, intercalated with buff-yellow marl. Massive to hard, buff dolomitic limestone marks the base of the overlying Wadi As Sir Limestone Formation (Turonian) (Sawariah and Barjous, 1993).

The overlying Wadi Umm Ghudran Formation (Coniacian-Santonian) is the basal unit of the overlying Belqa'a Group. The succeeding Amman Silicified Limestone Formation (Santonian-Campanian) is the youngest bedrock exposed in the study area. The formation composed of chert nodules, limestone, dolomitic limestone, marl, phosphatic chert, phosphate and apatite schist (Sawariah and Barjous, 1993).

Fluvial gravel, sand, silt and fine loess on hill slopes constitute Pleistocene Sediments, whereas thick soil up to 5 m in the Wadi and low topography of the Baqa'a basin. Holocene to Recent Alluvial and Wadi Sediments consist of sorted clasts in a sand matrix, clayey sand and clay are being deposited and reworked by the present-day drainage. Most of the soil can be considered as sandy loam to loamy sand.

Structurally, the area covers the northeastern part of the Wadi Shu'ayb structure. This structure is dominated by the northern extension of the NE-SW trending deformed belt (i.e. Wadi Shu'ayb structure), which consists of an echelon fold, monoclinal flexures and faults. The NNE-SSW trending Al Baqa'a asymmetrical anticline is 15 Km long and its width varies from 1 to 7 Km. This structure forms a negative geomorphological feature (i.e. depression) due to the high erodability of the Kurnub Group, which form the core, in contrast to the surrounding resistant Ajlun Group. The fault systems which are associated with the deformed belt are oriented NNE-SSE, SE-NW.

The topography reflects Neogene regional up-warping, folding and eastward beds tilting reflected on the terrain surface, accompanied by relative uplift in relation to block faulting west of Jordan Valley. The difference in the altitude is reflected in the westward direction of the river valleys. The drainage has rejuvenated during the tectonic phases, and a rapid incision into the main wadis has given rise to high relief with deep valleys and unstable slopes where mass movement takes place as landslides and debris flows (Sawariah and Barjous, 1993).

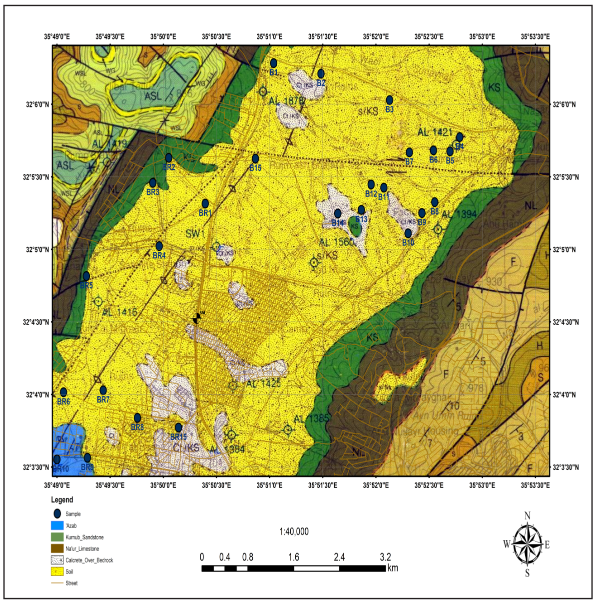

Figure 2. Geological map of the study area (modified after Sawariah and Barjous, 1993).

3. Materials and methods

3.1 The Soil Sampling

Thirty topsoil samples (0-20 depth cm) were collected from different localities of the study area with distance of samples from 0.500m up to 1 km and covered an area of about 20Km^2. ArcGIS " Geographic Information System" (version 10.2) was used to position the sampling sites with their attributes. For this purpose topographic map using coordinate system GCS WGS 1984 was prepared to locate the coordinates of the collected samples (Figure 3). The studied samples were selected during the winter season. The distance between samples differs and depend on the ease of access to the site and variability of the texture and the homogeneity of the soil. Three kilograms (3Kg) of each sample was collected with plastic tools and sorted into polyethylene bags. Standard methods were used for sample collection, preservation and analysis recorded by Ryan et al. (2001).

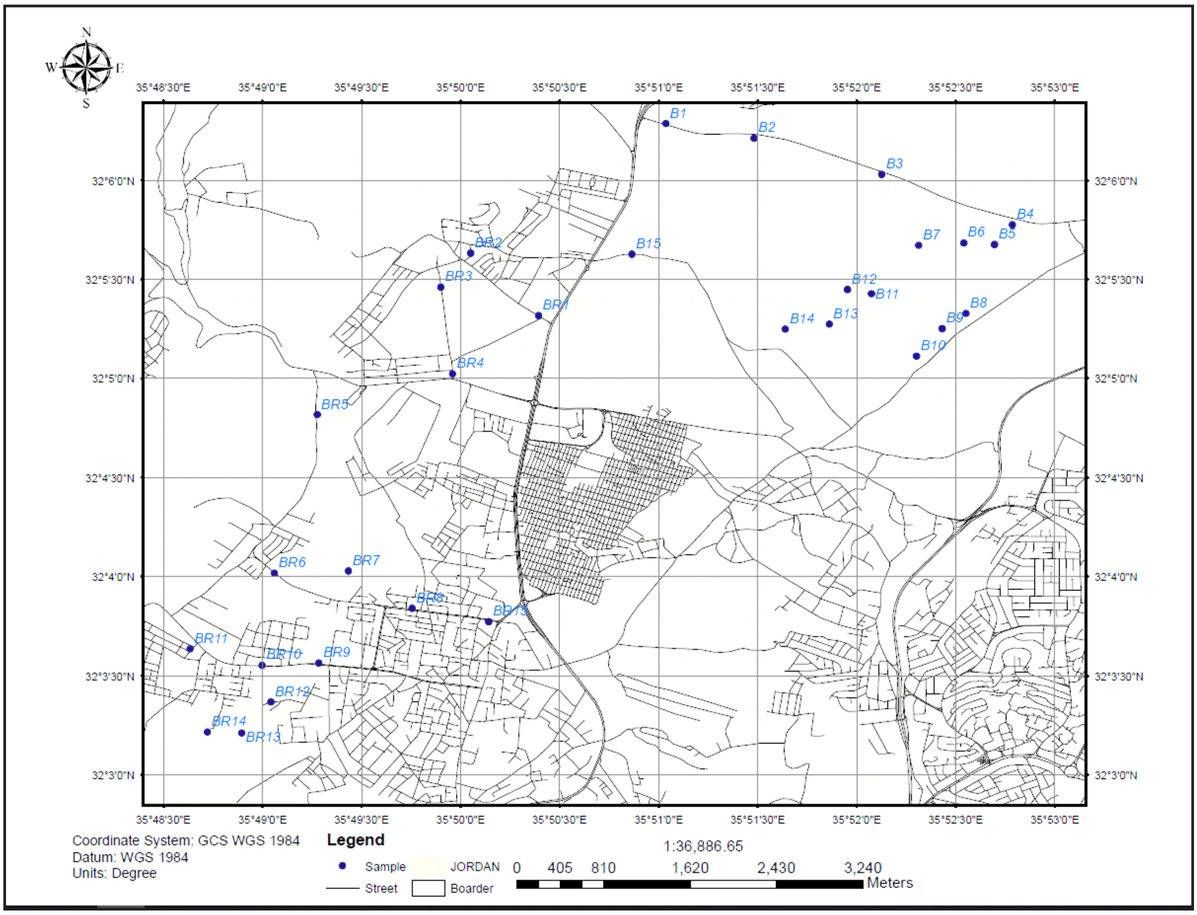

Figure 3. The map shows the sample location.

3.2 Granulometric Analysis

The studied samples were dried in the oven up to 100 C^o, then crushed and sieved through a 2 mm stainless sieve to remove debris. Sieve analysis has been carried out to determine the percentage of gravel, sand, and fine fraction using an ASTM sieve. About 100 g of soil sample was sieved at sieve No10, No 20 and No 200 prior to analysis. A hydrometer test was used to determine the percentage of silt and clay for representative samples (Table 1).

3.3 Physicochemical Methods

Soil texture and particle size distribution, moisture content, pH, EC and TDS were determined. Salinity is a measurement of all dissolved salts in water. It is usually measured indirectly and is derived from a conductivity reading using a conversion factor that would often be pre-programmed into the conductivity meter.

Salinity can affect the level of dissolved oxygen in the water. It is also called electrical conductivity (EC) which measures a substances ability to conduct an electrical current and this can be applied by using a conductivity meter. TDS, pH and EC parameters were determined by using the conductivity TDS meter (Model Hatch 44600). The procedure is done by mixing into a slurry with distilled or deionized water. Approximately 10 g of the air-dried sediments were suspended in 50 mL of deionized water and manually agitated for five minutes. The suspension was allowed to rest for about one hour with occasional shaking until pH, TDS and EC were determined (Table 1).

Inductively Coupled Plasma – Optical Emission Spectroscopy (ICP-OES) was used to determine the concentrations of heavy metals of Co, Cr, Cu, Mn, Ni, Pb, Zn, Cd and V. The samples were filtered by a membrane filter of a pore size of 0.45 µm before analyses using Standard Methods (APHA, 1995). Digestion solutions were measured for the total heavy metals using ICP-OES.

Selected samples were analyzed by XRD using 1 gram of a randomly oriented powder which put on a rotating sampler holder, and leveled with a glass slice to obtain a flat surface. XRD was also acquired using Zincite (ZnO) as internal standard.

Table 1. Grain size distribution and physical properties of the studied soil.

Site	Moisture	Sand	Silt	Clay	pH	TDS mg/l	EC 1500(µs/cm)
B1	17.6	83.07	15.50	1.43	8.54	106	275
B2	17.8	82.55	16.20	1.25	8.37	105	270
B3	17.2	82.95	15.70	1.35	7.70	103	265
B4	17.0	83.50	15.23	1.32	7.60	171	322
B5	16.5	80.30	18.40	1.30	8.22	140	205
B6	17.0	81.85	16.50	1.65	8.40	150	208
B7	17.3	82.74	15.70	1.56	8.40	155	206
B8	18.3	84.90	13.80	1.33	8.00	220	400
B9	17.5	83.95	14.50	1.55	8.65	200	399
B10	17.4	83.36	15.30	1.34	8.85	225	420
B11	17.3	83.99	14.78	1.23	8.90	226	427
B12	17.5	82.60	15.86	1.54	8.87	131	262
B13	16.9	87.20	11.50	1.31	8.37	230	460
B14	17.2	86.01	12.34	1.65	8.62	236	409
B15	17.6	85.13	13.53	1.34	8.62	110	144
BR1	16.8	86.13	12.33	1.54	7.40	220	480
BR2	16.7	83.22	15.34	1.44	8.35	225	481
BR3	16.7	84.70	13.45	1.85	8.39	75	150
BR4	16.5	83.96	14.70	1.34	8.26	76	151
BR5	16.2	83.01	15.65	1.34	8.56	78	144
BR6	16.5	85.24	13.33	1.43	8.39	77	156
BR7	16.9	82.32	15.80	1.88	8.26	80	154
BR8	16.3	81.32	17.34	1.34	8.34	86	150
BR9	17.0	82.67	16.90	1.33	8.39	88	148
BR10	17.3	83.36	14.77	1.87	8.59	89	188
BR11	16.6	85.11	13.44	1.45	8.32	86	210
BR12	16.3	86.33	12.34	1.33	7.59	78	189
BR13	16.9	87.01	11.54	1.45	8.35	88	166
BR14	16.8	87.11	11.56	1.33	7.57	89	123
BR15	16.9	87.20	11.58	1.37	8.60	90	156
Max	18.3	87.20	18.40	1.88	8.90	236	481
Min	16.2	81.32	11.50	1.23	7.40	75	123

3.4 Soil Contamination Assessment

The assessment of soil contamination was carried out. For this purpose, different indices have been applied to assess the heavy metal distribution and concentration. The indices of Geoaccumulation index (I_{geo}) and contamination factor (CF) were used to determine and define the contamination in sediments (Müller, 1969). A normalized indices approach for heavy element concentration is adopted in this study using World Uncontaminated Background Soil (Kabata-Pendias and Mukherjee, 2007), that compared to the average soil in the studied area as shown in Table 2.

3.4.1 Index of Geoaccumulation (Igeo)

The I_{geo} is calculated according to the method of Müller (1969) and Nowrouzi and Pourkhabbaz (2014). This index is calculated using the following mathematical relation:

$$I_{geo} = log2[\frac{Cn}{1.5Bn}] \quad \text{.......} (1)$$

Where C_n is the measurement of total concentration in soil metal n, and B_n is the background value for the metal n. Factor 1.5 is incorporated in relationship to accounting for possible variation in the background data due to lithologic effects.

Table 2. Salinity classes and relationship between $EC_{1:1}$ to ECe values.

	Degree of Salinity (Salinity Classes)					
	Non-Saline	Slightly Saline	Moderately Saline	Strongly Saline	Very Saline	Ration of EC1:1 to ECe
EC1:1 Method (Ds/m)						
Coarse to loamy sand	0-1.1	1.2-2.4	2.5-4.4	4.5-8.9	9.0+	0.56
Loamy fine sand to loam	0-1.2	1.3-2.4	2.5-4.7	4.8-9.4	9.5+	0.59
Silt loam to clay loam	0-1.3	1.4-2.5	2.6-5.0	5.1-10.0	10.1+	0.63
Silty clay loam to clay	0-1.4	1.5-2.8	2.9-5.7	5.8-11.4	11.5+	0.71
ECs Method (dS/m)						
All textures	0-2.0	2.1-4.0	4.1-8.0	8.1-16.0	16.1+	NA

3.4.2 Contamination Factor (CF) and Degree of Contamination (C_{deg})

Contamination factor was used to determine the contamination level of the sediments by applying the following equation:

$$CF = \frac{Cn}{Bn} \quad \text{.......} \quad (2)$$

Where Cn is the concentration of the heavy metal in the soil sample, and Bn is the background value for the same metal (Bambara et al., 2015 and Abrahim and Parker, 2008). The background concentration was calculated from the heavy metal concentration in unaffected soils (Kabata-Pendias and Mukherjee, 2007).

The degree of contamination (C_{deg}) was proposed by Hakanson (1980) as a generalized form and it can be calculated by the following equation:

$$C_{deg} = \Sigma\ (Cm/Bn)^{I} \quad \text{.......} \quad (3)$$

where i, represent the respective metals Co, Cr, Cu, Mn, Ni, Pb, Zn, Cd and V, while Cm is the measured metal concentration in the studied soil, and Bn is the background concentration value of metal concentration in unaffected soils (Kabata-Pendias and Mukherjee, 2007).

4. Results and discussion

4.1 Soil Physicochemical Properties

Soil texture and particle size distribution, moisture content, pH, EC and TDS were determined. The results are shown in Table 1. Particle-size distribution and soil texture classes showed that the soil is composed mainly of sand with silt and clay. The percentage of the sand varies between 81.32 and 87.20%, whereas the silt is between 11.50 and 18.40% and clay varies from 1.23 to 1.88%. Regarding these results, it can be noticed that most of the soil can be considered as sandy loam to loamy sand (Table 2).

Soil water affects the moisture content of the nature and amount of soluble materials, osmotic pressure and the pH of the soil solution (Paul, 2007). The current study showed a moisture content ranges from 16.2 to 18.3%. Insignificant differences with less than 1% were observed among the most studied sites (Table 1). It can be argued that lower pH corresponds with higher [H^+], while higher pH is associated with lower [H^+].

Measurement of pH of soil samples shows that some of them have pH higher than 8, while good soil ranges between 5.5-7. Results show that the soil pH varies from 7.40 to 8.90 (Table 1), with small significant differences ≤ of 0.6, that were observed among the studied sites. These results show that the studied soils are mostly in neutral to sub-alkaline conditions.

Results of the EC and TDS are related together and they increased. EC varies between 123 and 481(µs/cm), whereas the TDS varies between 75 and 235mg/l. EC and TDS measurements can vary greatly and are affected by several environmental factors including, climate, local biota (i.e. plants and animals), rock lithology and surficial geology, as well as human impacts on land. EC and TDS also are related to pH and their norms are within the type of most slightly to moderately saline for some samples as indicated in Table 2.

4.2 XRD Results

The soil samples were performed by using XRD. The results show that the major existing minerals quartz, while calcite, dolomite and kaolin are minor minerals (Figures 4, 5). These minerals are mainly related to the anthropologic processes and are part of the composition of the geological units surrounded the study area. The quartz is the dominant mineral in all tested samples and reached up to 95.53% by weight as indicated by granulometric analysis. Calcite and dolomite are present and most of these minerals considered as a main component of the limestone and dolomitic limestone rocks surrounding the area. Their presence could be explained also as a result of small leaching processes (Nada et al., 2019). Clay minerals also occur as minor minerals and could be explained by the chemical weathering of primary minerals as feldspar.

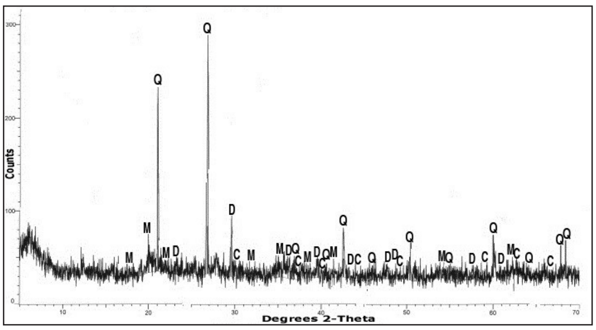

Figure 4. XRD of bulk sample from the study area (Q=Quartz; C=Calcite; D=Dolomite M=Montmorillonite).

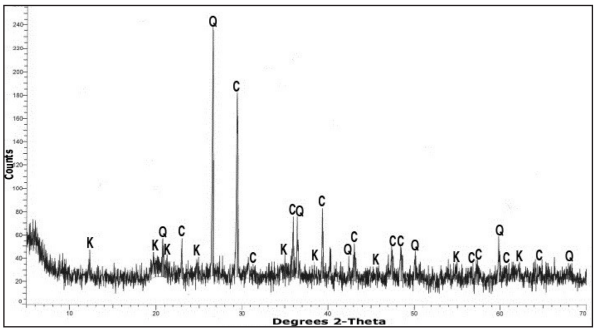

Figure 5. XRD of bulk sample from the study area (Q=Quartz; C=Calcite; D=Dolomite M=Montmorillonite).

4.3 Soil Metal Contamination

A normalized norm for heavy metals concentration, adopted in this study is based on the world uncontaminated soils used by Kabata-Pendias and Mukherjee (2007). The results and the norms of heavy metals are shown in Table 3. Nine heavy metals (Co, Cr, Cu, Mn, Ni, Pb, Zn, Cd and V) were determined in thirteen sites. As shown from the results, the average concentration of these metals is in the following sequence in (ppm): Co (15); Cr (182); Cu (27); Mn (737); Ni (90); Pb (10); Zn (87), Cd (0.10); and V (92). This allows for the arrangement of the heavy metals from the higher to lower mean content as follows: Mn > Cr >V >Ni >Zn > Cu > Co > Pb > Cd. The results show that the concentration of Cr, Co, Mn, Ni and Zn are higher in many samples, whereas the concentration of Cu, Pb, V and Cd are less than the norms. Small exceptions from the norms can be seen for some samples as in sample B1 for the heavy elements of Zn and Mn; sample BR4 and B11 for Co, Mn and Pb; BR13 and BR15 for Co, and BR11 with a high concentration of V. The soil is contaminated with Co, Cr, Mn, Ni and Zn that exceeding the standard levels in most of the sites, exception of this rule can be seen in some sites as indicated in B1, B3, B4, BR11, BR15. Sites B10, B12, B13 and B14 are contaminated with Mn that exceed 1000ppm. Site B14 represent the most contaminatedplace with Co, Cr, Mn, Ni, Zn and V. The values of these heavy metals in this site are twice the values of adopted norms. Most samples did not exceed the values approved in this study regarding the adopted norms. It can be argued that a high concentration of Co, Cr, Mn, Ni, Zn and V in some sites as indicated in sites B10, B12, B13 and B14 could be related to natural processes that include rock weathering and erosion, leaching and wind-blown dust. On the other hand, anthropogenic activities, including industrial, agricultural activity and motor vehicle traffic, are considered as one of the main sources of contamination that could be affected in some sites as seen clearly in site B14, and partially in other sites (B1, B3, B4, B10, BR 11, B12, B13, BR 15), that exceeds the adopted norms.

4.3.1 Index of Geoaccumulation (I_{geo})

The index of geoaccumulation (I_{geo}) for contamination levels in the soil have been taken after Rahman et al. (2012) and Odat (2015). It consists of seven grades from 0 to 6, ranging from uncontaminated to extremely contaminated (Table 4). The factor 1.5 incorporated in the relationship to account for possible variation in background data due to lithological effects. The calculated I_{geo} values are shown in Table 5. Compared to the average soil, the I_{geo} values indicated that the results reported uncontaminated soil (I_{geo} ≤ 0 for Cu, Pb, V and Cd), uncontaminated to moderately contaminated soil (0 <Igeo<1 for Co and Mn, Zn, Ni). It can be noticed that there is an exception in some sites in I_{geo} values as for Zn, Pb, and Ni. At the site, BR9 Ni value (I_{geo}=2.95), that can be considered moderately/strongly contaminated; I_{geo} value for Cr inmost of the samples are uncontaminated to moderately contaminated and highly contaminated (2 <Igeo<3), as seen in BR9 (Cr I_{geo}=2.98).Contaminated/ moderately contaminated/highly contaminated in some sites, as reported in site BR9, that could be attributed to high traffic and industrial activities, in addition to anthropogenic effects such as excavated construction materials and randomly dumping of the wastes nearby the site.

Table 3. Results of the ICP and the norms of the average world soil.

No	sites	Co	Cr	Cu	Mn	Ni	Pb	Zn	Cd	V
1	B-1	11	139	21	486	65	6	57	0.1	79
2	B-2	16	146	26	688	82	8	78	0.1	94
3	B-3	13	133	24	547	63	6	66	0.1	79
4	B-4	13	141	25	577	66	6	67	0.1	74
5	B-5	17	151	25	686	73	8	74	0.1	84
6	B-6	17	166	32	699	83	8	89	0.1	87
7	B-7	15	170	26	652	82	8	73	0.1	84
8	B-8	15	162	25	655	78	9	72	0.1	83
9	B-9	16	173	26	680	83	10	77	0.1	88
10	B-10	17	142	30	760	76	10	105	0.1	92
11	B-11	18	156	34	789	90	11	103	0.1	96
12	B-12	15	152	32	680	87	8	111	0.1	99
13	B-13	20	150	32	777	89	10	89	0.1	105
14	B-14	17	185	34	694	106	12	103	0.1	97
15	B-15	15	166	28	565	81	7	75	0.1	87
16	BR-1	17	157	32	745	76	10	92	0.1	98
17	BR-2	17	195	32	709	111	8	103	0.1	102
18	BR-3	17	160	34	747	79	9	107	0.1	97
19	BR-4	10	337	23	342	161	7	79	0.1	50
20	BR-5	13	145	26	580	65	13	85	0.1	78
21	BR-6	18	154	26	718	80	11	80	0.1	98
22	BR-7	18	152	35	788	84	13	106	0.1	98
23	BR-8	23	166	24	815	70	12	80	0.1	83
24	BR-9	15	703	34	524	336	11	88	0.1	79
25	BR-10	15	151	29	1000	78	47	104	0.1	75
26	BR-11	8	168	21	921	83	4	72	0	112
27	BR-12	12	166	20	1201	83	6	73	0.1	120
28	BR-13	9	180	23	1288	77	6	80	0.1	108
29	BR-14	20	117	20	1283	52	1	125	0.1	158
30	BR-15	5	166	22	807	69	8	97	0.1	86
Average		15	182	27	737	90	10	87	0.10	92
Min		5	117	20	342	52	1	57	0.0	50
Max		20	703	35	1288	336	47	125	0.10	158
Range		5-20	117-703	20-35	342-1288	52-336	1-47	57-125	0-0.10	50-158
Norms		11.3	59.5	38.9	488	29	27	70	0.41	129

Table 4. I_{geo} accumulation index values (Rahman et al., 2012).

I_{geo} Class	I_{geo} value	Contaminated level
0	Igeo≤0	uncontaminated
1	0 <1geo<1	Uncontaminated/moderately contaminated
2	1 <1geo<2	moderately contaminated
3	2 <1geo<3	Moderately/strongly contaminated
4	3<1geo<4	Strongly contaminated
5	4 <1geo<5	Strongly /extremely contaminated
6	5<1geo<6	extremely contaminated

Table 5. I_{geo} accumulation index value of the heavy metals in the study area.

	Co	Cr	Cu	Mn	Ni	Pb	Zn	V	Cd
B-1	-0.38	0.64	-1.47	-0.59	0.58	2.75	-0.47	-1.29	-2.62
B-2	-0.08	0.71	-1.17	-0.09	0.91	2.34	-0.02	-1.04	-2.62
B-3	-0.38	0.58	-1.28	-0.42	0.53	2.75	-0.26	-1.29	-2.62
B-4	-0.38	0.66	-1.22	-0.34	0.60	2.75	-0.24	-1.39	-2.62
B-5	0.00	0.76	-1.22	-0.09	0.75	2.34	-0.10	-1.20	-2.62
B-6	0.00	0.90	-0.87	-0.07	0.93	2.34	0.17	-1.15	-2.62
B-7	-0.18	0.93	-1.17	-0.17	0.91	2.34	-0.11	-1.20	-2.62
B-8	-0.18	0.86	-1.22	-0.16	0.84	2.17	-0.13	-1.22	-2.62
B-9	-0.08	0.95	-1.17	-0.11	0.93	2.02	-0.04	-1.14	-2.62
B-10	0.00	0.67	-0.96	0.05	0.80	2.02	0.41	-1.07	-2.62
B-11	0.09	0.81	-0.78	0.11	1.05	1.88	0.38	-1.01	-2.62
B-12	-0.18	0.77	-0.87	-0.11	1.00	2.34	0.49	-0.97	-2.62
B-13	0.24	0.75	-0.91	0.09	1.03	2.02	0.17	-0.88	-2.62
B-14	0.00	1.05	-0.78	-0.08	1.28	1.75	0.38	-1.00	-2.62
B-15	-0.18	0.90	-1.06	-0.37	0.90	2.53	-0.08	-1.15	-2.62
BR-1	0.00	0.81	-0.87	0.04	0.80	2.02	0.22	-0.98	-2.62
BR-2	0.00	1.13	-0.87	-0.05	1.35	2.34	0.38	-0.92	-2.62
BR-3	0.00	0.84	-0.78	0.03	0.86	2.17	0.44	-1.00	-2.62
BR-4	-0.76	1.92	-1.34	-1.10	1.89	2.53	0.17	-1.95	-2.62
BR-5	-0.38	0.70	-1.17	-0.34	0.58	1.64	0.10	-1.31	-2.62
BR-6	0.09	0.79	-1.17	-0.03	0.88	1.88	0.02	-0.98	-2.62
BR-7	0.09	0.77	-0.74	0.11	0.95	1.64	0.42	-0.98	-2.62
BR-8	-0.38	0.90	-1.28	-0.50	0.69	1.75	0.02	-1.22	-2.62
BR-9	-0.18	2.98	-0.78	-0.51	2.95	1.88	0.15	-1.29	-2.62
BR-10	-0.18	0.76	-1.01	0.45	0.84	0.21	0.40	-1.37	-2.62
BR-11	-1.08	0.91	-1.47	0.33	0.93	3.34	-0.13	-0.79	-2.62
BR-12	-0.50	0.90	-1.54	0.71	0.93	2.75	-0.11	-0.69	-2.62
BR-13	-0.91	1.01	-1.34	0.82	0.82	2.75	0.02	-0.84	-2.62
BR-14	0.24	0.39	-1.54	0.81	0.26	5.34	0.66	-0.30	-2.62
BR-15	-1.76	0.90	-1.41	0.14	0.67	2.34	0.30	-1.17	-2.62

4.3.2 Contamination Factor (CF)

The contamination factor (CF) is used to determine the contamination grade of heavy metals in the studied soil. Soil contamination categories based on CF proposed in this study was taken from Afrifa et al. (2003) and Hakanson (1980), as shown in Table 6. The calculated contamination factor values are shown in Table 7.

Table 6. Contamination categories based on contamination factor (CF).

CF value	Contamination Level
CF < 1	Low contamination
1<CF< 3	Moderate contamination
3<CF< 6	Considerable contamination
CF>6	Very high contamination

The results of the CF index of heavy metals of the studied samples indicated low contamination to considerable contamination. The maximum CF was found in site BR9 with high values (CF=11.82) for Cr and CF=11.59 for Ni, whereas values of CF for Cr in the rest of the samples are from moderate to considerable contamination as indicated in sites BR4 (CF=5.66) for Cr, and CF=5.55 for Ni. The values of CF for the heavy elements in the rest of the studied samples can be considered as moderate contamination levels.

4.3.3 Contamination degree (C_{deg})

To facilitate pollution control, Hakanson (1980) proposed a diagnostic tool named 'degree of contamination' (C_{deg}) as shown in Table 7. It is aimed at providing a measure of the degree of overall contamination in surface layers in a particular core or sampling sites. It can be concluded that the value of C_{deg} for most heavy metals in the studied samples indicated moderate to a considerable degree of contamination (Table 8). Exception of this conclusion can be noticed for some sites as indicated in Site BR9 that shows a high degree of contamination C_{deg}= 29.18. This site indicated highly contaminated as approved by CF and I_{geo} values and this could be due to to anthropogenic effects such as dumping of the wastes.

Table 7. Soil contamination categories based on contamination factor (CF).

C_{deg} value	Contamination level
C_d<6	Low degree of contamination
6<C_d<12	Moderate degree of contamination
12<C_d<24	Considerable degree of contamination
C_d> 24	High degree of contamination

Table 8. Contamination factor (CF) and Degree of contamination (Cdeg) of heavy metals in the study area.

	Co	Cr	Cu	Mn	Ni	Pb	Zn	V	Cd	Cdeg	Result
B-1	1.15	2.34	0.54	1.00	2.24	0.22	0.81	0.61	0.24	9.16	M
B-2	1.42	2.45	0.67	1.41	2.83	0.30	1.11	0.73	0.24	11.16	M
B-3	1.15	2.24	0.62	1.12	2.17	0.22	0.94	0.61	0.24	9.32	M
B-4	1.15	2.37	0.64	1.18	2.28	0.22	0.96	0.57	0.24	9.62	M
B-5	1.50	2.54	0.64	1.41	2.52	0.30	1.06	0.65	0.24	10.86	M
B-6	1.50	2.79	0.82	1.43	2.86	0.30	1.27	0.67	0.24	11.90	M
B-7	1.33	2.86	0.67	1.34	2.83	0.30	1.04	0.65	0.24	11.25	M
B-8	1.33	2.72	0.64	1.34	2.69	0.33	1.03	0.64	0.24	10.97	M
B-9	1.42	2.91	0.67	1.39	2.86	0.37	1.10	0.68	0.24	11.64	M
B-10	1.50	2.39	0.77	1.56	2.62	0.37	1.50	0.71	0.24	11.67	M
B-11	1.59	2.62	0.87	1.62	3.10	0.41	1.47	0.74	0.24	12.68	CM
B-12	1.33	2.55	0.82	1.39	3.00	0.30	1.59	0.77	0.24	11.99	M
B-13	1.77	2.52	0.80	1.59	3.07	0.37	1.27	0.81	0.24	12.45	CM
B-14	1.50	3.11	0.87	1.42	3.66	0.44	1.47	0.75	0.24	13.48	MC
B-15	1.33	2.79	0.72	1.16	2.79	0.26	1.07	0.67	0.24	11.04	M
BR-1	1.50	2.64	0.82	1.55	2.62	0.37	1.31	0.76	0.24	11.82	M
BR-2	1.50	3.28	0.82	1.45	3.83	0.30	1.47	0.79	0.24	13.69	MC
BR-3	1.50	2.69	0.87	1.53	2.72	0.33	1.53	0.75	0.24	12.18	CM
BR-4	0.88	5.66	0.59	0.70	5.55	0.26	1.27	0.39	0.24	15.55	CM
BR-5	1.15	2.44	0.67	1.19	2.24	0.48	1.21	0.60	0.24	10.23	M
BR-6	1.59	2.59	0.67	1.47	2.76	0.41	1.14	0.76	0.24	11.63	M
BR-7	1.59	2.55	0.90	1.61	2.90	0.48	1.51	0.76	0.24	12.56	C
BR-8	1.15	2.79	0.62	1.06	2.41	0.44	1.14	0.64	0.24	10.51	M
BR-9	1.33	11.82	0.87	1.05	11.59	0.41	1.26	0.61	0.24	29.18	C
BR-10	1.33	2.54	0.75	2.05	2.69	1.74	1.49	0.58	0.24	13.40	CM
BR-11	0.71	2.82	0.54	1.89	2.86	0.15	1.03	0.87	0.24	11.11	M
BR-12	1.06	2.79	0.51	2.46	2.86	0.22	1.04	0.93	0.24	12.13	CM
BR-13	0.80	3.03	0.59	2.64	2.66	0.22	1.14	0.84	0.24	12.15	CM
BR-14	1.77	1.97	0.51	2.63	1.79	0.04	1.79	1.22	0.24	11.96	M
BR-15	0.44	2.79	0.57	1.65	2.38	0.30	1.39	0.67	0.24	10.42	M

M: Moderate; CM: Considerable Moderate; C: Considerable; MC: Moderate Considerable

5. Conclusions

The study area is one of the hotspots affected by environmental pollution in Jordan. This is due to many factors that are related to industrial, commercial, agricultural activities and traffic load. The study objective was to determine the level of contamination of heavy metals in the soil and to indicate their potential sources of origin. The area is located on a flat plain represented by a depression surrounding by elevated areas and it is considered as an aquifer for groundwater. Samples were analyzed using granulometric analysis, pH, electrical conductivity (EC), Total dissolved solid (TDS), Inductive coupled plasma (ICP) and X-ray diffraction (XRD). Soil contamination was assessed using three indices including the index of geoaccumulation (I_{geo}), a contamination factor (CF) and degree of contamination (C_{deg}).

The geology of the study affected by the high deformation of the rocks and the processes of weathering, erosion and leaching that had a very strong effect on soil deposition. Soil cover topographical lows and the pediment slopes, together with calcrete obscures much of the bedrock. Particle-size distribution and soil texture classes showed that the soil composed mainly of sand with silt and clay. The studied soil can be considered as sandy loam to loamy sand. The characteristics of quality sediment show that the soil has a pH ranging from 7.80 and 8.90, which slightly neutral to subalkaline. EC ranged from 123 to 481 (µs/cm), while TDS vary from 75 to 235 mg/l. EC and TDS are affected by different environmental factors that are related to climate, bedrock and surficial geology, as well as human activities.

Quartz is the dominant mineral identified by XRD, while calcite, dolomite and kaolinite are secondary minerals. The presence of these minerals are related to the anthropologic processes and are part of the composition of the geological units in the area.

Results of heavy metals indicated by ICP show the following concentration in (ppm): Co (15); Cr (182); Cu (27); Mn (737); Ni (90); Pb (10); Zn (87), Cd (0.10); and V (92). This allows an arrangement of the metals in the following sequence: Mn > Cr > V >Ni > Zn > Cu > Co > Pb > Cd. The concentration of Cr, Co, Mn, Ni and Zn are higher in most samples, whereas the concentration of Cu, Pb, V and Cd are less than the norms of average.

The I_{geo} values indicated that the results reported uncontaminated soil ($I_{geo} \leq 0$ for Cu, Pb, V and Cd), uncontaminated to moderately contaminated soil (0<1geo<1) for Co and Mn, Zn, Ni. It can be noticed that there is an exception in some sites for I_{geo} values for Zn, Pb, and Ni.

CF index of heavy metals indicating low contamination to considerable contamination. This can be seen in site BR9 with high values (CF=11.82) for Cr and Ni (CF=11.59), while CF in some sites as BR4 (CF=5.66) for Cr and (CF=5.55) for Ni. It can be noticed that CF values in the rest of the studied samples can be considered at moderate contamination levels.

It can be concluded that the value of C_{deg} for most of the heavy metals in the studied samples indicated a moderate to a considerable degree of contamination. Exception of this conclusion can be noticed for some sites as indicated in Site BR9, which shows a high degree of contamination (C_{deg}= 29.18). This site indicated also highly contaminated as approved by CF and I_{geo} values. This conclusion could be due to anthropogenic effects such as dumping of the wastes in this area and industrial activities that increased the level of contamination.

Acknowledgement

This research has been granted from Amman Arab University. We would like to thank the University for supporting me to follow up on this research. Thanks to Eng. Khloud Hadad from the Ministry of Energy and Mineral Resources, for her help in analyzing the samples. Thanks also are extending to Prof. Hani Alnawafleh, Al Hussein Bin Talal University, Jordan for his help in the interpretation of the XRD results. Thanks also extend to the two reviewers for their critical comments.

References

Afrifa, C., Ofosu, F., Bamford, S., Wordson, D., Atiemo, S., Aboh, I., Adeti, J. (2013). Heavy metal contamination in surface soil dust at selected fuel filling stations in Accra, Ghana. American Journal of Scientific and Industrial Research 4(4): 404-413.

Al Obaidy, A., and Al Mashhadi, A. (2013). Heavy metal contaminations in urban soil within Baghdad City, Iraq. Journal of Environmental Protection 4: 72-82.

APHA (1995). American Public Health Association (APHA). Standard methods for the examination of water and wastewater. Washington, D.C. USA, 19th ed.

Asaah, A., and Abimbola, A. (2006). Heavy metal concentrations and distribution in surface soils of the Bassa Industrial Zone 1, Doula, Cameroon. The Journal for Science and Engineering 31(2A): 147-158.

Abrahim, G., and Parker, R. (2008). Assessment of heavy metal enrichment factors and the degree of contamination in marine sediments from Tamaki Estuary, Auckland, New Zealand. Journal of Environmenntal Monitoring Assessment 136: 227-238.

Bambara, L.T., Kabore, K., Zoungrana, M., Zougmore, F., Cisse, O., Bentil, N. (2015). Assessment of heavy metals contamination in agricultural soil of Loumbila and Paspanga, Burkina Faso. International Journal Advanced Research in Science, Engineering and Technology 2(1): 380-386.

Hakanson, L. (1980). Ecological risk index for aquatic pollution control. A sedimentlogical approach. Water Resources 14(5): 975-1001.

Jordan Meteorological Department (2018). Annual report.

Kabata-Pendias, A., and Mukherjee, A. B. (2007). Trace Elements from Soil to Human. Springer-Verlag Berlin Heidelberg.

Müller, G. (1969). Index of geoaccumulation in sediments of the Rhine River. Geological Journal 2: 108-118.

Nada, N., Chaden, H., Wala, D., Tarawneh, K., Frederic, V. (2019). Assessment of Heavey Metal Pollution in sediments of the Lower Litani River Basin, Lebanon. Jordan Journal of Earth and Environmental Sciences 10(2): 104-112.

Nowrouzi, M., and Pourkhabbaz, A. (2014). Application of geoaccumulation index and enrichment factor for assessing metal contamination in the sediments of Hara Biosphere Reserve, Iran. Chemical Speciation and Bioavailability 26(2) : 99-105.

Odat, S. (2015). Application of geoaccumulation index and enrichment factors on the assessment of heavy metal pollution along Irbid/Zarqa Highway-Jordan. Journal of Applied Sciences 15(11): 1318-1321.

Paul, E.A. (2007). Soil Microbiology, Ecology, and Biochemistry, Third edition, Elsevier Inc., UK.

Radojevic, M., and Bashkin, V. (2006). Practical Environmental Analysis, Second Edition, RSC Publishing.

Rahman, S., Khanam, D., Adyel, T., Islam, M., Mohammad, A., Akbor, M. (2012). Assessment of heavy metal contamination of agricultural soil around Dhaka Export Processing Zone (DEPZ), Bangladesh: Implication of seasonal processing zone, Bangladesh. Journal of Applied Sciences 2(3): 584-601.

Ryan, J., Estefan, G., Rashid, A. (2001). Soil and Plant Analysis Laboratory Manual, Second Edition, International Center for Agricultural Research in the Dry Areas (ICARDA), Aleppo, Syria.

Sawariah, A., and Barjous, M. (1993). Geological map of the Suwaylih area 3154 II, scale 1:50.000. Geological Mapping Division, Geology Directorate, Natural Resources Authority, Amman, Jordan.

Sharma, M., and Raju, N. (2013). Correlation of Heavy Metal contamination with Soil properties of Industrial areas of Mysore, Karnataka, India by Cluster analysis. International Research Journal of Environment Sciences 2(10): 22-27.

Stanley, H., Odu, N., Immanuel, O. (2014). Impact of cement dust pollution on physicochemical and microbiological properties of soil around Lafarge cement Wapco, Ewekoro, southwestern Nigeria. International Journal of Advanced Biological Research 4(4) 2014: 400-404.

JJEES

JJEES (2021) 12 (4): 295-305
ISSN 1995-6681

Jordan Journal of Earth and Environmental Sciences

Comparison between Weighted Arithmetic and Canadian Council of Ministers of the Environment Water Quality Indices performance in Amman-Zarqa Area, Jordan

Tasneem Hyarat and Mustafa Al Kuisi*

Department of Geology, School of Science, The University of Jordan, Jordan.

Received 3 March 2021; Accepted 25 March 2021

Abstract

Water Quality Indices (WQI's) are efficient and simplified tools to evaluate the situations of water quality based on the biological, physical, and chemical parameters. National and international institutions and agencies determined the limits of these parameters on a scientific basis. It converts the water quality into a single and simple value, simple enough for the laypeople to understand.

The present study compares the results of the CCME-WQI method with the WA-WQI method for drinking purposes. Fifty-nine groundwater wells were chosen from the Amman Zarqa Area for this purpose. Elevenparameters of water analysis during the period July to November 2020were obtained to determine water quality indices. These parameters are; EC, pH, Ca^{2+}, Na^+, Mg^{2+}, K^+, NO_3^-, HCO_3^-, $SO_4^{2-}$and Cl^-. The results of applying CCME-WQI and WA-WQI for assessing the water suitability in the study area showed that; CCME-WQI classified water samples as "26% Excellent", "49% Good", "8% Fair", "12% Marginal", and "5% Poor" while the WA-WQI classified it as "8% Excellent", "45% Good", "31% Poor", "14% very poor", "2% unsuitable for drinking purpose".By comparing the results of both methods the CCME-WQI with WA-WQI, the results show that the CCME-WQI is more flexible and yielded a higher value of water quality than WA-WQI. Also, the statistical test calculated for both indices showed a strong indication that the differences between the CCME-WQI and the WA-WQI mean values are statistically significant at a significance of (a = 0.05).

Keywords: Water Quality Index, Canadian Water Quality Index, Weighted Arithmetic Index, Amman Zarqa Basin.

1. Introduction

Water is an essential component of the ecosystem and is often found in the form of streams, springs, rivers, lakes, glaciers, rainfall, and groundwater. Over the years, many sources of surface and groundwater have been depleted and large parts of them have been subjected to pollution due to many reasons such as urbanization, growth of population, and industrial development, which contributed to changes in water quality (Imneisi and Aydin, 2016). Nowadays one of the most important issues throughout the world is water quality management and environmental protection. Many countries focused on assessing and monitoring the water situation depending on their physicochemical and biological characteristic for different uses.

Water Quality Index (WQI) concept had recently been innovated to become the most effective tool for evaluating water quality. Based on water characteristics (physical, chemical, and microbiological), the quality of water characterized. Over the years, several national and international organizations applied the water quality index for water quality assessment. Initially, Horton (1965) proposed the first index in the United States in an endeavor to describe the water quality by choosing the most water quality parameters used such as (pH, dissolved oxygen, specific conductance, coliforms, alkalinity and chloride, etc.) and calculated the WQI by using the arithmetic weighted mean technique (Horton, 1965). Brown et al. (1972) modified the Horton index, which is supported by the National Sanitation Foundation.WQI model proposed by Bhargava (1983), to assess the Ganga River in India based on the sensitivity function technique. Canadian Council of Ministers of the Environment (CCME) computed a Canadian WQI using the summation squares of harmonic numbers (CCME, 2001). Over the years, several water quality indices were formulated and used by organizations and researchers such as: a) Index of River Water Quality, b) The Scatter Score Index, c) Chemical Water Quality Index, d) Overall Index of Pollution, e) Universal Water Quality Index-UWQI, f) Iowa Water Quality Index, g) Oregon Water Quality Index, h) Weighted Arithmetic Water Quality Index (Oni and Fasakin, 2016).

Many international and local institutions and agencies sought to transform the huge water quality data into a simple formula or a simple number, simple enough for the laypeople to understand, and studied the water and analyzed all its physical, chemical, and biological elements and their effects to find out the suitability of water for human use and to define permissible standards for each element in drinking water. Among these Institutions are World Health

* Corresponding author e-mail: mkuisi@ju.edu.jo

Organization (WHO) and Centers for Disease Control (CDC), and Environmental Protection Agency (EPA) (Madalina and Gabriela, 2014).In Jordan, the Jordan Institute for Standards and Metrology has developed permissible standards for drinking water in Jordan (JISM, 2015).

On the other hand, many indices have been commonly used over the last decades, among these are, the Canadian Council of Ministers of the Environment (CCME-WQI), Oregon Water Quality Index (O-WQI), Weighted Arithmetic (WA-WQI), and National Sanitation Foundation (NSF-WQI) are the commonly used (Paun et al., 2016).

The interpretation of the obtained data from monitoring and water quality management improved the accuracy of the applied indices. For this purpose, many statistical methods were utilized such as principal components analysis (PCA), cluster analysis (CA), factor analysis (FA) discriminant analysis (DA), and artificial intelligence (AI) (Bilgin, 2018).

The main objectives of this study are: (1) to assess the water quality of the Amman Zarqa area using two methods of water quality indices (WA-WQI and CCME-WQI), and (2) to compare the results of both indices (WA-WQI and CCME-WQI) by emphasizing the merits and demerits of the two methods and figure out which method is more reliable and concise.

2. Material and Methods

2.1. Canadian Council of Ministers of the Environment (CCME-WQI)

In 1997, the Canadian Council of Ministers of the Environment established the CCME-WQI based on the British Colombia WQI (CCME, 2001). This index is used by many countries to assess water quality with a little modification for their ease to calculate and flexibility to choose the parameters that contribute to the calculation of the index.

In 1997, the Canadian Council of Ministers of the Environment established the CCME-WQI based on the British Colombia WQI (CCME, 2001). This index is used by many countries to assess water quality with a little modification for their ease to calculate and flexibility to choose the parameters that contribute to the calculation of the index.

CCME-WQI consists of three significant factors (Scope, F1; Frequency, F2; and amplitude, F3), denominated to calculate the final CCME Index as a dimensionless single number that describes the water quality condition from 0(poor quality) to 100(High quality) (CCME, 2003; Sutadian et al., 2016; Lopes et al., 2020).

In brief, the above factors are calculated as follows:

$$F_1 = \left(\frac{No.of\ failed\ variables}{Total\ no.of\ variables}\right)*100$$

Where, Scope factor F1= Number of variables, whose objectives are not met.

$$F_2 = \left(\frac{No.of\ failed\ tests}{Total\ no.of\ tests}\right)*100$$

Frequency factor F2 = number of times by which the objectives are not met. Amplitude factorF3= Amount by which the objectives are not met, which is calculated in three steps:

(a) Excursion = $\left(\frac{Failed\ test\ value}{Objective}\right) - 1$

(b) The normalized sum of excursions (nse) $= \frac{\Sigma\ excursions}{No.\ of\ tests}$

(c) F3 $= \frac{nse}{0.01nse + 0.01}$

Finally, calculation the CCME -WQI;

$$WQI = 100 - \frac{\sqrt{F1^2 + F2^2 + F3^2}}{1.732}$$

According to the final index score (0 to 100), The higher score the better the water quality, WQIiscategorized into the following five classes: “Poor;0–44”, “Marginal;45–64”, “Fair;65–79”, “Good;80–94”, “Excellent;95–100” (Table 1, CCME, 2003).

2.2. Weighted Arithmetic Water Quality Index (WA-WQI)

The Weighted Arithmetic WQIis considered one of the widely used method to classify water for drinking purposes. WA-WQI is easy and simple to use; it relies on weighing the water parameters, each according to their importance, let the user choose the water quality parameters incorporated in the process (Iticescu et al., 2019).

WA-WQI is calculated by using the following equation (Zotou et al., 2019):

$$WQI = \frac{\sum Q_i W_i}{\sum W_i}$$

The quality rating scale (Qi) for each parameter is calculated using this expression:

$$Qi = 100*\left[\frac{V_i - V_o}{S_i - V_o}\right]$$

Where, $V_i$is the estimated concentration of the i^{th} parameter in the analyzed water

V_o is the ideal value of this parameter in pure water Vo = 0 (except pH =7.0 and DO = 14.6 mg/L)

Si is the recommended standard value of the i^{th} parameter

The unit weight W_i for each water quality parameter is calculated by using the following formula:

$$W_i = \frac{K}{S_i}$$

Where, K = proportionality constant and can be calculated by using the following equation:

$$K = \frac{1}{\Sigma\left(\frac{1}{S_i}\right)}$$

The final rating of WA-WQI is an ascending scale that ranges from 0 to 100 (higher scores indicate higher pollution). The quality of the water body is categorized also into five classes: “Excellent,” “Good,” “Poor,” “Very poor and Unsuitable” for drinking purposes (Table 1, Tyagi et al., 2013).

Table 1. Water Quality Rating for CCME-WQI and WA-WQI.

Rating of Water Quality	Water Quality Value
Canadian Council of Ministers of Environment Water Quality Index (CCME-WQI)	
Excellent water quality	95-100
Good water quality	80-94
Fair water quality	65 -79
Marginal water quality	45 -64
Poor water quality	0-44
Weighted Arithmetic Water Quality Index (WA-WQI)	
Excellent water quality	0-25
Good water quality	26-50
Poor water quality	51-75
Very Poor water quality	76-100
Unsuitable for drinking purpose	Above 100

3. Study Area

Arid and semi-arid regions are characterized by water scarcity. To solve this problem; water conservation and management have become a priority, whether it is surface water or groundwater. Jordan has suffered for a long time from water scarcity because it is considered a semi-arid region. Due to the water shortage, Jordan is highly dependent on underground water sources to cover its water demand. Because of this significance, it is important to preserve and protect groundwater from pollutants, in addition, to reduce over-pumping by factories and farms, which leads to deteriorating the water quality and makes it unfit for drinking purposes. One of the main groundwater sources is the Amman Zarqa Basin (AZB) located in the central of Jordan covers around 4074 Km^2. The study area is representing the southeastern part and including three major cities of Jordan, Amman, Ruseifa, and Zarqa (Figure 1). This portion of the basin is highly developed and urbanized with more than 6 million inhabitants,and represents the home for about 60% of Jordan's population (DOS, 2020).

In the last decades, this area has witnessed a high population growth, which can be related to the sudden fluxes of relatively large numbers of refugees as a result of political instability in the region. This led to huge and instantaneous pressures on the stressed available water resources. Furthermore, the consequence has influenced the per capita share of freshwater resources in Jordan and particularly this area that has been declined to less than 90 m^3/year, which places Jordan way below the poverty limit of 1000 m^3/year (MWI, 2017).

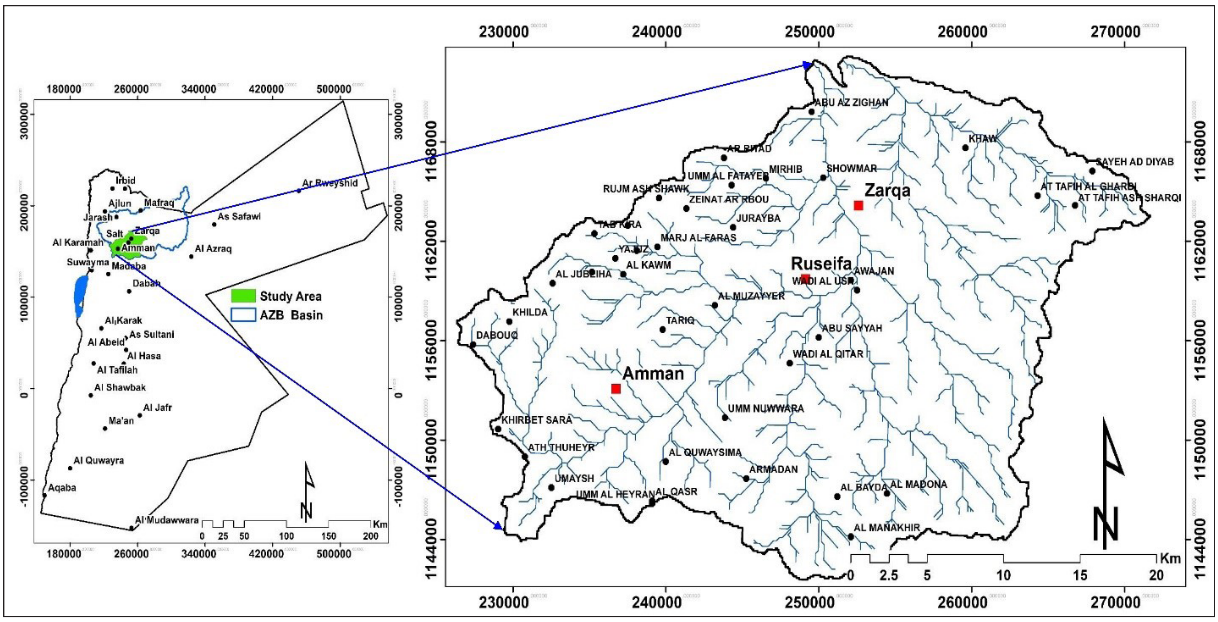

Figure 1. Location of the study area.

3.1. Hydrology and Hydrogeology

The climate of the area is hot and dry in the summer season, cold with rainfall in the winter season. The long term rainfall distribution ranges from around 400mm in the south to 120 mm in the northern parts of the study area. The mean monthly temperature in the area ranges from around 26 °C in summer to 8 °C in winter. The daily temperature ranges from over 30 °C in summer in the southeastern part to 35°C in the north and northeastern makes this area drier and hot (Atashi et al., 2020). The groundwater is exploited from two (shallow and deep) aquifers. The shallow aquifer consists of silicified limestone and limestone beds designated by Amman /Wadi Es Sir Aquifer (B2/A7) and the deep sandstone aquifer designated by the Kurnub Aquifer (K). The groundwater flow direction is from the south-west where recharge occurs along Seil el Zarqa north-west of the study area (Al Kuisi et al, 2014). The aquifer recharge depends on natural (infiltration from the rainfall directly) and artificial (such as leakage from water supply networks and irrigation return flow) sources. Many factors like geology, topographic relief, climate, and land use, affect the groundwater quality(UN-ESCWA and BGR, 2013; Al Kuisi et al., 2014).

Hundred public and private wells were drilled in the area for many purposes, increasing thus the pressure on the aquifers causing degrading the quality of water to become more saline and non-suitable for drinking purposes. The water level is declining in almost all wells in the study area. The Ministry of Water and Irrigation reported that the declines in the water level of the limestone aquifer (B2/A7) range between 0.67 m and 2 m per year (MWI, 2017).

3.2. Primary Data, Determinations, and Data Treatment

This study uses the available data of water quality (59groundwater wells × 11 water quality parameters) collected during 2020 from July to November systematically from the study area. Groundwater wells are distributed over an area of 85km^2. The location and coordinates of all the sample points were recorded using a GPS as present in Figure (2).

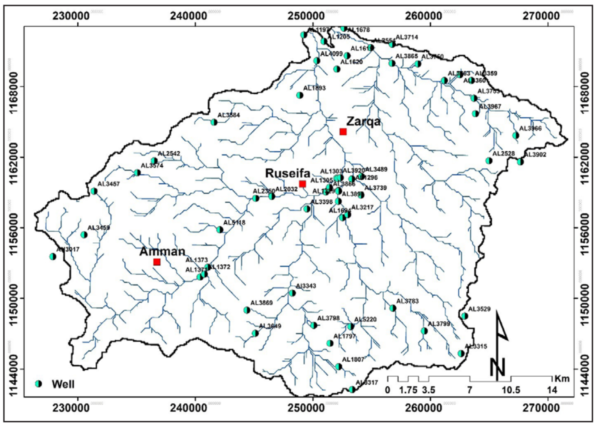

Figure 2. Location of the groundwater wells in the study area.

Before sample collection, the boreholes were pumped for up to 15 min to purge the aquifers and avoid contamination from the water to be sampled. Hydrogen ion concentration (pH), electrical conductivity (EC), and temperature were immediately measured during sampling by using a WTW-portable instrument. In addition, dissolved oxygen (DO) was determined by using calibrated portable DO meter and bicarbonate (HCO_3^-) by titration in the field. The water sample was collected from each well in 1000-mL polyethene bottles, which is rinsed many times before the sample storage and transferred to the laboratory of the Geology Department, at the University of Jordan. Where, different analytical methods and instruments measured Calcium (Ca^{2+}), Magnesium (Mg^{2+}), Potassium (K^+), Sodium (Na^+), Nitrite (NO_3^-), Sulfate (SO_4^{2-}) and Chloride (Cl^-). The accuracy of the analysis was calculated by the charge balance error equation, which resulted in ± 5% concentration of the major cations and anions.

Table 2 shows the selected parameters in CCME-WQI and WA-WQI calculations and their threshold values according to the Jordanian Institute of Standards and Metrology (JISM, 2015). The CCME-WQI and WA-WQI values were calculated for the groundwater samples collected in the Amman Zarqa area, applying the equations mentioned before. JISM Typology established by the Ministry of Water and Irrigation of Jordan was applied to classify the status of groundwater in the area.

Table 2. Statistics of the selected parameters for the classification of groundwater quality.

Chemical parameters	Mean	Max.	Min.	Std. Dev.	WHO (2017)*	JISM (2015)**
pH	7.19	8.03	6.5	0.35	8.5	6.5-8.5
EC (µS/cm)	1775.5	5490	372	1211.25	1500	1500
Dissolved Oxygen (DO) mg/L	3.74	8.6	0.10	2.22	5	5
Calcium (Ca^{2+}) mg/L	136.18	331	40	72.44	100	200
Magnesium (Mg^{2+}) mg/L	60.73	193	13	40.24	50	150
Sodium (Na^+) mg/L	148.87	544	3	140.82	200	200
Potassium (K^+) mg/L	5.78	37	0.03	6.70	20	10
Chloride (Cl^-) mg/L	340.96	1251	30	297.07	250	500
Nitrate (NO_3^-) mg/L	31.02	170	0.1	38.24	50	50
Sulfate (SO_4^{2-}) mg/L	146.76	712	14	151.69	250	500
Bicarbonate (HCO_3^-) mg/L	333.74	732	153	110.44	200	250

* WHO (The World Health Organization).

** JISM (Jordanian Institute of Standards and Metrology).

The CCME-WQI and WA-WQI adopts a “five-class” scale, while JISM endorses a “two-class” scale. To make a good comparison between these two WQI’s harmonization terms were used to merge the five classes of CCME-WQI and WA-WQI into two classes similar to JISM (Table 3). Precisely, the “Poor–marginal” CCME ratings and “unsuitable–Very Poor-Poor” WA ratings were both merged into “Class 1” which indicate the “bad” rating, and “Class 2” as given by JISMthe ratings “Excellent–Good–Fair” and “Excellent–Good” of CCME-WQI and WA-WQI, respectively, were harmonized into “Good” rating.

Table 3. Harmonization of WQI’s to JISM classes based on criteria given by WA, CCME, and JISM.

		Classes	1	2
CCME-WQI		**Rating Range**	**Poor - Marginal 0-64**	**Fair- Good- Excellent 65-100**
WA-WQI		**Rating Range**	**Poor–Very Poor -Unsuitable 51-100**	**Excellent–Good 0-50**
JISM	Units	Rating	Poor	Good
pH			<6.5 or >8.5	6.5–8.5
EC	µS/cm		>1500	<1500
DO	mg/L		<5	>5
Calcium (Ca^{2+})	mg/L	Range	>200	<200
Magnesium(Mg^{2+})	mg/L		>150	<150
Sodium (Na^{+})	mg/L		>200	<200
Potassium (K^{+})	mg/L		>10	<10
Chloride (Cl^{-})	mg/L		>500	<500
Nitrate (NO_3^{-})	mg/L		>50	<50
Sulfate (SO_4^{2-})	mg/L		>500	<500
Bicarbonate (HCO_3^{-})	mg/L		>250	<250

The spatial distributions of water quality parameters across 59 groundwater wells were investigated using the Kriging modules in the ArcGIS 10.8 Software. Kriging is defined as a spatial interpolation technique that uses the measured georeferenced samples to estimates values at unsampled locations based on a statistical model. To test the statistical variations of the water samples, Box-and-Whiskers plots were constructed (Microsoft Excel 2019 version). The plots represent a beneficial way to compare the distributions of the parameter values. It shows the principal statistical attributes such as median, minimum, maximum, upper and lower quartiles.

Paired samples t-test,also called the dependent samples t-test was applied to see if there are two measurements apply to the same samples with the same condition. A T-test is based on comparing the means of the two (pair) samples. The null hypothesis indicates that if the means of the two tests used are equal ($\mu_1 = \mu_2$), there is no statistical significance in the difference between the WA-WQI and CCME-WQI mean values. On the other hand, if the means of the two tests used are not equal ($\mu_1 \neq \mu_2$),this implies that there is a statistical significance in the difference between the WA-WQI and CCME-WQI mean values (Wackerly et al., 2002).

4. Results and Discussion

4.1. Spatial analysis of water quality

The study data set comprises11 water quality parameters (EC, pH, DO, Ca^{2+}, Na^{+}, Mg^{2+}, K^{+}, NO_3^{-}, HCO_3^{-}, SO_4^{2-}, Cl^{-}). The statistical variations of every parameter amongst the different groundwater wells were plotted using the Box-and-Whiskers as shown in Figure (3), whereas the spatial distribution maps were constructed using the ArcGIS 10.8 Software and are presented in Figure 4(a) - (k).

The study area is divided depending on the attribute classes of each parameter into four categories; 1-4. The pH values in all groundwater wells ranged between 6.5 and 8.03, which lie in the permissible limits of JISM as shown in Table (2). Most pH values (Figure 4a) were observed in categories 3 and 4 with a range from 7-8. Thus, the groundwater reflects neutral to slightly add pH values in the study region. The EC values of water samples ranged between 372 and 5490 µS/cm, these values are directly proportional to the total dissolved solids. 46 % of the samples show a high concentration of EC greater than the permissible limit set by JISM (2015). These excesses are shown in categories 2, 3, and 4 (Figure 4b). Dissolved oxygen (DO) refers to the amount of free non-compound oxygen dissolved in water. The minimum value of DO in the study area is 0.1 mg/L, while the maximum value equals 8.6 mg/L. Figure 4c shows that most of the DO concentrations occurred in category 3.

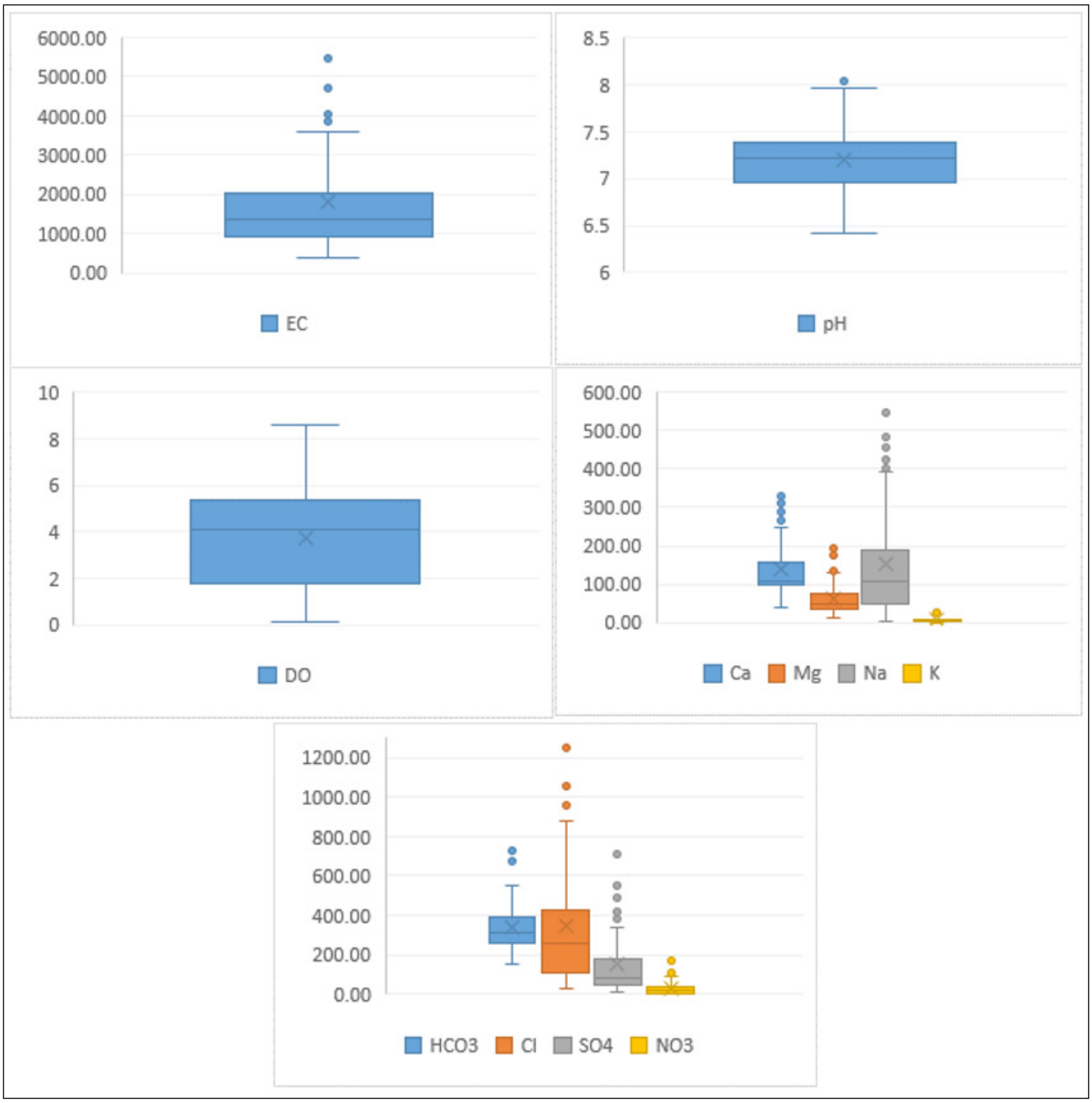

Figure 3. Box-and-Whisker plot of water quality parameters for the study area in the year 2020.

Calcium and magnesium values ranged from 40 to 331 and 13 to 193 mg/L, respectively. 17 % and 5 % of the calcium and magnesium concentration in the study area lie beyond the documented permissible limits of 200 mg/L for Ca^{2+} and 150 mg/L for Mg^{2+}. From the spatial distribution of calcium (Figure 4d), the higher concentration value was exhibited in the northern and northeast of the region. Figure 4e shows that most of the magnesium concentrations occurred in category 3. This is due to ion exchange in groundwater, dissolution of minerals, agronomic and industrial related activities (Fernandes et al., 2008 and Singh et al., 2011).

Spatial distribution of sodium and potassium concentrations are shown in Figure 4f-g where the high concentration of sodium is clear in categories 2 and 3, whereas the northeast part of the study area is distinguishing with high amounts of potassium values. Sodium and potassium values ranged between 3 and 544 mg/L and 0.03 to 37, respectively.24 % of the samples exceed the permissible limit of JISM (2015) for Na^{+} concentration while 5 % of the samples exceed the permissible limit of JISM (2015) for K^{+} concentration. High K^{+}concentration in water may lead to health concerns for people suffering from hypertension, kidney dysfunction, and diabetes (WHO, 2017). While, Na+ concentrations have a multifunction in the human body to maintain blood pressure, control fluid levels, for nerve and muscle function. However, a high level of Na^{+}isconsidered harmful to the human body (WHO, 2017). Sodium and potassium are present in the water through anthropogenic activities such as industrial discharges, fertilizer, and the release of wastewater around the wells (Al Kuisi et al., 2009).

Figure 4h-k shows the spatial distribution of Chloride, Nitrate, Sulfate, and Bicarbonate in the groundwater samples. Chloride values range from 30 to 1251 mg/L and 24 % of the samples exceed the JISM (2015) allowable limits (Table2). The high Cl^{-} content lies in the category 3 and 4 (Figure 4h). Chloride may get into water from a number of sources including the weathering of soils from industries and municipalities, agricultural activities and overexploitation of the aquifer (Al Kuisi et al, 2009). Nitrate concentrations ranged between 0.1 and 170 mg/L in the study area. Figure 4i indicates that high nitrate concentration is stationed in the northern part of the region. 22 % of the samples exceed the maximum permissible limit of NO_3^- according to JISM (2015).On the other hand,5 % of the samples exceed the permissible limit of sulfate according to JISM (2015). SO_4^{2-} concentrations ranged from 14 to 712 mg/L, and the spatial distribution of $SO_4^{2-}$is shown in Figure 4j. The highest concentration of sulfate is located in the northeast part of the region. Increasing nitrate and sulfate concentrations in the groundwater could be attributed to using chemical and natural fertilizers for agricultural activities and the wastewater effluents (Al Kuisi et al., 2009). Bicarbonate values in the analyzed samples ranged from 153 and 732 mg/L. The TheHCO_3^- content in 59 % of the samples has been found to exceed the maximum permissible limit for HCO_3^- in drinking water guidelines of JISM (2015). This is mostly observed in the northern part of the study area (Figure 4k). The carbon dioxide-charged water infiltrating through the soil zone under the influence of H_2CO_3 commonly encounters dissolvable minerals which are calcite and dolomite which could be dissolved through contact with the CO_2-charged seeping water. This process could be regarded as the major source of HCO_3- input into the groundwater system (Freeze and Cherry, 1979).

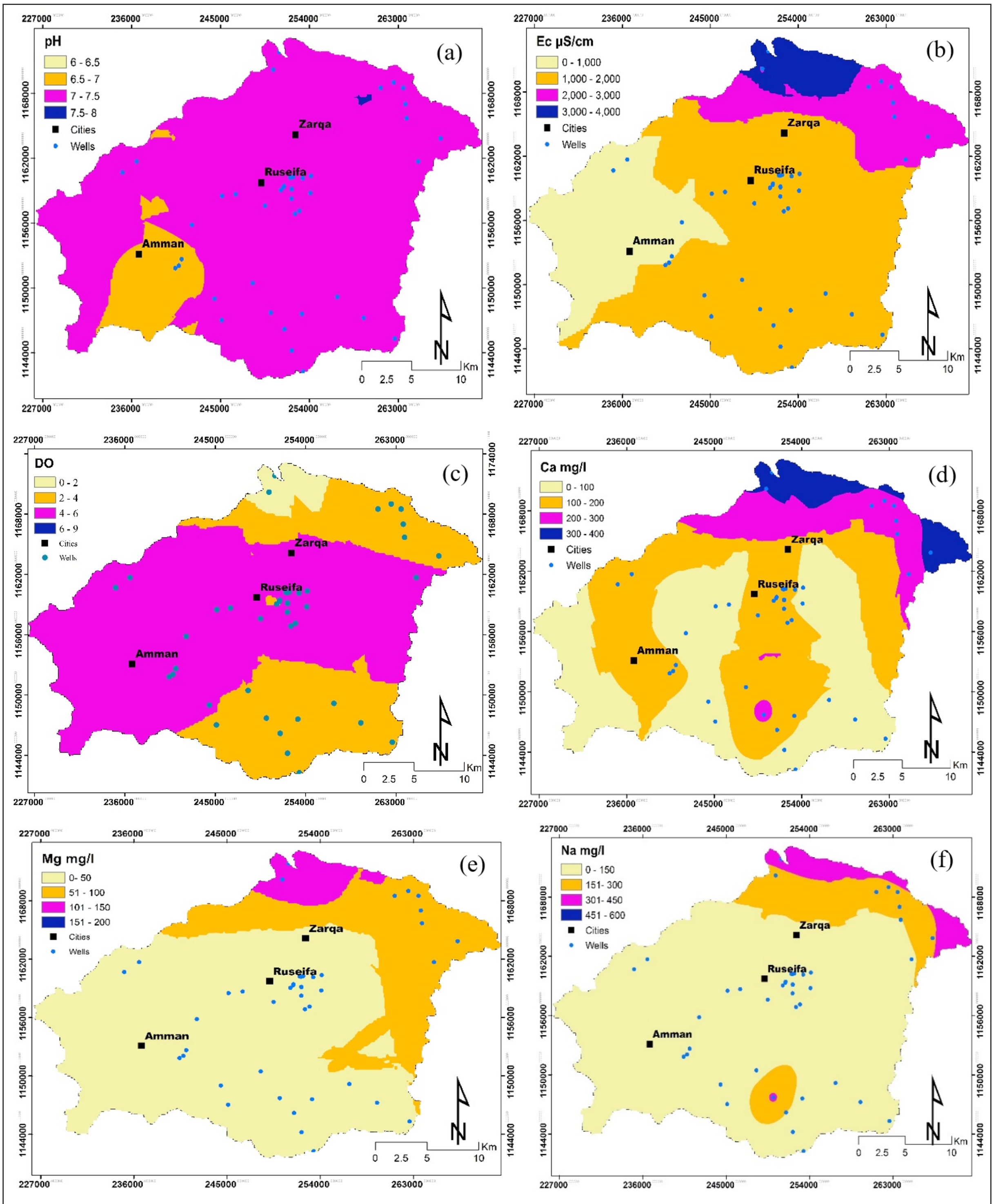

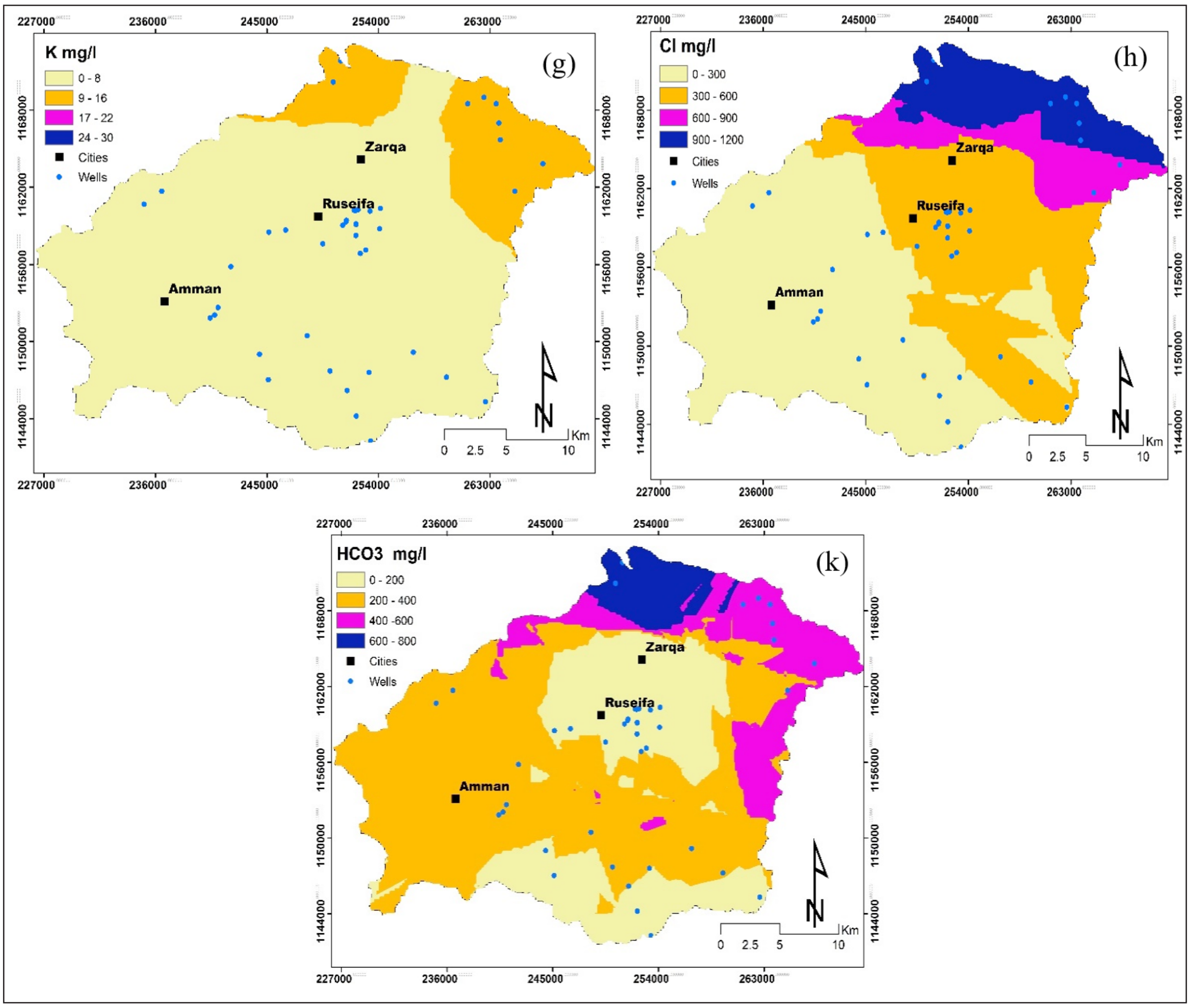

Figure 4. Spatial distribution for water quality parameters in the study area.

4.2. Comparison between CCME and WA water quality indices

Generally, most of the WQI's work is focused on the comparative performance of the various quality indices in surface water bodies rather than groundwater because the surface water is more vulnerable to pollution. Many researchers have discussed results related to the performance of WQI's in surface water bodies (Alexakis et al., 2016; Darvishi et al., 2016; Hamlat et al., 2017; Majeed, 2018; Noori, 2020).

Several researchers showed a clear interest in the WA-WQI, whereas the others, widespread overall the world, applied the CCME-WQI separately (Bilgin, 2018; Ewaid, 2016; Uddin et al., 2017; Ama et al., 2018; Dutta et al., 2018) and just a few of them focused on comparing indices performance for water quality management purpose such as Lopes et al., 2020; Wong et al., 2020; Ebraheim et al., 2020; Zotou et al., 2019. The lack of comprehensive and comparative studies of the performance of Water Quality Indices in the area under consideration prompted this study.

The first comparison made was carried out to check whether the two indices would yield similar results. The t-test rejected the null hypothesis regarding similarity at the 95% significance level. This means that the produced means using the two indices exhibit a significant statistical difference.

Figure 5 shows the calculations made using the WA and CCME indices. Both indices include 11 water quality variables (EC, pH, DO, Ca^{2+}, Na^{+}, Mg^{2+}, K^{+}, NO_3^{-}, HCO_3^{-}, SO_4^{2-}, Cl^{-}). Results observed show that CCME-WQI classify the groundwater samples as follows: "26% Excellent", "49% Good", "8% Fair", "12% Marginal", and "5% Poor" on the other hand, the WA-WQI classify the sample in the following manner: "8% Excellent", "45% Good", "31% Poor", "14% very poor", "2% unsuitable for drinking purpose". The results indicate that there is a minor disparity in rating groundwater by these two indices. The reason for this minor difference is related to weights, assignments, quality scales, and aggregation formulae. After reviewing the results of the analyzed parameters for the dissimilar samples between the two indices, it is clear that they are not exceeding the limits recommended by the JISM (2015). Although the Weighted Average water quality index classifies it as very bad to not suitable for drinking purposes.

Figure 5. Variations in water quality values obtained at the groundwater monitoring stations of the study area using the above mentioned indices.

In general, the comparison between the WA -WQI and CCME -WQI considering their merits and demerits is shown in Table 4 (Terrado et al., 2010; Abbasi and Abbasi, 2012;Yogendra and Puttaiah, 2008; Akoteyon et al., 2011).

Table 4. Merits and demerits of the selected water quality indices (Terrado et al., 2010; Abbasi and Abbasi, 2012;Yogendra and Puttaiah, 2008; Akoteyon et al., 2011).

Merits	Demerits
Weighted Arithmetic Water Quality Index	
1. Uses several parameters in a mathematical equation to obtain a rating of water quality. 2. Water quality is represented by one number, which facilitates the delivery of information to decision-makers and citizens. 3. It helps to describe the suitability of surface and groundwater sources for human use. 4. It requires fewer parameters compared to other water quality parameters for a specific use. 5. Several parameters and their composition can be used to assess and manage water quality.	1. The final water quality indicator number may not be a true description of water quality. 2. There are many parameters that are not taken into account in calculating the water quality index. 3. A bad value of any parameter may affect the calculation of the water quality index. 4. A water quality index based on important parameters can provide a simple water quality indicator.
Canadian Council Ministry of Environment Water Quality Index	
1. Convert the measure of the variable to a single number. 2. Flexibility to choose the parameters that contribute to the calculation of the index. 3. Adaptability to changing legal requirements and different uses of water. 4. Simplify the multivariate data statistically. 5. Understandable and clear diagnosis for decision-makers and the public. 6. An appropriate tool to assess the water quality at a specific location. 7. Easy to calculate. 8. Tolerance for lost data.	1. Loss of information of single variables. 2. Loss of information about the particular objectives for each location and specific utilizing of water. 3. Results are influenced by the formulation of the index. 4. Missing a lot of information about the interactions between variables. 5. The index is difficult to adapt to different ecosystem types. 6. Equal importance is given to all variables. 7. It cannot be used in combination with other indicators or biological data. 8. When few variables are considered or there is an excessive amount of covariance between them, F1 cannot work properly. 9. Gives a partial diagnosis of water quality.

Figure 6. shows the spatial variation of WQI's values in the studied wells within the study area. The CCME-WQI values range from 22 to 100, while the WA-WQI values range from 5 to 157.

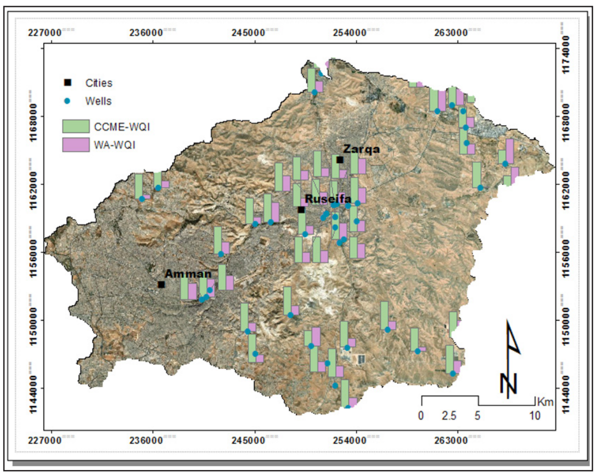

Figure 6. Spatial variation of CCME and WA-WQI values.

WQI's spatial distribution maps were constructed using kriging technique (Figures 7 and 8). The high CCME index value corresponds to excellent groundwater while the low value indicates poor water quality. On the other hand, the low WA index value corresponds to excellent groundwater while the high value indicates very poor and unsuitable water. A careful inspection of both figures 7 and 8 shows that there is a great similarity between both figures. Both indices characterized the northern part of the study area similarly, whereas the southern part differs slightly, in such a manner where the CCME-WQI index yielded more precise and detailed characterization. This reflects its superiority to WA-WQI especially in pinpointing specific areas of deteriorating water quality.

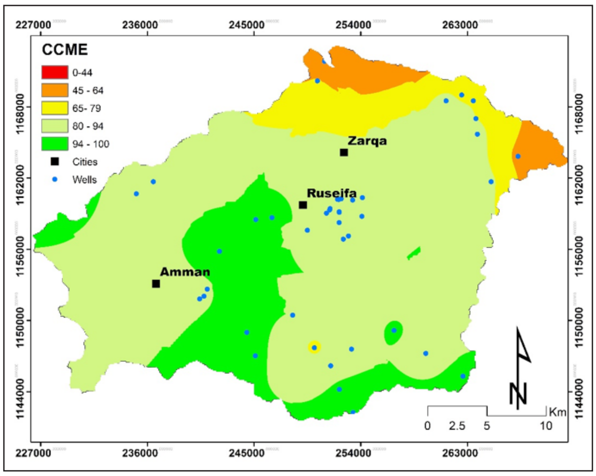

Figure 7. CCME-WQI prediction map for the study area.

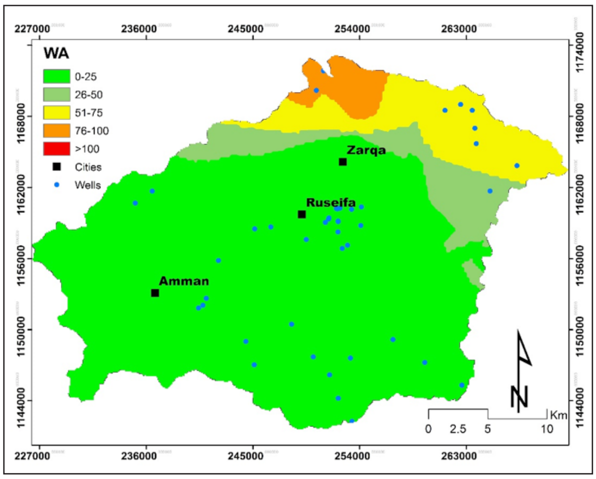

Figure 8. WA-WQI prediction map for the study area.

5. Conclusions

Water quality monitoring and evaluation indices based on water quality parameters are useful tools. They can reflect the water quality status and give an impression about the suitability of water for drinking purposes. Spatial and Statistical analyses were conducted to analyze 11 water quality parameters (EC, pH, DO, Ca^{2+}, Na^{+}, Mg^{2+}, K^{+}, NO_3^{-}, HCO_3^{-}, SO_4^{2-}, Cl^{-}) across the study area. The paired (two tail) t-test for the WQI values of the study area at a significance level (a = 0.05) shows that there is a strong indication that the difference between CCME-WQI and WA-WQI mean values are statistically significant. The grading of the study area quality varied due to the difference in the numbers and types of selected parameters, mathematical structures, weights, assignments, quality scales, and aggregation formulae in each index. The CCME-WQI proved to be a more accurate tool in characterizing the groundwater of the study area. The CCME-WQI has flexibility in the selection of parameters and simplicity in the calculation and pinpoints specific areas of deteriorating water quality.WA-WQI ranked 15% of the samples as "very bad" and "not suitable for drinking purposes" thoughthe parameters used in determining the water quality indices did not exceed the values allowed by the JISM.

Acknowledgments

The authors would like to extend their thanks to the anonymous reviewers for their valuable comments and suggestions which led to improving the quality of the original manuscript.

References

Abbasi, T., and Abbasi, S.A. (2012). Water quality indices. Elsevier.

Akoteyon, I.S., Omotayo, A.O., Soladoye, O., Olaoye, H.O. (2011). Determination of water quality index and suitability of urban river for municipal water supply in Lagos-Nigeria. European Journal of Scientific Research 54(2): 263-271.

Alexakis, D., Tsihrintzis, V.A., Tsakiris, G., Gikas, G.D. (2016). Suitability of water quality indices for application in lakes in the Mediterranean. Water resources management 30(5): 1621-1633. DOI: 10.1007/s11269-016-1240-y.

Al Kuisi, M., Al-Qinna, M., Margane, A., Aljazzar, T. (2009). Spatial assessment of salinity and nitrate pollution in Amman Zarqa Basin: a case study. Environmental Earth Sciences 59: 117–129. DOI: 10.1007/s12665-009-0010-z.

Al Kuisi, M., Mashal, K., Al-Qinna, M., Hamad, A.A., Margana, A. (2014). Groundwater vulnerability and hazard mapping in an arid region: case study, Amman-Zarqa Basin (AZB)-Jordan. Journal of Water Resource and Protection, 2014. DOI: 10.4236/jwarp.2014.64033.

Ama, I.N., Ebichime, N.G., Agbaire, P.O., Verla, A.W. (2018). Determination of water quality index of selected water bodies in Warri, Delta State, Nigeria.World News of Natural Sciences 16: 42-52.

Atashi, N., Rahimi, D., Al Kuisi, M., Jiries, A., Vuollekoski, H., Kulmala, M.,Vesala, T., Hussein, T. (2020). Modeling Long-Term Temporal Variation of Dew Formation in Jordan and Its Link to Climate Change. Water 2020, 12 (8), 2186. DOI: 10.3390/w12082186.

Bilgin, A. (2018). Evaluation of surface water quality by using Canadian Council of Ministers of the Environment Water Quality Index (CCME WQI) method and discriminant analysis method: a case study Coruh River Basin. Environmental monitoring and assessment 190 (9): 1-11. DOI: 10.1007/s10661-018-6927-5

Brown, R.M., Mccleiland, N.J., Deiniger, R.A., O'Connor, M.F. (1972). Water quality index crossing the physical barrier. (Jenkis, SH, ed.). Proceedings in International Conference on water pollution Research Jerusalem 6: 787-797.

Canadian Council of Ministers of the Environment (CCME). (2001). "Canadian water quality guidelines for the protection of Aquatic life": CCME Water Quality Index 1.0. Technical Report.

Canadian Council of Ministers of the Environment, Winnipeg, MB, Canada.

CCME. (2003). Water Quality Index Workshop; Canadian Council of Ministers of the Environment Winnipeg: Winnipeg, MB, Canada,.

Darvishi, G., Kootenaei, F.G., Ramezani, M., Lotfi, E., Asgharnia, H. (2016). Comparative investigation of river water quality by OWQI, NSFWQI and Wilcox indexes (case study: The Talar River–IRAN). Archives of Environmental Protection 42(1): 41-48.

Bhargava, D.S. (1983) Use of Water Quality Index for River Classification and Zoning of Ganga River. Environmental Pollution Series B, Chemical and Physical 6: 51-67. DOI:10.1016/0143- 148X(83)90029-0.

Department of Statistics (DOS) (2020) http://dosweb.dos.gov.jo/population/population-2/

Dutta, S., Dwivedi, A., Suresh Kumar, M. (2018). Use of water quality index and multivariate statistical techniques for the assessment of spatial variations in water quality of a small river. Environmental Monitoring and Assessment 190(12). DOI: 10.1007/s10661-018-7100-x.

Ebraheim, G., Zonoozi, M.H., Saeedi, M.A. (2020). Comparative study on the performance of NSFWQIm and IRWQIscin water quality assessment of Sefidroud River in northern Iran.Environ Monit Assess192(677) (2020). DOI: 10.1007/s10661-020-08630-6.

Ewaid, S.H. (2016). Water Quality Assessment of Al-Gharraf River, South of Iraq by the Canadian Water Quality Index (CCME WQI). Iraqi Journal of Science 57(2A): 878-885.

Fernandes, P.G., Carreira, P., da Silva, M.O. (2008). Anthropogenic sources of contamination recognition—Sines coastal aquifer (SW Portugal). Journal of Geochemical Exploration 98(1-2): 1-14.

Freeze A.R. and Cherry (1979) Groundwater. Englewood Cliffs, NJ, -Prentice-Hall, 590 pp.; USA

Hamlat, A., Guidoum, A., Koulala, I. (2017). Status and trends of water quality in the Tafna catchment: a comparative study using water quality indices. Journal of Water Reuse and Desalination 7(2): 228- 245. DOI: 10.2166/wrd.2016.155.

Horton, R.K. (1965). An index number system for rating water quality. Journal of Water Pollution Control Federation 37(3): 300-306.

Imneisi, I.B., and Aydin, M. (2016). Water quality index (WQI) for main source of drinking water (Karaçomak Dam) in Kastamonu City, Turkey. Journal of Environmental Analytical Toxicology l 6(407): 2161-0525. DOI:10.4172/2161-0525.1000407.

Iticescu, C., Georgescu, L.P., Murariu, G., Topa, C., Timofti, M., Pintilie, V., Arseni, M. (2019). Lower Danube water quality quantified through WQI and multivariate analysis. Water11(6), 1305. DOI: 10.3390/w11061305.

JISM, Jordanian Institute of Standards and Metrology (2015). Drinking water standards No. 286/2015, Amman, p 13.

Lopes, O.F., de Jesus, R.M., de Sousa, L.F., Rocha, F.A., da Silva, D.M.L., Amorim, A.F., Navoni, J.A. (2020). Comparison between water quality indices in watersheds of the Southern Bahia (Brazil) with different land use. Environmental Science and Pollution Research 1- 16. D10:1007/s11356-020-10941-7.

Madalina, P., and Gabriela, B.I. (2014). Water Quality Index-An Instrument For Water Resources Management. Aerul si Apa. Componente ale Mediului 391-398.

Majeed, S.A. (2018). Comparison of Water Quality Indices (Bani-Hassan River as a Case Study). Journal of Kerbala University16(1): 53-65.

Ministry of Water and Irrigation (2017). Water Yearbook Hydrological year 2016-2017. Ministry of Water and Irrigation, www.mwi.gov.jo.

Noori, M.D. (2020, February). Comparative analysis of weighted arithmetic and CCME Water Quality Index estimation methods, accuracy and representation. IOP Conference Series: Materials Science and Engineering 737(1 012174). IOP Publishing. DOI: 10.1088/1757-899X/737/1/012174.

Oni, O., and Fasakin, O. (2016). The use of water quality index method to determine the potability of surface water and groundwater in the vicinity of a municipal solid waste dumpsite in Nigeria.American Journal of Engineering Research (AJER) 5(10): 96-101.

Paun, I., Cruceru, L., Chiriac, F.L., Niculescu, M., Vasile, G., Marin, N.M. (2016). Water Quality Indices-methods for evaluating the quality of drinking water. NCD ECOIND – International Symposium-SIMI 2016. The Environment and the industry. Proceeding book.

Singh, C.K., Shashtri, S., Mukherjee, S. (2011). Integrating multivariate statistical analysis with GIS for geochemical assessment of groundwater quality in Shiwaliks of Punjab, India. Environmental Earth Sciences 62: 1387–1405. DOI: 10.1007/s12665-010-0625-0.

Sutadian, A.D., Muttil, N., Yilmaz, A.G., Perera, B.J.C. (2016). Development of river water quality indices—a review. Environmental monitoring and assessment 188(1), 58. DOI: 10.1007/s10661-015- 5050-0.

Terrado, M., Barceló, D., Tauler, R., Borrell, E., de Campos, S. (2010). Surface-water-quality indices for the analysis of data generated by automated sampling networks. TrAC Trends in Analytical Chemistry 29(1): 40-52. DOI: 10.1016/j.trac.2009.10.001.

Tyagi, S., Sharma, B., Singh, P., Dobhal, R. (2013). Water quality assessment in terms of Water Quality Index. American Journal of Water Resources 1(3): 34–38. DOI: 10.12691/ajwr-1-3-3.

Uddin, M.G., Moniruzzaman, M., Khan, M. (2017). Evaluation of groundwater quality using CCME water quality index in the Rooppur Nuclear Power Plant Area, Ishwardi, Pabna, Bangladesh. American Journal of Environmental Protection 5(2): 33-43. DOI: 10.12691/env-5-2-2.

UN-ESCWA, B.G.R. (2013). Inventory of shared water resources in Western Asia: Chapter 6 Jordan River Basin. United Nations Economic and Social Commission for Western Asia.Federal Institute for Geosciences and Natural Resources, Beirut.

Wackerly, D., Mendenhall, W., Scheaffer, R. (2002). Mathematical Statistics with Applications: Sixth edition. Duxbury Press.

Wong, Y.J., Shimizu, Y., He, K., Sulaiman, N.M.N. (2020). Comparison among different ASEAN water quality indices for the assessment of the spatial variation of surface water quality in the Selangor river basin, Malaysia. Environmental monitoring and assessment 192(10): 1-16. DOI: 10.1007/s10661-020-08543-40.

World Health Organization. (2017).Global diffusion of eHealth: making universal health coverage achievable: report of the third global survey on eHealth. World Health Organization.

Yogendra, K., and Puttaiah, E.T. (2008). Determination of water quality index and suitability of an urban waterbody in Shimoga Town, Karnataka. In: Sengupta, M., and Dalwani, R. (Eds.), proceedings of Taal 2007: The 12th world lake conference:342-346.

Zotou, I., Tsihrintzis, V.A., Gikas, G.D. (2019). Performance of seven water quality indices (WQIs) in a Mediterranean River. Environmental monitoring and assessment 191(8), 505. DOI: 10.1007/s10661- 019-7652-4.

JJEES

JJEES (2021) 12 (4): 306-314
ISSN 1995-6681

Jordan Journal of Earth and Environmental Sciences

Assessment of Drinking Water Quality Index (WQI) in the Greater Amman Area, Jordan

Ali El-Naqa[1*] and Amal Al Raei[2]

[1]Department of Water Management and Environment, Prince El-Ha ssan Bin Talal Faculty for Natural resources and Environment, The Hashemite University, Zarqa, Jordan.
[2]Water Quality inspector, Greater Amman Municipality, Jordan

Received 18 February 2021; Accepted 25 March 2021

Abstract

Abstract: The Water Quality Index (WQI) is considered the most effective method of measuring water quality. Several water quality parameters are included in a mathematical equation to rate water quality, determining the suitability of water for drinking purposes. This work aims to evaluate the quality of drinking water in Greater Amman using the water quality index method (WQI). For this purpose, twenty-six water sampling zones were used to calculate the WQI during the period 2012 to 2016. The water samples were analyzed for a various set of physicochemical parameters such as pH, turbidity, total dissolved solids, Sodium, Potassium, Calcium, Magnesium, Chloride, Sulfate, Bicarbonate, Total Hardness, Nitrate, and trace heavy metals such as(Ba, Cd, Cr, Cu, Fe, Mn, Ni and Zn). In addition, the biological parameters were also analyzed such as total coliform, Fecal coliform, Fungi and Pseudomonas.

The relative weight has assigned to each parameter and ranges from 1 to 5, based on the importance of the water quality parameters for domestic purposes. The computed WQI collected from twenty-six sampling zones in the Greater Amman area has a range from 29.17 to 62.32 The WQI analysis reveals that the water quality varies from excellent to good water quality. The water quality for potable drinking water was compared with the guidelines of the World Health Organization (WHO)and Jordan Drinking Water Standard (JS286) and the results indicate that water quality in the Greater Amman water is of high quality for drinking purpose.

The spatial distribution mapping of the water quality index (WQI) has been prepared using ArcGIS software. Comparing the WQI for the five years from 2012 to 2016) indicates that the water quality of potable drinking water has been deteriorated in 2016 due to the high population growth of Greater Amman in comparison to the precedent years.

Keywords: Water Quality, Index, Greater Amman, Drinking water, physio-chemical parameters

1. Introduction

One of the major challenges in the drinking water supply is the quality of the produced water. Water quality depends on water composition influenced by natural process and human activities. Eighty percent of drinking water in Jordan comes from groundwater and 20% from surface water sources. The average water demand in the distribution network is estimated to be 85 liters per capita per day (MWI, 2017). The main obstacles to potable water supply in Jordan are the shortage of water, and the water supply is intermittent, especially during the summer period; the deterioration of the water quality of different sources of water; the increasing of water demand; and the water leakage throughout the water distribution network is estimated to account for the loss of 45% of the total water distributed.

To assess the suitability of water quality for different uses, there is of utmost importance need to develop a quality index, which will classify the quality of water. World Health Organization (WHO) set guidelines for chemical contaminants in drinking water. Water Quality Index (WQI) is considered the most effective method of measuring water quality. Diverse water quality parameters are included in a mathematical equation to assess the water quality, determining the suitability for water for potable purposes (Ochuko et al., 2014). Water Quality Index (WQI) is used to assess the suitability of water for a variety of uses (Shala et al., 2020). WQI was introduced and demonstrated in the early 1970s but not widely used or accepted by water agencies that monitor the quality of water. (Cude, 2001). So WQI is used to relate a collective of variables to a common scale and combining them into a single numerical value according to a chosen model or method.

Clean potable water is an essential factor for human survival and the whole life. Due to many factors such as the population increase, the water demand is increasing steadily over time (Ramakrishnaiah et al., 2009). This challenge is leading to more demands for clean water and therefore the lack of water in many parts of the world is increasing consequently. Most of the diseases in human beings are water pollution according to WHO (World Health Organization). Because of these factors, it is necessary to monitor the water quality and to protect it from pollutants (Tiwari and Mishra, 1985). Water quality assessment can be evaluated

* Corresponding author e-mail: elnaqa@hu.edu.jo

for potable water purposes using physio-chemical and biological parameters. Hazards of drinking polluted water involve diseases like cholera, diarrhea, typhoid, parasitic worm. Consequently, there is an increasing attention to water quality aspects and guidelines, based on setting standards or guidelines of potable drinking water criteria (WHO, 2011).

Water quality is defined by pollutants, which can be grouped as physical, chemical and biological properties of the water. These variables can collectively be integrated into a systematically structured indexing scale, commonly known as the water quality index (WQI).

The WQI offers a single value that expresses water quality by integrating diverse variables of water quality (Stambuck-Giljanovic, 1999; Stigter et al. 2006; Saeedi et al. 2010). The traditional approaches for assessing water quality are mainly based on the comparison of analyzed parameters with the local or international standards. Various studies have suggested the use of a WQI (Cude, 2001; Saeedi et al., 2010; Lateef, 2011). There are various methods for calculating the WQI, considering a comparable physical and chemical parameter but varying in the way the parameters are valued (Abdulrasoul et al., 2015).

The WQI is capable of converting a large quantity of water pollution data into a single dimensionless index value, which represents the level of contamination of the water resources (Kalyani et al., 2016; Ponsadailakshmi et al., 2018 and Ewaid et al., 2018). Considering such ability to integrate a pool of water quality variables into a simple easily understood number, WQI is, therefore, regarded as a very effective and significant communication tool for water managers and policymakers (García-Ávila et al., 2018). Water quality indices are used to simplify and streamline what would otherwise be impractical assignments, thus justifying the efforts of developing such indices.

The main goal of this study is to assess the potable drinking water quality and introduce the use of the WQI as a potential monitoring tool for the drinking water quality of the Greater Amman area.

2. Materials and methods

2.1. Description of Study Area

Amman City is the capital of Jordan which is located between latitudes 220000 and 265000 E and longitudes 135000 and 165000 N and occupies an area of about 1680 km^2 (Figure 1). The population of Greater Amman is approximately 4,008,000 and is expected to increase in Amman at a rate of about 1.8 percent per year until 2030 (Jordan Department of Statistics, 2017). The climate in Jordan is of Mediterranean type. The summer season in Amman extending from May to September which is hot and dry with cool evenings, whilst the winter season starts from mid of October to the ends of April(Jordan Meteorological Department (JMD) (2019). The climate in Amman is overall mild and dry. Amman city is situated on the East Bank Plateau, an upland characterized by three major wadis which run through it. Originally, the city had been built on seven hills. Amman's terrain is typified by its mountains. The most important areas in the city are named after the hills or mountains they lie on. The area's elevation ranges from 700 to 1,100 m. The average elevation is around 800 meters above sea level and has an average temperature ranging from 8.5 °C in January to 26.5 °C in July and August. The mean annual temperature in Amman is 17 °C. The average minimum monthly temperature is 7.7 °C and the average maximum monthly temperature is 25.2°C. Rainfalls between November and March with an average annual of 250 mm/year. Spring is brief, mild and takes a little less than a month, from April to May. Sometimes snow is falling on the city during spring. Autumn is also mild and lasts from September to late November or December(Jordan Meteorological Department (JMD) (2019).

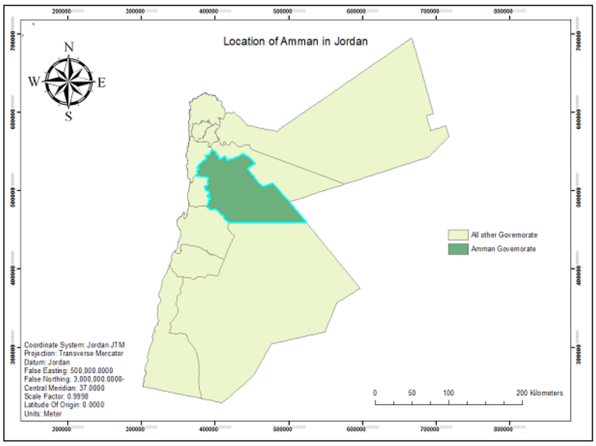

Figure 1. Location of Amman Governorate within Jordan map.

2.2. Water Sampling and Physicochemical Analyses

In this study, Greater Amman Municipality has divided into twenty-two (22) sampling zones according to the distribution of domestic water. The tap water samples were collected from the restaurants and service shops. The total number of water samples in this study was 180 samples. The hydrochemical data was collected during the period 2012-2016 from the Health and Business Inspection Department HBID laboratories of Greater Amman Municipality. The data included the routine analysis, in addition to turbidity, microbiological analysis such as E. coli, coliform, fungi and Pseudomonas.

A flowchart diagram representing the methodology layout to determine and evaluate the water quality index in Greater Amman (Figure 2). Data collection is an important stage in any research. The physicochemical analyses were taken from HBID laboratories-Greater Amman Municipality. Twenty-two (22) representative water samples from 22 sampling zones for five years period were collected from tanks (tap water) from restaurants, Bakery, beautification saloon, and all shops dealing with food. The samples were collected and analyzed in cooperation with HBID laboratories for their physiochemical constituents. The representative water samples were collected in polyethylene bottles of (500 ml volume) for chemical and physical analysis and (250 ml volume) for microbiological analysis- because chemical and physical tests need more quantities water than microbiological tests- after washing them twice by samples water to avoid contamination. The analysis of water samples waschecked, and the accuracy of the analysis should not exceed 5%.

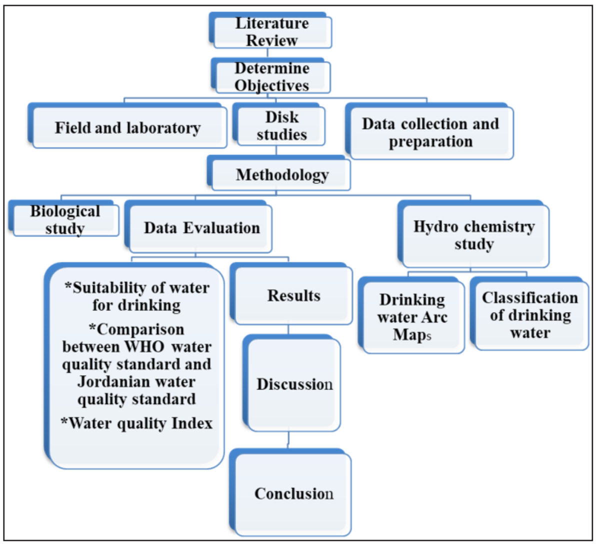

Figure 2. Flowchart illustrating the research stages.

The major, minor elements and trace elements analyses were conducted in the HBID Laboratories. These analyses aimed to determine the concentration of cations (Ca^{2+}, Mg^{2+}, Na^{+}, K^{+}) and the anions (HCO_3^{-}, SO_4^{2-}, Cl^{-}), Nitrate (NO_3^{-}), pH, TDS , Turbidity in addition to Total hardness and trace elements (Iron, Zinc, Manganese, Cadmium, Chromium, Copper, and Nickel) in the four private wells.

The water samples included 4 private wells (drinking water). These drinking water sampling zones include (AL-Madeenah (Mid Town), Swuayleh, Abu Nusayr, Shafa Badran, AL-Jubayhah, Tareq, Marka, Tla′a Ali, Badr AL-Jadeedah, Wadi AL-Seer, Marj AL-Hamam, Badr, Zahran, AL-Muqabalin, Khraibet AL-Souq, Ohoud, AL-Nasr, Ras AL-Ain, AL-Yarmouk, AL-Abdali, AL-Qwaismeh, and Basman) whilst wells sampling zones include Marj AL-Hamam, Sahab, AL-Jubayhah, Dwar Al-Waha, (Figure 3 and Figure 4).

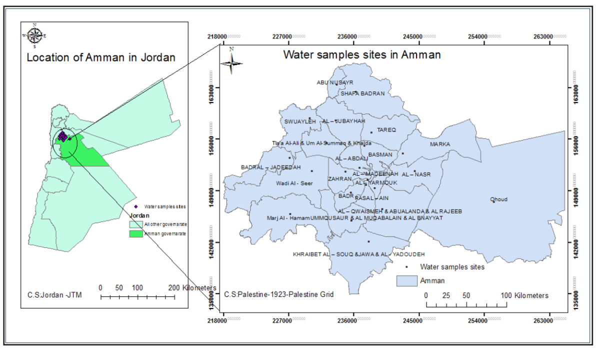

Figure 3. Drinking water sample sites in the Greater Amman area.

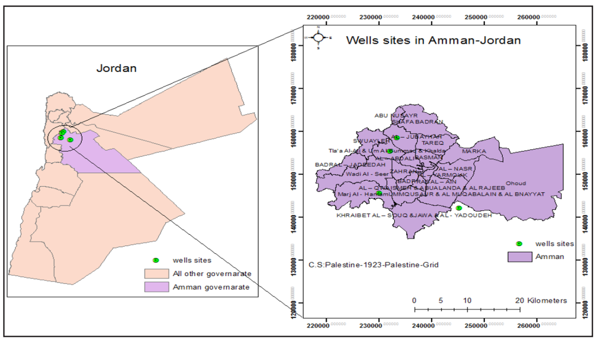

Figure 4. Groundwater sampling sites from 4 wells in the Greater Amman area.

2.3 Analytical Methods

Water chemical analyses were conducted to identify the quality of water according to standard methods for the standard methods for examination of water and wastewater22nd edition (Eugene, 2012). The pH of water samples was determined using a pH meter. The Total Dissolved Solids (TDS) was measured using the portable Electrical Conductivity (EC) meter. The concentrations of major cations and anions were determined using ICP-MS. Turbidity was determined by turbidity meter. The assessment of water quality in the greater Amman was considered the following analyzed parameters of drinking water including pH, Turbidity, Total Dissolved Solids, Total hardness, Calcium, Magnesium, Sulfate, Nitrate, Total alkalinity, Chloride, Iron, Cadmium, Chromium, Nickel, Zinc, Manganese, Sodium and Potassium.

Several microbiological analyses have been conducted including the total coliform, fecal coliform, fungi, and pseudomonas and Escherichia coli. The total number of colonies was determined by the nutrient agar method and the coliforms group and E. coli were determined by Colilert (defined substrate) method, as described by Maurice et al., 2008). The requisite data of various water quality parameters were analyzed monthly during the period from 2012 to 2016 which are available data at the laboratories of HBID.

2.4 Measurements of physiochemical Parameters

Physical parameters including turbidity, total dissolved solids (TDS) are measured directly in the field. The chemical analyses of Major ions (Ca^{2+}, Mg^{2+}, Na^{+}, K^{+}, Cl^{-}, SO_4^{2-}, HCO_3^{-} and CO_3^{2-}) and minor ions (NO_3^{-}) are carried out in the HBID laboratories. The chemical analyses of trace elements which are Cd, Cr, Ni, Mn, Cu, Fe, Zn, and B were carried out in HBID laboratory. Table (1) shows the physiochemical parameters for the sampling zones in Greater Amman area. The accuracy of the results of water samples analyses was estimated by calculating the absolute difference between total cations and the total anions as shown in Equation (1) (Hem, 1985):

$$Error\ (RD\%) = \frac{100 * \Sigma cations - \Sigma anions}{\Sigma cations + \Sigma anions} \quad \text{.... Eq. (1)}$$

Where:

RD %: Relative Difference

r ∑ Cations: Summation of positive ions concentrations in (meq/L).

r ∑ Anion: Summation of negative ions concentrations in (meq/L).

- If (RD ≤ 5%) the results could be accepted for interpretation.
- If (5% ≤ RD ≤ 10%) then the results are acceptable with risk.
- If the value (RD% > 10%) cannot depend on the results in hydrochemical interpretation (Hem, 1985).

2.5 Water quality assessment for drinking purposes.

The assessment of chemical characteristics for the potable water samples that were analyzed compared with World Health Organization (WHO, 2011) Guidelines and Jordanian water quality standards (JISM, 2015). Potable water quality was assessed by calculating the Water Quality Index (WQI) for each sample that indicates the impact of individual water quality parameters on the whole water quality. The Water Quality Index (WQI) was calculated for evaluating the influence of natural and anthropogenic activities based on several key parameters of drinking water chemistry (Krishna et al., 2014). The weight for the physio-chemical parameters has been assigned according to the relative significance of the parameter to the overall quality of water for domestic water purposes.

The spatial distribution for potable water quality parameters and water quality index maps for drinking purposes in the Greater Amman were done with the help of spatial analyst modules in ArcGIS software. Geographic Information System (GIS) is a powerful tool for creating solutions for assessing water quality and managing water resources. Inverse Distance Weight IDW interpolation technique was used for spatial modeling. The IDW referred to as the determinant interpolation techniques used because they assign values to locations based on the surrounding measured values and on specified mathematical formulas that determine the smoothness of the resulting surface (Selvam et al., 2015). Because the IDW is a weighted average, the distance the average cannot be greater than the highest or lesser than the lowest input, it determines the cell values using a linearly weighted combination of a set of sample points and controls the significance of known points upon the interpolated values (Selvam et al., 2015).

2.6 Classification of drinking water samples

Classification of all analyzed drinking water samples collected from the Greater Amman area has been done by using the software Aquachem, 2014. These classifications were done to determine the water types and the variations of water quality, these displayed graphical plots depending on the main cations and anions concentrations measured as milligrams per liter (mg/l) or milliequivalents per liter (meq/l). The distribution of water types in the Greater Amman is shown in Figure (5).

Table 1. The physio-chemical parameters of the analyzed water samples during the period (2012-2016).

ID	Site	HCO3 (mg/l	TH (mg/l)	Cl (mg/l)	SO4 (mg/l)	NO3 (mg/l)	Turbidity (NTU)	TDS (mg/l)	pH-Value	K (mg/l)	Na (mg/l)	Mg (mg/l)	Ca (mg/l)
1	AL-Madeenah	125.1	178.8	121.9	48.7	20.4	0.2	479.6	7.7	3.6	47.6	20.5	77.6
2	Swuayleh	16.0	135.8	80.7	45.4	10.7	0.3	341.9	7.7	5.0	20.0	15.0	30
3	Badr	200.2	132.6	74.4	41.0	12.8	0.3	338.2	7.6	2.4	30.9	15.4	58.2
4	AL-Muqabalin	110.1	155.1	81.8	37.0	13.7	0.1	351.0	7.5	3.5	65.0	22.0	25
5	Ras AL-Ain	110.0	124.4	78.6	32.9	12.6	0.1	283.7	7.7	2.5	60.0	18.0	22
6	Zahran	100.0	143.4	99.6	55.5	13.0	0.5	380.0	7.7	5.5	70.0	18.0	30
7	AL-Abdali	80.0	138.9	104.6	47.0	14.0	0.2	370.8	7.7	2.4	63.0	14.0	28
8	Marj Al-Hamam	110.0	104.6	74.7	37.1	11.5	0.2	320.4	7.5	1.3	55.5	10.4	38.7
9	AL-Yarmouk	105.0	114.2	78.5	41.1	12.1	0.2	342.8	7.7	3.0	60.0	15.0	22
10	Marka	130.0	190.6	150.1	39.3	25.2	0.2	516.5	7.6	5.0	100.0	25.0	35
11	Tareq	140.0	156.8	150.4	37.3	8.6	0.1	311.1	7.6	4.5	105.0	20.0	32
12	AL-Nasr	90.0	117.7	52.7	51.5	11.0	0.1	268.0	7.7	4.0	45.0	15.0	22
13	AL-Jubayhah	160.0	149.3	89.1	57.6	9.7	0.1	304.3	7.6	8.6	55.0	14.8	71.4
14	AL-Qwaismeh	70.0	97.9	44.9	36.8	13.7	0.1	256.7	7.7	3.0	32.0	12.0	20
15	Khraibet Al- Souq	70.0	105.4	60.1	25.8	11.2	0.3	272.4	7.6	2.5	35.0	12.0	22
16	Basman	120.0	174.9	95.6	39.5	12.8	0.1	347.7	7.6	5.6	65.0	21.0	36
17	Shafa Badran	115.0	137.7	96.7	41.0	11.4	0.1	320.0	7.7	6.5	70.0	16.0	30
18	Abu Nusayr	120.0	169.5	115.4	51.8	18.4	0.2	331.2	7.6	8.2	85.0	18.0	38
19	BadrAl-Jadeedah	200.2	162.6	156.2	39.9	2.7	0.1	216.4	7.2	3.5	70.0	18.0	100
20	Ohoud	53.0	62.9	50.1	10.2	4.2	0.1	188.9	7.8	1.5	30.0	7.0	14
21	Wadi AL- Seer	90.0	160.8	62.3	45.5	9.5	0.1	240.0	7.4	6.2	35.0	18.0	34
22	Tla΄a AL-Ali	53.0	158.7	70.1	31.6	8.2	0.1	244.7	7.5	5.0	50.0	21.0	28
	Mean	99.1	138.6	91.2	40.0	12.3	0.2	322.2	7.6	4.3	57.3	16.6	36.99

2.7 Water Quality Index (WQI) for Drinking Purposes

Water Quality Index has been successfully applied to assess the quality of potable drinking water in recent years due to its importance in understanding the water quality issues by integrating complex data and generating a score that describes water quality status (Othman et al., 2020).

Horton (1965) was first used the concept of WQI then developed by Brown et al. (1970) and improved by Deininger (Scottish development department, 1975). The development of WQI for water quality is described in the various studies (Backman et al., 1998; Stigter et al., 2006; Saeedi et al., 2010; Ramakrishnaiah et al., 2009; Prasada and Siddaraju, 2012) and Krishna Kumar (2015).

The chemistry of drinking water is often used as a tool for discriminating the drinking water quality (Subba Rao, 2006). The water quality index (WQI) is an important parameter for identifying the water quality and its sustainability for drinking purposes (Magesh et al., 2013). WQI is defined as a method of rating that provides a composite influence of individual water quality parameters on the whole water quality (Mitra, 1998).

The water quality index (WQI) was calculated for evaluating the influence of natural and anthropogenic activities based on several key parameters of drinking water chemistry Idris and Aydın (2016). World Health Organization (2011) Guidelines for drinking water quality have been used to calculate the WQI. To calculate the WQI, the weight has been assigned for the physicochemical parameters according to the relative importance of certain parameter to the overall water quality for domestic water purposes. The greatest weight of five (5) was assigned to the parameter nitrate, potassium and total dissolved solids due to its importance in the assessment of water quality; the weight of four (4) has been assigned to the parameters pH,sulfate and total Hardness; the weight of three (3) has been assigned to parameters chloride and bicarbonate; while the weight of two (2) has been assigned to the parameters calcium, and sodium, based on their importance in the quality of water for drinking purposes. Magnesium is assigned the minimum weight of one because it plays a fewer role in the water quality assessment. The relative weight is computed from the equation (Eq.2):

$$Wi = wi \Big/ \sum_{i=1}^{n} wi \quad \text{............} \quad \text{Eq. (2)}$$

Where:
Wi is the relative weight.
wi is the weight of each parameter.
n is the number of parameters.

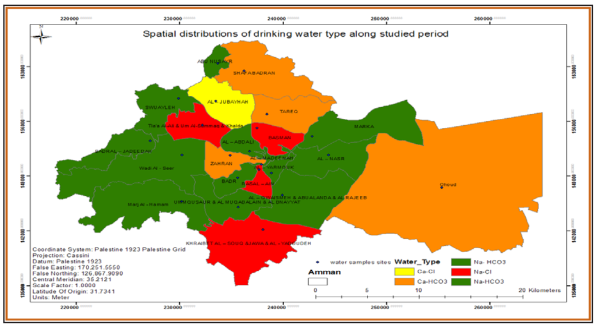

Figure 5. Spatial distributions of water type in the Greater Amman Area.

The quality rating scale for each parameter is calculated by dividing its concentration in each water sample by its respective standards of WHO (2011) and multiplied the results by 100 (Eq.3).

$$qi = \left(\frac{Ci}{Si}\right) * 100 \quad \text{............} \quad \text{Eq. (3)}$$

Where:
qi is the quality rating.
Ci is the concentration of each chemical parameter in each sample in milligrams per liter.
Si is the World Health Organization Guidelines for each chemical parameter in milligrams per liter according to the guidelines of the WHO (2011).

For computing the final stage of WQI, the SI is first determined for each parameter (Eq.4). The sum of SI values gives the water quality index for each sample (Eq.5).

$$SIi = Wi * qi \quad \text{............} \quad \text{Eq. (4)}$$

$$WQI = \sum SIi \quad \text{............} \quad \text{Eq. (5)}$$

Where:
SIi is the sub-index of ith parameter.
qi is the rating based on the concentration of ith parameter.

The relative weight (w_i) was assigned for water quality parameters based on their relative importance on water quality for domestic purposes (Table 2). The computed WQI is shown in Table (3) where the WQI varies from “excellent water” to “good water for potable drinking purposes. The calculation of the WQI for potable water for the five periods from 2012 to 2016 are shown in Figures (6 to 10). The WQI for the whole period from 2012 to 2016 is shown in Figure (11). The WQI in the Greater Amman showed that the WQI for drinking water exceeding the value of 50 increases with time. The water quality of less than 50 is excellent in terms of chemical and physical characteristics and the greater than 50 can be classified as good water quality for drinking purposes. This means that 2012 was the lowest value of 50 and therefore the water quality was better than 2013, 2014 and 2015, but the year 2016 has the worst water quality index.

Table 2. Relative weight of chemical of physiochemical parameters.

Parameter	WHO Guidelines (2011)	Weight (wi)	Relative weight (Wi) $Wi = wi \Big/ \sum_{i=1}^{n} wi$
pH (on scale)	6.5 – 8.5	4	0.114
TH	300-600	4	0.114
TDS (mg/l)	500	5	0.143
HCO_3^- (mg/l)	500	3	0.086
Cl^-(mg/l)	250	3	0.086
SO_4^{2-}(mg/l)	250	4	0.114
NO_3^-(mg/l)	45	5	0.143
Ca^{2+}(mg/l)	75-200	2	0.057
Mg^{2+}(mg/l)	50-150	1	0.029
Na^+(mg/l)	200	2	0.057
K^+(mg/l)	10 – 50	2	0.057
		$\sum wi = 35$	$\sum wi = 1$

Table 3. WQI of water samples during the years 2012- 2016.

ID	Site	WQI/2012	WQI/2013	WQI/2014	WQI/2015	WQI/2016
1	AL-Madeenah	78.9	63.1	52.4	56.1	56.5
2	Swuayleh	59.2	40.4	39.1	50.2	42.3
3	Badr	43.6	47.6	43.8	43.1	41.2
4	AL-Muqabalin	43.6	47.6	44.9	44.8	48.6
5	Ras AL-Ain	59.7	45.7	35.7	45.9	31.9
6	Zahran	69.7	51.5	44.6	49.7	48.3
7	AL-Abdali	60.9	52.1	39.7	51.1	45.8
8	Marj Al-Hamam	52.3	0	40.2	43.9	34.4
9	AL-Yarmouk	43.9	38.2	42.9	46.9	32.5
10	Marka	72.9	54.8	60.5	71.5	62.3
11	Tareq	85.9	27.2	40.1	48.6	52.1
12	AL-Nasr	64.7	41.4	48.8	30.5	33.6
13	AL-Jubayhah	64.3	39.6	32.1	65.5	46.2
14	AL-Qwaismeh	30.3	40.2	30.9	41.9	36.7
15	Khraibet Al- Souq	43.3	33.9	42.5	27.8	43.8
16	Basman	61	43.8	42.3	51.8	42.7
17	Shafa Badran	75.2	25.6	43	35.3	48.1
18	Abu Nusayr	61.4	49.8	49.3	55	37.6
19	BadrAl-Jadeedah	47.6	0	17.6	47.7	17.3
20	Ohoud	0	0	0	26.8	26.9
21	Wadi AL- Seer	0	34.6	19.2	40.9	38.1
22	Tla′a AL-Ali	0	21.1	19	39.4	39

The WQIof twenty-two sampling zones shows lower values which classified as excellent water, and six sampling zones are classified as good water according to the classification of water quality based on WQI values (Table 4). The high value of WQI at these zones has been is attributed mainly to the higher values of TDS, Ca^{2+}, K^{+}, Cl^{-}, HCO_3^{-}, NO_3^{2-} and SO_4^{2-}.

Table 4. Classification of water quality based on WQI values.

Range	Type of water
< 50	Excellent water
50 – 100	Good water
100 – 200	Poor water
200 – 300	Very poor water
> 300	Water unsuitable for drinking purposes

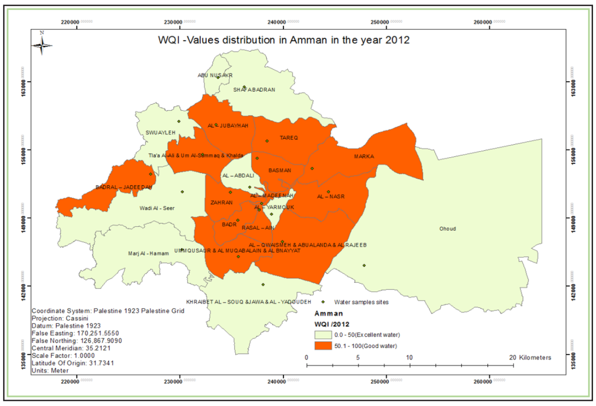

Figure 6. WQI-values in Greater Amman Area in the year 2012.

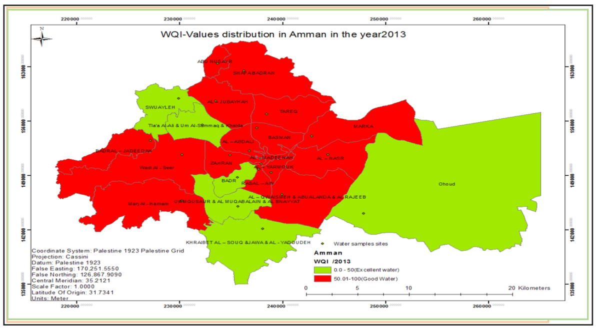

Figure 7. WQI-values in Greater Amman Area in the year 2013.

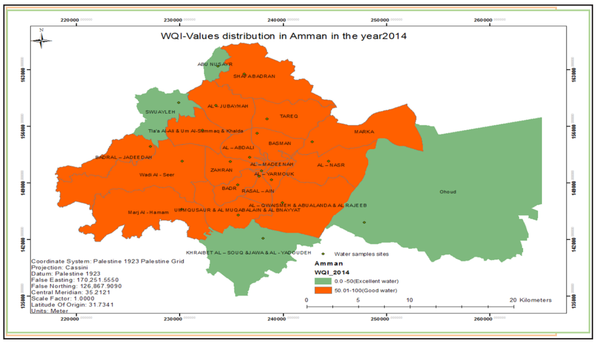

Figure 8. WQI-values in Greater Amman Area in the year 2014.

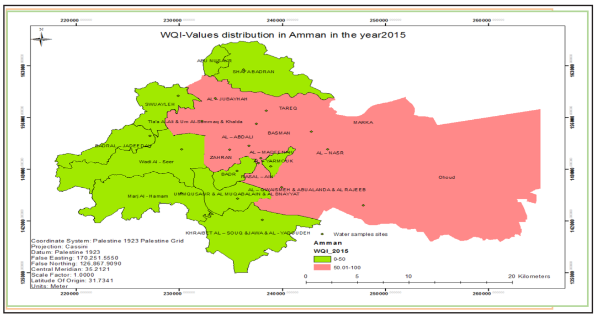

Figure 9. WQI-values in Greater Amman Area in the year 2015.

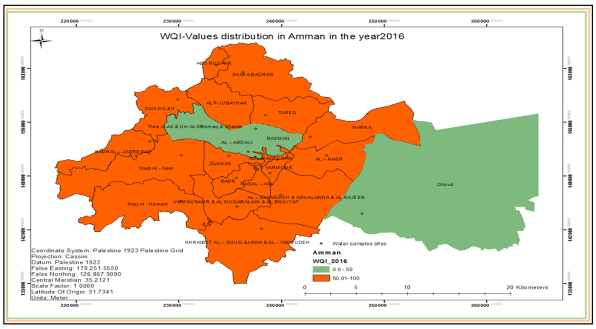

Figure 10. WQI-values in Greater Amman Area in the year 2016.

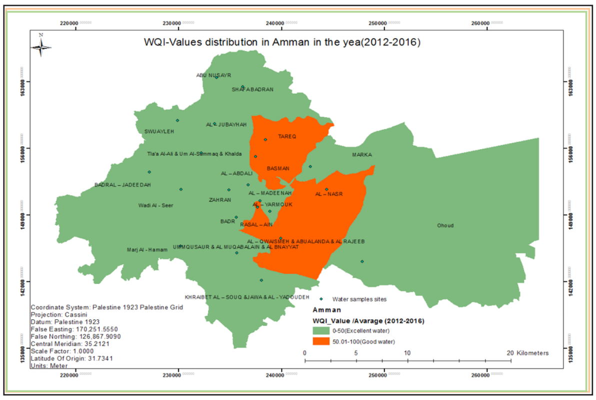

Figure 11. WQI-values in Greater Amman Area during the years 2012-2016.

3. Results and Discussion

Assessment of drinking water quality in a timely requirement where availability of safe water is at risk due to natural and man-made activities. This study conducted in the Greater Amman area to help in measuring drinking water quality using WQI which provide the composite effect of chemical parameters on water quality. The present study is contributing to designing and improving the monitoring programs in the city.

The study findings revealed that drinking water was slightly alkaline, although the ideal pH for human consumption is stated to be 7.6. The maximum permissible limit for pH in drinking water as given by the WHO is 8.5 (WHO, 2011). The values of pH in the drinking water samples in this study varied from 7.2 at Badr AL-Jadeedah to 7.8 at Ohoud with an average value of 7.6. It tends to be alkaline. A controlled pH of water is suggested in WHO guideline to reduce the corrosion and contamination of drinking water having health consequences. This explained higher alkalinity by the presence of two common ions calcium and magnesium, affecting the hardness of the water.

The maximum acceptable and potable limit of TDS value for drinking water of the Jordanian standard1000 mg/l, whereas lower TDS values of drinking water samples (<1000 mg/l) then the TDS values started to increase in the middle of Amman (Zahran, Basman, Bader, Tareq, Abdali, AL-Muqabalin Yarmouk).It is clear that Marka showed the highest TDS of 516.5 ppm value in comparison with other sites where the lowest value of TDS was measured in Ohoud with a value of 188.9 ppm. The average value of TDS was 319.4 ppm.

Turbidity is important because it affects both the acceptability of water to consumers, and the selection and efficiency of treatment processes. Turbidity is measured utilizing electronic meters. The turbidity of water samples in the Greater Amman varies from 0.1 to 0.5 and the maximum turbidity values were reported in Zahran area.

Nitrate is the most available indicator for pollution and it is well-dissolved in water. The concentration of NO_3^- is often an indicator of water deterioration due to agricultural impact. The consumption of water with high nitrate concentration causes several health disorders, such as gastric cancer, goiter, birth malformations and decreasing oxygen-bearing capacity of the blood. The acceptable limit of NO_3^- for drinking water is 50 ppm (WHO, 2011). In the study area, the minimum NO_3 concentration was observed of 2.7 at Badr AL-Jadeedah and a maximum of 25.2mg/l at Marka with an average of 12.3 mg/l. The middle parts of Amman have the highest values comparing to other parts.

The total hardness (TH) of the collected water samples ranges from 62.9 at Ohoud to 190.6 mg/l at Marka with an average value of 138.6 mg/l.According to WHO guidelines, the maximum allowable limit of TH for drinking purposes is 600 mg/l and the most desirable limit is 300 mg/l. The spatial distribution of total hardness concentration of water samples in the Greater Amman area indicated that the middle part of the Greater Amman have the highest values comparing with other parts.

The overall suitability of drinking water was assessed using a combined measure of water quality parameters: the WQI. The water quality index (WQI) was calculated for evaluating the influence of natural and anthropogenic activities based on several key parameters of drinking water chemistry. To calculate the WQI, the weight has been assigned for the physicochemical parameters according to the parameters relative importance in the overall quality of water for drinking water purposes. The assigned weight ranges from 1 to 5. The maximum weight of 5 has been assigned for NO3 and TDS; the weight 4 is assigned for pH, TH and SO_4; the weight 3 is assigned for HCO_3 and Cl; the weight 2 is assigned for Ca, Na and K and the weight 1 is assigned for Mg.

The chemical parameters of water samples were used to calculate the WQI value at each sampling site. The weighted arithmetic WQI method is applied to calculate WQI values. In this method, the permissible WQI value for drinking is considered to be 100, the water quality is considered poor if the value exceeded this acceptable limit. The water quality during the period 2012-2016 was found to good at these sites AL-Madeenah, Marka and Abu Nusayr areas due to low chemical parameter values contributing to lower composite effect on drinking water quality. The water quality was water was classified as excellent for drinking at most sample sites in the Greater Amman area.

The study had some limitations since it would have been better to collect samples throughout the year addressing seasonality. In addition, the testing of drinking water samples from all sites was not possible for this study due to limited resources.

4. Conclusions

The chemical and physical parameters were measured to determine the quality of drinking water of the collected samples in Greater Amman Municipality. The accuracy of the chemical analyses was checked using the charge balance error, which ranges between 0.05 to 5% for all analyzed water samples.

The quality of drinking water was assessed using the WQI which is a tool used for discriminating the water quality. The computed WQI values for twenty-six water sampling zones from different sites of the Greater Amman area were analyzed. The WQI was computed based on the eleven (11) chemical parameters such as nitrate, total dissolved solids, pH, turbidity, sulfate, bicarbonate, chloride, calcium, sodium and potassium and magnesium. The assigned weight for each parameter ranges from 1 to 5 based on their importance for analysis.

The WQI values calculated during the study period showed that the WQI value of more than 50 increases each year more than the preceding year in the different studied areas. Water quality of less than 50 is excellent in terms of chemical and physical characteristics. This means that 2012 was the lowest value of 50 and therefore the water quality was better than 2013, 2014 and 2015, but the year 2016 has the better water quality index which is below 50. It should be noted that these values in all years did not exceed 100 which means the water quality is good in general. The spatial distribution of WQI during the period 2012-2016 for Greater Amman area shows that most of the quality of drinking water in different zones are of excellent water quality which reflects the continuous monitoring by the governmental agencies responsible for the control on the quality of drinking water.

References

Al-Omran, A., Al-Barakah, F., Altuquq, A., Aly, A., Nadeem, M. (2015). Drinking water quality assessment and water quality index of Riyadh, Saudi Arabia. Water Quality Research Journal 50(3): 287–296. DOI: 10.2166/wqrjc.2015.039.

Aquachem Software (2014). Water Quality Analysis Software. Waterloo Hydrogeologic, Inc., Canada.

Backman, B., Bodis, D., Lahermo, P., Rapant, S., Tarvainen, T. (1998). Application of a groundwater contamination index in Finland and Slovakia'' Environmental Geology 36(1–2): 55–64. DOI: 10.1007/s002540050320.

Brown, R., McClelland, N.I. Deininger, R.A., Tozer, R.G. (1970). A water quality index:Do we dare?'' Water and Sewage Works 117(10): 339–343.

Krishna Kumar, S; Logeshkumaran, A; Magesh, N S; Godson, Prince S; Chandrasekar, N. (2015). Hydro-geochemistry and application of water quality index (WQI) for groundwater quality assessment, Anna Nagar, part of Chennai City, Tamil Nadu, India. Applied Water Science 5: 335–343. DOi: 10.1007/s13201-014-0196-4.

Cude, C. Oregon Water Quality Index (2001). A Tool for Evaluating Water Quality Management Effectiveness. Journal of the American Water Resources Association. 37: 125-137. DOI: 10.1111/j.1752-1688.2001.tb05480.x.

Department of Statistics. (2017). "Estimated population of 2017 from CensusData". http://dosweb.dos.gov.jo/population/population-2/. Hashemite Kingdom of Jordan.

Eugene W. Rice. (2012). Standard methods for the examination of water and wastewater 22 ed., 2012.

Ewaid, S.H., Abed, S.A., Kadhum, S.A. (2018). Predicting the Tigris River water quality within Baghdad, Iraq by using water quality index and regression analysis. Environmental Technology and Innovation. 11: 390-398.

García-Ávila, F., Ramos- Fernández, L., Pauta, D., Quezada, D. (2018). Evaluation of water quality and stability in the drinking water distribution network inthe Azogues city, Ecuador. Data in Brief. 18 : 111-123.

Hem, J.D. (1985) Study and Interpretation of the Chemical Characteristics of Natural Water. 3rd Edition, US Geological Survey Water-Supply Paper 2254.

Horton, R.K. (1965). An index number system for rating water quality''Water Pollution Control Federation 37: 300-305.

Idris, B., and Aydin, M. (2016). Water Quality Index (WQI) for Main Source of Drinking Water (Karaçomak Dam) in Kastamonu City, Turkey. Journal of Environmental and Analytical Toxicology 6(5): 1-8. DOI: 10.4172/2161-0525.1000407.

Jordanian Institute for Standards and Metrology (JISM) (2015). Jordan Water Quality Standards (JWQS). Unpublished report.

Jordan Meteorological Department (JMD) (2019). "Annual Report of Jordan Meteorological Department," Amman.

Kalyani, R.A., Rao, S.G., Nageshwarao, B., Thirupathi, B. (2016). Water Quality Index in Four Sites of the Cherlapally Lake, Telangana State. International Journal for Innovative Research in Science and Technology 3: 66-73.

Lateef, K. (2011). Evaluation of groundwater quality for drinking purpose for tikrit and samarra cities using water quality index. Lateef KH (2011) Evaluation of groundwater quality for drinking purpose for Tikrit and Samarra cities using water quality index. European Journal for Science Researchs 58(4): 472–481.

Magesh, N., Krishna, K., Subbiah, N., Chandrasekar, N. (2013). Groundwater quality assessment using WQI and GIS techniques, Dindigul district, Tamil Nadu, India . Arabian Journal of Geosciences 6: 4179–4189 . DOI: 10.1007/s12517-012-0673-8.

Mitra, B.K. (1998): Spatial and temporal variation of groundwater quality in sand dune area of Aomori Prefecture in Japan'' ASABE Member (1998).

Maurice, B., Maheux, A., Picard, F. (2008). Analytical comparison of nine PCR primer sets designed to detect the presence of Escherichia coli/Shigella in water samples.

Ministry of Water and Irrigation (MWI) (2017). Jordan Water Sector Facts and Figures. 30pp.

Ochuko, U., Thaddeus, O., Oghenero, O.A., John, E.E. (2014). A comparative assessment of water quality index (WQI) and suitability of river Ase for domestic water supply in urban and rural communities in Southern Nigeria. International Journal of Humanities and Social Science 4(1): 234–45.

Othman, F., Alaaeldin, M., Seyam, M., Najah, A., Fang, A. Teo, Y. (2020). Efficient river water quality index prediction considering minimal number of inputs variables. Engineering Applications of Computational Fluid Mechanics 14(1): 751-763, DOI: 10.1080/19942060.2020.1760942.

Ponsadailakshmi, S., Sankari, S. G., Prasanna, S.M. Madhurambal, G. (2018). Evaluation of water quality suitability for drinking using drinking water quality index in Nagapattinam district, Tamil Nadu in Southern India. Groundwater for Sustainable Development. 6: 43-49.

Prasada, A.G. and Siddaraju, K. (2012) Application of CCME Water Quality Index (CWQI) to the Lakes of Mandya, Karnataka State, India. Online International Interdisciplinary Research Journal 2 (1): 108-114.

Ramakrishnaiah, C.R., Sadashivaiah, C., Ranganna, G. (2009): Assessment of Water Quality Index for the Groundwater in Tumkur Taluk, Karnataka State, India. E-Journal of Chemistry 6: 523-530.

Saeedi, M., Abessi, O., Sharifi, F., Meraji, H. (2010): Development of groundwater quality index. Environ Monit Assess 163:327–335.

Selvam, S., Venkatramanan, S., and Singaraja, C. (2015): A GIS-based assessment of water quality pollution indices for heavy metal contamination in Tuticorin Corporation, Tamilnadu, India. Arabian Journal of Geosciences 8(12). DOI 10.1007/s12517-015-1968-3.

Shala, A., Durmishi, B., Sallaku, F., Çadraku, H., Fetoshi, O., Ymeri, P., Bytyçi, P. (2020). Assessment of water quality of Sitnica River by using water quality index (WQI). Rasayan Journal of Chemistry 13(1): 146 - 159. DOI: 10.31788/RJC.2020.1315344.

Stambuck-Giljanovic, N. (1999): Water quality evaluation by index in Dalmatia. Water Resources 33(16): 2440–3423.

Stigter, T.Y., Ribeiro, L., Carvalho, Dill, A.M.M. (2006). Evaluation of an intrinsic and a specific vulnerability assessment method in comparison with groundwater salinisation and nitrate contamination levels in two agricultural regions in the south of Portugal. Journal of Hydrogeology 14(1–2): 79–99. DOI:10.1007/s10040-004-0396-3.

Subba Rao N (2006) Seasonal variation of groundwater quality in a part of Guntur district, Andhra Pradesh, India. Environ Geol 49:413–429.

Tiwari, T.N. and Mishra, M.A. (1985): A Preliminary Assignment of Water Quality Index of Major Indian Rivers. Indian Journal of Environmental Protection 5: 276-279.

WHO (2011) Guidelines for Drinking Water Quality. 4th edn. World Health Organization, 20 Avenue Appia, 1211 Geneva 27, Switzerland.

JJEES

JJEES (2021) 12 (4): 315-325
ISSN 1995-6681

Jordan Journal of Earth and Environmental Sciences

Review of the Early/Middle Eocene biostratigraphy and paleoenvironment of the Rus Formation and Wadi Al Nahayan Member of the Dammam Formation, western limb of Jabal Hafit, United Arab Emirates

Haidar Anan

Emeritus, Former Vice President for Academic Affairs, Al Azhar University-Gaza

Received 29 January 2021; Accepted 28 March 2021

Abstract

The present study presents an amended two planktic foraminiferal biozones using the modified ranges of *Acarinina cuneicamerata* and *Turborotalia frontosa* index species from sixteen species of six genera throughout E7a,b biozone, and revised calibration datum of the Early/Middle Eocene (EME) bioevent in the western limb of Jabal Hafit, Al Ain area, United Arab Emirates (UAE). Sixteen planktic foraminiferal diagnostic species are recorded and illustrated from the upper part of the Rus Formation (late Early Eocene = late Ypresian, E7a) and the lower part of the Wadi Al Nahayan Member of the Dammam Formation (early Middle Eocene = early Lutetian, E7b).

Keywords: Eocene, Biostratigraphy, Paleoenvironment, Rus Formation, Dammam Formation, Jabal Hafit, UAE.

1. Introduction

The present paper is a continuation of the studies concerned with the complete record of the foraminiferal content of the Paleogene rocks in the Al Ain area of the United Arab Emirates (UAE), particularly Jabal Hafit which located to the southwest of Al Ain city, and represents the third part of the sequence outcropping in the western limb in Jabal Hafit: the top Early Eocene (Anan, 1996) and the Early/Middle Eocene (EME) sequence (Anan, 2015a). Jabal Hafit is located to the southeast of Al Ain city, Emirate of Abu Dhabi, UAE (Figure 1).

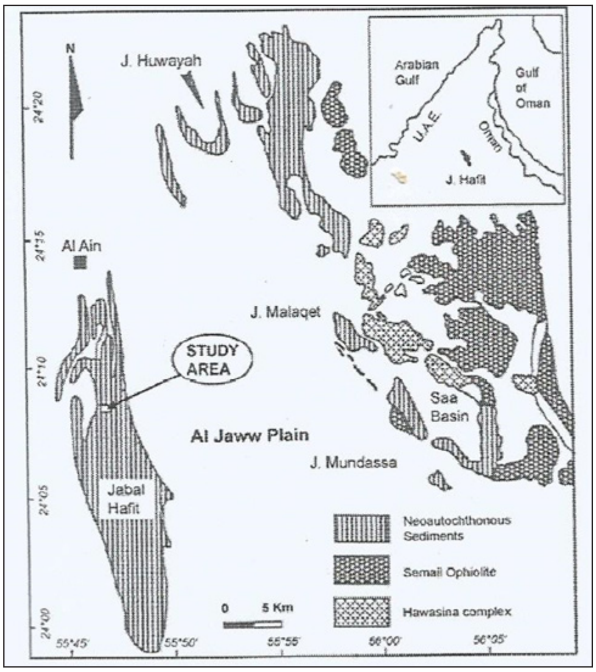

Figure 1. Location map of Al Ain area , UAE including Jabal Hafit (west of Al Jaww Plain), J. Malaqet and J. Mundassa, east Al Jaww Plain (after Anan, 2015a).

The base Middle Eocene succession (about 17 m thick) is located about 5m above the upper Early Eocene intraformational conglomeratic bed in K4 (about 50 m thick), along the asphalted road climbing to the top of the Jabal at the western limb of Jabal Hafit anticline (Figure 2). The previous studies of Cherif et al. (1992), Anan et al. (1992), Anan (1996, 2015a, b), Boukhary et al. (2006) on the planktic, nummulitic foraminifera and nannoplankton content around the EME boundary in Jabal Hafit are pertinent to the present study. The paleontology, stratigraphy, paleoenvironment and also the lacuna around the EME boundary in UAE and some other parts in the Tethys are presented.

2. Material of study

Eighteen soft marl and gypsiferous shale samples alternated with other hard and Nummulitic and Alvelinid large benthic foraminiferal beds were collected from the inclined succession of the Early-Middle Eocene rocks of the western limb of Jabal Hafit (Lat. 24° 4’ 40’’ N, Long. 55° 46’ 54’’ E), which is located to the south of Al Ain city, and exposed along the asphalted road climbing to the top of the Jabal with about 70 m thick in K4 (Figure 3). The study gypsiferous shale and marl samples yield well-preserved and diverse planktic foraminiferal assemblage and have supplied the morphotype of the illustrated sixteen species of six genera.

* Corresponding author e-mail: profanan@gmail.com

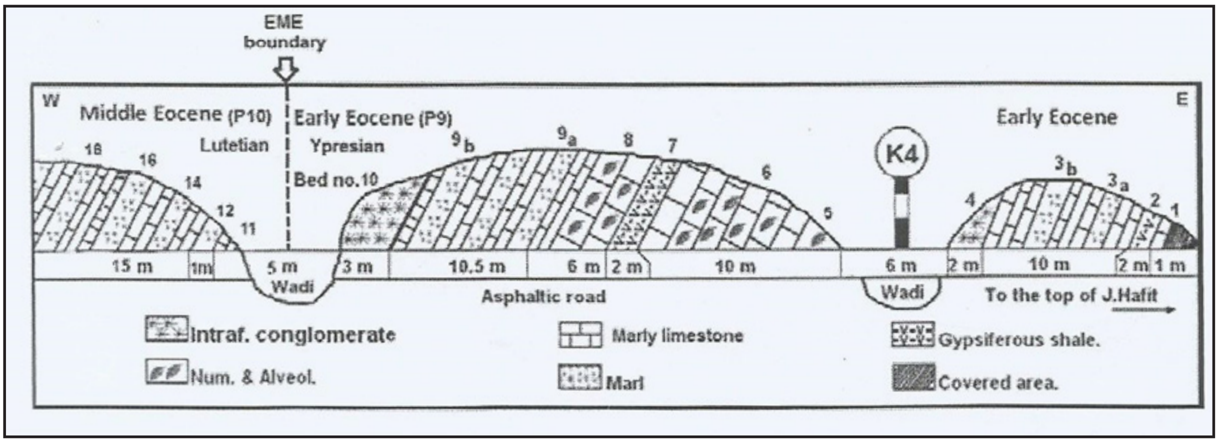

Figure 2. Schematic section of the Early/Middle Eocene succession at K4 of J. Hafit (after Anan, 2015a).

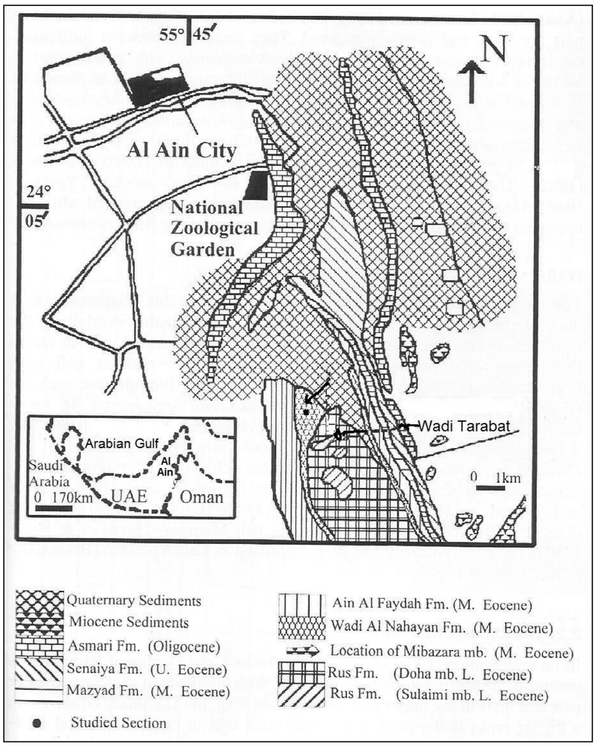

Figure 3. Geologic map of Jabal Hafit (UAE) including the study section of the Middle Eocene Wadi Al Nahayan Member of the Dammam Formation (after Hamdan and Bahr, 1992) outcropping at the western limb of Jabal Hafit (after Boukhary et al., 2006).

3. Stratigraphy

According to Payros et al. (2007), an attempt is made at a new Ypresian/Lutetian boundary biomagneto chronology based on data from the Gorrondatxe section, which shows that the boundary between Zones P9 (=E7, approximately) and P10 (=E8, approximately) is 3.1 Myr younger than hitherto considered, and the duration of the Early Eocene, most commonly defined according to this planktic foraminiferal zonal boundary, has generally been underestimated over the last four decades. After that, Molina et al. (2011) noted that it was conceptually agreed that the Lutetian GSSP should be placed somewhere in the interval between the top of the historical Ypresian Stage defined in Belgium and the bottom of the historical Lutetian Stage stratotype defined in Paris. A major problem to this end is the scarcity of continuous sections at the Ypresian/Lutetian transition due to the large offlap/sea level fall event that cuts out part or all of the NP13/14 calcareous nannofossil interval in many sections. Consequently, the Ypresian/Lutetian boundary interval is represented by a hiatus in most sections worldwide (see Anan, 2015b).

The stratigraphic succession exposed in the northern part of Jabal Hafit (UAE) ranges from Early Eocene to Miocene (Figure 3). The basal Middle Eocene succession (Wadi Al Nahayan Member of the Dammam Formation) is represented by a thick sequence of limestone, marl and shale intercalation. The lower Eocene rocks (Ypresian) belong to Hili Member of the Rus Formation (after Hamdan and Bahr, 1992). It is represented by a thick sequence of bedded limestone with flint in the lower part and marl intercalation in the upper part (about 50m), which ends by an intraformational conglomeratic bed (Figure 4).

Figure 4. The late Early Eocene intraformational conglomeratic bed at EME boundary in K4, western limb of J. Hafit, UAE.

On the other hand, Boukhary et al. (2006) noted that the diagnostic conglomeratic bed (around the Ypresian and Lutetian) yields large benthic foraminiferal assemblage as *Assilina spira, Somalina praestefaninii* and *Nummulites perplxus* similar to the basal Lutetian assemblage of Italy and regarded this conglomeratic bed as a new member (Mibazara Member) in the Middle Eocene Wadi Al Nahayan Formation of the Dammam Group (Figure 5). The lower Eocene rocks (Ypresian) belong to Hili Member of the Rus Formation (after Hamdan and Bahr, 1992).

Figure 5. The early Middle Eocene Mibazara Member of the Dammam Formation overly the late Early Eocene Rus Formation, according to Boukhary et al. (2006).

Based on the stratigraphic distribution of the planktic foraminiferal species of the Early/Middle Eocene (EME)(= Ypresian/Lutetian, Y/L) boundary in K4, two biozones are recognized, from base to top (after Anan, 1966, 2015a): the late Early Eocene *Acarinina pentacamerata* Zone (P9 of Blow, 1969 = E7 of Berggren and Pearson, 2006), and early Middle Eocene *Hantkenina nuttalli* Zone (P10=E8), or *Acarinina bullbrooki* Zone, or *Subbotina frontosa* Zone as treated in UAE (Anan, 2015a). The planktic foraminifera zonation around EME boundary is adapted here to accommodate the modern studies of some authors, i. e. Wade et al. (2011) and Karoui-Yaakoub et al. (2015) for the late Ypresian to become: *Acarinina pentacamerata* (E6), *Acarinina cuneicamerata* (E7a) and the lowest part of *Turborotalia frontosa* (E7b) biozones, while the early Lutetian biozones are: the upper part of *Turborotalia frontosa* (E7b) and *Guembelitrioides nuttalli* (E8).

4. Planktic foraminiferal biostratigraphy

Amendment to the planktic foraminiferal assemblages around the EME biozones in the present study are diversified and enable the biozones of *Acarinina cuneicamerata* (E7a) and *Turborotalia frontosa* (E7b):

E7a: *Acarinina cuneicamerata* Lowest-occurrence Subzone (top Early Eocene), which definedasinterval between the LO (lowest occurrence) of the nominate taxon *Acarinina cuneicamerata* and the LO *Guembelitrioides nuttalli*. According to Karoui-Yaakoub et al. (2015) the upper boundary is detected also by the LO of *Turborotalia frontosa* and *Acarinina bullbrooki*.

E7b: *Turborotalia frontosa* Lowest-occurrence Subzone (topmost Early Eocene to lowest Middle Eocene), which defined as the interval between the LO of the nominate taxon *Turborotalia frontosa* and the *LO Guembelitrioides nuttalli*.

5. Taxonomy and systematic description

The taxonomy followed here is that of Pearson et al. (2006). The stratigraphic distribution of the planktic foraminiferal species around the EME of Jabal Hafit is presented in Table 1. Two species of *Morozovella (M. caucasica and M. crater)* are restricted in the top Ypresian and don't cross the EME boundary. The other nine species *(Morozovella aragonensis, Parasubbotina inaequispira, Subbotina linaperta, S. yeguaensis, Acarinina bullbrooki, A. cuneicamerata, A. pentacamerata, A. praetopilensis and Pseudohastigerina micra)* are recorded in the top Ypresian and continue in the base Lutetian. Five species *(Subbotina eocaena, S. hagni, S. patagonica, Acarinina berwaliana and Turborotalia frontosa)* appear only in the base Lutetian (illustrated in Plate 1).

Table 1. The planktic foraminiferal distribution in the Early-Middle Eocene transition of the western limb of J. Hafit, Al Ain area, UAE. The neglected samples (see Figure 2) are related to hard limestone or nummulitic limestone beds (don't yields planktic foraminifer), - = not recorded, x= recorded species. Θ = illustrated species.

no	Early-Middle Eocene Planktic foraminiferal Species		Western Limb of Jabal Hafit														
		Bed no.	1					2					3				
		Sample no.	2	3a	3b	4	5	6	7	8	9a	9b	10	12	14	16	18
1	Parasubbotina	inaequispira	x	x	x	-	-	-	x	-	x	x	-	Θ	x	x	x
2	Subbotina	eocaena	-	-	-	-	-	-	-	-	-	-	-	Θ	x	x	x
3		hagni	-	-	-	-	-	-	-	-	-	-	-	Θ	x	x	x
4		linaperta	x	x	Θ	-	-	-	x	-	x	x	-	x	x	x	x
5		patagonica	-	-	-	-	-	-	-	-	-	-	-	x	Θ	x	x
6		yeguaensis	x	x	x	-	-	-	x	-	-	-	-	x	Θ	x	x
7	Acarinina	berwaliana	-	-	-	-	-	-	-	-	-	-	-	Θ	x	x	x
8		bullbrooki	x	x	x	-	-	-	x	-	x	x	-	Θ	x	x	x
9		cuneicamerata	x	x	x	-	-	-	x	-	x	Θ	-	-	x	x	x
10		pentacamerata	x	x	x	-	-	-	x	-	-	Θ	-	x	x	x	x
11		praetopilensis	x	x	x	-	-	-	x	-	x	Θ	-	-	-	-	-
12	Morozovella	aragonensis	x	x	x	-	-	-	x	-	x	x	-	x	x	Θ	x
13		crater	x	Θ	x	-	-	-	x	-	x	x	-	-	-	-	-
14		caucasica	x	x	x	-	-	-	x	-	Θ	x	-	-	-	-	-
15	Turborotalia	frontosa	-	-	-	-	-	-	-	-	-	-	-	Θ	x	x	x
16	Pseudohastigerina	micra	Θ	x	x	-	-	-	x	-	x	x	-	x	x	x	x

Genus Parasubbotina Olsson et al., 1992
Type species *Globigerina pseudobulloides* Plummer, 1926

***Parasubbotina inaequispira* (Subbotina, 1953)**
Pl. 1, fig. 1

1953 *Globigerina inaequispira* Subbotina, p. 84, pl. 6, fig. 1.
2006b *Parasubbotina inaequispira* (Subbotina) - Olsson et al., p. 101, pl. 5.11, figs. 1-15.
2017 *Parasubbotina inaequispira* (Subbotina) - Seferinov, p. 79, pl. 1, figs. 5-6.

This species has low trochospiral test with 4-4½ globular well separated chambers in the final whorl, umbilical aperture with lip. It is recorded around the EME boundary of J. Hafit, UAE.

Genus *Subbotina* Brotzen and Požaryska, 1961
Type species: *Globigerina triloculinoides* Plummer, 1927

***Subbotina eocaena* (Gümbel, 1868)**
Pl. 1, fig. 2

1868 *Globigerina eocaena* Gümbel, p. 662, pl. 2, fig. 109.
1992 *Subbotina eocaena* (Gümbel) - Cherif et al., p. 46, pl. 1, fig. 36.
1995 *Globigerina eocaena* Gümbel - Anan, p. 8, pl. 1, fig. 10.
2006a *Globigerina eocaena* Gümbel - Olsson et al., p. 134, pl. 6.9, figs. 1-16.
2018 *Subbotina eocaena* (Gümbel) - Wade et al., p. 315, pl. 10. 3, figs. 1-16.

This species was originally described from the MLE rocks in Texas, and later found in some localities of the Tethys (Italy, Egypt, UAE, India, Australia). Berggren, 1965 (after Subbotina, 1960) considered that the Early-Late Eocene S. eocaena has evolved from the Early Eocene *S. pseudoeocaena* (Subbotina). Olsson et al. (2006a) noted that *S. eocaena* is closely related Eocene large-sized subbotinids, which includes *S. hagni* (Gohrbandt, 1967) and S. corpulenta (Subbotina, 1953). It is recorded from the early Middle Eocene (EME) of Jabal Hafit.

***Subbotina hagni* (Gohrbandt, 1967)**
Pl. 1, fig. 3

1967 *Globigerina hagni* Gohrbandt, p. 324, pl. 1, figs 1-3.
2002 *Subbotina hagni* (Gohrbandt) - Hancock et al., p. 40.
2006a *Subbotina hagni* (Gohrbandt) - Olsson et al., p. 142, pl. 6.11, figs. 1-17.
2020 *Subbotina hagni* (Gohrbandt) - Anan, p. 10, pl. 1, fig. 3.

This species was originally described from the Middle Eocene of Austria, and later found in some parts of the Tethys (Austria, Bulgaria, Egypt, UAE, Australia). It is recorded herein from the EME of Jabal Hafit.

***Subbotina linaperta* (Finlay, 1939)**
Pl. 1, fig. 4

1939 *Globigerina linaperta* Finlay, p. 125, pl. 13, figs. 54-57.
1976 *Globigerina* (Eoglobigerina) linaperta Finlay - Hillebrandt, p. 331, pl. 1, figs. 14-15.
1980 *Subbotina linaperta* (Finlay) - Barr and Berggren, p. 185, pl. 2, fig. 19.
2006a *Subbotina linaperta* (Finlay) - Olsson et al., p. 149, pl. 6.14, figs. 1-16.
2020 *Subbotina linaperta* (Finlay) - Anan, p. 10, pl. 1, fig. 5.

This species was originally described from the Paleocene-Middle Eocene rocks in Trinidad, and later in other localities of the Tethys (Spain, Italy, Egypt, UAE, Qatar, India, Indian Ocean, New Zealand). It is considered as a basic stock for all Eocene Globigerinids by some authors (Stainforth et al., 1975; Haggag and Luterbacher, 1991 and Anan, 1995). Olsson et al. (2006a) considered this species belongs to a tightly coiled subbotinids, which includes *S. angiporoides* (Hornibrook, 1965) and *S. patagonica* (Todd and Kniker, 1952), which may be derived from the latter species. It is recorded around the EME rocks of Jabal Hafit.

***Subbotina patagonica* (Todd and Kniker, 1952)**
Pl. 1, fig. 5

1952 *Globigerina patagonica* Todd and Kniker, p. 26, pl. 4, fig. 32.
2006a *Subbotina patagonica* (Todd and Kniker) - Olsson et al., p. 154, pl. 6.15, figs. 1-16.
2019 *Subbotina patagonica* (Todd and Kniker) - Solé et al., p. 1047, figs. 4-5.

This species was originally recorded from the Early Eocene of Chile, and later of London clay and the Indian Ocean as noted by Olsson et al. (2006a). It is characterized by its compact low trochospiral test, the final chamber making up about ½ the test and semicircular aperture. It is recorded here, for the first time, from the EME rocks of Jabal Hafit.

***Subbotina yeguaensis* (Weinzierl and Applin, 1929)**
Pl. 1, fig. 6

1929 *Globigerina yeguaensis* Weinzierl and Applin, p. 409, pl. 43, fig. 1.
2006b *Subbotina yeguaensis* (Weinzierl and Applin) - Olsson et al., p. 162, pl. 6.18, figs. 1-16.
2017 *Subbotina yeguaensis* (Weinzierl and Applin) - Seferinov, p. 90, pl. 3, figs. 6-7.

This species was originally recorded from the Middle Eocene of Yegua Formation, USA. Olsson et al. (2006b) considered the figured form of G. p. pseudoeocaena Subbotina (1953) as a junior synonym of *Subbotina yeguaensis* Krasheninnikov and Hoskins (1973) include two other subspecies *G. pseudoeocaena compacta* and *G. pseudoeocaena trilobata* in the species concept of G. p. pseudoeocaena Subbotina. It is recorded around the EME rocksof J. Hafit.

Genus *Acarinina* Subbotina, 1953
Type species: *Acarinina acarinata* Subbotina, 1953

***Acarinina berwaliana* (Mohan and Soodan, 1969)**
Pl. 1, fig. 7

1969 *Globorotalia berwaliana* Mohan and Soodan, p. 9, text-fig. 1 A-F.
2015a *Acarinina berwaliana* (Mohan and Soodan) - Anan, p. 13, pl. 1, fig. 2.

This species was originally recorded in the early Middle Eocene *Hantkenina aragonensis* Zone (=*H. nuttalli* Zone, P10) in the Kutch, India and continue in the younger zone. Berggren et al. (2006) treated this species as a doubtful species of *Acarinina cuneicamerata* (Blow). It is regarded here as a separate species, and recorded from the EMEof Jabal Hafit.

***Acarinina bullbrooki* (Bolli, 1957)**
Pl. 1, fig. 8

1957 *Globorotalia bullbrooki* (Bolli), p. 167, pl. 38, fig. 5.
1996 *Acarinina bullbrooki* (Bolli) - Anan, p. 158, fig. 6.9.
2006 *Acarinina bullbrooki* (Bolli) - Berggren et al., p. 269, pl. 9.6, figs. 1-16.
2020 *Acarinina bullbrooki* (Bolli) - Alhejoj et al., p. 5, fig. 2.Z.

This species was originally described from the Early-Middle

Eocene (EME) succession of Trinidad, and found later in some localities of the Tethys (Tunisia, Egypt, Jordan, UAE). Berggren et al. (2006, p. 271) treated *Acarinina spinuloinflata* (Bandy) as a junior synonym of *A. bullbrooki*. It is recorded around the EME rocks of Jabal Hafit.

***Acarinina cuneicamerata* (Blow, 1979)**

Pl. 1, fig. 9

1979 *Globorotalia (Acarinina) cuneicamerata* Blow, p. 924, pl. 146, figs. 6-8.

2006 *Acarinina cuneicamerata* Blow - Berggren et al., p. 280, pl. 9.9, figs. 1-16.

2019 *Morozovella cuneicamerata* (Bolli) - Solé et al., p. 1047, fig. 4. 4.

This EME species is characterized by its 5-6 subtriangular to wedge-shaped cuneiform chambers in the last whorl than 4-4½-5 subangular chambers in Early Eocene *A. angulosa.* Berggren et al. (2006) noted that *A. cuneicamerata* probably evolved from *A. angulosa*. The illustrated forms of the latter species by Anan (2015a) and Karoui-Yaakoub et al. (2015) are closely related to *A. cuneicamerata*.

***Acarinina pentacamerata* (Subbotina, 1947)**

Pl. 1, fig. 10

1947 *Globorotalia pentacamerata* Subbotina, p. 128, pl. 7, figs. 12-17, pl. 9, figs. 24-26.

1953 *Acarinina pentacamerata* (Subbotina) - Subbotina, p. 233, pl. 23, fig. 8, pl. 24, fig. 6.

2015a *Acarinina pentacamerata* (Subbotina) - Anan, p. 14, pl. 1, fig. 5.

This species was originally described from the Middle Eocene in Caucasus, and found later in many localities of the Tethys (UAE, Egypt, Tunisia, Spain, Mexico). A. pentacamerata Zone (P9) represents the top EarlyEocene zone in Jabal Hafit (after Blow, 1969), and represents the pre-top Early Eocene zone (E7) for Berggren et al. (2006). It is recorded in samples around the EME boundary of Jabal Hafit.

***Acarinina praetopilensis* (Blow, 1979)**

Pl. 1, fig. 11

1979 *Globorotalia (Truncorotaloides) topilensis praetopilensis* Blow, p. 1043, pl. 155, fig. 9.

2006 *Acarinina praetopilensis* Blow - Berggren and Pearson, p. 300, pl. 9.16, figs. 1-16.

2020 *Acarinina praetopilensis* Blow - Alhejoj et al., p. 5, fig. 2. AC.

This species was recorded in the South Atlantic and Southern Tethys (Egypt, Jordan, UAE) from E7-E12 Zones. The figured specimens from Egypt (Youssef et al., 1983) and UAE of Anan (1996, 2015a) as *Acarinina triplex* is closely related to *A. praetopilensis.* It is recorded around the EME rocks of Jabal Hafit.

Genus Morozovella McGowran, 1968

Type species: *Pulvinulina velascoensis* Cushman, 1925

***Morozovella aragonensis* (Nuttall, 1930)**

Pl. 1, fig. 12

1930 *Globorotalia aragonensis* Nuttall, p. 288, pl. 24, figs. 6-11.

1976 *Globorotalia (Morozovella) aragonensis* Nuttall - Hillebrandt, p. 348, pl. 4, figs. 2- 5.

1980 *Morozovella aragonensis* (Nuttall) - Barr and Berggren, p. 185, pl. 2, fig. 6.

2006 *Morozovella aragonensis* (Nuttall) - Berggren and Pearson, p. 349, pl. 11.3, figs. 1-16.

2020 *Morozovella aragonensis* (Nuttall) - Alhejoj et al., p. 5, fig. 2.W.

This species was originally described from the EME rocks in Mexico and found later in some localities of the Tethys (Spain, Tunisia, Egypt, UAE, Australia). Toumarkine and Luterbacher (1985) noted that one branch of *Morozovella subbotinae* lineage develops to a series of species starting with *M. lensiformis*, evolving towards *M. aragonensis*. Berggren and Pearson (2006) regarded that this species evolved from *M. lensiformis* and does not appear to have left any descendants. This species is recorded around the EME boundary of Jabal Hafit.

***Morozovella crater* (Hornibrook, 1958)**

Pl. 1, fig. 13

1958 *Globorotalia crater* Hornibrook, p. 33, pl. 1, figs. 3-5.

1996 The transitional form between *M. lensiformis and M. caucasica* - Anan, p. 154, fig. 5.11.

2006 *Morozovella crater* Hornibrook - Berggren and Pearson, p. 358, pl. 11.5, figs. 1-16.

2015a *Morozovella* sp. 2 - Anan, p. 24, pl. 1, fig. 9.

2019 *Morozovella* crater Hornibrook - Sharma et al., p. 2, pl. 1, figs. 4-5.

This species has plano-convex test, 4½-5 chambers in the last whorl, thickened circumumbilical rim of elevated chamber shoulders. It evolved from *M. lensiformis* and evolved into *M. caucasica* as noted earlier by Anan (1996) and later Berggren and Pearson (2006). It is recorded in the top Early Eocene of Jabal Hafit.

***Morozovella caucasica* (Glaessner, 1937)**

Pl. 1, fig. 14

1937 *Globorotaliaaragonensis* Nuttall var. caucasica Glaessner, p. 31, pl. 1, fig. 6.

1996 *Morozovella caucasica* Glaessner - Anan, p. 154, fig. 5. 9,10.

2006 *Morozovella caucasica* Glaessner - Berggren and Pearson, p. 354, pl. 11.4, figs. 1-16.

2018 *Morozovella caucasica* Glaessner - Seferinov, p. 41, pl. 2, figs. 11-13.

This species was described originally from the Early Eocene of Caucasus, but around EME boundary in some localities in the Tethys (i. e. Mexico, Spain, Qatar, Australia). Stainforth et al. (1975), Hillebrandt (1976), Haggag and Luterbacher (1991), Anan (1996, 2015a) and Molina et al. (2000) noted that this species restricted only in the Early Eocene, while it was found also in the early Middle Eocene in some localities in the Tethys by some authors, i. e.: Blow (1969), Toumarkine and Luterbacher (1985), Pearson (1993). As noted by Anan (2015b) its absence in many localities in the Tethys (Australia, New Zealand, India, Turkey, Arabia, Egypt, Libya, France, Bulgaria, Spain, USA, Argentina, Chile) most probably due to a lacuna (*pentacamerata* event of Anan, 2015b) around the EME boundary. It is recorded in the top Early Eocene of Jabal Hafit.

Genus *Turborotalia* Cushman and Bermúdez, 1949

Type species: *Globorotalia centralis* Cushman and Bermúdez, 1937

***Turborotalia frontosa* (Subbotina, 1953)**

Pl. 1, fig. 15

1953 *Globigerina frontosa Subbotina*, p. 84, pl. 12, fig. 3.

1980 *Subbotina frontosa* (Subbotina) - Barr and Berggren, p. 185, pl. 2, fig. 18, pl. 5, fig. 16.

1985 *Turborotalia cerroazulensis frontosa* (Subbotina) -

Toumarkine and Luterbacher, p. 136, fig. 34. 11.
2005 T*urborotalia frontosa* (Subbotina) - Mukhopadhyay, p. 37, pl. 1, figs. 1-7, pl. 3, fig. 20.
2020 *Turborotalia frontosa* (Subbotina) - Alhejoj et al., p. 5, figs. 2. AF, AG.
This species was originally described from the EME rocks in Caucasus, and later found in some localities of the Tethys (Italy, Libya, Egypt, UAE, India, Australia). Toumarkine and Luterbacher (1985) treated it as the first member of the *Turborotalia cerroazulensis* lineage *(Subbotina frontosa-Turborotalia cerroazulensis cunialensis lineage).* It is recorded here from the EME rocks of Jabal Hafit.

Genus *Pseudohastigerina* Banner and Blow, 1959
Type species: Nonion micrus Cole, 1927
Pseudohastigerina micra **(Cole, 1927)**
Pl. 1, fig. 16

1927 *Nonion micrus* Cole, p. 22, pl. 5, fig. 12.
1953 *Globigerinella micra* (Cole) - Subbotina, p. 122, pl. 13, figs. 16-17.
1956 *Globanomalina ovalis* Haque, p. 147, pl. 14, fig. 3.
1959 *Pseudohastigerina micra* (Cole) - Banner and Blow, p. 19, pl. 3, fig. 6, text-figs. 4 g—i.
2018 *Pseudohastigerina micra* (Cole) - Seferinov, p. 46, pl. 3, figs. 7-8.
This species was originally described from the Early Eocene-Early Oligocene succession in Mexico, and later from some localities of the Tethys (Spain, Bulgaria, Libya, Egypt, UAE, Pakistan, India). Loeblich and Tappan (1988) noted that the illustrated topotype specimens of *Globanomalina ovalis* Haque (1956) as well as the topotype of *Nonion micrus* Cole (1927) show no appreciated differences and are regarded as congeneric. It is recorded around the EME rocks of Jabal Hafit.

6. The Ypresian/Lutetian (Y/L) boundary in the UAE

1. Anan (1996) suggested that the intraformational conglomeratic bed at the top Lower Eocene succession of Jabal Hafit (Fig. 4) is likely an indicator of a hiatus between the Lower Eocene and Middle Eocene succession at Jabal Hafit. This tectonic event which synchronous with the active tectonic and eustatic sea-level changes at the end of the Ypresian (Vail et al., 1977; Haq et al., 1987). This bed was deposited as submarine debris flows in the basin, not as subaerial denudation, which and has a homogenous thickness, about 3 m. Moreover, Anan (1996) studied in detail the foraminiferal assemblage of the Lower Eocene section at K4 which consists of about twenty alternating soft and hard beds of about seventy m thick. The intraformational conglomeratic bed (which consists of angular to subangular limestone detritus of different sizes with fine-grained marl matrix) ends the Lower Eocene rocks in this section (=Mibazara Member of Boukhary et al., 2006), and represents the lithological indicator for the EME lacuna which associated with the major sea-level lowering of Vail et al., 1977 (Figure 6), besides the faunal gap of some diagnostic planktic species, especially the existence of *Morozovella caucasica* only in the Lower Eocene rocks, but its absence in the younger Middle Eocene horizon.

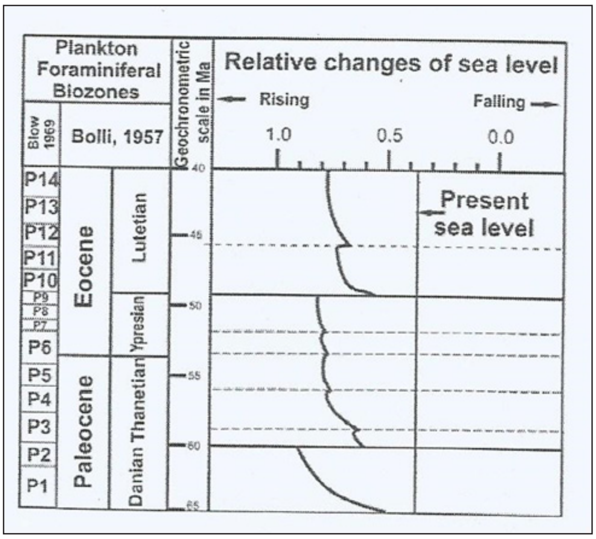

Figure 6. The Ypresian/Lutetian boundary relative to the global sea level fluctuation of Vail et al. (1977).

2. Boukhary et al. (2006) found rich large benthic foraminiferal species in the fine reddish matrix of marly limestone carbonates which cements the conglomerate clastic in the intraformational conglomeratic bed. These taxa are *Assilina spira abrardi, Somalina praestefaninii and Nummulites perplxus,* which are similar to the basal Lutetian assemblage of Italy. Consequently, these authors considered this conglomeratic bed as representing the basal part of the Middle Eocene, and considered it as a basal Lutetian with a new member (the Mibazara Member) in the Dammam Formation. According to these authors, the nannofossil assemblage at the EME boundary coincides with the NP13/NP14 boundary which lies within the top Lower Eocene of Jabal Hafit.

3. Anan (2014, 2015a,b) noted that the core of Jabal Hafit in Al Ain area (UAE) contains late Ypresian sediments (about 55 m) ends by an intraformational conglomeratic bed (about 3 m). The upper Early Eocene succession is separated from the early Middle Eocene by erosional wadi (about 5 m), which stratigraphically is located above the upper Early Eocene intraformational conglomeratic bed. This conglomeratic bed was most probably controlled by active tectonic and eustatic sea-level changes, at the end of the Ypresian. It represents a major, but short-lived regression in Jabal Hafit, and the lacuna at the EME boundary is associated with the major sea-level lowering (Vail et al., 1977 and Haq et al., 1987), just before the end of the Early Eocene, at 49 Ma. Moreover, the '*pentacamerata* event' of Anan (2015b) most probably synchronous with the early/middle Eocene spreading system of the Indian Ocean, and coincident with the reactivation movement of the Syrian Arc folding.

7. The Ypresian/Lutetian (Y/L) boundary in the Tethys

Vrielynck et al. (1995) noted that for 260 Ma, the Tethys Ocean covered much of the face of the earth, from the Caribbean domain to the west to the Indonesian domain to the east. From the Late Cretaceous to the present, the Tethys has been closing, with sediments in the Caribbean, Alpine-Himalayan, and Indonesian belts. Before that, Tethys had spread and cut Pangaea as early as the Permian. Remnants of this ocean are found only in the Central Atlantic and the Mediterranean Sea.

1. Mohan and Soodan (1970) noted that the Middle Eocene (Lutetian) sediments disconformably overlie the Early Eocene (Ypresian) sediments in western Kutch, India.
2. Malumián and Caramés (1997) presented a correlation chart that shows an irregular stratigraphic lacuna around the EME boundary, and also at the Cretaceous/Paleogene and Paleocene/Eocene boundaries at Argentina and Chile
3. Moore et al. (1978) noted that a lacuna occurs near the base of the Middle Eocene (48-50 Ma) and it is seen only as a shoulder in the hiatus abundance curves of the World Ocean.
4. Haq and Aubry (1980) noted that North Africa and Middle East formed important parts of the Tethyan link between the Atlantic and the Pacific Oceans during the early Cenozoic.
5. Al-Hashimi (1980) noted that the lower-middle Eocene contact in Wadi Hauran (west of Iraq) is marked by a one-meter thick bed of conglomerate (it consists of nodular phosphate, glauconite and fish teeth), and this deposition indicates a break in sedimentation before the Middle Eocene transgression. He also added that similar lower-middle Eocene unconformity of the Dammam Formation is encountered throughout south and southwestern Iraq.
6. Berggren and Miller (1988) noted that the global sea level lowering (and associated hiatus/unconformity) characteristics of the EME interval, may place in apparent juxtaposition or overlap, biostratigraphic events which are normally separated in space and time.
7. Haggag (1992) detected an unconformity in Wadi Ed Dakhl (Eastern Desert of Egypt) which represents a gap across the EME boundary.
8. Janin et al. (1993) evidenced a well-known hiatus between the Cuisian (Early Eocene) and Lutetian (Middle Eocene) in the French type localities.
9. Browning et al. (1996) suggested that the major unconformity at the EME boundary (in New Jersey coastal plain, USA) is associated with major facies changes and sea-level lowering at the top of C22n (49 Ma, at P9/P10 boundary, within NP14a).
10. Molina et al. (2000) noted that the base of *Hantkenina nuttalli* Zone (P 10), at an exposed section near Agost (Southern Spain), which is often used to set the boundary between the Lower and the Middle Eocene (Y/L) falls facies changes from a limestone bank to marls just below the first occurrence of *H. nuttalli* implies a short hiatus at the lithological boundary.
11. Orue-Etxebarria et al. (2006) presented a comparison of all traditionally events used to place the EME boundary (by planktic foraminifera, calcareous nannofossil, large benthic foraminifera) which have been identified in the Gorrondatxe section (northern Spain) give evidence that all these events (previously considered as simultaneous) occur at very different levels. Accordingly, the stratigraphical position of the Ypresian-Lutetian (Y/L) boundary is still a matter of controversy between the calcareous nannoplankton, planktic foraminiferal and large benthic foraminifera faunal biostratigraphic schemes (Figure 7).

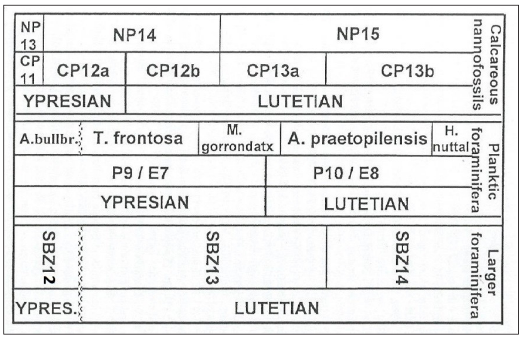

Figure 7. The position of the boundary between the Ypresian and Lutetian based on different biostratigraphic zones of calcareous nannoplankton, planktic foraminifera and larger foraminifera in Gorrondatxe beach section, Basque Country, W. Pyrenees, northern Spain (after Orue-Etxebarria et al., 2006).

12. Ortiz et al. (2008) noted that the Ypresian–Lutetian (Y–L; early-middle Eocene) transition at the continuous Agost section, southeastern Spain (115-m-thick) shows such markers and characterize palaeoenvironmental turnovers, which consists of hemipelagic marls intercalated with hemipelagic limestones and turbidity sandstones, spans from planktic foraminiferal Zones P9 to P12 (E7 to E10) and found that the most abundant planktic species belong to the genera *Acarinina, Morozovella, Subbotina,* and *Pseudohastigerina*. They also distinguished several mineralogical boundaries at the Agost section, each associated with lithological facies changes suggesting a change in provenance rather than changes in weathering conditions. Benthic foraminiferal and trace fossil assemblages also suggest an associated relative fall of sea level from upper-middle bathyal to sublittoral depths.
13. Payros et al. (2009) noted that the Global Stratotype Section and Point of the Lutetian Stage, which is still pending definition, should be placed at a globally correlatable event included within that unrepresented interval. This common evolution can be readily interpreted in terms of a sea-level driven depositional sequence whose low stand and transgressive systems tracts are included within the Ypresian/Lutetian boundary interval.
14. Molina et al. (2011) noted that the Ypresian/Lutetian boundary stratotype has to be defined at a level equivalent with the base of the Lutetian, which is the lowermost standard stage of the middle Eocene. The boundary stratotype must be defined by a lithostratigraphic level coinciding with an easily correlatable event that allows correlation, in a suitable marine continuous section, preferably out of the Paris basin where the Lutetian stage was defined since the Lutetian in the Paris basin is a sedimentary sequence between two hiatuses. Consequently, the GSSP has to be located in a deep-water section with minimal evidence of disturbance, transport and erosion. The LO of *Hantkenina nuttalli*, frequently used by planktic foraminiferal specialists to mark this boundary is younger than the base of the Lutetian in the Paris Basin, according to the new data from the Agost section.

15. Wade et al. (2011) noted that the early-middle Eocene First Appearance Datum of Turborotalia frontosa has resulted in large changes in the duration of Biochrons E7a,b.
16. Karoui-Yaakoub et al. (2015) noted that the Y/L transition at Sejnen section of Tunisia allowed tracing a precise correlation with the Global Stratotype Section and Point (GSSP) for the Y/L boundary recently defined at Gorrondtxe of Spain. The planktic foraminifera assemblages are diversified and enable the biozones of *Acarinina pentacamerata* (E6), *Acarinina cuneicamerata* (E7a), *Turborotalia frontosa* (E7b), and *Guembelitrioides nuttalli* (E8) to be identified.
17. Anan (2015b) noted that the fossil assemblage around the EME boundary (equivalent to Y/L boundary) provides a good database for biostratigraphic subdivisions, and the time-interval corresponding to the late Early Eocene planktic foraminiferal *Acarinina pentacamerata* Zone (P9) and early Middle Eocene *Hantkenina nuttalli* Zone (or *Acarinina bullbrooki* Zone, P10) around the boundary and this interval is called 'pentacamerata event'. This event is marked by important changes of the depositional setting and stratigraphic lacuna mainly due to tectonic activity in combination with lowering sea-level in many localities in the Tethys, i.e., New Zealand, Australia, India, Pakistan, Iraq, Qatar, UAE, Saidi Arabia, Kuwait, Jordan, Palestine, Egypt, Libya, Turkey, Ireland, Spain, France, USA, Argentina and Chile.
18. Alqudah et al. (2019) noted that the Y/L boundary could be correlated with angular unconformity at Bekaa Valley, Lebanon.
19. Alhejoj et al. (2020) noted that the Y/L boundary at Jabal Ghuzayma in central Jordan is placed near the base of the planktic foraminiferal E7b Subzone (lower occurrence of the Turborotalia frontosa) at the transition from the massive argillaceous limestone and the overlaying bedded limestone with flint bands.

8. Paleoenvironment

In the study section, the planktic foraminiferal species are numerous in the gypsiferous shale and marl samples around the EME boundary which represent the middle-upper neritic environment. The nummulitic and alveolinid limestone samples represent a shallow inner neritic environment. The intraformational beds of the top Early Eocene horizon and limestone samples around the EME boundary are barren. Anan (1996) suggested that the intraformational conglomeratic bed around EME boundary in Jabal Hafit (Figure 4) was deposited as submarine debris flows in the basin with a short distance of transportation on a slightly deepening pale slope from the positive localized source area, not as subaerial denudation, which consists of angular to subangular limestone detritus of different sizes with fine-grained marl matrix and has a homogenous thickness, about 3 m. Strougo and Haggag (1983) noted that the occurrence of deposits of an intraformational conglomeratic bed suggests a minimal reworking and accumulation in a low-energy environment with a short distance of transportation on a slightly deepening pale slope from the positive localized source area during the time of active tectonics. Browning et al. (1996) suggested that the EME boundary in the New Jersey coastal plain (USA) is associated with major facies changes and sea-level lowering at the top of the P9/P10 boundary (49 Ma). Molina et al. (2000) noted that the boundary between theY/L falls a facies changes from a limestone bank to marls just below the first occurrence of H. nuttalli implies a short hiatus at the lithological boundary. Jauhri and Agarwal (2001) noted that the Early Paleogene succession of the sedimentary facies in the south Shillong Plateau in NE India seems to be the result of sea-level and climate changes controlled by major tectonic reshuffling. Ortiz et al. (2008) noted that the Y–L(early-middle Eocene) transition at the continuous Agost section, southeastern Spain (115-m-thick) shows such markers and characterize palaeoenvironmental turnovers, which consists of hemipelagic marls intercalated with hemipelagic limestones and turbidity sandstones. Payros et al. (2009) noted that the Early/Middle Eocene (=Ypresian/Lutetian) transition is represented by a hiatus in many North European sections, including those in which the classic stratotypes were originally defined. Anan (2015b) noted that the fossil assemblage around the EME boundary in UAE is marked by important changes of the depositional setting and stratigraphic lacuna mainly due to tectonic activity in combination with lowering sea-level in many other localities in the Tethys. Khawaj et al. (2018) noted that the Eocene is an important Epoch for carbonate depositions, and it was the time of marine transgression.

9. Conclusions

The analysis of the EME planktic foraminiferal species in the western limb of Jabal Hafit, Al Ain area, United Arab Emirates (UAE)led to the following conclusions:

1. The paleontology, biostratigraphy and paleoenvironmental remarks are presented to sixteen planktic foraminiferal species from six genera have been recorded and illustrated.
2. Two modern planktic foraminiferal biozones are amended using the modified ranges of *Acarinina cuneicamerata* and *Turborotalia frontosa* index species throughout E7a,b biozone, and revised calibration datum of the EME bioevent in this study.
3. The lower Eocene rocks (Ypresian) belong to Hili Member of the Rus Formation and represented by a thick sequence of bedded limestone with flint in the lower part and marl intercalation in the upper part (about 50m), which ends by an intraformational conglomeratic bed, which was deposited as submarine debris flows in the basin, not as subaerial denudation, during the time of active tectonics and synchronous with the eustatic sea-level changes at the end of the Ypresian.
4. The basal Middle Eocene succession (Wadi Al Nahayan Member of t he Dammam Formation) is represented by a thick sequence of limestone, marl and shale intercalation.
5. The planktic foraminiferal analysis around the EME boundary is unconformable, which emphasized by the existence of an intraformational conglomeratic bed at the end of the Ypresian.
6. The lacuna around EME boundary has been reported from different parts of the world, which named as global " *pentacamerata* event" by Anan (2015b).

Acknowledgement

Gratitude is expressed to my colleague Prof. Mona Haggag, Ain Shams University (Egypt) for her kind help in photography of the fauna in Tubingen University(Germany). My sincere appreciation to the editor of JJEES and the three unknown reviewers for thorough scrutiny, helpful criticism and valuable comments. Thanks also extended to my daughter Dr. Huda Anan for her help in the development of the figures.

References

Al-Hashimi, H.A.J. (1980). Biostratigraphy of Eocene-Lower Oligocene of western desert, Iraq - Actes du colloque de Africain de Micropaleontologie, Tunis 1974. Annals des Mines et la Geologie 28(3): 209-229.

Alhejoj, I, Farouk, S., Bazeen, Y., Ahmad, F. (2020). Depositional sequences and sea-level changes of the upper Maastrichtian-middle Eocene succession in central Jordan: Evidence from foraminiferal biostratigraphy and paleoenvironments. Journal of African Earth Sciences 161: 1-13.

Alqudah, M., Monzer, A., Sanjuan, J., Salah, M.K., Alhejoj, I. (2019). Calcareous nannofossil, nummulite and ostracod assemblages from Paleocene to Miocene successions in the Bekaa (Lebanon) and its paleogeographic implications. Journal of African Earth Sciences 151: 82-94.

Anan, H.S. (1995). Late Eocene biostratigraphy of Jabals Malaqet and Mundassa of Al Ain region, United Arab Emirates. Revue de Micropaléontologie 38 (1): 3-14.

Anan, H.S. (1996). Early Eocene foraminifera of Jabal Hafit, United Arab Emirates. Middle East Research Center, Ain Shams University. Earth Science Series 10: 147-162.

Anan, H.S. (2014): Significant episodes of tectonic activities in the Paleogene of Al Ain area, United Arab Emirates. International Journal of Chemical and Natural Science 2 (6): 180-188.

Anan, H.S. (2015a). Planktic foraminifera around the Early/Middle Eocene boundary in the United Arab Emirates and other Tethyan localities. Revue de Paléobiologie 34 (1): 11-25.

Anan, H.S. (2015b). The global 'pentacamerata event': A diagnostic episode of tectonic activity in combination with lowering sea-level around the Early/Middle Eocene boundary in the world. International Journal of Chemical and Natural Sciences 3 (4): 287-296.

Anan, H.S. (2020). Taxonomical considerations, phylogeny, paleogeography and paleoclimatology of the Middle Eocene (Bartonian) planktic foraminifera from Jabal Hafit, Al Ain area, United Arab Emirates. Earth Sciences Pakistan (ESP) 4 (1): 10-20.

Anan, H.S., Bahr, S.A., Bassiouni, M.A., Boukhary, M.A., Hamdan, A.R. (1992). Contribution to Early Eocene-Oligocene biostratigraphy of Jabal Hafit succession, United Arab Emirates.Middle East Research Center, Ain Shams University. Earth Science Series 6: 225-247.

Banner, F.T. and Blow, W.H. (1959). The classification and stratigraphical distribution of the Globigerinacea.Palaeontology 2: 1-27.

Barr, F.T., Berggren,W.A. (1980). Lower Tertiary Biostratigraphy and Tectonics of Northeastern Libya. The Geology of Libya 1: 163-192.

Berggren, W.A. (1965). Some problems of Paleocene-Lower Eocene planktonic foraminiferal correlations. Micropaleontology 11 (3): 278-300.

Berggren, W.A. and Miller, K.G. (1988). Paleogene tropical planktic foraminiferal biostratigraphy and magnetobiochronology. Micropaleontology 34 (4): 362-380.

Berggren, W.A. and Pearson, P.N. (2006). Taxonomy, Biostratigraphy and phylogeny of Eocene Morozovella. Cushman Foundation Special Publication 41: 343-376.

Blow, W.H. (1969). Late Middle Eocene to Recent plankticforaminiferal biostratigraphy. 1st International Conference of Planktic Microfossils (Geneva 1967) 1: 199-422.

Blow, W.H. (1979). Danian to Oligocene planktic foraminiferal biostratigraphy, in the Cenozoic Globigerinida. A study of the morphology, taxonomy, evolutionary relationships and the stratigraphical distributions of some Globigerinida (mainly Globigerinacea). Leiden: E.J. Brill, 3, 753-1413.

Bolli, H.M (1957). The genera Globigerina and Globorotalia in the Paleocene-Lower Eocene Lizard Springs Formation of Trinidad. B.W.I. United States Natural Museum Bulletin 215: 61-81.

Boukhary, M., El Safori, Y.A., Decrouez, D., Faris, M.M. (2006). Bio-and isotope stratigraphy of the Lower/Middle Eocene section at Gebel Hafit area, United Arab Emirates. Neues Jahrbuch für Geologie und Paläontologie Monatshefte 8: 477-497.

Browning, J.V., Millar, K.G., Pak, D.K. (1996). Global implication of lower to middle Eocene sequence boundaries on the New Jersey coastal plan: icehouse cometh. Geology 24 (7): 639-642.

Cherif, O.H., Al-Rifaiy, I.A. El Deeb, W.Z. (1992). "Post-Nappes" early Tertiary foraminiferal paleoecology of the northern Hafit area, south of Al Ain City (United Arab Emirates). Micropaleontology 38 (1): 37-56.

Cole, W.S. (1927). A foraminiferal fauna from the Guayabal Formation in Mexico. Bulletins of American Paleontology 14: 1-46.

Finlay, H.J. (1939). New Zealand foraminifera: Key species in stratigraphy, 3. Transactions of the Royal Society of New Zealand 69: 309-329.

Glaessner, M.F. (1937). Planktonforaminiferen aus der Kreide und dem Eozän und ihre stratigraphische Bedeutung. Etyudy po Mikropaleontologiy, Paleontologicheskava Laboratoria Moskovskogo Gosudarstvennogo Universiteta 1 (1): 27-46.

Gohrbandt, K. (1967). Some new planktic foraminiferal species from the Austrian Eocene. Micropaleontology 13: 319-326.

Gümbel, C.W. (1868). Beiträge zur Foraminiferenfauna der nordalpinen Eocängebilde. Abhandlungen der K. Bayerische Akademie der Wissenschaften, Cl. II, 10 (2): 579-730.

Haggag, M.A. (1992). Planktic foraminiferal groups and zonation of the Paleocene/Eocene of the South Galala and environs. Egyptian Journal of Geology 35 (1-2): 37-50.

Haggag, M.A., Luterbacher, H. (1991). Middle Eocene planktic foraminiferal groups and biostratigraphy of the Wadi Nukhul section, Sinai, Egypt. Neues Jahrbuch für Geologie und Paläontologie, Monatshefte 6: 319-334.

Hamdan, A. R., Bahr, S.A. (1992). Lithostratigraphy of Paleogene succession of northern Jabal Hafit, Al Ain area, United Arab Emirates.Middle East Research Center, Ain Shams University. Earth Science Series 6: 201-224.

Hancock, H.J., Chaproniere, G.C., Dickens, G.R., Henderson, R.A. (2002). Early Paleogene planktic foraminiferal and carbon isotope stratigraphy, Hole 762C, Exmouth Plateau, northwest Australian margin. Journal of Micropalaeontology 21: 29-42.

Haq, B.U., Aubry, M.-P. (1980). Early Cenozoic calcareous nannoplankton biostratigraphy and palaeobiogeography of North Africa and the Middle East and Trans-Tethyan correlations. The Geology of Libya (1). 2nd Symposium of the Geology of Libya, Tripoli: 271-304.

Haq, B.U., Hardenbol, J., Vial, P.R. (1987). Chronology of fluctuating sea level since the Triassic. Science 235: 1156-1167.

Haque, A.F.M. (1956). The foraminifera of the Ranikot and the Laki of the Nammal Gorge, Salt Range, Pakistan. Pakistan Geological Survey Memoir, Palaeontologica Pakistanica 1: 1-229.

Hillebrandt, A.V. (1976). Los foraminifors planctonicos, nummulitidos y coccolitoforidos de la zone de Globorotalia palmerae del Cuisiense (Eoceno inferior) en el SE de España, (Provincias de Murcia y Alicante). Revue Española de Micropaleontologia 8 (3): 323-394.

Mohan, M. and Soodan, K.S.(1970). Middle Eocene planktic foraminiferal zonation of Kutch, India. Micropaleontology 16 (1): 37-46.

Molina E., Alegret L., Apellaniz E., Bernaola, G., Caballer, F., Dinarès-Turell, J., Hardenbol J., Heilmann-Clausen, C., Larrasoaña, J.C., Luterbacher, H., Monechi, S., Ortiz1, S., Orue-Etxebarria, X., Payros, A., Pujalte, V., Rodríguez-Tovar, F.J., Tori, F., Tosquella, J., Uchman, A. (2011). The Global Stratotype Section and Point (GSSP) for the base of the Lutetian Stage at the Gorrondatxe section, Spain. Episodes 34 (2): 86-108.

Molina, E., Cosovic, V., Gonzalvo, C., Von Salis, K. (2000). Integrated biostratigraphy across the Ypresian/Lutetian boundary at Agost, Spain. Revue de Micropaléontologia 43(3): 381-391.

Moore, Jr., T.C., van Andel, Tj. H., Sancetta, C., Pisias, N. (1978). Cenozoic hiatuses in pelagic sediments. Micropaleontology 24 (2): 113-138.

Mukhopadhyay, S.K. (2005). Turborotalia cerroazulensis group in the Paleogene sequence of Cambay Basin, India with a note on the evolution of Turborotalia cunialensis (Toumarkine and Bolli). Revue de Paléobiologie 24 (1): 29-50.

Nuttall, W.L.F. (1930). Eocene foraminifera from Mexico. Journal of Paleontology 4: 271-293.

Olsson, R.K., Hemleben, C., Huber, B.H., Berggren, W.A. (2006a). Taxonomy, biostratigraphy and phylogeny of Eocene Globigerina, Globoturborotalia, Subbotina and Turborotalia. (in Atlas of Eocene Planktic Foraminifera). Cushman Foundation Special Publication 41: 111-168.

Olsson, R.K., Pearson, P.N., Huber, B.T. (2006b). Taxonomy, biostratigraphy, and phylogeny of Eocene Catapsydrax, Globorotaloides, Guembelitrioides, Paragloborotalia, Parasubbotina and Pseudoglobigerinella n. gen. Cushman Foundation Special Publication (Chapter 5), 41, 67-110.

Ortiz, S., Gonzalvo, C., Molina, E., Rodríguez-Tovar, F.J., Uchman, A., Vandenberghe, N., Zeelmaekers, E. (2008). Palaeoenvironmental turnover across the Ypresian–Lutetian transition at the Agost section, Southastern Spain: In search of a marker event to define the Stratotype for the base of the Lutetian Stage. Marine Micropaleontology 69: 297–313.

Orue-Etxebarria, X., Bernaola, G., Payros, A., Dinarès-Turell, J., Tosquella, J., Apellaniz, E., Caballer, F. (2006). The Ypresian/Lutetian boundary at the Gorrondatxe Beach section (Basque Country, W Pyrenees). In: Climate and Biota of the Early Paleogene, Mid-Conference Field Excursion Guidbook: Azkorri-Gorrondatxe, Bilbao, 36 pp.

Payros, A, Bernaola, G., Orue-Etxebarria, X., Dinarès-Turell, J., Tosquella, J. (2007). Reassessment of the Early–Middle Eocene biomagnetochronology based on evidence from the Gorrondatxe section (Basque Country, western Pyrenees). Lethaia 40 (2): 183-195.

Payros, A., Tosquella, J., Bernaola, G., Dinarès-Turell, J., Orue-Etxebarria, X., Pujalte, V. (2009). Filling the North European Early/Middle Eocene (Ypresian/Lutetian) boundary gap: Insights from the Pyrenean continental to deep-marine record. Palaeogeography, Palaeoclimatology, Palaeoecology 280: 313–332.

Pearson P.N. (1993). A lineage phylogeny for the Paleogene plankticforaminifera. Micropaleontology 39 (3): 193-232.

Pearson, P.N., Olsson, R.K., Huber, B.T., Hemleben, C., Berggren, W.A. (2006). Atlas of Eocene planktic foraminifera. Cushman Foundation for Foraminiferal Research Special Publication 41, 513p.

Seferinov, S. (2017). Family Globigerinidae Carpenter, Parker and Jones, 1862 from the Paleocene and Eocene in Lom Depression. Review of the Bulgarian Geological Society 78 (1–3): 73–95.

Seferinov, S. (2018). Paleocene and Eocene planktonic foraminifera of the Families Hantkeninidae Cushman, 1927, Truncorotaloididae Loeblich and Tappan, 1961 and Hedbergellidae Loeblich and Tappan, 1961 from the Lom Depression. Review of the Bulgarian Geological Society 79 (1–2): 29–50.

Sharma, B., Kumar, Ch., Malarkodi, N. (2019). Late Palaeocene-Early Eocene Morozovella from Pondicherry Area, Cauvery Basin, Southern India. International Journal of Paleobiology and Paleontology 2 (1): 1-8.

Solé, F., Noiret, C., Desmares, D., Adnet, S., Taverne, L., De Putter, T., Mees, F., Yans, J., Steeman, T., Louwye, S., Folie, A., Stevens, N.J., Gunnell, G.F., Baudet, D., Yaya, N.K., Smith, T. (2019). Reassessment of historical sections from the Paleogene marine margin of the Congo Basin reveals an almost complete absence of Danian deposits. Geoscience Frontiers 10: 1039-1063.

Stainforth, R.M., Lamb, J.L., Luterbacher, H.P., Beard, J.H., Jeffords, R.M. (1975). Cenozoic planktic foraminiferal zonation and characteristics of index forms. Paleontological Contribution, University of Kansas 62: 163-425.

Strougo, A. and Haggag, M.A. (1983). The occurrence of deposits of Paleocene age at Abu Roash, west of Cairo, Egypt. Neues Jahrbuch für Geologie und Paläontologie, Monatshefte 11: 677-686.

Subbotina, N.N. (1947). Foraminifery Datskikh i Paleogenovykh otlozheniy severnogo Kvkaza [Foraminifera of the Danian and Paleogene deposits of the northern Caucasus] in Mikrofauna Neftanykh Mestorozhdeiny. Emby i Sredny Azii. Leningrad: Vsesoyuzhnyy Neftyanoy Nauchno - issledovatel'skiy Geologo-razvedochnyy Institut (VNGRI): 39-160.

Subbotina, N.N. (1953). Fossil foraminifers of the USSR, Globigeriniidae, Hantkeninidae and Globorotaliidae]. Trudy Vsesoyuznogo Neftyanogo Naucho-issledovatel'skogo Geologorazvedochnogo Instituta (VNIGRI) 76: 1-296 (in Russian, translated into English by E. Lees, 1971).

Subbotina, N.N. (1960). Pelagic foraminifera of the Paleogene deposits of the southern part of the U.S.S.R. [in Russian]. Akad. Nauk U.S.S.R.: 24-36.

Todd, R. and Kniker, H.T. (1952). An Eocene foraminiferal fauna from the Agua Fresca Shale of Magallanes Province, southernmost Chile. Cushman Foundation for Foraminiferal Research, Special Publication 1: 1-28.

Toumarkine, M. and Luterbacher, H. (1985) Paleocene and Eocene Planktic Foraminifera. In: Bolli, H.M., Saunders, J.B., Perch-Nielsen, K., (Eds.), Plankton Stratigraphy, Cambridge University Press, Cambridge: 87-154.

Vail, P.R., Mitchum, R.M., Thompson, S. III (1977). Seismic stratigraphy and global changes of sea level. In: Payton, C. E. (Ed.), Stratigraphic Interpretation of Seismic Data. The American Association of Petroleum Geologists Memoir 26: 83-97.

Vrielynck B., Dercourt J., Cottereau N. (1995). The Tethys. In: Nairn A.E.M., Ricou LE., Vrielynck B., Dercourt J. (Eds.), The Tethys Ocean. Springer, Boston, MA. https://doi.org/10.1007/978-1-4899-1558-0_16.

Wade, B.S., Pearson, P.N., Berggren, W.A., Pälike, H. (2011). Review and revision of Cenozoic tropical planktic foraminiferal biostratigraphy and calibration to the geomagnetic polarity and astronomical time scale. Earth Science Reviews 104: 111–142.

Wade, B.S., Olsson, R.K., Pearson, P.N., Edgar, K.M., Premoli Silva, I. (2018). Taxonomy, biostratigraphy, and phylogeny of Oligocene Subbotina. Cushman Foundation Special Publication 46: 307-330.

Weinzierl, L.L. and Applin, E.R. (1929). The Claiborne formation on the coastal domes. Journal of Paleontology 7: 384-410.

Youssef, M.I., Bassiouni, M.A., Boukhary, M.A., Anan, H.S. (1983). Paleogene planktic foraminifera from Abu Gharadig Basin (Subsurface), north Western Desert, Egypt. 1st Jordanian Geological Conference: 123-156.

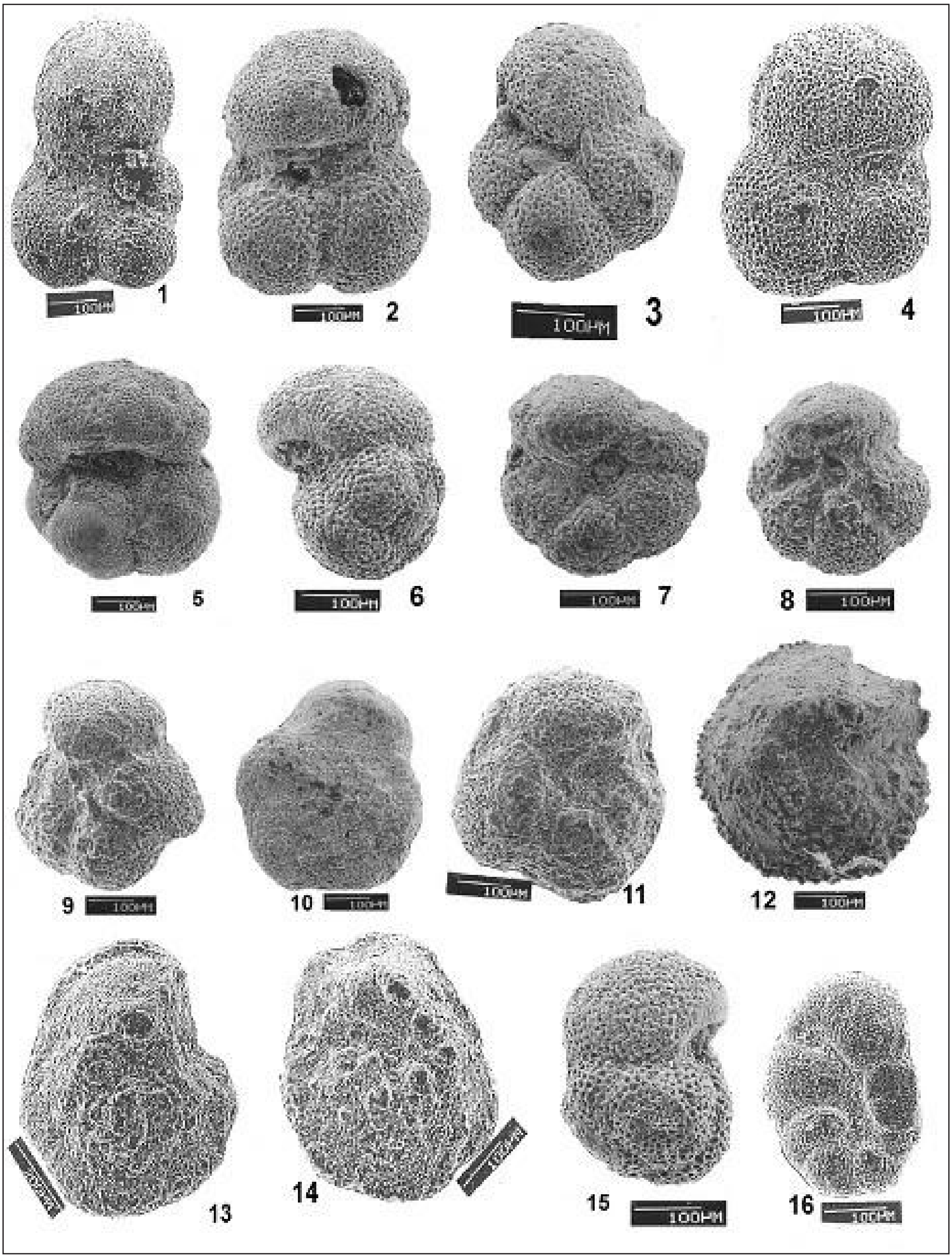

Plate 1.

1. Parasubbotina inaequispira (Subbotina, 1953), sample 12.
2. Subbotina eocaena (Gümbel, 1868), sample 12.
3. S. hagni (Gohrbandt, 1967), sample 12.
4. S. linaperta (Finlay, 1939), sample 3.
5. S. patagonica (Todd and Kniker, 1952), sample 16.
6. S. yeguaensis (Weinzierl and Applin, 1929), sample 14.
7. Acarinina berwaliana (Mohan and Soodan, 1969), sample 12.
8. A. bullbrooki (Bolli, 1957), sample 12
9. A. cuneicamerata (Blow, 1979), sample 9a.
10. A. pentacamerata (Subbotina, 1947), sample 9b.
11. A.praetopilensis (Blow, 1979), sample 9b.
12. Morozovella aragonensis (Nuttall, 1930), sample 16.
13. M. crater (Hornibrook, 1958), sample 3.
14. M. caucasica (Glaessner, 1937), sample 9a.
15. Turborotalia frontosa (Subbotina, 1953), sample 12,
16. Pseudohastigerina micra (Cole, 1927), sample 2.

JJEES

JJEES (2021) 12 (4): 326-336
ISSN 1995-6681

Jordan Journal of Earth and Environmental Sciences

Spatio Temporal Analysis and Simulation Pattern of Land Use and Land Cover Change in Odeda Peri-urban of Ogun State, Nigeria

Anthony Tobore[1*], Bolarinwa Senjobi[1], Ganiyu Oyerinde[2]

[1]Department of Soil Science and Land Management, Federal University of Agriculture Abeokuta, Nigeria.
[2]Department of Soil Science, Faculty of Agriculture, University of Abuja, Nigeria.

Received 5 January 2021; Accepted 4 April 2021

Abstract

Land use and land cover (LULC) change at the peri-urban is a complex and dynamic process that involves global environmental change. The substantial increase in the human population has led to threats of peri-urban. This study identified the pattern of the LULC change for the years 2014 and 2019 using Landsat satellite images. Soil samples were collected, analyzed, and classified. Principal component analysis (PCA) and Contamination factor (CF) were also determined on the soil nutrients. The Markov Chain (MC) and Cellular Automata (CA) methods were utilized to simulate the LULC maps for the year 2024. Variations among the soil properties decrease across the soil depths and the soils were classified as Mollic Cambisols and Abruptic Eutric. Bioaccumulation index varied substantially with high significant contamination of soil iron. The accuracy of LULC simulation models is more than 85% based on the validation results. The simulation result shows that if the current encroachment continues, the built-up areas will increase by 32% and thus would leading to loss of farmlands and a decrease in food production. Moreover, the rate of economic development in the urban has caused rapid expansion and migration of people into the study area. This study is helpful for planners and decision-makers in ensuring sustainable land-use systems for peri-urban planning.

Keywords: land use, land cover, Peri-urban, Markov Chain, Cellular Automata model.

1. Introduction

Land use and land cover (LULC) change are some of the major global changes predicted for the future (Su et al., 2012). LULC change at the peri-urban is a complex and dynamic process that involves both natural and human activities (Xiao et al., 2006). LULC is also the primary driving force of sustainable development and global environmental change (Wali et al., 2019). The change in LULC varies from region to region, in rural areas is attributed due to agriculture expansion while in urban areas it is attributed to urban development. The causes and consequences of LULC change are related to human-induced activities which are largely been examined independently (Basommi et al., 2016). Global environmental changes such as emissions of greenhouse gases, global climate change, loss of biodiversity, and loss of soil resources have been closely linked to LULC changes (Li et al., 2016). Additionally, LULC changes are also faced with threats of rapid economic development such as commercialization and urbanization (Hyandye et al., 2017). However, this threat has led to the loss of lands suitable for farming especially in developing countries such as Nigeria (Li et al., 2016).

Studies have shown that urbanization is a major concern of many world regions. It was estimated that the urban population will increase from 3.3 billion in 2007 to 6.4 billion in the year 2050 (United Nations, 2008). Due to this reason, more attention has been given to peri-urban areas as a means to alleviate poverty and ensure food security (Tiani et al., 2015). Globally, about 800 million people engaged in peri-urban agriculture (FAO, 1999). According to FAO, (2010) peri-urban can be described as “the area of transition between well recognized urban and rural land uses. It has also been conclusively shown that peri-urban contributes to food security (FAO, 2010). Despite their importance, peri-urban are still faced with anthropogenic activities such as discharge of effluents and vicinity dumpsite, etc. (Awoniran et al., 2013).

Monitoring and assessing LULC change at the peri-urban calls for detail and accurate information. Although, assessing LULC changes in developing countries requires urgent attention especially in the spatial environment of today (Tobore et al., 2021). Satellite remote sensing (SRS), in conjunction with Geographic information systems (GIS), have been widely applied and are recognized as an indispensable tool in obtaining accurate and timely spatial data for LULC changes (Mishra et al., 2016; Khan et al., 2016). SRS provides cost-effective valuable information using multispectral and temporal data which is very useful in monitoring and evaluating LULC change (Hua, 2017). For instance: Landsat imagery has been applied extensively for predicting and monitoring LULC change efficiently at different scales and times (Hua, 2017). GIS provides a flexible user environment for collecting, storing, displaying, and analyzing spatial data (Khan et al., 2016). However, the commonly used models for monitoring and predicting LULC changes are Analytical equation-based models (Shamsi, 2010), Statistical models (Hyandye et al., 2017), Evolutionary models (Aitkenhead and Aalders, 2009), Cellular automata

* Corresponding author e-mail: toboreao@funaab.edu.ng

models (Singh et al., 2015), Markov-chain models (Yang et al., 2012), Expert system models (Stefanov et al., 2001), and Multiagent models (Ralha et al., 2013). At present, the most widely used models in the monitoring and prediction of LULC change are Cellular automata and Markov chain (Sohl and Claggett, 2013; Myint and Wang, 2006). Markov chain models can quantitatively predict the dynamic changes in LULC patterns (Wu et al., 2010). In contrast, cellular automata models can predict the spatial distribution of landscape patterns but cannot predict temporal changes (He et al., 2006). Integration of Cellular automata and Markov chain (CA- Markov) model in LULC studies has advantages such as dynamic simulation capability; high efficiency with spatial and non-spatial data, scarcity and simple calibration; and ability to predicts complex and multiple lands covers patterns (Hyandye et al, 2017; Ansari, 2016). Moreover, many studies have applied CA- Markov model in monitoring and predicting LULC change in the urban (Shahidul Islam and Ahmed, 2011). Thus, few studies have been applied to predict changes in the peri-urban area using the CA - Markov model especially in developing countries such as Nigeria. Hence, this study seeks to integrate the CA-Markov model to evaluate the impacts of LULC change in peri-urban of Odeda Local government area (LGA) of Ogun State, Nigeria. More specifically, the study is targeted to map the spatial and temporal changes in LULC for the years 2014 and 2019. Therefore, the objectives of this study are:

1. To assess, characterize and classify the soil nutrients of the study area.
2. To predicts the LULC change of the study area for 5 years using the CA–Markov model.

2. Materials and methods

2.1 Description of the study area

The study area is located at Odeda Local Government Area (LGA) of Ogun State, southwestern Nigeria. Odeda falls in the peri-urban area of Abeokuta, close to the city of Ogun State. It falls between latitude 7^0 49’ to $7^0$13’ and longitude $3^0$79’ to 3^0 14’ zones 31 North (Figure 1). It has a total surface area of 1,560 km² and a population of 109,449 according to the National population census (2006). Agriculture is the main source of occupation and it also serves as their major livelihood. The crops grown in the area are majorly arable, and permanent crops, such as maize, rice, and oil palm (Dada, 2017).

2.2 Climate

The climate of the study area is monsoonal and like all monsoonal climates: it has a contrast between well-defined dry and wet seasons (Adeleye et al., 2020). The wet season lasts from April to October with an annual rainfall of about 2500 mm at the coast and about 1220 mm at the northern limit of the forest belt. The monthly mean minimum temperature is about 22.48°C while the monthly mean maximum temperature is about 31.24°C with an average yearly temperature of about 26.6°C (Adeleye et al., 2020).

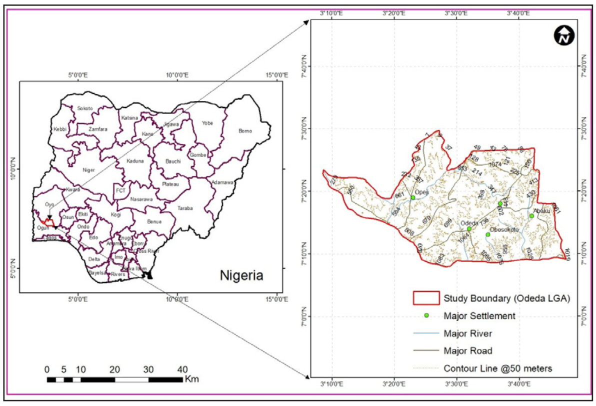

Figure 1. The study area (Odeda LGA) showing the contours and some major settlements.

2.3 Data Description

Multi-spectral Landsat satellite data for the years 2014 and 2019 were acquired from the United States Geological Survey (USGS) to assess the LULC change. Due to atmospheric error and avoidance of seasonal variation, the Landsat images were downloaded during the period of the dry season. Since the Landsat satellite data are free of radiometric and geometric distortions, there was no additional geo-rectification or image-to-image registration needed for image pre-processing. Information of the images acquired from the USGS online data repository (image type, date, spatial resolution, number of bands, Path and row, and bands composite) are shown in Table 1.

Table 1. Details of the Landsat images acquired for the assessment of the Odeda LULC study

Image Type	Acquisition date	Path and row	Bands composite	No of bands	Spatial Resolution
LandSat 7	19/01/2014	P191, R55	432	10	30 Meter
LandSat 8	20/01/2019	P191, R55	652	11	Meter

2.4 Multi-temporal land cover mapping

The collected satellite images were enhanced in Idrisi selva Software via (3 by 3) majority filter techniques for better visibility. True Color Composite (TCC) was generated using suitable combinations of bands for the satellite images (d’Entremont and Thomason, 1987; Good and Giordano, 2019). Considering the “Nigeria Land Classification System” and the goal of this study, Anderson and Hardy (1976) classification scheme II and prior knowledge of the study area for over 5 years was used to identify the Area of interest (AOI) features. The images obtained from the Landsat image are classified into 5 LULC classes based on the Maximum Likelihood Supervised Classification (MLSC) technique(Table 2). The MLCS operation is carried out due to its good performance, visualization, and easy classification algorithm (Liu, 2005; Sun et al., 2013; Biro et al., 2013; Zhang et al., 2015). The accuracies of land cover maps were evaluated using 150 ground truth points from the field and with the support of the year 2019 Google Earth image. These 150 pixels were selected through the random sampling process. The Kappa statistics and confusion matrix was calculated for accuracy assessment (Foody, 2002; Pontius Jr and Millones, 2011; Story and Congalton, 1986).

Table 2. The Description of the land categories.

No	Class name	Description
1	Builtup Area	Residential, commercial, industrial services, and transportation network
2	Vegetation	Mixed forest and grass
3	Bareland	Vacant land, open space, sand, bare soils, and landfill sites
4	Farmland	Rainfed cropping planted cropping areas.
5	Waterbodies	River, wetlands, lakes, ponds, and reservoirs.

2.5 Simulation Pattern Analysis

To simulate the future LULC pattern of the study area, the Markov Chain (MC) and Cellular automata (CA) model method was applied. MC performs better at modelling LULC in both temporal and spatial dimensions for its higher accuracy (Pontius and Jeffrey, 2007). CA underlies the dynamics of LULC change for any location (cells) based on the concept of proximity (Balogun and Ishola, 2017). The CA-Markov model was implemented in the Landsat images of the years2014 and 2019 in the Idrisi Selva environment (Tobore et al., 2021). The LULC change prediction was based on the dependent and independent variables. The dependent variable used includes the Digital elevation model (DEM), aspect, distance from a major road, and distance from the river (Figure 2a and 2b). The DEM and aspect were derived from the Shuttle radar topographic mapper (SRTM) of 30-meter resolution downloaded from the USGS website. The DEM ranges from the lowest value of 33 meters to the highest value of 266 meters from mean sea level (MSL) in the study area. The aspect maps indicate a more or less flat surface presence in the study area. Distance from major roads and rivers were derived from vector layers from an open street map. The analysis of the dependent variable was carried out using the ArcGIS 10.5 environment using Euclidean distance operation. The independent variables are the LULC of the year 2014 and 2019 classification maps. The independent and dependent variables were used as input parameters to generate the transition probability matrix. The transition matrix analysis generates an empirical likelihood image that estimated the probability of change between LULC in the study area. The random sampling method was applied using the maximum iteration and neighbourhood of 3 by 3 cells i.e. 9 cells. The Cellular automata and Markov Chain were predicted according to Ma et al. (2016):

$$S_{t+1} = P_{iJ} \times S_t \quad \text{.......... Eq. 1}$$

Where: : represent the land-use status

T, and t+1 represent the time point

P_{iJ}: represent the state transition probability matrix

$$P_{iJ} \begin{bmatrix} P_{11}, & \square & P_1, P_1, \\ \cdots, & \cdots & \cdots \\ P_{11} & P_{11} & P_{11} \end{bmatrix} \quad \text{.......... Eq. 2}$$

2.6 Accuracy assessment

To ensure the validity of the model for predicting LULC change for the projected year, a validation process was performed using the existing database. The CA-Markov model was validated to simulate the LULC of the year 2019, which is compared to the estimated LULC map of the same year. The validation process was performed in the Idrisi selva environment producing several Kappa (K) parameters: kappa for grid cell level location (Klocation), kappa for no information (Kno), kappa for stratum-level location (KlocationStrata), and kappa standard (Kstandard) following the standard procedure of Pontius Jr and Millones (2011).

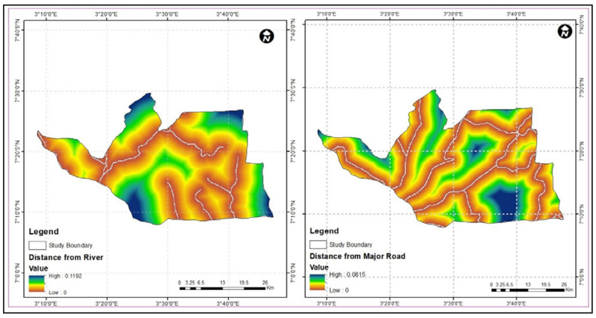

Figure 2a. The study area (Odeda LGA) showing the distance from Major Road and River.

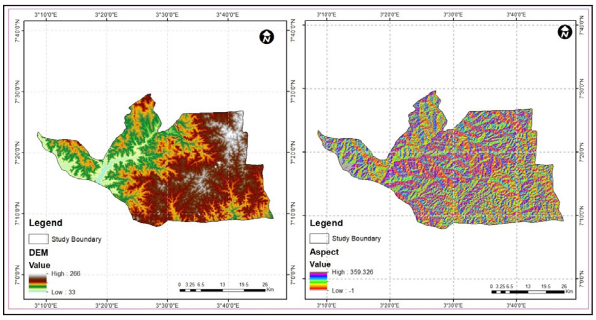

Figure 2b. The study area (Odeda LGA) showing the digital elevation model and Aspect.

2.7 Vegetation Cover analysis

Vegetation indices derived from satellite remote sensing data are one of the primary sources of information for monitoring the Earth's vegetation cover (Gilabert et al., 2002). Vegetation indices are usually developed to extract vegetation information from two or more spectral bands. In this study, LULC changes were assessed with Soil adjusted vegetation index (SAVI) for the years 2014 and 2019. SAVI has a better efficiency to calculate vegetation index by reducing the influence of soil background (Gilabert et al., 2002). Afterwards, SAVI was used to identify significant changes in the vegetation cover of the study area. The equation is given by (Huete, 1988):

$$SAVI = \frac{(\mathrm{NIR} - \mathrm{RED})}{\mathrm{NIR} + \mathrm{RED} + \mathrm{L}}(1 + L) \quad \text{.......... Eq. 3}$$

where: NIR represents the spectral reflectance measurements in the near-infrared regions of band 5; Red represents the Spectral reflectance measurements in the visible red of the band 4 and L is the constant or correction factor, ranges from 0 to 1.

2.8 Soil mapping

The study area was sampled using reconnaissance and stratified grid sampling. The slopes from which transects were cut for soil mapping include pedon 1 (Odeda), pedon 2 (Olodo), and pedon 3 (Isolu). Soil sampling was collected at the soil depth of 0 -15cm and 15 – 30cm for soil analysis. A total number of 74 soil samples were collected for this study. Soil sampling coordinate point was recorded using a Global positioning system (GPS). At each pedon, representative soil profile pits measuring 2 m by 1.5 m by 2 m (meters) were dug at the predominant slope i.e. Crest, middle and lower slope. A total of 9 soil profile pits were dug and described based on soil morphology, chemical, and physical which was suggested by FAO, (2009) procedure. Soil samples were collected from the different pedogenic horizons and then processed in the laboratory after air-drying at room temperature.

2.9 Soil classification

Based on morphological characteristics and laboratory data of the soil mapping, the soils of the study area were classified using the USDA Soil Taxonomy (Soil Survey Staff, 2010) and the World Reference Base (WRB) system of FAO/IUSS Working Group (2006).

2.10 Soil pollution load assessment model

Pollution by soil heavy metals has been widely studied using several indices (Odukoya et al., 2016). In this study, the Contamination factor (CF) index was used to assess the soil heavy metal concentration. CF is used to assess contamination level relative to the average concentration of the respective heavy metals in the environment i.e. soil to the measured background values from the previous study with similar geological origin or uncontaminated soil (Sutherland, 2000; Tijani et al., 2004; Uriah and Shehu, 2014). The CF is often expressed based on the formula previously described by Hakanson (1980) and has been applied by Odukoya et al. (2016).

$$CF = \frac{\text{C metal}}{C\ Bkg} \quad \text{.......... Eq. 4}$$

Where C: metal represents the concentration (mg/kg^{-1}) of a given heavy metal in soil

C Bkg: represent the background or preindustrial concentrations (mg/kg^{-1}).

2.11 Geospatial mapping of soil heavy metals

Among the metal concentration, iron (Fe), zinc (Zn), and manganese (Mn) were selected to assess the level of heavy metals using 0 -15 cm soil depth. According to Obiora et al. (2016), Fe, Zn, and Mn are the most common contaminated heavy metals found in Nigeria's soils and environment. The collected coordinates of the soil heavy metals concentration were processed in an excel spreadsheet and saved as text delimited. Each of these metal concentrations was plotted and display in the ArcMap. Thereafter, the Inverse difference weight (IDW) technique was used for the interpolation of soil data according to Li and Heap (2008). Raster calculator tool in ArcGIS 10.5 environment was used to assess the formula described by Odukoya et al. (2016) for soil concentration mapping for the study area. Due to no data information of preindustrial or preanthropogenic activities in southwestern Nigeria, geochemical background concentration values of 9 mg/kg^{-1} were used to assess the quality of the soil in the study area according to Pejman et al. (2009) as described in table (3).

Table 3. Geochemical and pollution indices

Classes	Pollution Intensity	Soil Quality
0 -1	0	Unpolluted
1-2	1	Unpolluted to moderately polluted
2-3	2	Moderately polluted
3-4	3	Moderately to highly polluted
4-5	4	Highly polluted
5-6	5	Highly to very highly polluted
6-7	>5	Very highly polluted

Source: Pejman et al. (2009)

2.12 Soil samples analysis

The soil samples were air-dried and passed through a 2mm diameter sieve before analysis for the soil's physical and chemical properties. Afterwards, soil pH was determined in potassium chloride and water suspensions with a glass electrode pH meter (McLean et al., 1982). Soil organic carbon (OC) was determined by the chromic acid oxidation method (Walkley and Black, 1939). The total nitrogen (TN) of the soil was determined by the macro Kjeldahl method. The soil available phosphorus (P) was determined according to the Bray-1 method. Exchangeable bases Calcium, Magnesium, Potassium, and Sodium ($Ca^{2+,}$ Mg^{2+} K + and Na+) in the soil were extracted with 1 N ammonium acetate solution. The Ca^{2+} and Mg^{2+} were determined with atomic absorption spectrophotometer (AAS) while (K+) and (Na+) were read on a flame photometer. Exchangeable acidity (H+) in the soil was extracted with 1N Kcl and measured using the titration method (Anderson and Ingram, 1993). Effective cation exchange capacity (ECEC) was estimated by the summation of the exchangeable acidity and exchangeable bases. Base saturation (BS) was calculated as the percentage ratio of the exchangeable bases to the ECEC following the procedure of Udo et al. (2009). The particle size distribution of the soil was determined by the hydrometer method (Bouyoucos, 1962). For heavy metal analyses, sub-samples (0.5 g) of each of the soil were digested. Digestion was done with 10 ml of a mixture of nitric (HNO3) and perchloric (HClO4) acid in ratio 2:1 (v/v) for 90 min, initially at 150° C. After which 2ml of concentrated HCL was added to the mixture. The temperature of the digest was then increased to 230° C for another 30 minutes on the digester. On completion of digestion, digests were allowed to cool down at room temperature. Thereafter, the content of each digestion tube was transferred into a 50 ml volumetric flask and made to volume with distilled water.

2.13 Statistical analysis

The relationship across the soil nutrients was subjected to Principal component analysis (PCA), correlation, and regression analysis using R- statistics v4.0.3. The correlation coefficients were estimated for all possible variable combinations to generate a correlation matrix.

3. Results and Discussion

3.1 Land use/cover mapping

Periodical assessment characteristics and colour composite were used to classify the LULC change of the studied area. Results of the MLSC algorithm for evaluating LULC changes between the year 2014 and 2019 patterns are presented in Figure (3) and (4). Overall classification accuracy of MLSC was 94.10% and 95.87% in the years 2014 and 2019 respectively (Table 4). For validation, the predicted LULC map of 2019 was compared with the observed LULC map of 2019 using kappa index statistics. Based on the evaluation of predicted LULC with observed LULC scenarios, a kappa statistic for quantity and location was derived. The statistics showed that Kno, Klocation, KlocationStrata, and Kstandard values were 0.8603, 0.8869, 0.8743, and 0.8645 (overall kappa), respectively. After the prediction, it was found out that all kappa index values were > 0.86 showing high agreement between predicted and observed LULC maps. The statistical analysis of the multi-temporal LULC maps revealed that significant changes have occurred. From the change analysis of LULC between 2014 and 2019, it was observed that there was an increase in farmland, built-up, bare land, and water bodies with a value of 30.80%, 20.18%, 17.63%, and 1.92% respectively while vegetation was decreased from 60.51% to 29.43% (Table 5).

To predict future LULC change, the land use map of 2014 and 2019, and then the output was used to predict future LULC for the year 2024 using the CA-Markov model (Figure 5). The significant changes that are predicted to occur between 2019 and 2024 would be due to the conversion of bare land, water bodies, and vegetation. Therefore, change analysis of LULC between 2019 and 2024 indicated that built-up and farmland will increase in the order of 163.87 ha (Hectare) and 124.36 ha, while bare land, vegetation, and water bodies were decreased by –140.13ha, 132.67ha, and -15.43ha, respectively (Table 6). The results revealed that a sudden increase in farmland and built-up area can be attributed to a substantial increase in human activities. Besides, the increase observed in farmland could also be traced to the over-exploitation of land resources which serves as a means of livelihood and source of occupation for the majority of people living in the peri-urban area. Also, an increase in the built-up area by the next 5 years, may lead to more people migrating from urban to peri-urban due to unplanned population growth in the city. However, the main reason for these changes could be attributed to some factors such as agricultural land use expansion, biodiversity loss, pollution of water and soils in the studied area. Weng and Yang (2004) pinpointed that both geopolitical and economic factors contribute to the increases in human activities and thus leading to built-up expansion. Adepoju et al. (2006) also stated that LULC change has been recognized as an important driver of global environmental changes. The present study also corroborates with Nachtergaele et al. (2011) who found out that peri-urban areas are rapidly experiencing biodiversity decrease and high human activities thereby leading to the sudden decrease in vegetation cover and built-up expansion. However, further studies supporting this study results can be found in Bankole and Bakare (2011).

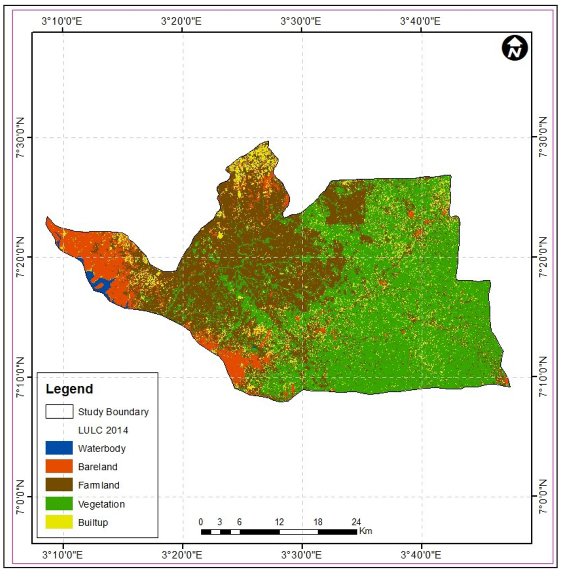

Figure 3. The study area (Odeda LGA) showing the year 2014 LULC changes.

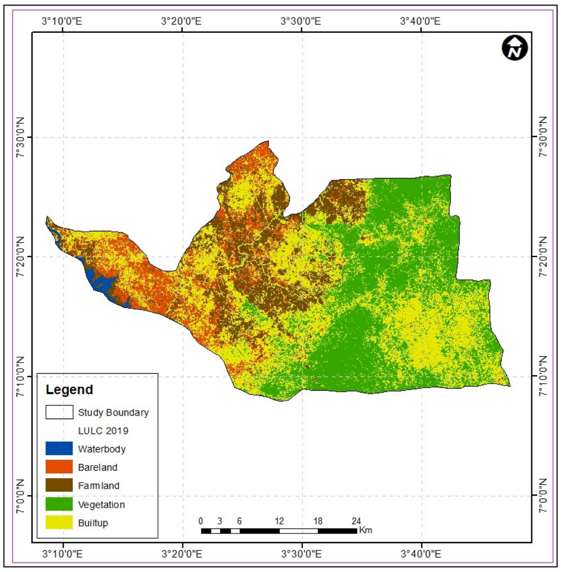

Figure 4. The study area (Odeda LGA) showing the year 2019 LULC changes.

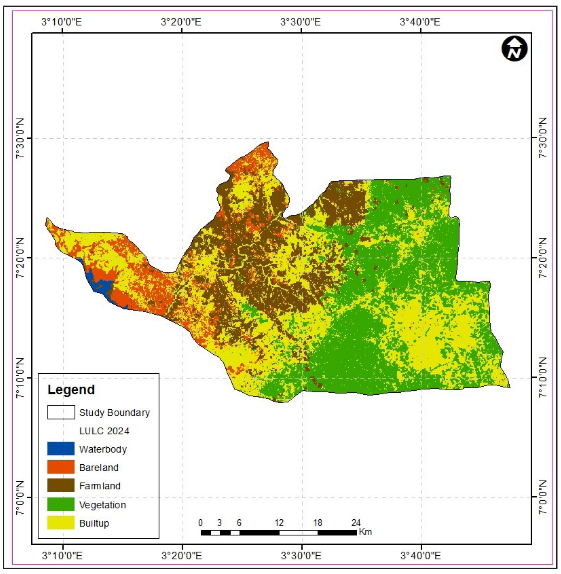

Figure 4. The study area (Odeda LGA) showing the year 2019 LULC changes.

Table 4. Accuracy assessment of the LULC classified maps (Odeda LGA) for the years 2014 and 2019.

User Accuracy (%)							Producer Accuracy (%)					
LULC	WB	BL	VG	FD	BA	Overall Classified Accuracy	WB	BA	VG	FD	BA	Overall Statistic Kappa
2014	98.4	98.9	98.5	94.3	97.2	94.10%	98.5	96.4	95.8	88.8	95.3	0.9488
2019	98.2	97.5	98.7	94.9	96.5	95.87%	99.8	95.9	88.2	96.8	97.5	0.9365

LULC: WB: Waterbodies; BL; Bareland; FD: Farmland; VG; Vegetation; BA

Table 5. Change analysis of LULC (Odeda LGA) between the years 2014 and 2019.

LULC	Area in 2014		Area in 2019		Change in 2014 -2019
	(ha)	(%)	(ha)	(%)	(ha)
Waterbodies	18.33	1.34	26.32	1.92	7.99
Bareland	135.21	9.90	240.82	17.63	105.61
Farmland	256.93	18.81	420.63	30.80	163.70
Vegetation	826.14	60.51	401.89	29.43	- 424.25
Builtup	128.66	9.42	275.61	20.18	146.95
Total	1365.27	100	1365.27	100	

Table 6. Change analysis of LULC(Odeda LGA) between the years 2019 and 2024.

LULC	Area in 2019		Area in 2024		Change in 2019 -2024
	(ha)	(%)	(ha)	(%)	(ha)
Waterbodies	26.32	1.92	10.89	0.79	-15.43
Bareland	240.82	17.63	100.69	7.37	-140.13
Farmland	420.63	30.80	544.99	39.91	124.36
Vegetation	401.89	29.43	269.22	19.71	-132.67
Builtup	275.61	20.18	439.48	32.18	163.87
Total	1365.27	100	1365.27	100	

3.2 Satellite-based vegetation Assessment

Vegetation indices have been used to monitor temporal changes associated with vegetation and spectral reflectance (Gilabert et al., 2002). One of these commonly used vegetation indices is the SAVI. SAVI appears to be more reliable and less noisy than the NDVI (Normalized difference vegetation index) (Waswa et al., 2012). In this study, the SAVI vegetation index was used and the vegetation cover ranged from -0 to 0.2715 for the year 2014 and 0 to 0.0317 for the year 2019 (Figure 6). The results revealed that during the year 2019, low vegetation-covered was experienced when compared to that of the year 2014. The effects of the low vegetation observed in the year 2019 might be traced to the rate of human activities experienced in the study area such as farmland and built up expansion. Additionally, indiscriminate grazing of cattle might also be responsible for the low vegetation observed in the year 2019 especially during the dry season when the chlorophyll content is low.

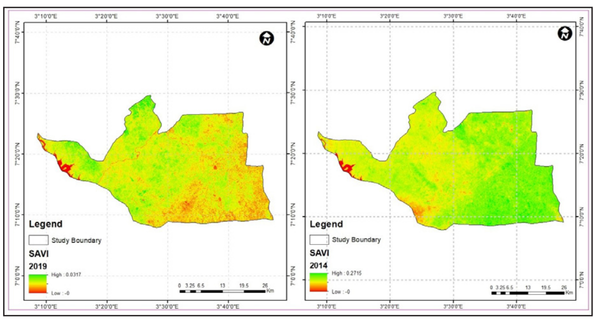

Figure 6. The study area (Odeda LGA) showing the year 2014 and 2019soil adjusted the Vegetation index.

3.3 Soil fertility variation at 0 -15cm depth

As shown in Figure 7, cluster variations were observed among the chemical soil properties. The soil zinc (Zn) was observed along the same dimension (dimension 2) with exchangeable acidity and iron (Fe). This simply means that as Zn decreases exchangeable acidity and soil iron also decrease. The exchangeable bases; magnesium (Mg), sodium (Na), potassium (K), and effective cation exchanged capacity (ECEC) were also observed along the same dimension (dimension 3). This confirms the fact that an increase in exchangeable bases will lead to higher ECEC in the studied soil. The soil pH, available phosphorus (P), soil total nitrogen (TN), and soil organic carbon (OC) were found in the same dimension. The calcium, soil Fe, Mg, and base saturation also behaved the same way.

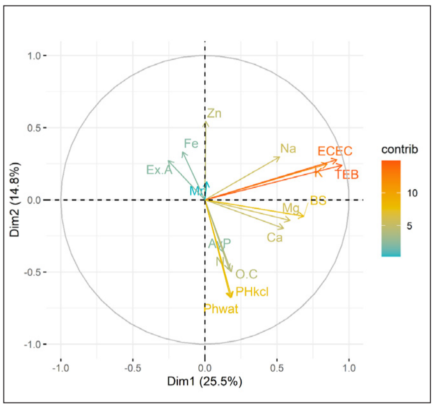

Figure 7. Variable factor map of Principal component analysis for soil sampled at 0 - 15cm depth.

3.4 Correlation among soil properties at 015-cm.

From Table 7, high R squared (R^2) values were observed among soil OC versus TN, K versus Total exchangeable bases (TEB), ECEC, and TEB versus ECEC (Figure 8 - 10). The linear regression plots and modelling equation shows how the soil properties could be predicted in the study area (Table, 7).

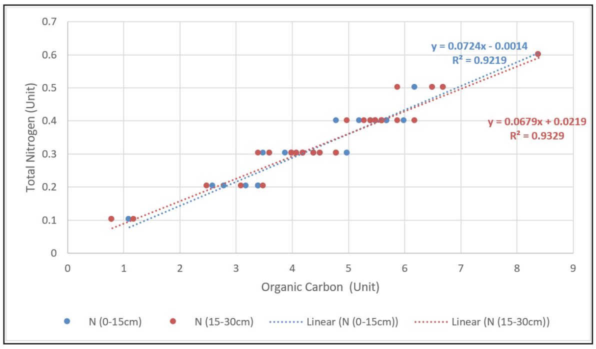

Figure 8. The study area (Odeda LGA) showing the linear regression between Nitrogen and Organic Carbon.

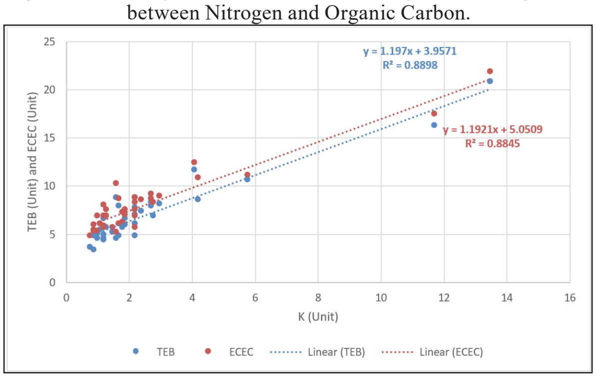

Figure 9. The study area (Odeda LGA) showing the linear regression among K versus TEB/ECEC.

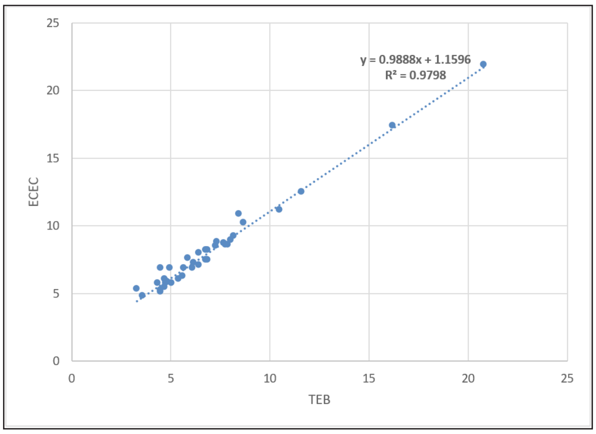

Figure 10. The study area (Odeda LGA) showing the linear regression between TEB and ECEC.

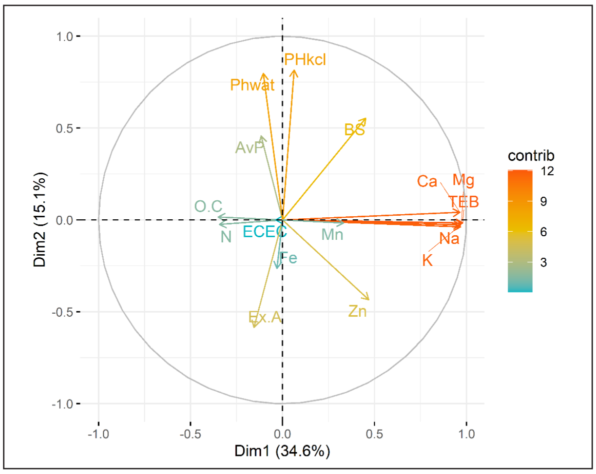

Figure 11. The study area (Odeda LGA) showing the variable factor map of principal component analysis for soil samples at 15-30 cm.

Table 7. The study area (Odeda LGA) showing the R2 correlation among soil properties at 0-15cm soil depth.

	O.C	AvP	N	Ex.A	Na	K	Ca	Mg	TEB	ECEC	BS	pHkcl	pHwater	Fe	Zn
AvP	0.029														
N	0.922	0.028													
Ex.A	0.001	0.046	0.000												
Na	0.004	0.044	0.002	0.001											
K	0.011	0.014	0.020	0.001	0.108										
Ca	0.019	0.002	0.001	0.099	0.005	0.059									
Mg	0.002	0.003	0.000	0.001	0.048	0.108	0.270								
TEB	0.009	0.002	0.010	0.006	0.298	0.890	0.159	0.205							
ECEC	0.008	0.000	0.010	0.004	0.304	0.884	0.126	0.210	0.980						
BS	0.001	0.029	0.000	0.666	0.108	0.177	0.227	0.065	0.290	0.179					
pHkcl	0.001	0.043	0.001	0.020	0.004	0.000	0.006	0.039	0.001	0.000	0.026				
pHwater	0.003	0.028	0.009	0.027	0.004	0.000	0.022	0.033	0.000	0.000	0.034	0.578			
Fe	0.013	0.010	0.006	0.077	0.028	0.000	0.008	0.083	0.008	0.017	0.026	0.138	0.058		
Zn	0.030	0.009	0.032	0.000	0.002	0.011	0.000	0.018	0.008	0.008	0.001	0.101	0.022	0.045	
Mn	0.035	0.196	0.022	0.000	0.003	0.002	0.000	0.001	0.000	0.000	0.001	0.000	0.022	0.022	0.158

3.5 Correlation among soil properties at 15 -30cm depth

In Figure 11, Soil O.C and N followed a similar direction which indicates correlation among the soil properties and thus affected by the same factors. Both soil pH (water and potassium chloride) along with available P is found around dimension 2. All the Exchangeable bases (Ca, Mg, Na, K, and Mn) and TEB have good relationships as displayed in dimensions 2 and 3. In line with the PCA, soil O.C and N have a high correlation. The exchangeable bases also showed great relationships as highlighted in yellow (Table 8).

Table 8. The study area (Odeda LGA) showing the R2 correlation among soil properties at 15-30cm.

	O.C	AvP	N	Ex.A	Na	K	Ca	Mg	TEB	ECEC	BS	pHkcl	pHwater	Fe	Zn
AvP	0.044														
N	0.933	0.029													
Ex.A	0.015	0.108	0.039												
Na	0.040	0.026	0.034	0.001											
K	0.053	0.016	0.043	0.003	0.925										
Ca	0.038	0.007	0.032	0.011	0.917	0.916									
Mg	0.048	0.012	0.040	0.003	0.965	0.952	0.965								
TEB	0.047	0.016	0.039	0.004	0.969	0.985	0.959	0.985							
ECEC	0.011	0.024	0.013	0.012	0.004	0.002	0.007	0.017	0.000						
BS	0.013	0.032	0.034	0.648	0.129	0.147	0.157	0.108	0.145	0.093					
pHkcl	0.002	0.041	0.001	0.033	0.006	0.002	0.009	0.005	0.004	0.001	0.054				
pHwater	0.004	0.037	0.002	0.021	0.012	0.008	0.002	0.007	0.008	0.001	0.030	0.602			
Fe	0.002	0.009	0.006	0.068	0.008	0.003	0.011	0.008	0.006	0.004	0.019	0.135	0.117		
Zn	0.010	0.020	0.007	0.008	0.167	0.156	0.135	0.142	0.157	0.013	0.007	0.075	0.094	0.032	
Mn	0.048	0.161	0.091	0.002	0.060	0.043	0.057	0.060	0.052	0.017	0.007	0.000	0.008	0.012	0.150

3.6 Soil Mapping of the (Odeda LGA) study area

The diagnostic criteria of the pedons were classified according to the USDA Soil Taxonomy (Soil Survey Staff, 2010) and World Reference Base for Soil Resources (FAO/ ISRIC/IUSS, 2006). The differentiating properties used for the soil classification include physical, chemical, and morphological soil properties. The particle size distribution classification indicated that the soil texture ranged from sandy to sandy loam.The high preponderance of sand indicated a dominance of low activity clay such as kaolinite. There was a consistent clay increase across the pedons leading to the formation of the argillic horizon. The soils were strongly acidic to neutral with a soil pH ranging from 5.1 to 7.3. Available phosphorus (< 8 to 20 mg/kg), and total nitrogen ranged from low to medium (<0.1 to 0.2%). Organic carbon had higher levels (1.0 to >20%) in the analyzed soils. The high content of soil OC observed could be traced to the presence of deposition or dumping of waste material into the vicinity of the studied area. ECEC of the soils is more than 1.5 cmol/kg^{-1} in the studied soils and this may be responsible for the intense leaching of the exchangeable cations due to the parent material.

3.7 Soil Classification of the (Odeda LGA) study area

All the pedons were well-drained and dry for as long as 90 cumulative days with a mean annual soil temperature of 22^{0}C, thus considered as Udic moisture regime and classified as Isohyperthermic. This is also in consonance with the work done by Amusan and Ashaye (1991) which states that soil temperature regime in Southwestern - Nigeria can be classified as isohyperthermic. The pedons had base saturation of > 50% with a colour value from < 4 and chroma 3 or less, and soil OC content of more than 0.6% (Soil Survey Staff, 2010). This implies that the studied soils can be considered as mollic Epipedon. At the Order level, pedons 1 and 2 were classified as Inceptisol due to little or no soil profile development across the horizons (Soil Survey Staff, 2010), while at pedon major processes such as erosion, and highly leached soils due to slope position (>2 mm in diameter) were observed and therefore classified as Ultisols. At the suborder level, there was high sandy distribution and irregular clay movement down the horizon at the soil profile. Therefore, at the suborder, the soils can be classified as Typic Kandiudult with ECEC of more than 1.5 cmol/kg^{-1}. According to the World Reference Base for Soil Resources, pedons 1 and 2 were classified as Mollic Cambisols (Endo – Skeleton, Eutric) due to the beginning or incipient subsurface horizon differentiation and alteration while pedon 3 were classified as Haplic Gleysols (Abruptic, Eutric) due to saturated groundwater and gleyic colour pattern (FAO/ ISRIC/IUSS,2006).

3.8 Geoconcentration of heavy metals in studied (Odeda LGA) soils

The assessment of pollution levels of heavy metals soil contamination is significant to human health and environmental management. In this study, the soil heavy metals were interpolated and classified according to Pejman et al. (2009) soil quality. The order of contribution of the heavy metals to soil contamination increased in the following order: Fe > Mn > Zn. The overall pollution load index indicated that the soils ranged from unpolluted to highly polluted (Figure 12). The soil heavy metal reveals that vicinity waste and effluent discharge into rivers and streams could be responsible for the rate of contamination in the studied soils. According to Mazurek et al. (2017), heavy metals pollution in the soil varies according to its chemical and physical characteristics including texture, and buffering ability. Mazurek et al. (2017) and Pająk et al. (2015) also reported that the distribution and arrangement of soil heavy metals depend on landscape and/or topography. Hence, this could account for variation found among the soil heavy metals. The results are also in consonance with the studies of Ajmone-Marsan and Biasioli (2010) as well as that of Obiora et al. (2016) who reported that soil Fe, Mn, and Zn are among the most common contaminated heavy metals found in Nigeria soils and environment.

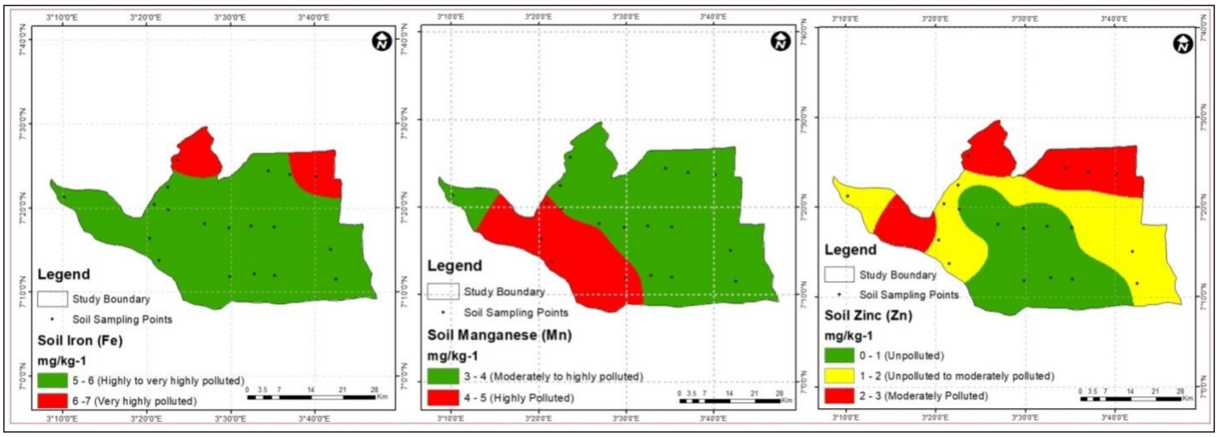

Figure 12. The study area (Odeda LGA) showing the Geoconcentration of soil iron, manganese, and zinc.

4. Conclusions

The study objective was to evaluate the significance of LULC change from the year 2014 to 2024 using GIS, RS data, and the CA-Markov model in Odeda LGA, Ogun State, Nigeria. Prediction of future LULC changes at the study area can help to manage the sudden encroachment. The finding reveals that built-up area and farmland was increased by 32.18% and 39.91% from the year 2014 to 2019, which leads to a decrease in vegetation by (19.71%), bareland (7.37%), and water bodies (0.79%). The increase in built-up area and farmland could be attributed to the increase in human activities such as built-up expansion through the sudden encroachment of people migrating from urban to the study area. The soil nutrients variation shows a good relationship and decreases across the soil depths. Concentrations of soil Zn, Fe, and Mn in the study soils varied substantially with high significant contamination of soil Fe. The rate of human activities such as vicinity dumpsite, and discharge of industrial waste into the streams and river can lead to the transferring of toxic metals to the food chain; thereby leading to a potential risk to human health and a decrease in food production in the studied area. The present study demonstrated the efficiency of GIS and RS data in the study of LULC change using the Cellular Automata and Markov chain model.

Acknowledgements

The authors are sincerely grateful to farmers in the study area for their understanding and for allowing us to carry out this study on their farms. We are equally thankful to the USGS for assisting this research with data sets.

Funding

This research did not receive any specific grant from funding agencies in the public, commercial, or not-for-profit sectors.

References

Adeleye, N., Osabuohien, E., Adeogun, S., Fashola, S., Tasie, O., Adeyemi, G. (2020). Access to Land and Food Security: Analysis of ‘Priority Crops’ Production in Ogun State, Nigeria. In, Osabuohien. E (Ed.), The Palgrave Handbook of Agricultural and Rural Development in Africa (pp. 291-311). Cham-Switzerland: Palgrave Macmillan. DOI: https://doi.org/10.1007/978-3-030-41513-6_14.

Adepoju, M.O., Millington, A.C., Tansey, K.T., (2006). Land Use/Land Cover Change Detection in Metroploitian Lagos (Nigeria): 1984-2000. AASPRS 2006 Annual Conference, Reno Nevada, May 1-5, 2006, Maryland: American Society for Photogrammetry and Remote Sensing.

Ajmone-Marsan, F., and Biasioli, M.(2010).Trace elements in soils of urban areas. Water, Air, and Soil Pollution 213: 121 –143. DOI: 10.1007/s11270-010-0372-6.

Amusan, A.A., and Ashaye, T.I. (1991). Granitic-gneiss derived soils in humid forest tropical southwestern Nigeria I: Genesis and classification. Ife Journal of Agriculture 13 (1-2): 1 – 20.

Anderson, J.M., and Ingram, J.S.L. (1993). Tropical soil biology and fertility: handbook of Method of Analysis. UK:International Wallingford, (pp. 38–39).

Anderson, J.R., and Hardy, E.E. (1976). A Land Use and Land Cover Classification System for Use with Remote Sensor Data. Geological Survey Professional.

Ansari, A. (2016). The final report of the research project “Identification of harvesting centres’ and effective factors of dust storms in Michigan Desert Wetland’’ Arak University.

Aitkenhead, M.J., and Aalders, I.H. (2009). Predicting land cover using GIS, Bayesian and evolutionary algorithm methods. Journal of Environmental Management 90(1): 236–50. https://doi.org/10.1016/j.jenvman.2007.09.010 PMID: 18079039.

Awoniran, D.,R., Adewole, M.B., Adegboyega, S.A, Anifowose, A. Y. B. (2013). Assessment of environmental responses to land-use / land-cover dynamics in the lower Ogun River Basin, South-western Nigeria. International Journal of Sustainable Land use and Urban Planning 1(2):16-31.

Balogun, I., and Ishola, K. (2017). Projection of future changes in land-use/ land-cover using cellular automata/Markov model over Akure city, Nigeria. Journal of Remote Sensing Technology 5 (1): 22–31.

Bankole, M.O., and Bakare, H.O. (2011). Dynamics of urban land-use changes with remote sensing: Case of Ibadan, Nigeria. Journal of Geography and Regional Planning 4(11): 632-643.

Basommi, L.P., Guan, Q.F., Cheng, D.D., Singh, S.K. (2016). Dynamics of land-use change in a mining area: a case study of Nadowli District, Ghana. Journal of Mountain Science 13(4): 633–42. https://doi.org/10.1007/s11629-0153706-4.

Biro, K., Pradhan, B., Buchroithner, M., Makeschin, F.(2013). Land use/Land cover change analysis and its impact on soil properties in the northern part of Gadarif region, Sudan. Land Degradation and Development 24(1): 90–102. https://doi.org/10.1002/ldr.1116.

Bouyoucos, G.H. (1962). Hydrometer method for making particle size analysis of soils. Agronomy Journal 54: 464-465. DOI: 10.2134 /agronj1962.00021962005400050028x.

Dada, S. (2017). Public-Private Dialogue Report on Land Administration, Registration and Acquisition in Ogun State. Nigeria: Deutsche Gesellschaft für Internationale Zusammenarbeit (GIZ).

D'Entremont, R.P., and Thomason, L.W. (1987). Interpreting meteorological satellite images using a colour-composite technique. Bulletin of the American Meteorological Society 68(7): 762-768.

FAO-ILASA-China-Dokuchaev (1999). CD-ROM on Soil and Terrain Database for North and Central Eurassia (Version 1.0), FAO, ROME.

FAO/IUSS Working Group (2010). A framework for land evaluation.Rome: Soils Bulletin 31,

FAO, pp 25-42.

FAO, Rome (2006). The State of Food Insecurity in the World. Food and Agriculture Organization of the United Nations, Rome.

FAO, Rome (2009). The State of Food Insecurity in the World. Food and Agriculture Organization of the United Nations, Rome.

Foody, G.M. (2002). Status of land cover classification accuracy assessment. Remote Sensing of Environment 80 (1): 185–201.

Gilabert, M. A., González-Piqueras J., García-Haro F. J., Meliá J., (2002). "A generalized soil-adjusted vegetation index." Remote Sensing of Environment 82(2):303-310. DOI:10.1016/S0034-4257(02)00048-2.

Good, T., and Giordano, P.A., (2019). Methods for Constructing a Color Composite Image: Google Patents.

He, C., Okada, N., Zhang Q., Shi, P., Zhang, J. (2006). Modeling urban expansion scenarios by coupling cellular automata model and system dynamic model in Beijing, China. Applied Geography 26(3): 323–45. https:// doi.org/10.1016/j.apgeog.2006.09.006.

Hua, A.K. (2017). Analytical and Detection Sources of Pollution Based Environmetric Techniques in Malacca River, Malaysia. Applied Ecology and Environmental Research 15 (1): 485-499.

Hakanson, L. (1980). An ecological risk index for aquatic pollution control of sediment ecological approach. Water Research 14: 975–1000.

Huete, A.R. (1988). A soil-adjusted vegetation index (SAVI). Remote Sensing of Environment 25: 295-309.

Hyandye, C, Mandara, G., Safari, J. (2017). GIS and Logit Regression Model Applications in Land Use/Land Cover Change and Distribution in Usangu Catchment. American Journal of Remote Sensing 3(1): 6–16. doi: 10.11648/j.ajrs.20150301.12.

Pejman, A.H., Bidhendi, G.R.N., Karbassi, A.R., Mehrdadi, N., Bidhendi, M.E. (2009). Evaluation of spatial and seasonal variations in surface water quality using multivariate statistical techniques. International Journal of Environmental Science and Technology 6: 467–476 (2009). DOI: 10.1007/BF03326086.

Khan, S., Cao, Q., Zheng, Y.M., Huang, Y.Z., Zhu, Y.G. (2016). Health risks of heavy metals in contaminated soils and food crops irrigated with wastewater in Beijing, China. Environmental Pollution 152(3): 686–692. https://doi.org/10.1016/j.envpol.2007.06.056.

Li, X., Min, X.U., Cao, C., Singh, P.R., Chen, W., Ju, H. (2016). Land use and land cover changes and their influence on the Ecosystem in Chengdu City during the period of 1982 – 2018. Sustainability 10: 3580.

Li, J., and Heap, A.D. (2008).A Review of Spatial Interpolation Methods for Environmental Scientists. Geoscience Australia, Record 2008/23, 137 pp.

Liu, H. (2005). Accuracy analysis of remote sensing change detection by rule-based rationality evaluation with post-classification comparison. International Journal of Remote Sensing 25(5): 1037–1050. http://dx.doi.org/10.1080/014311603 1000150004.

Ma, X., Zuo, H., Tian, M., Zhang, L., Meng, J., Zhou, X., Min, N., Chang, X., Liu, Y. (2016). Assessment of heavy metals contamination in sediments from three adjacent regions of the Yellow River using metal chemical fractions and multivariate analysis techniques. Chemosphere 144:264-72. DOI: 10.1016/j.chemosphere.2015.08.026.

McLean, E. O., Dumford, S. W. F., Coronel, S.W. (1982). A comparison of several methods of determining lime requirements of the soil. Soil Science Society of America Journal 30(1): 26-30.

Mazurek, R., Kowalska, J., Gasiorek, M., Zadrozny, P., Jozefowska, A., Zaleski, T. (2017). Assessment of heavy metals contamination in surface layers of Roztocze National Park forest soils (SE Poland) by indices of pol- lution. Chemosphere 168: 839–850.

Mishra, VN., Rai, PK., Kumar, P., Prasad, R. (2016). Evaluation of land use/land cover classification accuracy using multi-resolution remote sensing images. Geographic Forum XV(1):45–53. https://doi.org/10.5775/ fg.2016.137.i.

Myint S.W., and Wang, L. (2006). Multicriteria decision approach for land use land cover change using Markov chain analysis and a cellular automata approach. Canadian Journal of Remote Sensing 32(6): 390–404. https://doi.org/ 10.5589/m06-032.

Nachtergaele, F.O., Velthuizen, H., Van, Verelst, L., Batjes, N.H., Dijkshoorn, J.A., Engelen, V.W.P. van, Fischer, G., Montanarella, L., Petri, M., Prieler, S., Teixeira, E., Wilberg, D., Shi, X. (2011). World Soil Database.Version 1.0. http://www.fao.org/nr/water/docs/Harm-World-Soil-DBv7cv.pdf (accessed November 2015).

National Population Commission, Nigeria (2006). Census Report.

Obiora, S.C., Chukwu, A., Davies, T.C. (2016). Heavy metals and health risk assessment of arable soils and food crops around Pb–Zn mining localities in Enyigba, southeastern Nigeria. Journal of African Earth Sciences 116: 182-189. DOI: 10.1016/j.jafrearsci.2015.12.025.

Odukoya, A.M., Olobaniyi, S.B., Abdussalam, M. (2016). Metal pollution and health risk assessment of soil within an urban industrial estate, southwest Nigeria. Ife Journal of Science 18(2): 573 – 583.

Pająk, M., Halecki, W., Gąsiorek, M. (2015). Accumulative response of Scots pine (Pinussylvestris L.) and silver birch (Betulapendula Roth) to heavy metals enhanced by Pb-Zn ore mining and processing plants: Explicitly spatial considerations of ordinary kriging based on a GIS approach. Chemosphere 168: 851–859. DOI: 10.1016/j. chemosphere.2016.10.125.

Pontius, G.R., and Malanson, J. (2005) Comparison of the structure and accuracy of two land change models. International Journal of Geographical Information Science 19(2): 243-265. DOI: 10.1080/13658810410001713434.

Pontius, Jr. R. G., and Millones, M., (2011). Death to Kappa: birth of quantity disagreement and allocation disagreement for accuracy assessment. International Journal of Remote Sensing 32 (15): 4407–4429. https://doi.org/10.1080/01431161.2011.5529 23.

Ralha, C.G., Abreu, C.G., Coelho, C.G.C., Zaghetto, A, Macchiavello, B, Machado, R.B. (2013). A multi-agent model system for land-use change simulation. Remote Sensing of Environment 42: 30–46. https://doi.org/10. 1016/j.envsoft.2012.12.003.

Shahidul Islam, M.D., and Ahmed, R. (2011). Land-use change prediction in Dhaka city using GIS aided Markov chain modeling. Journal of Life and Earth Science 6: 81-89.

Shamsi, S.R.F., (2010). Integrating Linear Programming and Analytical Hierarchical Processing in Raster-GIS to Optimize Land Use Pattern at Watershed Level. Journal of Applied Sciences and Environmental Management 14(2): 81–5.

Singh, S.K., Mustak, S., Srivastava, P.K., Szabo, S., Islam, T. (2015). Predicting Spatial and Decadal LULC Changes Through Cellular Automata Markov Chain Models Using Earth Observation Datasets and Geo-information. Environmental Processes 2(1):61–78.

Sohl, T.L., and Claggett, P.R. (2013). Clarity versus complexity: Land-use modeling as a practical tool for decision-makers. Journal-Environ Manage 129: 235–43. PMID:23954777. https://doi.org/10.1016/j.jenvman.2013.07.027.

Soil survey staff. (2010). Keys to soil taxonomy,. Washington D. C.: USDA soil conservation service revised edition (9th).

Stefanov W.L., Ramsey M.S., Christensen P.R. (2001). Monitoring urban land cover change: An expert system approach to land cover classification of semiarid to arid urban centers. Remote Sensing of Environment 77 (2): 173–85.

Su, C., Jiang, L., Zhang, W. (2012). A review on heavy metal contamination in the soil worldwide: Situation, impact and remediation techniques. Environmental Skeptics and Critics 3(2): 24–38. https://doi.org/10.1016/j.envint.2014.04.014.

Sun, Y., Zhou, Q., Xie, X., Liu, R. (2013). Spatial, sources and risk assessment of heavy metal contamination of urban soils intypical regions of Shenyang, China. Journal of Hazardous Materials 174(1–3): 455–462. DOI: 10.1016/j.jhazmat.2009.09.074.

Sutherland, R. (2000). Bed sediment-associated trace metals in an urban stream, Oahu, Hawaii. Environmental Geology 39(6): 611–627. DOI: 10.1007/s002540050473.

Story, M., and Congalton, R.G. (1986) Accuracy Assessment: A User's Perspective. Photogrammetric Engineering and Remote Sensing 52: 397-399.

Tiani, A.M., Besa, M.C., Devisscher, T., Pavageau, C., Butterfield, R., Bharwani, S. Bele, M. (2015). Assessing Current Social Vulnerability to Climate Change: A Participatory Methodology. Working Paper 169. Bogor: Center for International Forestry Research.

Tijani, M.N., Kenneth, J., Yoshinar, H. (2004). Environmental impact of heavy metals distribution in water and sediment of Ogunpa River, Ibadan area, South Western Nigeria. Journal of Mining and Geology 40(1): 73 – 83. DOI: 10.4314/jmg.v40i1.18811.

Tobore, A., Senjobi B., Ogundiyi, T., Samuel, B. (2021). Geospatial assessment of wetlands soils for rice production in Ajibode using Geospatial Techniques. Open Geosciences 13: 310-320. https://doi.org/10.1515/geo-2020-0227.

Udo, E.J., Ibia, T.O., Ogunwale, J.A., Ano, A.O., Esu, I.E. (2009). Manual of soil, plant and water analyses. Lagos: Sibon Books Ltd 183 pp.

United Nations. (2008). World Urbanization Prospects: The Revision United Nations (Population Division of the Department of Economic and Social Affairs) New York.ESA/P/WP/224,2012.

Uriah, L.A., and Shehu, U. (2014). Environmental risk assessment of heavy metals content of municipal solid waste used as organic fertilizer in vegetable gardens on the Jos Plateau, Nigeria. American Journal of Environmental Protection 3(6 – 2): 1 – 13.

Walkley, A., and Black, I. A. (1939). An examination of the Degtjareff method for determining soil organic matter and a proposed modification of the chromic acid titration method. Soil Science 37:29 –38. DOI: 10.1097/00010694193401000-00003.

Wali, E., Phil-Eze, P.O., Nwankwoala, H.O., Bosco-Abiahu, L.C., Emelu, V.O., (2019). Analysis of land use and land cover changes in the wetland ecosystem of Port-Harcourt metropolis, Nigeria. International Journal of Ground Sediment and Water 9: 503-524.

Waswa, B. S., Vlek, P. L., Tamene, L. Okoth, P. F. (2012). Mapping land degradation patterns using NDVI as a Proxy: a case study of Kenya. Resilience of Agricultural Systems Against Crises (Tropentag, September 19-21 2012), Göttingen-Kassel/Witzenhausen.

Wu, C.D., Cheng, C.C., Lo, H.C., Chen, Y.K. (2010). Application of SEBAL and Markov Models for Future Stream Flow Simulation Through Remote Sensing. Water Resource Manag. 24(14): 3773–97. https://doi. org/10.1007/s11269-010-9633-9.

Weng, Q., and Yang, S. (2004). Managing the adverse thermal effects of urban development in a densely populated Chinese city. Journal of Environmental Management 70: 145-156.

Xiao, J., Shen, Y., Ge, J., Tateishi, R., Tang, C., Liang, Y. (2006). Evaluating urban expansion and land-use change in Shijiazhuang, China by using GIS and remote sensing. Landscape and Urban Planning 75: 69-80. http://dx.doi.org/10.1016/j.landurbplan.2004.12.005.

Yang, X., Zheng, X., Lv, L. (2012). A spatiotemporal model of land use change based on ant colony optimization, Markov chain and cellular automata. Ecol Model 233:11–19. doi:10.1016/j.ecolmo del.2012.03.011.

Zhang, J., Niu, J., Bao, T., Buyantuyev, A., Zhang, Q., Dong, J., Zhang, X. (2015). Human-induced dry-land degradation in Ordos plateau, China, revealed by multi-level statistical modelling of normalized difference vegetation index and rainfall time series. Journal of Arid Land 6: 219–229. https://doi.org/10.1007/s40333-0130203-x.

JJEES

JJEES (2021) 12 (4): 337-343
ISSN 1995-6681

Jordan Journal of Earth and Environmental Sciences

An object oriented classification approach for mapping land cover from Landsat and Sentinel image data in the north of Ivory Coast

Daouda Sylla[1], Habib Mouissa[2*], Léocadie M-Cakadje-Konan[1], Célestin Hauhouot[1]

[1]*Institut de Géographie Tropicale, Université Félix Houphouët-Boigny, Abidjan (Côte d'Ivoire).*
[2]*Département des sciences agronomiques, Université Ziane Achour –Djelfa (Algérie), Laboratoire de recherche Conservation, gestion et amélioration des écosystèmes forestiers, ENSA – Kasdi Merbah (Algérie).*

Received 15 December 2020; Accepted 14 April 2021

Abstract

Monitoring and analyzing land cover changes help to provide relevant information for the establishment of diagnostics and the preparation of environmental forecasts. The objective of this work is to apply an "object-oriented" classification method to three satellite images for monitoring and detecting land cover changes in the North of Ivory Coast. The landscape complexity of this environment and the low resolution of the images (30 m and 20 m) constitute an important limitation for conventional classification methods using the "pixel by pixel" approach. Two Land sat images TM/ ETM + (1986; 2002) and a Sentinel-2 image (2019) were used in this study. The method developed for monitoring and detecting changes in land cover is carried out through 1) a classification of land cover using the «object-oriented» method based on fuzzy logic and 2) detecting changes of land cover by the post-classification method followed by the integration within a GIS of the three land cover maps obtained. The Kappa coefficients of the classified land cover maps were 86, 88, and 84.55% at the level of the 1986 images; 2002 and 2019, respectively. For the period of interest (33 years), we mapped and quantified land-use changes in this complex environmental context. Our study shows that the study area is undergoing major changes in land cover. The modifications identified in the study area concern all the topics of interest.

Keywords: Land cover, North of Ivory Coast, Object-oriented approach, Post classification method.

1. Introduction

Environmental management and the preservation of biodiversity are now considered a priority in the context of the acceleration of global changes that affect the physical and biological resources of the earth. Further amplified by the inappropriate modes and systems of exploitation of the available resources, these changes raise fears of a «Desertification of landscape and flora» in the northern region of Ivory Coast (8 ° and 10 ° North latitude and 3 ° and 6 ° West longitude). The study area located northwest of the Ivory Coast is the savannah formations' domain. Agro-pastoral activities' growth endangers and increases the risks of degradation in this fragile environment (Geerling and Diakité, 1988).To study the degradation phenomenon of natural resources, numerous works based on optical remote sensing exist (Vägen et al., 2013; Mouissa et al., 2018). These studies generally use conventional classification methods (Maximum likelihood) which have recourse to the "pixel by pixel" approach (Podest and Saatchi, 2002; Mouissa and Fournier, 2013). However, the landscape complexity of the areas of interest and the great spectral heterogeneity of the images reduces the statistical dispersal of the classes, inducing an imprecision of the cartographic results (Chust et al., 2004). Also, several studies in optical remote sensing have used textural image information on the one hand and classification by object-oriented method on the other to improve the quality of the purely spectral classification (He et al., 1994). Thus, Galletti and Myint (2014) compared classifications by the "object-oriented" approach to the classic classification methods which use the "pixel by pixel approach". From an ASTER image, the authors proceeded to an "object-oriented" segmentation and classification of the Arizona "Sun Corridor" following six thematic classes of interest. With respectively 93.71% of overall processing precision and 0.92 of Kappa coefficient, Galletti and Myint (2014) concluded the contribution of textural information is essential if we want to improve qualitatively the results obtained from the purely spectral classification. Moran (2010), explored different classification methods from a QuickBird image taken on June 20, 2008, on the Lucas do Rio Verde (Mato Grosso, Brazil) to improve the mapping of occupation and land use in the urban area. Ultimately, Moran (2010) concludes that the integration of textural and spectral images improves the overall classification accuracy by 11.7% and the Kappa coefficient by a score of 0.14. Also, the use of the "object-oriented" classification method based on segmentation constitutes an effective approach to considerably improve the mapping of land cover. Johansen et al. (2007) explored from the "object-oriented" method, the potential of using textural information from a QuickBird image with very high spatial resolution from June 2005 for discrimination and mapping of the structural stages of vegetation in adjacent forest and riparian ecosystems on Vancouver Island. Following a geostatistical study using semivariograms, the authors concluded that the contribution of textural parameters (dissimilarity; contrast

* Corresponding author e-mail: habib.mouissa@gmail.com

and homogeneity) to the spectral data greatly improves, on the one hand, the discrimination of the structural classes of vegetation (between 2 -19%) and on the other hand, the overall accuracy of the cartographic results with 78.95%. Herold et al. (2002) evaluate the use of the "object-oriented" approach for land cover mapping in the Santa Barbara area (California). To do this, a set of treatments is carried out: geometric and atmospheric corrections, a segmentation of seven IKONOS images and then their classification using their spectral and textural properties. With a map with an overall accuracy of 79%, Herold et al. (2002) concluded that the object-oriented approach has enormous potential to report detailed and precise information on the physical structure of urban areas. Ultimately, though many studies in optical remote sensing use textural parameters and segmentation, few use principal component analysis (PCA) and an "object-oriented" approach to execute classifications based on fuzzy logic. In this context, the objectives of this work are twofold: 1) to use on three satellite images an object-oriented classification approach and 2) to detect changes in land use.

2. Literature review

The landscape's complexity and the relatively low resolution of the images used in this study (30 m and 20 m) constitute an important limitation for conventional classification methods which proceed "pixel by pixel" (Jukka and Aristide, 1998). Unlike these classifiers, the "object-oriented" classification does not treat the pixel in isolation but its context, by grouping pixels within objects whose spectral value, size, shape and context constitute the key to interpretation (Dell'acqua and Gamba 2006). Otherwise, the semantic information necessary for the interpretation of the image is not represented in isolated pixels, but rather in objects having a particular meaning, as well as in their mutual relationships (Schwarzer et al., 2009). The "object-oriented" classification is organized in two main stages (Stow et al., 2008): 1) a multi-resolution segmentation whose purpose is the establishment of a hierarchical network of objects representing different levels of reality on the ground (Wemmert et al., 2009); 2) a supervised classification based on different algorithms (Maximum likelihood, Fuzzy logic, etc.).

The assessment of cartographic accuracy is very important for understanding the results obtained. The success of change mapping and the GLCM method through the use of remote sensing data also necessitates the careful choice of textural parameters to use as neo-channels in the subsequent classification process. In this perspective, the approach by the co-occurrence matrix of the grey levels is retained (Kayitakire et al., 2002) and applied to the eight textural parameters calculated respectively on the 7x7 and 17x17 windows and generated from each of the images available for this study. Two textural parameters, the mean and the correlation are chosen because of their weak correlations with the other six and added as neo-channels to the main components 1 (CP1) of the images of interest to drive and improve the "oriented" classification object" (Cruse et al., 1984). The most common elements include the assessment of overall accuracy, producer accuracy, user accuracy and the Kappa coefficient (White et al., 2007). The literature provides detailed information on the methods for calculating these elements (Congalton et al., 1983; Congalton, 1991; Congalton and Green, 1999).

In the field of land cover mapping, textural information of satellite images is of the first importance. It is established that the contribution of textural information improves the quality of the purely spectral classification (He and Wang, 2010). To do this, Haralick et al. (1973) proposed for the calculation of textural parameters, the method of grey level co-occurrence matrices (GLCM) mostly used in the analysis of remote sensing data (Del Frate et al., 2008). The success of this method requires the prior determination of three parameters: 1) the appropriate distance between pixels; 2) the appropriate direction between pixels; 3) the optimal window for calculating the textural parameters on the study area. In this study, the first two parameters are chosen according to the indications in Haralick (1979) and Safia and He (2015): an interpixel distance of 1 is used and the textural parameters used correspond to the average values in the four directions (0°; 45°; 90° and 135°) likely to carry all the textural information derivable from the Gray Level Co-occurrence Matrices (GLCM). The choice of the optimal window is more sensitive because it depends on the satellite data used and on the study objectives. It is achieved through the calculation of the coefficient of variation (standard deviation/average) of any textural parameter in the image (Puissant et al., 2005). Ultimately, the window for which the coefficient of variation is stable and lower for the majority of land use classes is chosen (Puissant et al., 2005).

3. Materials and Methods

3.1. Study area

The study area [9 ° 27'to 9° 57' N; 5° 39'to 5° 58' W] is located in the northwest of Ivory Coast (Figure 1).

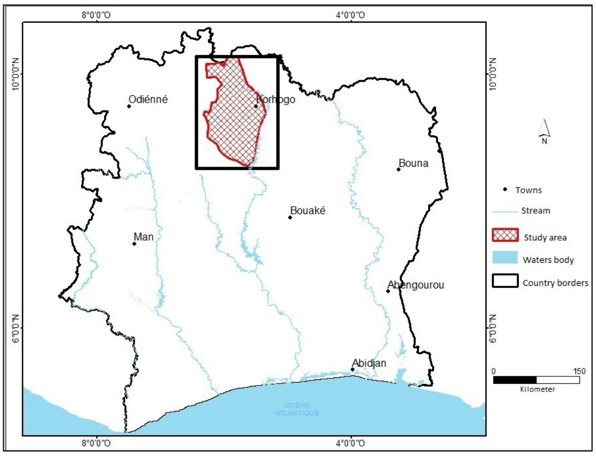

Figure 1. Study area located at (9 ° 27' to 9° 57' N; 5° 39' to 5° 58' W) in the northwest of Ivory Coast.

Here, the relief is a vast peneplain of 300 to 500 m altitudes interspersed with buttes, armoured plateaus and isolated inselbergs like Mount Korhogo. The region has a tropical Sudano-Guinean climate characterized by the existence of two very contrasting seasons (Géomines, 1982): a rainy season which lasts from May to October, with maximum rainfall in July-August and a dry season, well-marked from November to April. In terms of land cover, plant formations of the savannah, tree or shrub type are more widespread in the Center with a grassier tendency in the North and clear forest in the South and the West. Forest galleries highlight certain rivers and classified forest islands and "sacred woods" are found on the outskirts of villages. The demography of the department of Korhogo is one of the most dynamic in the Ivory Coast with 763,852 inhabitants in 2014 (INS, 2014). This population (Sénoufo, Malinké) is mainly rural and cultivates corn, sorghum, yam, rainfed or irrigated rice, cotton and cashew. Land tenure in the Senoufo country is democratic as all individuals have access to land. This status of the land leads to competition in its access and appropriation. As a result, people cultivate large areas and would not hesitate to migrate to new cropland at the first signs of soil degradation.

3.2. Satellite images and Data

Three satellite images, including two Landsat TM / ETM + images (Scene 197-53 acquired from http://earthexplorer.usgs.gov/) taken in the dry season, on January 16, 1986, and January 21, 2002, respectively and a Sentinel-2 (Acquired from (https://scihub.copernicus.eu/dhus/#/home) image which was acquired February 12, 2019, were used to perform this study. In addition to these images, there are also field data relating to 69 ground control points (GCPs). The Landsat TM / ETM + and Sentinel-2 images have a spatial resolution of 30 m and 20 m respectively. In this study, the GCPs would help to learn and validate the method of mapping and detecting changes in land cover. Also, 50% of the GCPs are integrated as learning points for conducting the images classification and 50% of the points as validation for accuracy assessment.

4. Methodological approach

A preliminary step consists of processing the images of interest (radiometric and geometric correction, generation of different indices, resampling, etc.) by ENVI 5.3 software. The method of mapping and detecting changes in land use are developed and carried out through 1) a Principal Component Analysis (PCA) transformation applied to the three satellite images; 2) classification and detection of land-use changes from Landsat TM/ETM+ and Sentinel-2 images using i) textural information of the images and ii) the «object-oriented» method based on the fuzzy logic according to the land use classes (open forest; wooded savannah; humanized areas and ponds or water).

Figure 2 presents the methodological flowchart of this project. Details of the different methodological aspects of monitoring and detecting land-use changes are presented in the following subsections.

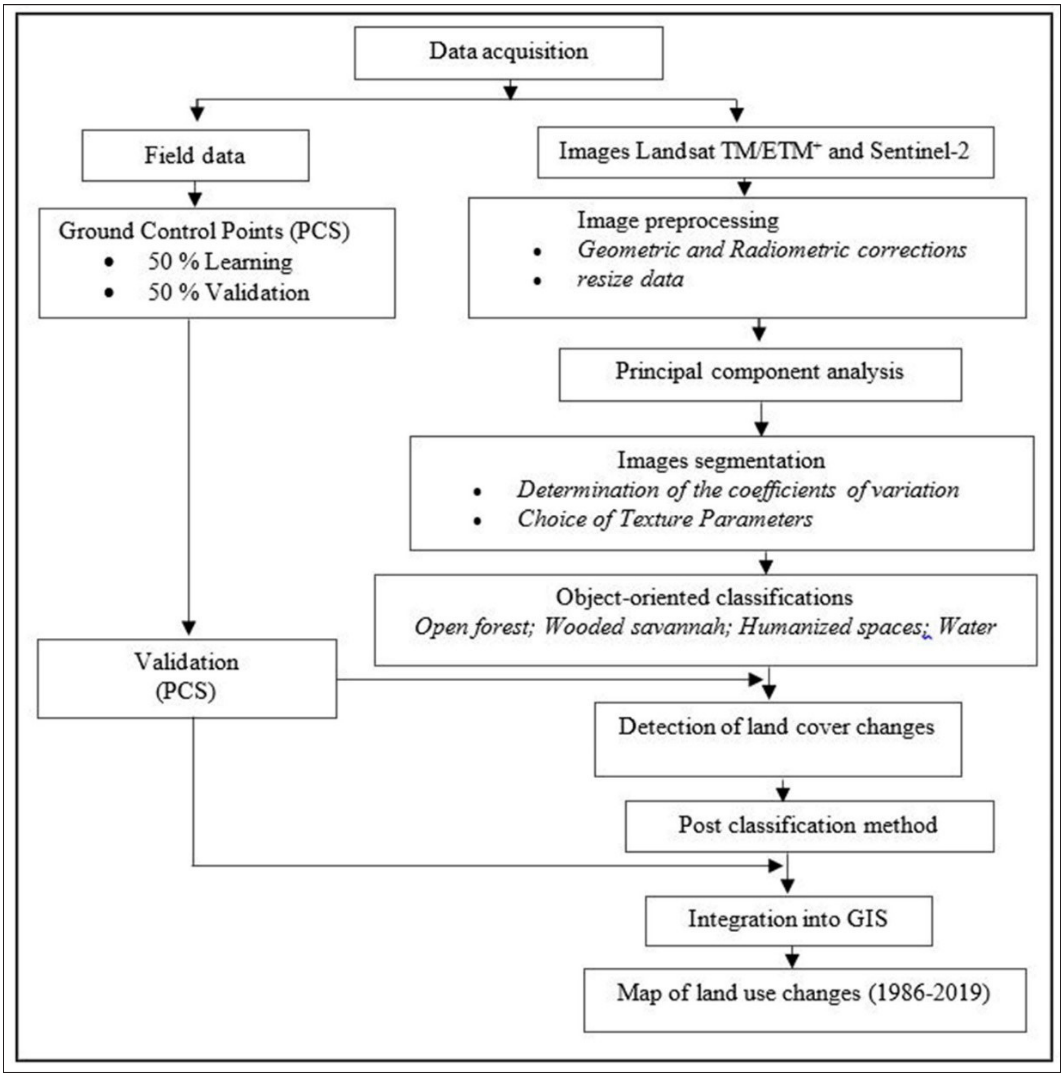

Figure 2. Methodological flowchart of monitoring and detecting land-use changes in the department of Korhogo.

4.1. Principal Component Analysis (PCA)

Satellite images of the same scene recorded according to the different spectral bands of a multispectral sensor (Landsat TM / ETM +; Sentinel-2) are generally strongly correlated. In this study, PCA is therefore used to eliminate redundancy in information and to retain for each image, the only components with significant information content (greater than 85%) and therefore optimal for mapping and fine detection of changes in land use (Jensen, 2005). Indeed, PCA makes it possible to synthesize a set of data initially expressed by highly correlated variables into a reduced number of new «uncorrelated» variables which express the maximum variance in the raw data (Carvalho and Gherardi, 2008).

4.2. Land cover mapping

4.2.1. Textural information of satellite images

To determine the optimal window size (size from 3 to 21) for each satellite image in this study, the second angular momentum and contrast parameters are chosen from the eight textural parameters (homogeneity; contrast; dissimilarity; mean; standard deviation; entropy; second angular momentum and correlation). These parameters are the least correlated and the most used in remote sensing (Solberg, 1999). The evolution of the coefficient of variation of these parameters on the different windows for the four lands' types allows identifying the windows' size of 7x7 and 17x17 as optimal for calculating the textural parameters. Figure 3 presents the evolution of the coefficient of variation for the Sentinel-2 image of February 12, 2019.

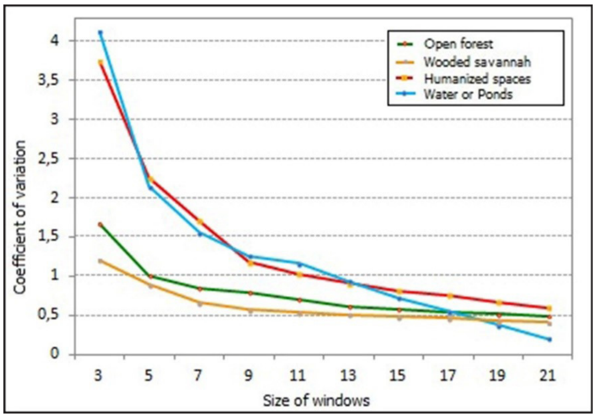

Figure 3. Coefficient of variation of the contrast parameter (Sentinel-2 of February 12, 2019).

When using the sizes 3 and 5 as windows, the coefficients of variation were low for three out of four land use. Thus, on the 7x7 window, they stabilize and reach low values for two classes of land cover. Beyond the 7x7 window, the coefficients of variation, although small, become divergent. Regarding the image of February 12, 2019, we observe that for window sizes less than 17x17 (Figure 2), the coefficients of variation of the four land cover classes are high and dependent on the window size. On the 17x17 window, they stabilize and reach very low values. Beyond the 17x17 window, the coefficients of variation are small and divergent (Figure 3).

4.2.2. Object-oriented image classification

For the present study, different thresholds are respectively tested on the 1986 image sets; 2002 and 2019 (CP1 and the two textural images selected). These thresholds identified the segmentation parameters (scale from 500 to 25 and heterogeneity criteria: shape and compactness from 1 to 0) adapted to the study area. In the present context, this approach is well suited because it calls on membership functions taking into account the notion of uncertainty through the formulation of a certain number of knowledge rules defined for each type of object to be classified (Jensen, 2005). These membership functions are obtained from the two textural neo-channels (Average and Correlation) or combinations of these neo-channels with the CP1s of the two images of interest (Castaneda and Ducrot, 2009).

4.3. Detection of changes in land cover and accuracy assessment

The post-classification approach is carried out by superimposing two or more multi-temporal images of the same scene, classified independently and then comparing the thematic classes of interest on a "pixel" basis. It generates a complete matrix of change information and indicates both the nature of the change and its magnitude (Jensen, 2005).

In this study, we limit the process of assessing overall accuracy to the Kappa index. And as already indicated, 50% of the ground control points (GCPs) were used for this validation purpose.

5. Results and Discussion

5.1. Principal component analysis

The multispectral bands of the Landsat TM / ETM + and Sentinel-2 images used in this study have strong correlations. Also, these spectral bands are subjected to an ACP transformation. The first main components (CP1) concentrate 88.08%, 84.76% and 78.14% variance for the satellite images of 1986, 2002 and 2019, respectively. Therefore these components (Figure 4a (1986) and 4b (2019)) are used for the implementation of multi-resolution segmentation.

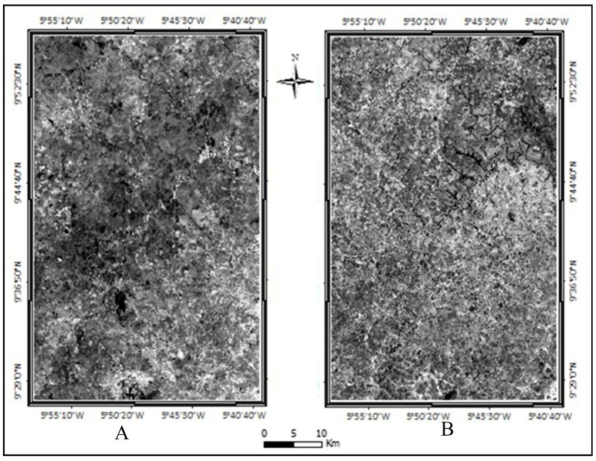

Figure 4. Result of the ACP transformation. A) Main component1 (Landsat TM, January 16, 1986); B) Main component1 (Sentinel-2, February 12, 1919).

5.2. Classification and validation of land cover

Fine mapping of land use according to the four classes of interest was obtained using a segmentation which let to identify fairly precise geographic objects on the three satellite images. This mapping of land use reached Kappa coefficients of 86, 88 and 84.55% for the maps of 1986, 2002 and 2019 respectively (Figure 5, Figure 6, Figure 7 and Table 1). These statistics represent a very acceptable overall precision as reported by Chalifoux et al. 2006). As to confirm the effectiveness of the segmentation and membership functions chosen, we note for the image sets (CP1 and textural images) of 1986; 2002 and 2019 that the segmentation is efficient with an overall scale factor of 125 and shape and compactness values of 0.4 and 0.9 respectively. The geographic objects thus identified are precise enough to discriminate between the four land cover classes. Regarding the supervised classification, fuzzy logic (Sparfel et al., 2008) is applied to the study site characterized by land use classes with fuzzy semantic and spatial limits.

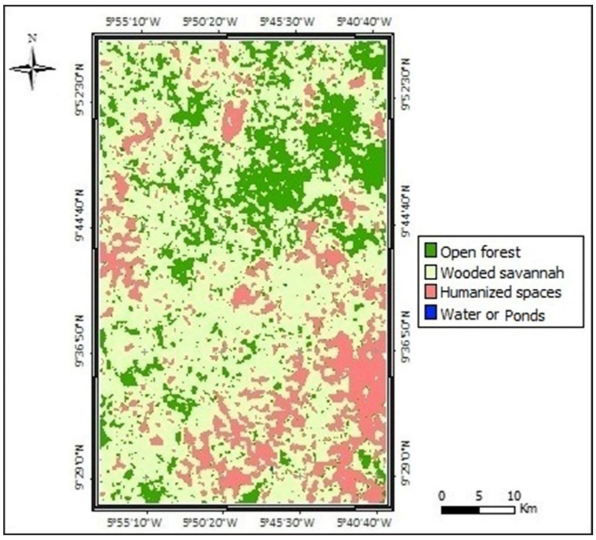

Figure 6. Result of the classification of the land cover of the study area in 2002.

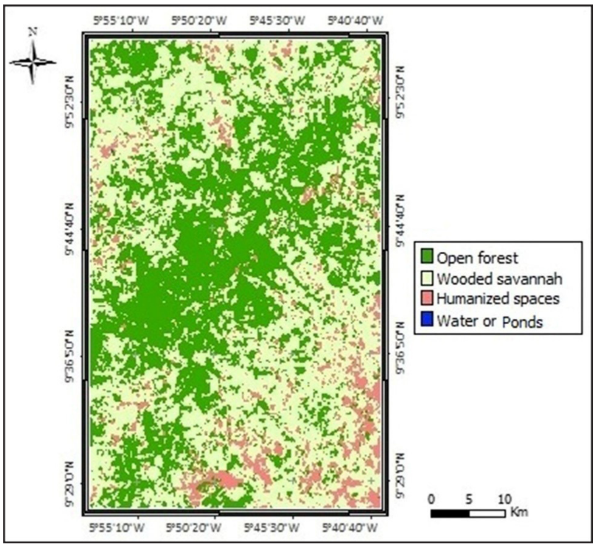

Figure 5. Result of the classification of the land cover of the study area in 1986.

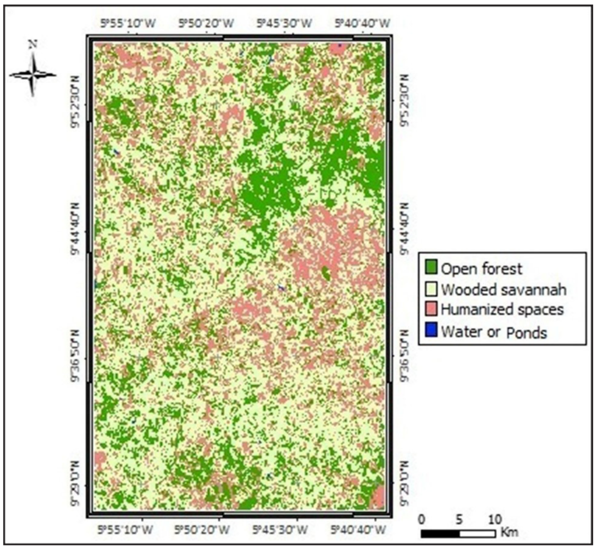

Figure 7. Result of the classification of the land cover of the study area in 2019.

Table 1. Land cover and areas mobilized in 1986, 2002 and 2019.

Land cover	Area of 1986 (ha)	(%)	Area of 2002 (ha)	(%)	Area of 2019 (ha)	(%)
Water or ponds	18	0.01	35	0.02	105	0.06
Humanized areas	13782	7.86	31755	18.11	36385	20.75
Open forest	72892	41.57	34456	19.65	46397	26.46
Wooded savannah	88656	50.56	109102	62.22	92461	52.73
Total	**175348**	**100**	**175348**	**100**	**175348**	**100**

The Analysis of maps (Figures 5, 6 and 7 and Table 1) shows that the study area is undergoing major changes in land cover. These findings are corroborated by Agouale et al. (2017).The modifications identified in the study area concern all the topics of interest. However, a more detailed thematic analysis makes it possible to detect certain specificities. These include the open forest experienced a reduction of more than half of its area from 1986 to 2002 (- 52.73%). Between the intermediate analysis period (2002) and the year 2019, the open forest increased (+ 36.56%). Wooded savannah was subjected to significant mutations (Wendpouiré, 2020). Between 1986 and 2002, it experienced a 23.06% increase in its surface areas. But since 2002, a decreasing trend was observed and the wooded savannah areas decreased to 92 461 ha. An extension of the floodable or marshy areas was observed. Indeed, the Water (dams-ponds-ponds) and floods and/or swampy areas complex which mobilized in 1986 only 0.01% of the area or 18 ha increased in 2019 and now covers 0.06% of the area is 105 ha.

Overall, from the change detection approach used in this study it noted that a significant part of the study area (+ 79%) is covered with plant formations (Clear forest and/or wooded savannah and wooded savannah and/or shrubby). This situation is certainly the result of a change in peasant land management practices and the strengthening of measures to protect and conserve classified areas (Korhogo and Badénou classified forests). In fact, due to the increase in the purchase price of cashew nuts, the favourable land of open forest and wooded savannah were transformed into cashew and mango plantations (Gansaonré, 2018).

5.3. Detection of changes in land cover

The detection of land cover changes by the post-classification method is carried out by superimposing the three previously obtained maps (Figures 5-7). Analysis of the global map of land cover changes (Figure 8) shows that the proportions of the different rights-of-way reflect those from the maps of 1986 2002 and 2019. It is thus noted that more than 2/3 of the study area (72.18%) is affected by modifications in land use (Table 2).

Table 2. Global change Statistics map (1986-2019).

Land cover	Area (ha)	Area (%)
Water or ponds	53	0.03
Humanized areas	2122	1.21
Open forest	12134	6.92
Wooded savannah	34473	19.66
Changes	*126566*	*72.18*
Total	**175348**	**100**

This area of 126,566 ha mostly coincides with the southern and central part of the study area where the agricultural plots are mainly established (Figure 8).

On these portions of the area, the interannual changes (1986-2019) of land use make their identification and recognition by remote sensing difficult and complex. In addition, the methodological approach (post-classification method) implemented in this study for the detection of changes has as a corollary, the generation of a class of changes grouping all the geographic objects having an interannual movement. However, these objects cannot be immediately assigned to a type of land cover without further analysis (Sylla, 2012). Also, the complex nature of the study area and the state of the available data require that the notions of uncertainty and imprecision be taken into account for the monitoring and detection of changes in land use. The Dempster-Shafer theory, an expert-type model, could help in the identification and better detection of land-use changes (Sylla, 2012). Indeed, the Dempster-Shafer probabilistic fusion rule makes it possible to combine different sources of data with a view to better decision-making (Corgne, 2004; Mora, 2009). Also, we are considering the use of specific spectral indices such as the three decorrelated indices (brightness, greenness and wetness) from the Tasseled Cap transformation. These indices allow the characterization of agricultural areas in numerous studies (Mora, 2009; Mouissa et al., 2018).

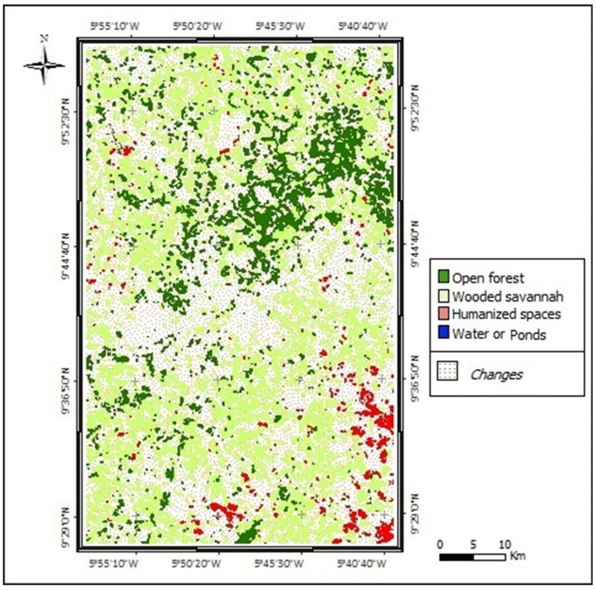

Figure 8. Global map of changes (1986-2019).

6. Conclusions

The study area is a complex environment. Monitoring and detecting land cover changes in such an environment was a real challenge. With the «object-oriented» method, we monitored and detected land cover changes from three satellite images (Landsat TM / ETM + and Sentinel-2 images). For the period of interest, the methodology developed in this study reached a fine detection of changes in land cover. The final map of land cover changes is intended to serve as a decision-making tool for planning agricultural activities. Dempster-Shafer's probabilistic combination rule is well suited for this purpose.

References

Agouale, Y. J., Vei, K. N., Affro, M. J. (2017). Anthropic pressures and dynamics of land cover in Katiola sub-prefecture. Ivorian. Journal of Savannah Geography 1: 78-86.

Carvalho, M., and Gherardi, D. F. M. (2008). Mapping the environmental sensitivity to the oil spill and land use/land cover using spectrally transformed Landsat 7 ETM data. Brazilian Journal of Aquatic Science and Technology 2: 1-9.

Castaneda, C., and Ducrot, D. (2009). Land cover mapping of wetland areas in an agricultural landscape using SAR and Landsat imagery. Journal of Environmental Management 7: 2270-2277.

Chalifoux, S., Nastev, M., Lamontagne, C., Latifovic, R., Fernandes, R. (2006). Land cover and land use mapping using Landsat imagery in hydrogeology. Télédétection 1: 9-17.

Chust, G., Ducrot, D., Pretus, J. LL. (2004). Land cover discrimination potential of radar multitemporal series and optical multispectral images in a Mediterranean cultural landscape. International Journal of Remote Sensing 17: 3513-3528.

Congalton, R. G., Oderwald, R. G., Mead, R. A. (1983). Assessing Landsat classification accuracy using discrete multivariate analysis statistical techniques. Photogrammetric Engineering and Remote Sensing 12: 1671-1678.

Congalton, R. G. (1991). A review of assessing the accuracy of classifications of remotely sensed data. Remote Sensing of Environment 1: 35- 46.

Congalton, R. G., and Green, K. (1999). Assessing the Accuracy of Remotely Sensed Data: Principles and Practices. Boca Raton, FL, USA: CRC/Lewis Press, USA.

Corgne, S. (2004). Predictive modelling of land use in an intensive agricultural context: application to winter soil cover in Brittany. PhD. Dissertation, University of Rennes 2-Haute-Bretagne (France).

Cruse, D., Oddy, C. J., Wright, A. (1984). A Segmented Image Data Base (SID) for Image Analysis. In: 7th International Conference on Pattern Recognition (ICPR). Montreal, Canada July, Institute of Electrical and Electronics Engineers: 493-496.

Del Frate, F., Pacifici, F., Solimini, D. (2008). Monitoring Urban Land Cover in Rome, Italy, and Its Changes by Single-Polarization Multitemporal SAR Images. Institute of Electrical and Electronics Engineers Journal of Selected Topics in Applied Earth Observations and Remote Sensing 2: 87-97.

Dell'acqua, F., and Gamba, P. (2006). Discriminating urban environments using multiscale textural and multiple SAR images. International Journal of Remote Sensing 18: 3797-3812.

Galletti, C. S., and Myint, S. W. (2014), Land-Use Mapping in a Mixed Urban-Agricultural Arid Landscape Using Object-Based Image Analysis: A Case Study from Maricopa, Arizona. Remote Sensing 7: 6089-6110.

Gansaonré, R.N. (2018). Dynamique du couvert végétal et implications socio-environnementales à la périphérie du parc W/Burkina Faso. VertigO La revue électronique en sciences de l'environnement 18 (1): 1-19.

Geerling, C., and Diakité, M. D. (1988). Final report of the Research project for the rational use of prey in the Sahel (RURGS). Department of Nature Planning, Wageningen Agronomic University, Wageningen, 93 p.

Géomines, (1982). Hydrogeological inventory of Ivory Coast applied to village hydraulics. Ministry of Public Works and Transport.Central Directorate of Hydraulics.The Republic of Ivory Coast.Map of Gagnoa. Cahier n° 24, 31 p.

Haralick, R. M. (1979). Statistical and Structural Approaches to Texture. Proceedings of the Institute of Electrical and Electronics Engineers 67 (5): 786-804.

Haralick, R. M., Shanmugam, K., Dinstein, I. (1973), Textural Features for Image Classification. Institute of Electrical and Electronics Engineers Transactions on Systems, Man, and Cybernetics 6: 610-621.

He, D.-C.; Wang, L.; Baulu, T.; Morin, D.; Bannari, A. (1994). Classification spectrale et texturale des données d'images SPOT en milieu urbain. International Journal of Remote Sensing 15(10): 2145-2152.

He, D. C., and Wang, L. (2010). Simplified texture spectrum for texture analysis. Journal of Communication and Computer 8: 44-53.

Herold, M., Scepan, J., Müller, A., Günther, S. (2002). Object-oriented mapping and analysis of urban land use/cover using IKONOS data. Proceedings of 22nd EARSel Symposium Geoinformation for European-wide integration, 8 p. Prague, Czech Republic, June 4-6.

INS, (2014). General Population and Housing Census in 2014. Global results, Permanent Technical Secretariat of the GPHC, Technical Committee of GPHC, 26 p.

Jensen, J. R. (2005). Introductory digital image processing: A remote sensing perspective, (3rdEd). Pearson Prentice Hall Upper Saddle River, USA.

Johansen, K., Coops, N. C., Gergel, S. E., Stange, Y. (2007). Application of high spatial resolution satellite imagery for riparian and forest ecosystem classification. Remote Sensing of Environment 1: 29-44.

Jukka, H., and Aristide, V. (1998). Land cover/land use classification of urban areas: a remote sensing approach. International Journal of Pattern Recognition and Artificial Intelligence 4: 475-489.

Kayitakire, F., Giot, P., Defourny, P. (2002). Automated delineation of the forest stands using digital colour orthophotos: A case study in Belgium. Canadian Journal of Remote Sensing 5: 629-640.

Mora, B. (2009). Mapping of forest parameters by obvious fusion of multi-source geospatial data; application to regenerating forest stands and mature hardwoods in southern Quebec. PhD. Dissertation, University of Sherbrooke, Canada.

Moran, E. F. (2010). Land Cover Classification in a Complex Urban-Rural Landscape with Quickbird Imagery. Photogrammetric Engineering and Remote Sensing 10: 1159-1168.

Mouissa, H., and Fournier, R. A. (2013). Mapping stand volumes of Pinus halepensis Mill in a semi-arid region using satellite imagery of the Sénalba Chergui forest in north-central Algeria. Journal of Arid Environments 92: 63-75.

Mouissa, H., Fournier, R.A., Oldache, E.H., Bellatreche, M. (2018).Detection of changes in forest cover in a semi-arid environment from 1984 to 2009: Case of the Senalba Chergui forest in Djelfa (Algeria). Canadian Journal of Remote Sensing 2: 113-130.

Podest, E., and Saatchi, S. (2002). Application of multiscale texture in classifying JERS-1 radar data over tropical vegetation. International Journal of Remote Sensing 7: 1487-1506.

Puissant, A., Hirsch, J., Weber, C. (2005). The utility of texture analysis to improve per-pixel classification for high to very high spatial resolution imagery. International Journal of Remote Sensing 4: 733-745.

Schwarzer, S., Allenbach,K., Jaquet, J.M. (2009). Semi-automated, multi-source cartography of land cover. Archives des Sciences 62: 107-124.

Solberg, A. S. (1999). Contextual data fusion applied to forest map revision. IEEE Transactions on Geoscience and Remote Sensing 3: 1234-1243.

Sparfel, L., Gourmelon, F. Le Berre, I. (2008). Object-oriented approach of coastal land cover. Revue Télédétection 4: 237-256.

Stow, D., Hamada, H., Coulter, L., Anguelova, Z. (2008). Monitoring shrubland habitat changes through object-based change identification with airborne multispectral imagery. Remote Sensing of Environment 3: 1051-1061.

Safia, A., He, D-c. (2015). Multiband compact texture unit descriptor for intra-band and inter-band texture analysis. ISPRS Journal of Photogrammetry and Remote Sensing 105: 169-185.

Sylla, D. (2012). Spatio-temporal modelling of environmental vulnerability to soil degradation in the semi-arid area from radar data. PhD. Dissertation, University of Sherbrooke, Canada.

Vägen, T. G., Winowiecki, L. A., Abegaz, A., Hadgu, K. M. (2013). Landsat-based approaches for mapping of land degradation prevalence and soil functional properties in Ethiopia. Remote Sensing of Environment 134: 266-275.

Wemmert, C., Puissant, A., Forestier, G., Gançarski, P. (2009). Multiresolution remote sensing image clustering. IEEE Geoscience and Remote Sensing Letters 3: 533-537.

Wendpouiré, A. Z. (2020). Dynamics of forest coverage of Sahelian agrosystems of northern Burkina Faso after the droughts of 1970-1980: implication of land management practices. PhD. Dissertation, University of Québec at Montréal, Canada.

White, J. C., Wulder, M. A., Grills, D. (2007). Assessing the accuracy of mountain pine beetle red attack damage maps generated from satellite remotely sensed data. Canadian Forest Service Publications 36: 1- 4.

JJEES

JJEES (2021) 12 (4): 344-352
ISSN 1995-6681

Jordan Journal of Earth and Environmental Sciences

Assessment of the surface water suitability for irrigation purposes: Case of the Guenitra dam watershed (Skikda, NE Algeria)

Selma Hadef, Faouzi Zahi*, Taha-Hocine Debieche, Abdelmalek Drouiche, Abdelmalek Lekoui

Geological Engineering Laboratory (LGG), Department of Earth Sciences and the Universe, Faculty of Nature and Life Sciences, University of Mohamed Seddik Benyahia - Jijel, Algeria.

Received 22 February 2021; Accepted 14 April 2021

Abstract

This paper aims to determine the water suitability for irrigation purposes originated from the Guenitra dam and its tributaries. This dam is located downstream of the Guenitra watershed (sub-catchment from the Guebli watershed). This watershed is considered among the highly influenced areas by anthropogenic activities including mostly urban wastes and leachate products of the abandoned polymetallic sulphide mine of SidiKamber. Two water sampling campaigns were carried out, during rainy and dry seasons, namely December 2017 and September 2019 respectively. The Physico-chemical parameters (hydrogen potential (pH) and electrical conductivity (EC) were measured in-situ while the major elements were analysed in the laboratory. The obtained results have been interpreted and evaluated by using indicators of water irrigation quality such as sodium absorption ratio (SAR) and percentage of sodium (%Na), in combination with electrical conductivity, in addition, the residual sodium carbonate (RSC) and the permeability index (PI). As a result, the water of Guenitra dam and its tributaries exhibit good to admissible quality for irrigation, excluding the waters of wadi Essouk tributary those are of poor quality due to direct discharge of the leachate product of SidiKamber abandoned mine, causing acidic character (3.09 to 5.30) as well as an important mineralization content (2550 to 2900 µS/cm) of water.

Keywords: water quality, irrigation, surface water, Guenitra dam, Skikda, Algeria.

1. Introduction

Algeria, similar to all the countries of the Mediterranean basin, has suffered water stress due to climate change, urban and demographic growth (Touati, 2010). Since the beginning of the 21st century, a new water policy has been undertaken by the Algerian government to mobilize new water resources by building dams. Currently, Algeria accounts for about 83 dams, which are an important source for drinking water supply, irrigation and industrial purposes (Allalgua et al., 2017; Touhari et al., 2018). The physicochemical composition of dam waters is mainly related to the nature of the geological formations crossed by the draining tributaries of the watershed (Lakhili et al., 2015; Ouhmidou et al., 20015; Bouguerne et al., 2017) and to the influence of anthropogenic discharges that lead to the degradation of the surface waters quality makes the wadi and dams water useless. Since 1980, the Skikda region has experienced several problems regarding water quality, in response to population growth, industrial and agricultural development (Bahroun et al., 2017). Urban and industrial discharges are the main causes, they are often dumped into rivers without any prior treatment (Belhadj and Boudoukha, 2014). The Guenitra dam watershed is considered among the influenced areas by anthropogenic activities, mainly the leachate product impact from the SidiKamberabandoned mine (Issaad et al., 2019). Previous studies carried out on the SidiKamberabandoned mine by (Boukhalfa, 2007; Medjram and Khalfaoui, 2014; Gherib et al., 2017; Issaad et al., 2019; Charchar et al., 2020) have been focused on acid mine waste in addition to the effects of heavy metals on the microbial quality of soils and surface waters of wadi Essouk, which drains the abandoned mine and discharges directly into the Guenitra dam. In this study, we report Physico-chemical data of the Guenitra dam water and its tributaries to shed the light on their suitability for irrigation, to qualify the possible risks of its waters on soil degradation, the effect of rainy and dry periods as well as the leachate product impact on surface water quality.

2. Materials and methods

2.1. Study area

The Guenitra dam, the studied area, is in the northeast of Algeria (Figure 1a), about 30 km south of Collo town (Wilaya of Skikda) (Figure 1b). It occupies the downstream part of its watershed (202 km2 of surface area) which is characterised by a dense hydrographic network. The main wadis that feed the Guenitra dam are wadi Fessa, wadi Charfa, wadi Magramene, wadi Malouh and wadi Essouk (Figure 1c). The dam (120 hm3of total capacity) ensures drinking water supply to Skikda city (37000 m3), the surrounding towns, the industrial zone (16000 m3) (Medjram and Khalfaoui, 2014) and the irrigation of EmdjezEdechich and the Saf-Saf valley perimeters (area of 5650 hectares) (Boukhalfa, 2007; Mecibah, 2017). Surface waters of Guenitra dam watershed are subjected to nocive anthropogenic activities such as, discharges of wastewater from OumToub and BeniOulbane townships and agricultural water as well as leachates product from SidiKamberabandoned mine, which could cause

* Corresponding author e-mail: f_zahi@univ-jijel.dz

deterioration of the dam water quality.

According to the weather station of Guenitra dam, the mean annual rainfall in the study area is 650 mm/year (1989-2004) (Issaad et al., 2019). It is characterised by a Mediterranean climate with two distinct seasons;(i) rainy humid season extending from October to April with a maximum rainfall average of 78 mm/month and a minimum temperature average of 13.5°C/month; (ii) Dryless rainy season extending from May to September with low monthly average rainfall (20 mm/month) and relatively high monthly temperatures (≈ 25°C/month) (Mecibah, 2017).

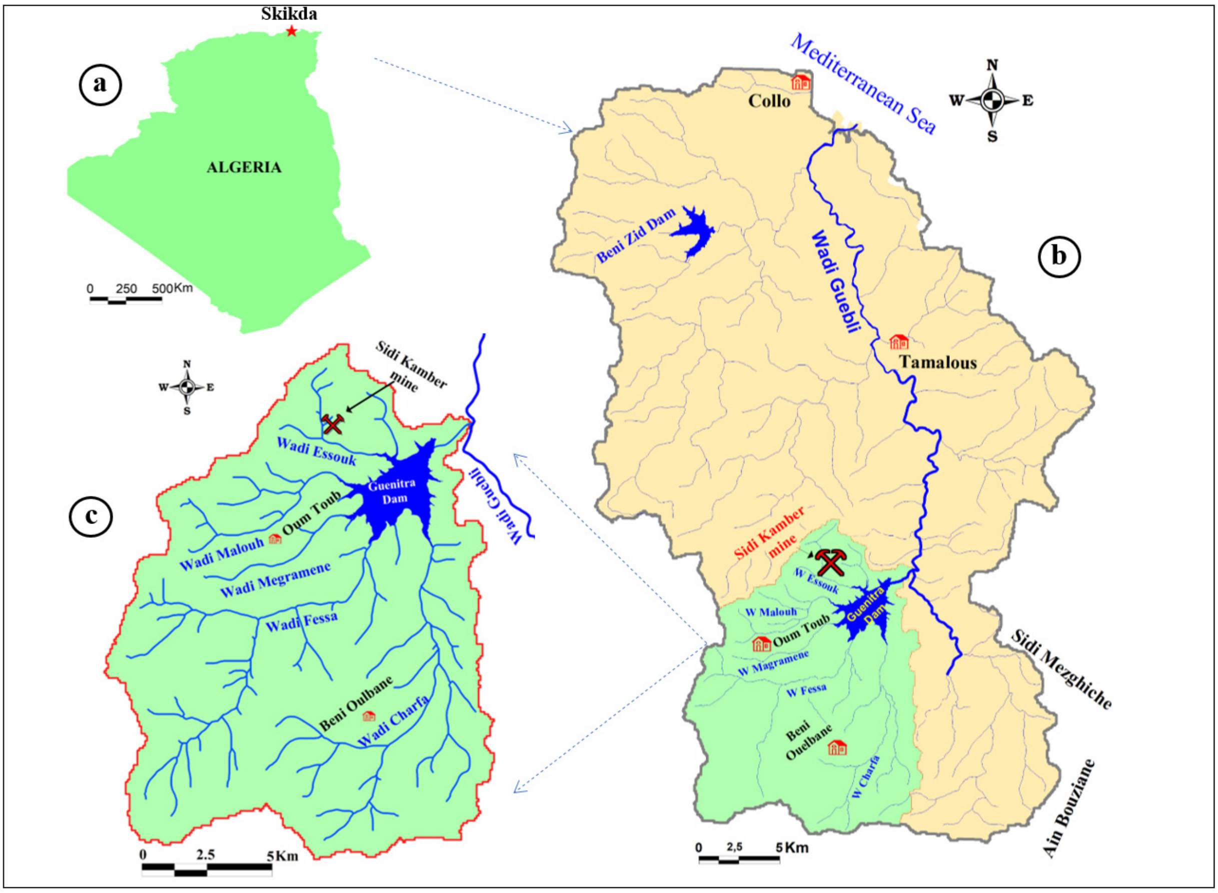

Figure 1. The geographical location of the Guenitra watershed; a. Map of Algeria, b. wadi Guebli watershed area, c. Guenitra watershed.

The Geology of the Guenitra watershed comprises different structural domains that belong to the so-called "internal zones" of the Maghrebid chain (Figure 2). According to Mahdjoub (1991) metamorphic rocks (Kabyle basement) of the Proterozoic to Lower Palaeozoic age are the most widespread and are surmounted by their Mesozoic calcareous cover (calcareous chain). In addition, Tellian units and flysch formation could also be present with a lesser importance. The Kabyle basement formations, mainly represented by gneisses and different types of schists, outcrops in the northwestern part (Figure2). Although, in the best part of the area, it outcrops as tectonic windows (Mahdjoub, 1991). These metamorphic formations host the Pb-Zn-Fe-Ba sulphide mineralization of SidiKamber Igneous rocks, solely represented by microgranites, are less widespread and are intruded in the Kabyle basement as a dyke shape. The Flysch formations of cretaceous ageoccupy the core of the watershed while the upstream part is dominated by carbonate formations (marl, limestone, marly limestone) of the Tellian units. The Numidian nappe of Miocene age is the most recent formation, it occupies the upper parts, therefore it covers all the older formations mentioned above.

The SidiKamber abandoned mine (North-West of the Guenitra dam) has been installed above the Kabyle basement. It should be noted that the deposit is composed of a series of massive sulphide veins scattered on both sides of the Essouk wadi. The sulphide mineralization is represented by galena (PbS), sphalerite (ZnS), pyrite-marcasite (FeS_2) and barite ($BaSO_4$) (Issaad et al., 2019). In 1976, mining activities of the Pb-Zn deposit have been ceased, since the only barite has been mined by open-pit until 1984, when the mine was definitively closed, however, the resulted leachate products have continued to flow into watercourses without prior treatment (Boukhalfa, 2007).

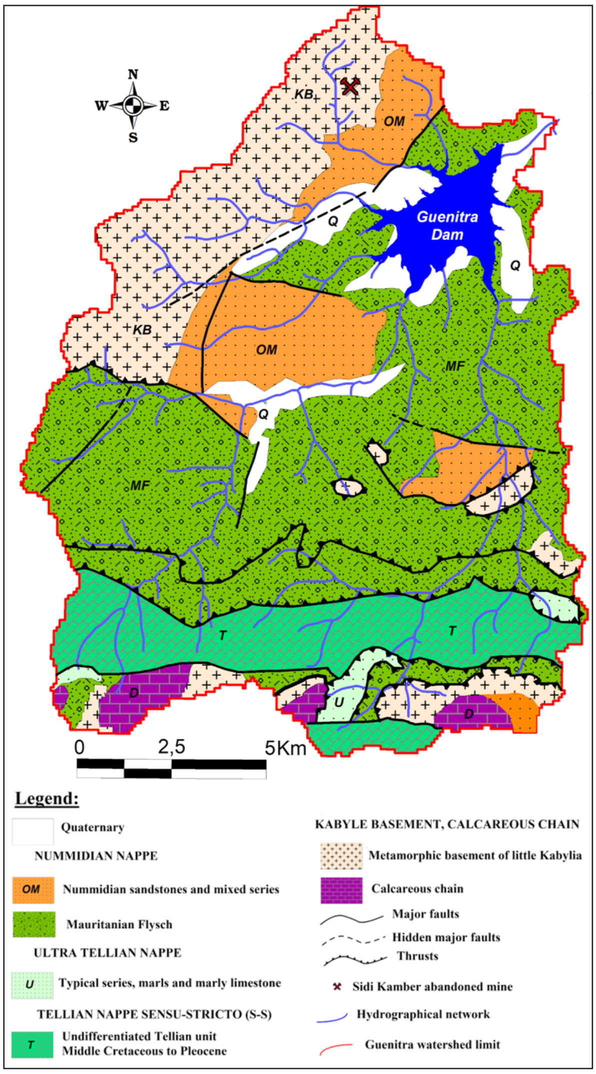

Figure 2. Geological map of the study area (Vila, 1980).

2.2. Sampling and analysis methods

For a good spatio-temporal characterization of Guenitra watershed water chemistry and its dam, two water sampling campaigns were carried out; (1) during the rainy season (December 2017) where the effect of dilution is important, and (2) during the dry season (September 2019) where the effect of dilution is negligible. During the two campaigns, 17 samples were collected from 10 sampling sites (Figure 3) where: eight (08)sites are located in the dam's tributaries to characterize the water inflows from the dam, one (01) site located in the dam lake (near the dam seawall) to evaluate the quality of the dam water which is used for irrigation purposes, and the last station located in the downstream (after the dam) to evaluate the quality of the dam water discharged into wadi Guebli (Figure 1b). Three (3) samples were not collected: one (O2) during the September 2019 campaign and two (O9 and B1) during the December 2017 campaign.

The samples were preserved according to Rodier et al. (2009). In-situ measurements of the physico-chemical parameters (hydrogen potential (pH) and electrical conductivity (EC)) were done using the Hanna portable pH-metre (HI 8424) and conductivity metre (HI-8733).

The major chemical elements analysis (Ca^{2+}, Mg^{2+}, Na^+, K^+, Cl^-, SO_4^{2-}, HCO_3^- and NO_3) was carried out at the Geological Engineering Laboratory (LGG) of Mohamed Seddik Benyahia-Jijel University using a spectrophotometer (UV 1600 PC), flame spectrophotometry (AFP 100) and volumetric titration. The protocols and methods of chemical analysis are done according to Rodier et al. (2009). The verification of analytical error of analysed ions concentration was done by the electro neutrality (charge-balance error) according to the following equation:

$$CBE = \frac{\sum cations - \sum anions}{\sum cations + \sum anions} \; x\,100$$

The major chemical elements analysis (Ca2+, Mg2+, Na+, K+, Cl-, SO42-, HCO3- and NO3) was carried out at the Geological Engineering Laboratory (LGG) of Mohamed Seddik Benyahia-Jijel University using a spectrophotometer (UV 1600 PC), flame spectrophotometry (AFP 100) and volumetric titration. The protocols and methods of chemical analysis are done according to Rodier et al. (2009). The verification of analytical error of analysed ions concentration was done by the electro neutrality (charge-balance error) according to the following equation:

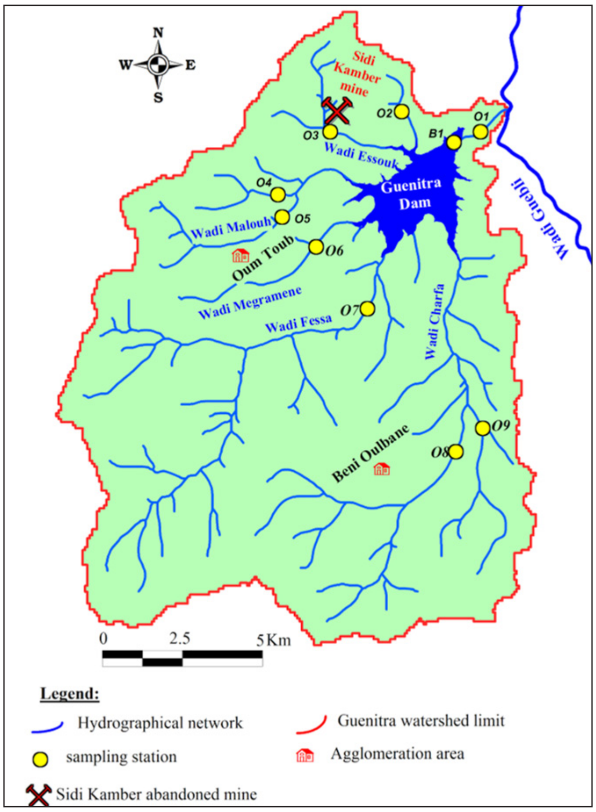

Figure 3. Water sampling map in Guenitra watershed.

3. Results and discussion

Results of physico-chemical analyses of Guenitra Dam surface waters and its tributaries of the two campaigns (December 2017 and September 2019), as well as the irrigation water quality indicators (SAR, %Na, RSC and IP) are shown in Table 1.

Table 1. Physico-chemical parameters of surface waters of Guenitra watershed.

Campaign	Samples	EC	pH	Ca^{2+}	Mg^{2+}	Na^{+}	K^{+}	Cl-	SO_4^{2-}	HCO_3^-	CO_3^{2-}	NO_3^-	SAR	%Na	RSC	IP
		µS/cm	/	meq/L	meq/L	meq/L	meq/L	meq/L	meq/L	meq/L	meq/L	meq/L	/	%	meq/L	%
First Campaign (December 2017)	O1	740	7.95	1.60	3.65	2.87	0.12	3.20	1.23	2.8	0	0.01	1.77	36.33	-2.45	55.16
	O2	896	7.93	1.60	4.78	3.28	0.12	3.70	1.14	3.08	0	0.17	1.84	34.71	-3.30	51.48
	O3	2550	5.30	10.42	12.56	4.88	0.16	6.35	1.35	0.16	0	0.09	1.44	17.99	-22.82	18.84
	O4	1856	7.81	2.24	9.88	3.43	0.07	9.50	3.11	4.00	0	0.21	1.40	22.43	-8.13	34.76
	O5	1160	7.8	3.21	3.89	3.83	0.34	3.60	0.76	5.64	0	0.01	2.03	36.99	-1.46	55.07
	O6	1604	7.85	3.29	4.13	6.62	0.44	6.30	2.48	6.24	0	0.01	3.44	48.77	-1.18	62.98
	O7	1008	8.39	3.77	4.94	2.53	0.08	1.90	2.72	3.92	0.1	0.19	1.21	23.06	-4.69	39.80
	O8	1750	7.72	8.82	5.51	4.96	0.32	6.30	2.97	6.48	0	0.17	1.85	26.90	-7.85	38.28
Second Campaign (September 2019)	O1	653	7.64	2.57	3.04	1.72	0.12	2.90	0.81	3.16	0	0.02	1.03	24.64	-2.45	46.99
	O3	2900	3.09	11.86	1.68	4.31	0.20	4.70	12.98	0.00	0	0.01	1.66	24.98	-13.54	23.89
	O4	2900	7.62	5.21	15.28	7.48	0.26	14.20	2.12	11.2	0	0.01	2.34	27.42	-9.29	38.35
	O5	1400	7.88	3.37	5.68	5.52	0.55	4.10	1.21	9.2	0	0.01	2.60	40.18	0.15	56.57
	O6	2190	7.70	4.09	4.16	6.59	0.78	10.00	1.03	5.12	0	0.01	3.25	47.19	-3.13	56.69
	O7	1200	7.73	2.32	6.16	3.06	0.13	3.60	2.54	5.00	0	0.01	1.49	27.35	-3.48	45.35
	O8	800	7.85	2.24	2.40	2.84	0.07	2.50	0.63	4.2	0	0.01	1.87	38.58	-0.44	64.70
	O9	830	7.80	2.97	2.72	2.77	0.21	2.70	1.13	4.28	0	0.01	1.64	34.38	-1.41	55.84
	B1	620	8.69	1.76	2.32	1.73	0.13	2.80	1.26	2.32	0.2	0.01	1.21	31.26	-1.56	54.70

3.1. Physico-chemical parameters of surface waters

Statistical analysis of surface waters of Guenitra watershed in terms of maximum (max), minimum (min), standard deviation (ST.D.) and mean values are shown in Table 2.

pH values of waters for all tributaries of the dam's watershed range from 7.62 to 8.39 (avg. 7.83), which is acceptable compared to the acceptable pH limit for irrigation water (6.5to 8.5) according to the Food and Agriculture Organization of the United Nations (FAO,1985). The dam water is slightly alkaline (pH of 8.69). However, the pH of wadi Essouk waters, which drains the abandoned mining area of SidiKamber, is very acidic (3.09 to 5.3) due to the oxidation of the sulphide minerals and the generation of the acid mine drainage (Issaad et al., 2019). Irrigation with acid and mineralized water leads to the degradation of soil structure, the reduction of biological activities and an increase in the risks of induced toxicity (Lal, 2015). Besides, when the pH values exceed 6.0 the repulsive force generated by the negative charges on soil particles decrease the permeability index resulting in accelerated erosion by water (Matsumoto et al., 2018).

Electrical Conductivity (salinity) values range between 620 to 2900 µS/cm (avg. 1474 µS/cm) (Table 2) indicating that the waters are lightly mineralized to mineralized. The high electrical conductivity values were recorded in the main wadis; wadi Charfa (1750 µS/cm), wadi Magramene (2160 µS/cm), wadi Malouh (2900 µS/cm) and wadi Essouk (2550 to 2900 µS/cm). They are more mineralized in the dry season (September 2019) than in the rainy season (December 2017). According to FAO (1985), the dam waters and their tributaries are acceptable for irrigation (EC < 3000 µS/cm as limit value).

Table 2. Statistical analysis of surface waters of Guenitra watershed.

Parameters	Units	**December 2017**(8 samples)				**September 2019**(9 samples)				Mean
		Min	Max	Mean	ST.D	Min	Max	Mean	ST.D	
EC	µS/cm	740	2550	1485	606	620	2900	1546	930	1473
pH	/	5.30	8.39	7.44	0.95	3.09	8.69	7.07	1.62	7.46
Ca^{2+}	meq/L	1.60	10.42	4.37	3.36	1.76	11.86	4.04	3.12	4.21
Mg^{2+}	meq/L	3.65	12.56	6.17	3.26	1.68	15.28	4.83	4.21	5.50
Na^{+}	meq/L	2.53	6.62	4.05	1.35	1.72	7.48	4.00	2.10	4.03
K^{+}	meq/L	0.07	0.44	0.21	0.14	0.07	0.78	0.27	0.24	0.24
Cl^{-}	meq/L	1.90	9.50	5.11	2.45	2.50	14.20	5.28	4.07	5.20
SO_4^{2-}	meq/L	0.76	11.35	3.47	4.09	0.63	12.98	2.63	3.93	3.05
HCO_3^{-}	meq/L	0.16	6.48	4.04	2.10	00.00	11.20	4.94	3.41	4.49
CO_3^{2-}	meq/L	00.00	00.10	00.01	00.04	00.00	00.20	00.02	00.07	00.05
NO_3^{-}	meq/L	0.01	0.21	0.12	0.09	0.01	0.02	0.01	00.00	0.07
SAR	/	1.21	3.438	1.96	0.69	1.03	3.25	1.94	0.71	1.89
%Na	%	17.99	48.77	31.40	10.12	24.64	47.19	33.44	7.8	31.95
RSC	meq/L	-22.82	-1.18	-6.50	7.11	-13.54	0,15	-3.93	4.53	-5.14
IP	%	18.84	62.98	44.55	14.29	23.89	64.70	49.23	12.26	47.03

Chloride and bicarbonate ions are present in most samples, the average chloride and bicarbonate contents varied respectively from 5.11 to 5.28 meq/L and from 4.04 to 4.94 meq/L, particularly recorded in the wadis Fessa, Charfa, Magramene and Malouh. On the other hand, sulphate ions are dominant especially in the water of Essouk wadi with average contents oscillating between 2.63 to 3.47 meq/L. Regarding cations, magnesium is the most important element with average concentrations ranging between 4.83 and 6.17 meq/L (Table 2). While calcium and sodium contents varied from 4.04 to 4.37 meq/L and from 4.00 to 4.05 meq/L respectively.

The nitrate concentrations recorded in this study are low and range between 0.01 meq/L and 0.21 meq/L (avg. 0.06meq/L) (Table 2). While carbonate ions are present only in wadi Fessa water (0.1 meq/L) during the first campaign (December 2017) and in the dam water (0.2 meq/L) during the second campaign (September 2019) (Table 2).

3.2. Hydrogeochemical facies

To know the hydrogeochemical regime of the studied area, analytical data obtained from the hydrochemical analysis are plotted on the Piper tri-linear diagram (Piper, 1944) to deduce the hydrogeochemical facies.

This diagram reveals a variability of chemical facies relative to the Guenitra watershed waters with three distinct groups (Figure 4). This variability could be explained, in part by the geological nature of the terrains crossed and also to anthropogenic pollution : (i) calcium-magnesium bicarbonate facies (G1: wadi Fessa and wadi Charfa) due to the dissolution of carbonate formations of SidiDriss mountains; (ii) sodium-calcium chloride sulphate facies (G2: wadi Magramene, wadi Malouh and Guenitra dam) linked to urban discharges from neighbouring towns (OumToub and BeniOulbane); (iii) calcium sulphate facies at wadi Essouk (G3) linked to acid mine drainage (AMD) from the SidiKamber mine and the oxidation of its metallic sulphide minerals contained in the mine discharges, in particular iron disulphide pyrite (Boukhalfa, 2007; Issaad et al., 2019).

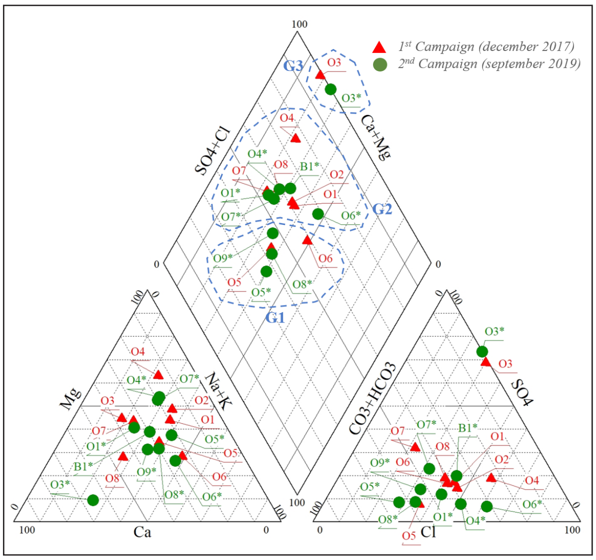

Figure 4. Piper diagram showing surface water samples from the watershed of Guenitra

3.3. Suitability of water irrigation

Water quality, soil types and agricultural activities are determinable factors for an appropriate irrigation practice (Kaka et al., 2011). For the water quality assessment in terms of irrigation, several criteria were used to monitoring the water quality intended for agricultural activity, namely; sodium absorption ratio(SAR) and percentage of sodium (%Na) in combination with electrical conductivity (EC); residual sodium carbonate index (RSC) and permeability index (PI). These methods describe the potential risk of soil salinization and the negative effects of irrigation on soils and plants (Rouabhia and Djabri , 2010; Kaka et al., 2011; Li et al., 2016; Li et al., 2019; Orou et al., 2016; Towfiqul Islam et al., 2017; Safiur Rahman et al., 2017; Singh et al., 2019; Saadali et al., 2019).

3.3.1. Sodium absorption ratio (SAR): it measures the relative proportion of sodium ions of water compared to calcium and magnesium ions. It can be calculated according to the equation of Richards (1954), where all ion contents are expressed in meq/L:

$$SAR = \frac{Na^+}{\sqrt{\frac{Ca^{2+} + Mg^{2+}}{2}}}$$

Indeed, high sodium water is generally unsuitable for soil irrigation due to deterioration of soil characteristics, such as clays dispersion, structure degradation, permeability diminution and plants asphyxiation (Richards, 1954; Orou et al., 2016). SAR has been plotted versus EC (µS/cm) on the Richards'united States salinity diagram to graphically demonstrate the suitability of this water for irrigation purposes in terms of quality. Five water classes were defined: excellent, good, acceptable, poor and bad (Table 2).

Table 2. Classification of water by degree of irrigation ability using the SAR method (Richards, 1954)

Degree	Quality	Class	State of use
1	Excellent	C1-S1 C1-S2	Safe use for irrigation of most crops on most soils.
2	Good	C2-S1 C2-S2	Suitable for plants that have the tolerance to salts, however, its use can cause problems for clays.
3	Acceptable	C3-S1 C2-S3 C3-S2	Salinity must be controlled, irrigation of tolerable crops to salts on well-drained soils.
4	Poor	C4-S1 C4-S2 C3-S3	Highly mineralized water, used only for very salt-resistant plants with good soil permeability.
5	Bad	C3-S4 C4-S3 C4-S4	Unsuitable

Obtained results of calculated SAR of surface waters vary from 1.21 to 3.44 (avg. 1.96) for the first campaign (December 2017) while for the second campaign (September 2019) it varies between 1.03 and 3.25 (avg. 1.94) (Table 2). According to Richards diagram (SAR vs EC), the water of the majority of tributaries in the watershed is mainly in classes C2S1 and C3S1 (Figure 5), which correspond respectively to a low and medium water salinity (good to acceptable quality). These waters are suitable for irrigation of salt-tolerant crops on well-drained soils with continuous control of the salinity evolution. However, waters of wadi Malouh (O4) and wadi Magramene (O6) in September 2019 and wadi Essouk (O3 and O3*) for both campaigns correspond to a poor-quality class (C4S1) (Figure 5), these mineralized waters are only authorized for the irrigation of certain salt-tolerant species and on well-drained and leached soils (Richards, 1954).

3.3.2. Percentage of sodium (%Na): Sodium is one of the most undesirable elements in irrigation water due to its effect on soil permeability and water infiltration. It substitutes calcium and magnesium adsorbed on clay particles and causes soil particles dispersion, making consequently the soil hard and compact when it's dry and excessively water-impermeable (Kaka et al., 2011; Singha, 2017; Singh et al., 2019). The percentage of sodium is calculated according to the following formula (Todd, 1980), where all ion contents are expressed in meq/L:

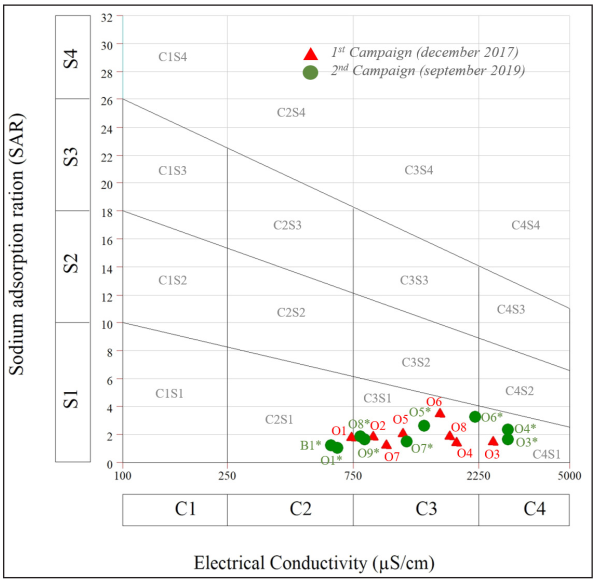

Figure 5. Irrigation water suitability of Guenitra watershed according to Richards (1954).

In December 2017, the sodium percentage in water oscillates between 17.99% and 48.77% (avg. 31.40%) (Table 2).In September 2019, it varies from 24.64% to 47.19% (avg. 33.44%).Wilcox's diagram (1948), sodium percentage versus electrical conductivity (Figure 6) shows that the waters of the majority of tributaries belong to the "excellent, good to permissible" quality during both campaigns (20% < %Na < 50% and EC < 2000 µS/cm), excluding the waters of wadi Malouh (O4*) and wadi Magramene (O6*) in September 2019 and wadi Essouk (O3 and O3*) for the two campaigns (December 2017 and September 2019) which correspond to Doubtful to Unsuitable quality for irrigation (EC > 2000 µS/cm) (Figure 6).

Generally, there is a slight deterioration in water quality during the second campaign (Low-water period; September 2019), this reflects the increase of salinity due to temperature increasing due to the surface water evaporation.

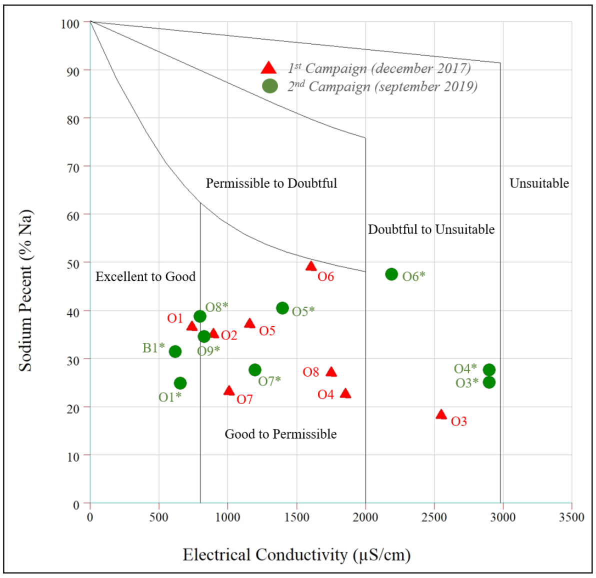

Figure 6. Irrigation water suitability of Guenitra watershed according to Wilcox's(1948).

3.3.3. Residual Sodium Carbonate (RSC): Residual sodium carbonate has been calculated to determine the hazardous effect of carbonate and bicarbonates on irrigation water quality. It is calculated according to the following formula (Kaka et al., 2011; Li et al., 2016; Li et al., 2019), where all ion contents are expressed in meq/L:

$$RSC = (CO_3^{2-} + HCO_3^-) - (Ca^{2+} + Mg^{2+})$$

Bicarbonate is an important constituent during the assessment of irrigation water quality. The RSC is used to quantify the impact of water with high carbonate content on soil and plant growth. An excess of RSC sterilises soils due to the deposition of sodium carbonate (Joshi et al., 2009). Water with an RSC < 1.25 is safe for irrigation, and an RSC> 2.5 is considered unsuitable for irrigation (Richards, 1954; Kaka et al., 2011; Towfiqul Islam et al., 2017; Safiur Rahman et al., 2017; Li et al., 2016, 2019; Singh et al., 2019).

In our case, the RSC of Guenitra dam water and its tributaries varies from -9.29 to 0.15 (avg. -3.39), except wadi Essouk waters those are influenced by acid mine drainage from SidiKamber abandoned mine (3.09 < pH < 5.3) where the RSC is about -22.82 and -13.54 for December 2017 and September 2019 respectively (Table 2). All values indicate that the waters of the study area are suitable for irrigation.

3.3.4. Permeability index (PI): Soil permeability is also affected by the continuous use of irrigation water with the influence of Ca^{2+}, Mg^{2+}, $Na^{+}$and HCO_3^- contained in the soil. Doneen (1964) and Ragunath (1987) developed a criterion for assessing water suitability for irrigation based on a permeability index (Figure 7).Accordingly, water can be classified into three classes; Class I (water excellent quality for irrigation), class II (water of acceptable quality) and class III (water unsuitable for irrigation) (Kaka et al., 2011; Li et al., 2016; Singha, 2017; Safiur Rahman et al., 2017; Towfiqul Islam et al., 2017; Singh et al., 2019). The permeability index (PI) can be written according to the following equation, where all ion contents are expressed in meq/L:

$$PI = \frac{Na^+ + \sqrt{HCO_3^-}}{Ca^{2+} + Mg^{2+} + Na^+} \times 100$$

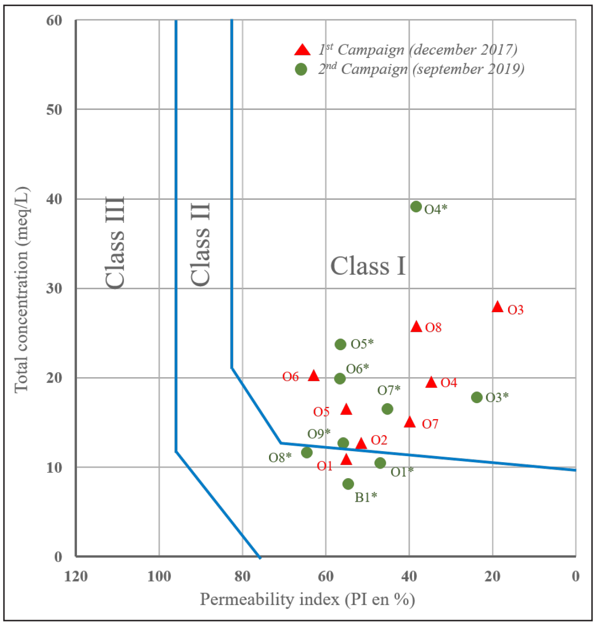

Figure 7. Classification of irrigation water based on permeability index.

Permeability index (PI)of waters of the Guenitra watershed varies between 18.84% and 62.98% (avg. 44.55%) during the first campaign (December 2017) and oscillates between 23.89% and 64.70% (avg. 49.23%) during the second campaign (September 2019) (Table 2). the results show that 76.47% of water samples plot in class I (Figure7), corresponds to all tributaries of the dam's watershed. 23.53% of water samples plot in class II, corresponding to the dam (B1) and its outlet (O1). In resume, the waters of the study area are suitable for irrigation (excellent to acceptable water for irrigation) without any effect on soil properties.

3.4. Discussion

pH values of waters for all tributaries of the dam's watershed range from 7.62 to 8.39 which is acceptable compared to the acceptable pH limit for irrigation water (6.0 to 8.5) according to FAO (1985). However, the pH of wadi Essouk water is very acidic (3.09 to 5.3) influenced by the oxidation of the sulphide minerals and the generation of the acid mine drainage. Electrical Conductivity values range between 620 to 2900 µS/cm, according to FAO (1985), the dam waters and its tributaries are acceptable for irrigation (EC < 3000 µS/cm as limit value).

Piper diagram reveals a variability of chemical facies relative to the Guenitra watershed waters with three distinct groups (calcium-magnesium bicarbonate facies, sodium-calcium chloride sulphate facies and calcium sulphate facies). This variability could be explained, in part by the geological nature of the terrains crossed and also by anthropogenic pollution.

Irrigation water quality indicators (SAR, %Na, RSC and PI) show that the water from the dam and most tributaries of the watershed display good to admissible quality and suitable for irrigation of most crops, excluding wadi Essouk tributary waters which drain the SidiKamber abandoned mining area (acidic and important mineralized water) those are of poor quality, influenced by the acid leachate product, Therefore, continuous monitoring of the impact of the wadi Essouk pollution on the dam water quality is necessary. The wadi Essouk waters could be only intended for irrigation of salt-tolerant crops on well-drained soils. Waters of the wadis Malouh and Magramene have undergone very remarkable quality degradation during the second campaign (September 2019); they were changed from good to poor quality due to the low-water period (negligible dilution effect) and high temperatures (high evaporation effect) which cause an increase in water salinity.

4. Conclusions

This study highlighted the devastating effect of acid leachate products from the abandoned mine on surface water quality and their presumed risk for irrigation as well as the effect of dry periods on the deterioration of surface water quality. This situation becomes seriously worrying in the presence of anthropogenic discharges of acidic nature and/or with high mineralization (rich in chemical elements undesirable for agriculture). The hydrodynamic exchange between surface water (wadi or dam) and groundwater by the over-pumping for irrigation will cause the drainage of polluted water from the wadis, which could lead to the water contamination from wells, intended mostly for drinking water supply, hence the direct risk on human health.

The water chemistry of Guenitra dam and its tributaries is mainly affected by the geological formations (mostly carbonate); particularly, carbonate formations occupy the southern and south-western parts of the watershed. On the other hand, discharges from urban areas (OumToub and BeniOulbane townships) as well as acid mine discharges fromSidiKamber mine through the oxidation of metallic sulphide minerals, in particular iron disulphide pyrite, have played a major role in deteriorating the water quality.

Finally, to protect water resources, particularly dams, against all types of water pollution, either for drinking water supply or for irrigation, it's well recommended to manage contaminated sites, especially abandoned mining areas, and to pre-treat its mining discharges, as well as the purification of wastewater discharges from urban areas located upstream of dams.

Acknowledgements

The authors of this article would like to thank the General Directorate of Scientific Research and Technological Development (DGRSDT), for their help in carrying out this scientific research, and the managers of the Guenitra dam for all the facilities they have given us to acquire the data necessary to carry out this work.

References

Abreha, A.G. (2014). Hydrogeochemical and water quality investigation on irrigation and drinking water supplies in the Mekelle Region, Northern Ethiopia, M.sc.Thesis, University of Twente.

Al-Shujairi, S.O.H. (2016). Reliability of water resources quality monitoring program data. College of Engineering Journal (NUCEJ) 19 (2): 246-254.

Allalgua, A., Kaouachi, N., Boualeg, C., Ayari, A., Bensouileh, M. (2017). Physico-chemical characterization of the waters of the Forum El-Khanga dam (Souk-Ahras region, Algeria). European scientific Journal 13 (12) : 258-275. http://dx.doi.org/10.19044/esj.2017.v13n12p258

Bahroun, S., Chaib, W.,Halimi, S. (2017).Suitability of Cheffia dam surface waters for irrigation (El Tarf area). Journal of Biodiversity and Environmental Sciences10 (6): 274-282. http://www.innspub.net

Belhadj, M.Z., and Boudoukha, A. (2014). Degradation of surface water of Zit-Embadam wilaya of Skikda by contamination of heavy metals and anthropogenic pollution. Scientific and Technical Review, The Water and Environment Journal, LJEE 24 and25:9-19.

Bouguerne, A., Boudoukha, A., Benkhaled, A., Mebarkia, A. (2017). Assessment of surface water quality of Ain Zada dam (Algeria) using multivariate statistical techniques. International Journal of River Basin Management 15 (2): 133-143. http://dx.doi.org/10.1080/15715124.2016.1215325.

Boukhalfa, C. (2007). Heavy metals in the water and sediments of wadi Essouk, Algeria, a river receiving acid effluents from an abandoned mine. African Journal of Aquatic Science 32 (3):245-249. https://doi: 10.2989/ AJAS.2007.32.3.3.302

Charchar, N., Bouchaala, L., Bouyahmed, H., Gherib, A.F.,Lehout, A. (2020). Effect of heavy metals on soil microbial quality of an abandoned mining area SidiKamber, North-East of Algeria. Eurasian Journal of Soil Science 9 (3): 254-263. https://doi.org/10.18393/ejss.735971

Doneen, L.D. (1964). Notes on water quality in agriculture. Published as a Water Science and Engineering, paper 4001, Department of water sciences and engineering, University of California, Davis.

FAO. (1985). Water quality for agriculture. Food and Agriculture Organization. http://www.fao.org/3/T0234E/T0234E01.htm#tab1 (Dec. 16,2020).

Gherib, A.F., Djebaili, H., Bouchaala, L., Charchar, N., Aissaoui, A., Lehout, A. (2017). Physiological and biochemical markers in the process of resistance and/or tolerance of heavy metals in the abandoned mining area of SidiKamber, Skikda, Algeria. International Journal of Environmental Studies:1-15. http://dx.doi.org/10.1080/00207233.2017.1284381

Hem, J.D. (1985). Study and interpretation of the chemical characteristics of natural water. United States Geological Survey. Water-Supply Paper 2254, 263p.

Hounslow, A.W. (1995). Water quality data: analysis and interpretation. CRC Press LLC, Lewis Publishers, New York.

Issaad, M., Boutaleb, A., Kolli, O., Edahbi, M., Benzaazoua, M., Hakkou, R. (2019). Environmental characterization of mine waste at the Pb-Zn SidiKamber abandoned mine (NE Algeria). RendicontiLincei. ScienzeFisiche e Naturali30 : 427-441. https://doi.org/10.1007/s12210-019-00806-8

Joshi, D.M., Kumar, A., Agrawal, N. (2009).Assessment of the irrigation water quality of river Ganga in Haridwar district. RasayanJournal of Chemistry 2(2): 285-292.

Kaka, E.A., Akiti, T.T., Nartey, V.K., Bam, E.K.P., Adomako, D. (2011). Hydrochemistry and evaluation of groundwater suitability for irrigation and drinking purposes in the southeastern Volta river basin: Manyakroboarea, Ghana.Elixir Agriculture 39: 4793-4807.

Katz, B.G., and Collins, J.J. (1998). Evaluation of chemical data from selected sites in the Surface-Water Ambient Monitoring Program (SWAMP) in Florida, Open-File Report 98-559, U.S Geological Survey, 51p.

Lakhili, F., Benabdelhadi, M., Bouderka, N., Lahrach, H., Lahrach, A. (2015). Study of the physico-chemical quality and metallic contamination of surface waters in Beht watershed (Morocco). European Scientific Journal 11 (11):132-147.

Lal, R. (2015). Restoring soil quality to mitigate soil degradation. Sustainability 7 (5):5875-5895.https://doi:10.3390/su7055875.

Li, P., Zhang, Y., Yang, N., Jing, L., Yu, P. (2016). Major ion chemistry and quality assessment of groundwater and around a mountainous tourist town of China. Exposure and Health 8: 239-252. https://doi 10.1007/s12403-016-0198-6.

Li, P., Tian, R., Liu, R. (2019). Solute geochemistry and multivariate analysis of water quality in the Guohuaphosphorite Mine, Guizhou Province, China. Exposure and Health 11:81-94. https://doi.org/10.1007/s12403-018-0277-y.

Mahdjoub, Y. (1991). Kinematics of deformations and ante-alpine and alpine P-T evolution in Lesser Kabylia (North-Eastern Algeria). Ph.D. Thesis, University of Science and Technology HouariBoumediene, Algeria.

Matsumoto, S., Ogata, S., Shimada, H., Sasaoka, T., Hamanaka, A., Kusuma, G.J. (2018). Effects of pH-induced changes in soil physical characteristics on the development of soil water erosion. Geosciences 8 (134):1-13.http://doi:10.3390/geosciences8040134w

Mecibah, I. (2017).Water resources and integrated management of the OuedGuebli catchment area (North-East Algeria). Ph.D.Thesis, University of Annaba, Algeria.

Medjram, M., and Khalfaoui, M. (2014). Study and evaluation of risk related to waters contamination of dam of Guenitra, by heavy metals, from the mine of SidiKamber. Journal of Selçuk University Natural and Applied Science, Digital Proceeding of the International Conference on Environmental Science and Technology ICOEST'2014, SIDE, pp268-274.

Orou, R., Soro, G., Soro, D., Traoré, A., Fossou, R., Soro, N. (2016). Groundwater suitability for agriculture in the Agboville department (South-East Ivory Coast). European Scientific Journal 12 (21): 81-100. https://doi.org/10.19044.

Ouhmidou, M., Chahlaoui, A., Kharroubi, A., Chahboune, M. (2015). Study of the physico-chemical and bacteriological quality of the barrage Hassan Addakhil of Errachidia (Morocco). Journal of Materials and Environmental Science 6 (6): 1663-1671.

Piper, A.M. (1944). A graphic procedure in geochemical interpretation of water analysis. American Geophysical Union Transom 25, pp 914-923.

Ragunath, H.M. (1987). Groundwater 2ndEd., Wiley Eastern Ltd., New Delhi, India.

Richards, L.A. (1954).Diagnosis and improvement of saline and alkali soils. United States Department of Agriculture Edition, Agricultural Handbook 60, Washington.

Rodier, J.,Legube, B.,Merlet, N., Brunet, R. (2009). Water Analysis 9th Ed., Natural Waters, Waste Water, Sea Water. Edition Dunod, 1600p.

Rouabhia, A., and Djabri, L. (2010).Irrigation and the risk of salt pollution. Example of groundwater in the Miocene aquifer of the El-Ma El-Abiod plain. Underground and Surface Hydraulics Research Laboratory. Larhyss Journal 08:55-67.

Saadali, B., Zerrouki, H., Hamzi, A., Bouhdid, C.,Khiari, A. (2019). Geochemical assessment of water quality and its suitability for agricultural use in the Djedra wadi subwater shed, Northeast Algeria. Euro-Mediterranean Journal for Environmental Integration 4:33. https://doi.org/10.1007/s41207-019-0121-1.

Safiur Rahman, M., Saha, N., Towfiqul Islam, A.R.M., Shen, S.,Bodrud-Doza, M. (2017). Evaluation of water quality for sustainable agriculture in Bangladesh. Water, Air &Soil Pollution228,385. https://doi.org/10.1007/s11270-017-3543-x.

Singha, D. (2017). A study on groundwater quality analysis in the district of Idukki, Kerala.International Journal of Scientific and Engineering Research 8 (3): 842-858.

Singh, K.R., Goswami, A.P., Kalamdhad, A.S., Kumar, B. (2019). Development of irrigation water quality index incorporating information entropy. Environment, Development and Sustainability 22:3119-3132. https://doi.org/10.1007/s10668-019-00338-z.

Todd, D.K. (1980). Groundwater Hydrology. 2nd Ed., Wiley, New York.

Touati, B. (2010). Dams and hydraulic policy in Algeria: status, diagnosis and prospects for sustainable development. PhD thesis, University of Constantine, Algeria.

Touhari, F., Mehaiguene, M., Messelmi, H. (2018). Evolution of water quality of dams in the Upper Cheliff basin. Agriculture Systems and Environment 2 (1): 41-57.

Towfiqul Islam, A.R.M., Shen, S., Bodrud-Doza, M.,Safiur Rahman, M. (2017). Assessing irrigation water quality in Faridpur district of Bangladesh using several indices and statistical approaches. Arabian Journal of Geosciences 10, 418. https://doi.org/10.1007/s12517-017-3199-2

Vila, J.M. (1980).The Alpine chain of eastern Algeria and the Algerian-Tunisian borders. Ph.D. Thesis,Pierre and Marie Curie University, Paris 6.

Wilcox, L.V. (1948). The quality of water for agricultural use. EditionUnited States Department of Agriculture, Technical Bulletin, vol. 962, Washington.

JJEES

JJEES (2021) 12 (4): 353-359
ISSN 1995-6681

Jordan Journal of Earth and Environmental Sciences

A review Research on Wind Erodibility of Some States and Their Interrelationships in Sudan

Motasim Abdelwahab[1] and Mukhtar Mustafa[2]

[1]*Associate Professor, Department of Arid Land and Desert Agriculture, Faculty of Agriculture, Omdurman Islamic University, Omdurman, Sudan*

[2]*Professor, Soil Sciences /Desertification, Faculty of Agriculture, University of Khartoum, Khartoum*

Received 27 November 2020; Accepted 24 May 2021

Abstract

Wind erodibility of soils (WE) is a prime indicator of soil susceptibility to wind erosion. It is used for the prediction of wind erosion. The pooled data of the six states of non –erodible soil particles (NEP), WE and soil physicochemical properties were treated statistically. The main objectives of this paper are to present a review of research on wind erodibility; generation of statistical empirical relationships between NEP and WE with soil physiochemical properties and derived the relationship for the pooled data of the six states. The overall mean NEP of the six states ranged from 27.2 to 62.4 with a mean of 41.9% and CV of 27.7%, and the overall mean of WE ranged from 46.8 to 236.9 with a mean of 140.4 ton/ha and CV of 43.2%. The overall mean NEP of the six states gave a highly significant positive correlation with clay content with coefficients ranging between 0.8945 and 0.6731 with a mean of 0.8044 and a CV of 10.2%. The overall mean NEP was in the following order: Gezira> the Red Sea> Northern> River Nile> Kassala> North Darfur. The overall mean WE of the six states gave a highly significant negative correlation with clay content with coefficients ranging between - 0.8794 and - 0.6567 with a mean of - 0.8004 and a CV of 9.6%. The overall mean WE was in the following order: North Darfur> Kassala> River Nile> Northern> the Red Sea> Gezira. The pooled data of the six states gave a highly significant negative correlation between NEP and (sand/clay) ratio, which accounted for 70% of the variation of NEP. The pooled results of the six states gave a highly significant positive correlation between WE and (sand/clay) ratio, which accounted for 70% of the variation of WE. Sand particles that limit soil aggregation and their presence increases WE and decreases NEP, so the ratio is useful for the prediction of wind erosion. The five states were dominated by course to medium textured wind erodibility groups (WEGs). The five states are described as highly susceptible to wind erosion because of their texture.

Keywords: Wind erodibility, Non–erodible soil particles, Soil physiochemical properties, Wind erodibility groups, States Sudan.

1. Introduction

Wind erosion occurs in a two-step process, namely detachment of primary soil particles from the soil mass and their transport by erosive winds $V \geq 5.4$ m/sec (Skidmore and Woodruff, 1968). When the wind velocity or energy is below the threshold value to transport soil particles, deposition occurs. Soil particles are transported by three mechanisms according to their diameter: suspension ($d < 0.1$ mm), saltation ($d = 0.1$-0.5 mm) and surface creep ($d > 0.5$ mm). The conducive conditions to wind erosion include: loose, dry, and dispersed soil particles, smooth surface soil, lack or sparse vegetative cover, large and extensive field and erosive winds (Mustafa, 2007).

Wind erosion is governed by two main factors namely wind erosivity and soil erodibility. Wind erosivity is a measure of the ability of wind to pick the soil particles from the soil surface and transport them by saltation or push them on the soil surface (surface creep) or blow them and transport them by suspension (Mustafa, 2007).

Soil wind erodibility (WE) is the susceptibility of dry soil or its ease of detachment and transport by wind. WE are a prime indicator of the susceptibility of the soil to wind erosion and hence it is used for the prediction of wind erosion by the soil loss equation proposed by Woodruff and Siddoway (1965). Chepil (1953) found that soil particles > 0.84 mm, were resistant to entrainment by common erosive winds. Thus, these particles were considered non-erodible particles (NEP) and wind erodibility is estimated from knowledge of the percentage of NEP (Woodruff and Siddoway, 1965). Wind erodibility of cultivated soils is affected mainly by soil texture and various other soil physical, chemical characteristics and processes that influence soil aggregation (Harris et al., 1966; Wishmeier and Mannering, 1969; Romken et al., 1977; Young and Muchler, 1977; Lyles and Tatarko, 1986; Black and Chanasyk, 1989; Kheir El Seid, 1998).

National research project on the assessment and mapping of wind erodibility in various states was undertaken in the Desertification and Desert Cultivation Studies Institute (Medani and Mustafa 2003; Mustafa and Medani 2003; Rehan and Mustafa, 2005; Abdelwahab et al., 2009; Mohammed and Mustafa, 2011; Hassan and Mustafa, 2011 and Abdelgadir et al., 2013). Soil indicators were recommended for the prediction of non-erodible soil particles (NEP) and wind

* Corresponding author e-mail: abdo.momti76sag@gmail.com

erodibility (WE) of the soils. For example, Mustafa and Medani (2003) recommended the use of the (Silt and Sand) / (Clay + $CaCO_3$) ratio for the prediction of NEP and WE of the soils of Khartoum State. WE showed a quadratic increase with the increase of this ratio. It was concluded that this indicator is a better indicator than the clay ratio alone, which was previously recommended by other authors. The present study was undertaken to achieve the following objectives:

1. Estimation and comparison of overall mean WE and NEP of the six states.
2. Identification of the correlation between (WE and NEP) with soil indices at the six states.
3. Generation relationships between (sand/clay) ratio, examined with (NEP and WE).
4. Establishment of wind erodibility groups (WEGs) for the studied states.

2. Materials and methods

2.1 Study area

The study was conducted in Sudan (1,882,000 Km^2), that locates in northeast Africa at latitudes 14° and 22° north and longitudes 22° and 38° east. Sudan is dominated by two types of winds, the dry north-easterly wind in winter (October, November, December, January and February) and the humid southerly wind in the rainy season during (May, June, July, August and September). There is a high variation in the spatial and temporal distribution of rainfall in Sudan. Lines of equal rainfall depth (isohyets) were used by (Harison and Jakson, 1958) to classify the vegetation zone of Sudan. Aridity index (AI) is defined as a measurement of precipitation divided by evapotranspiration. Five degrees of aridity were defined (0.03 - 0.65) by Dregne et al., (1991) and become a global measure.

2.2 Soil sampling and methods

Wind erodibility of selected farms was estimated using bulked surface (0-3cm) soil samples carefully collected at random, after completion of land preparation, from transects delineated across the field of each of (28-50) agricultural farms in each studied state accounted 268 samples. The soil samples were carefully saved in bags to avoid aggregate fragmentation.

Wind erodibility of soils was determined by the dry sieving method proposed by Chepil or Woodruff (1959). The soil samples were air-dried, and straw and stones, if any, were removed. One kilogram of an air-dry soil sample was sieved with a 0.84 mm diameter sieve. The mass of soil aggregates greater than 0.84 mm, considered to be non-erodible particles (NEP). Non-erodible particles were calculated for each sample, and its equivalent WE (ton/ha) was obtained from a standard table established by Woodruff and Siddoway (1965). Furthermore, the main soil physicochemical properties were determined by acceptable standard methods. Particle-size distribution was determined using the hydrometer method described by Black et al. (1965). By Chapman and Pratt (1961), organic carbon (OC) was determined by the dry-aching method of Fredrick, described by Ibrahim (1991), and organic matter (OM) was then calculated.

Statistical empirical relationships between NEP and WE and soil properties for six individual states were derived. The relationships for the pooled data of the six states were also derived by "Microsoft Excel 2003"

3. Results and discussion

3.1 Relationships in individual states

Table 1 shows the range of the mean soil particle-size distribution, organic matter (OM), NEP, WE, of the farm soils in each of the six studied states. The relatively high CV of the particle-size distribution in each state may be partially attributed to wind erosion. The data collected from farms in the Northern State will be presented as an example of the six studied states. Regression analysis of the data collected from farms in the Northern State showed that NEP significantly increased linearly with increase of clay (r^2 = 0.402) , silt (r^2 = 0.317), OM (r^2 = 0.139), and $CaCO_3$ (r^2 =0.279),(Fig.1, 2, 3 and 4)and decreased with increase of sand (r^2 = 0.410), and increase of (silt sand)/clay ratio (r^2 = 0.440) (Fig.5 and 6). The reverse correlation trends were obtained with WE (Abdelwahab, 2005, Abdelwahab and et al., 2009). Multiple regression analysis yielded a highly significant (P < 0.001, r = 0.718) correlation between NEP and multiple soil variables as follows:

$$NEP\% = 365.6 – 2.3\ Clay\% - 3.7\ Sand\% - 4.0\ Silt - 3.0\ CaCO_3$$

According to this relationship, the four soil properties account for 52% of the variation of NEP. The negative sign of the coefficients of clay and $CaCO_3$ is contrary to logical expectation but such anomalies are known in empirical statistical models.

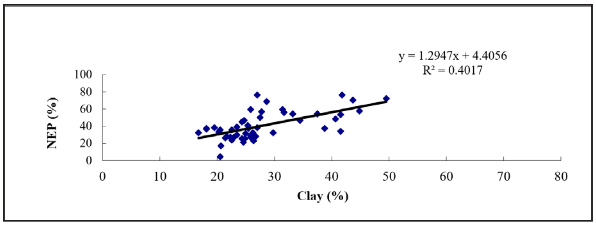

Figure 1. Mean non-erodible soil particles (NEP) versus clay content

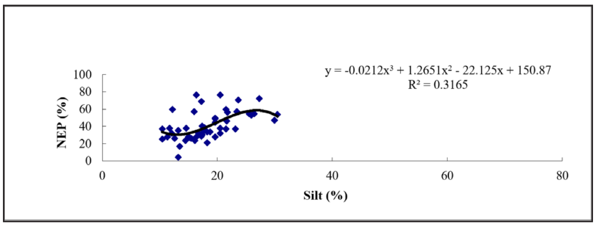

Figure 2. Mean non-erodible soil particles (NEP) versus silt content

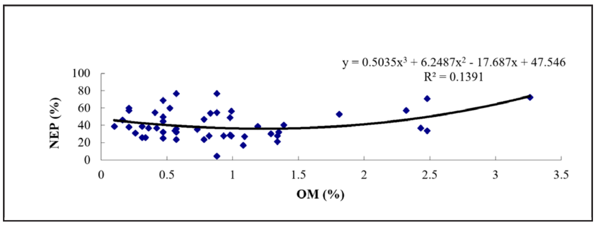

Figure 3. Mean non-erodible soil particles (NEP) versus silt content

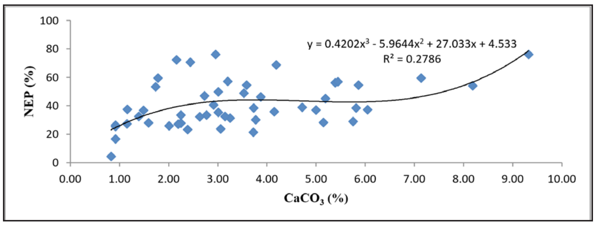

Figure 4. Mean non-erodible soil particles (NEP) versus CaCO3 content

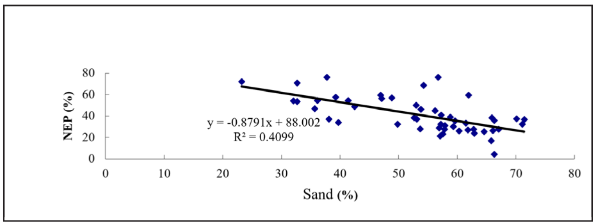

Figure 5. Mean non-erodible soil particles (NEP) versus sand content

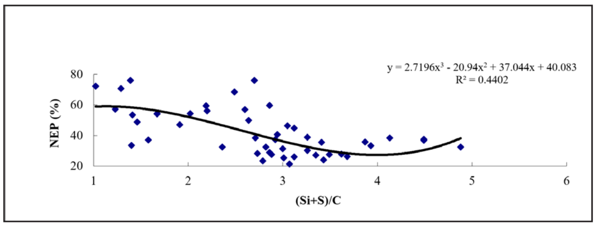

Figure 6. Mean non-erodible soil particles (NEP) versus (Si+S)/(C) ratio

Table 1. Range of mean soil physical properties, non-erodible soil particles (NEP) and wind erodibility (WE) of a number (n) of soil samples randomly collected from various agricultural farms in the six studied states

Soil characteristics	Range	Mean	CV
	Northern State(n = 50)		
Organic matter, %	0.10 – 3.26	0.91	76.3
Clay, %	16.8 – 49.5	28.1	28.1
Silt, %	10.4 – 30.5	18.2	26.6
Sand, %	23.2 – 71.4	53.7	21.9
NEP, %	4.2 – 76.1	40.8	39.5
WE, ton/ha	9.6 – 474.1	142.7	56.7
	Kassala State (n = 50)		
Organic matter, %	0.0 – 1.54	0.70	63.8
Clay, %	2.0 – 33.0	17.5	39.0
Silt, %	1.0 – 50.0	21.3	52.2
Sand, %	37.0 - 97.0	62.0	20.5
NEP, %	15.0 - 66.9	41.6	34.1
WE, ton/ha	34.2 – 262.0	124.2	47.8
	North Darfur State (n = 40)		
Organic matter, %	0.7 – 9.3	3.3	79.0
Clay, %	5.9 – 61.8	15.6	89.3
Silt, %	0.0 – 46.1	7.8	125.9
Sand, %	26.3 – 93.9	76.6	27.9
NEP, %	0.4 – 71.0	27.2	82.5
WE, ton/ha	25.0 – 695.0	236.9	69.2
	River Nile State (n = 50)		
Organic matter, %	0.01 - 0.60	0.10	109.8
Clay, %	5.7 - 47.8	29.2	33.2
Silt, %	4.1 – 32.8	11.2	42.2
Sand, %	34.6 – 87.5	59.8	18.9
NEP, %	4.3 - 98.1	43.6	61.7
WE, ton/ha	0.0 – 470.4	148.1	73.0
	Red Sea State (n = 28)		
Organic matter, %	0.05 - 0.68	0.20	104.6
Clay, %	21.3 – 60.9	37.6	22.4
Silt, %	7.9 – 38.1	14.7	49.1
Sand, %	11.0 – 68.0	47.7	27.0
NEP, %	17.0 – 57.2	36.0	30.3
WE, ton/ha	49.6 – 244.0	143.5	35.6
	Central Gezira (n = 50)		
Organic matter, %	0.15 – 0.57	0.31	30.8
Clay, %	24.0 – 60.0	38.9	26.6
Silt, %	14.0 – 46.0	29.6	28.0
Sand, %	17.0 – 48.0	31.9	24.1
NEP, %	36.0 – 85.5	62.4	16.3
WE, ton/ha	0.0 – 141.0	46.8	61.6

Wind erodibility data collected from farms in North Darfur State showed that NEP significantly ($P < 0.001$), increased linearly with increase in OM ($r^2 = 0.825$), logarithmically with clay ($r^2 = 0.754$), cubically with silt ($r^2 = 0.737$).

Furthermore, NEP rendered quadratic decrease with increase in sand ($r^2 = 0.761$), and linear decrease with increase of (silt+sand)/ clay ratio ($r^2 = 0.766$) (Medani, 2001; Medani and Mustafa, 2003). In this and other states, lower coefficient of determination and regression trends in reverse to those derived for NEP versus soil properties were derived for WE versus soil properties. Multiple regression analysis yielded a highly significant ($P < 0.001$, $r = 0.910$) correlation between NEP and the four prime soil properties as follows:

NEP%=28.7-0.41Clay%-0.23Silt%-0.27Sand%+8.42OM%

The results of a similar wind erodibility study in the River Nile State showed a highly significant ($P < 0.001$) power increase of NEP with increase of clay ($r^2 = 0.7214$), $CaCO_3$ ($r^2 = 0.2904$) and OM ($r^2 = 0.3155$), and power decrease with increase of sand ($r^2 = 0.5515$), and increase of (silt+sand)/ clay ratio ($r^2 = 0.7200$). Multiple regression analysis yielded a highly significant ($P < 0.001$, $r = 0.8056$) correlation between NEP and multiple soil variables as follows:

NEP% = 21.78 +1.44 Clay% - 0.51 Sand% + 2.59 $CaCO_3$ + 14.10 OM%

According to this relationship, the four soil properties account for 65% of the variation of NEP. It was evident that clay alone or the compound indicators gave better accountability than these multiple variables (Hassan and Mustafa, 2011). Regression analysis of the data collected from farms in the Red Sea State showed a highly significant linear increase of NEP with an increase of clay percent ($r^2 = 0.8001$), and logarithmic increase with the increase of OM ($r^2 = 0.3824$), and quadratic decrease with the increase of sand ($r^2 = 0.8001$). The results also showed a highly significant quadratic decrease in NEP with an increase of (silt+sand)/clay ratio ($r^2 = 0.8094$). Reverse correlation trends were obtained with WE (Mohamed, 2008; Mohamed and Mustafa, 2011). Multiple regression analysis yielded a highly significant ($P < 0.001$, $r = 0.9001$) Correlation between NEP and multiple soil variables as follows:

NEP% = -6.06 +1.10 Clay% - 0.67 Sand% - 2.68 OM% +1.23 $CaCO_3$

According to this relationship, the four soil properties account for 81% of the variation of NEP. The negative sign of the coefficient of OM may be attributed to the empiricism of the equation. Clay, sand or the compound indicators gave nearly similar accountability as the multiple soil variables.

The wind erodibility study of the farms in Kassala State gave highly significant ($P < 0.001$) power increase of NEP with increase of clay content ($r^2 = 0.4245$), and quadratic increase with increase of OM ($r^2 = 0.9200$), and significant ($P < 0.05$, $r^2 = 0.0796$) exponential decrease with increase of sand. Furthermore, it gave highly significant ($P < 0.001$) power decrease of NEP with increase of (silt+sand)/clay ($r^2 = 0.3353$), (silt+sand)/ (clay+$CaCO_3$) ($r^2= 0.3386$), and (silt+sand)/ (clay+OM) ($r^2 = 0.4611$), and a significant ($P < 0.05$) exponential decrease with increase of sand (0.0796) (Abdelgadir, 2007; Abdelgadir et al., 2013)

The wind erodibility study of the farms in Gezira State showed that NEP significantly increased linearly with increase of clay ($r^2 = 0.8236$), and OM ($r^2 = 0.6632$), and quadratic increase with increase of CaCO3 ($r^2 = 0.3254$), and c/ (si+s) ratio ($r^2 = 0.7813$). Furthermore, it gave quadratic decrease with increase of silt ($r^2 = 0.4162$), sand ($r^2 = 0.3486$) and (silt+sand)/clay ratio ($r^2 = 0.7125$). The reverse correlation trends were obtained with WE. Multiple regression analysis yielded a highly significant ($P < 0.001$, $r = 0.845$) Correlation between NEP and multiple soil variables as follows:

NEP% = 84.4+ 0.27 Clay% - 0.60 Sand% - 0.55 Silt + 0.66 $CaCO_3$

According to this relationship, the four soil properties account for 71.4% of the variation of NEP. The signs of the coefficient of the multiple variables are referred to as the type of impact (Rehan, 2004; Rehan and Mustafa, 2005). In all cases, lower correlation coefficients and regression trends in reverse to those derived with NEP and the studied soil properties were obtained with WE.

The mean NEP increased and WE decreased for the studied farms in the different states with an increase of the mean clay content. This is because clay particles form floccules and in the presence of cementing agents, e.g. polysaccharides, which is a microbial derivative of organic matter are responsible for the formation of stable soil aggregates that are not vulnerable to erosion (Emerson, 1959). This explains why the data in all states showed a highly significant ($P < 0.001$) increase in NEP and consequent decrease in WE with an increase of clay content in all states (Table 2). Because of its very low content and high variability in the drylands of Sudan, OM yielded a significant correlation with neither NEP nor WE. Furthermore, WE increased with the increase of the mean sand content, because sand is chemically neutral and it's nearly spherical shape is amenable to transport.

3.2 Wind erodibility groups of the individual states

Table 3 presents the mean non-erodible NEP and equivalent mean WE of the soil samples studied in each state having similar soil textures. Thes soil samples where thus placed into one class referred to as wind erodibility group (WEG) (Chepil, 1962; Hayes, 1965; Black and Chanasyk, 1989; Mustafa and Medani, 2003; Medani and Mustafa, 2003). Five states were dominated by coarse and medium-textured WEG.

Gezira is fine–textured WEG. In the six states, there were 280 WEG, 41% of them were coarse-textured (sand, loamy sand, and sandy loam), 42.8% have medium-textured (loam, sandy clay loam, clay loam) and 16.2% are fine-textured.

Table 2. The linear trend lines of non-erodible soil particles (NEP) and their equivalent wind erodibility (WE) as a function of clay content in the studied states [NEP or WE = a + b Clay %]

	a	b	r^2	r
	North Darfur (n = 40)			
NEP (%)	7.5512	1.2577	0.6105	0.7813
WE (ton/ha)*	2831.1	-1.1231	0.7243	- 0.8511
	Kassala(n = 50)			
NEP (%)	12.276	1.6737	0.6497	0.8060
WE (ton/ha)	246.29	-6.9727	0.6428	- 0.8017
	Northern State (n = 50)			
NEP (%)	5.7388	1.2407	0.4531	0.6731
WE (ton/ha)	287.7	-5.2674	0.4313	- 0.6567
	River Nile State (n = 50)			
NEP (%)	-19.854	2.1757	0.6122	0.7824
WE (ton/ha)	408.4300	-8.9278	0.6367	- 0.7979
	Red Sea State (n = 28)			
NEP (%)	-7.4978	1.157	0.8001	0.8945
WE (ton/ha)	343.85	-5.3239	0.7733	0.8794
	Central Gezira (n = 50)			
NEP (%)	28.278	0.8773	0.7906	0.8892
WE (ton/ha)	52.602	-0.2920	0.6652	- 0.8156

* *Power relationship:* $Y = aX^b$,

3.3 Relationships of the pooled data of the six states

Table 3 shows the mean non-erodible soil particles for the main textural groups found in the studied farms in the various states based on previous findings for the individual states, (sand/clay) ratio was used for predicting NEP and WE for all states. These results show that NEP decreased and WE increased significantly ($P < 0.01$) with an increase of (sand/clay) ratio content according to the following equation:

$$\text{NEP (\%)} = -\,9.5427\left(\frac{Sand}{Clay}\right) + 61.689$$
$$(r^2 = 0.7429) \ldots\ldots\ldots (1)$$

$$\text{WE (ton/ha)} = 51.965\left(\frac{Sand}{Clay}\right) + 9.6781$$
$$(r^2 = 0.7048) \ldots\ldots\ldots (2)$$

Although these two empirical relationships are highly significant, the coefficients of determinations account for 74.3% and 70.5% of the variability NEP and WE. Other variables that may affect the aggregation process and consequently affect NEP are silt, $CaCO_3$ and OM (Mustafa and Medani, 2003; Medani and Mustafa, 2003). For example, Mustafa and Medani (2003) recommended the use of the $(Si + S) / (C + CaCO_3)$ ratio for the prediction of NEP and WE of the soils of Khartoum State. WE showed a highly significant quadratic increase with an increase of this ratio. However, the present relationships depict linear relationships indicating a direct correlation with NEP or WE, which can be predicted from knowledge of routinely available sand and clay contents only. The weighted mean basic characteristics of the pooled wind erodibility groups of the six studied states are depicted in Table 4.

Conclusions and Recommendations

1. The overall mean NEP of the six states ranged from 27.2 to 62.4 with a mean of 41.9% and CV of 27.7%, and the overall mean of WE ranged from 46.8 to 236.9 with a mean of 140.4 ton/ha and CV of 43.2%.
2. The overall mean NEP of the six states gave a highly significant positive correlation with clay content with coefficients ranging between 0.8945 and 0.6731 with a mean of 0.8044 and a CV of 10.2%.
3. The overall mean NEP was in the following order: Gezira> the Red Sea> Northern> River Nile> Kassala> North Darfur.
4. The overall mean WE of the six states gave a highly significant negative correlation with clay content with coefficients ranging between - 0.8794 and - 0.6567 with a mean of - 0.8004 and a CV of 9.6%.
5. The overall mean WE was in the following order: North Darfur> Kassala> River Nile> Northern> the Red Sea> Gezira.
6. The pooled data of the six states gave a highly significant negative correlation between NEP and (sand/clay) ratio, which accounted for 70% of the variation of NEP.
7. The pooled results of the six states gave a highly significant positive correlation between WE and (sand/clay) ratio, which accounted for 70% of the variation of NEP.
8. Organic matter content did not yield a significant correlation with either NEP or WE due to its very low content and high variability in the drylands of Sudan.
9. The six states were dominated by coarse to medium textured WEGs. The Gezira was dominated by fine-textured WEG.

Table 3. The mean non-erodible soil particles for the main textural groups found in the studied farms in the various states

Texture*	Number of samples	Mean NEP	Texture	Number of samples	Mean NEP
Northern State	Nile State				
SL	38	36.4	SL	7	17.3
SCL	9	54.0	SCL	30	38.5
L	2	50.7	CL	3	80.5
CL	1	72.2	SC	5	67.0
			C	5	80.5
Red Sea State	Central Gezira				
SCL	16	53.9	L	5	37.6
CL	2	38.9	SCL	4	45.5
SC	5	47.1	CL	21	32.8
C	5	31.6	C	21	27
North Darfur State	Kassala				
S	15	7.5	S	1	15
LS	10	20.6	LS	3	22.5
SL	6	41.7	SL	19	39.7
L	1	42.4	SCL	20	46.8
CL	2	57.4	L	3	43.1
SCL	4	60.5	CL	1	65.9
C	2	59.3	SiL	1	30.9
			SC	1	25.2

** S = sand, Si = Silt, C = clay, L = loam*

Table 4. The weighted mean measured non-erodible soil particles (NEP) and its equivalent wind erodibility, silt, clay, sand (%) and (sand/clay) ratio for the wind erodibility groups (WEG) of their number of samples in the six studied states

WEG	Number of samples	NEP (%)	WE (ton/ha)	Silt (%)	Clay (%)	Sand (%)	Sand/clay (%)
S	16	8.0	336.0	8.9	15.7	75.4	4.8
LS	13	21.0	213.0	10.4	16.0	73.6	4.6
SL	70	35.8	142.0	38.9	19.7	41.4	2.1
SiL	1	30.9	161.5	15	15	70	4.7
C	33	37.8	135.0	17.7	35.8	46.5	1.3
L	11	41.9	117.4	10.1	29.0	60.9	2.1
CL	30	42.0	117.0	15.1	39.7	50	1.3
SCL	83	46.5	103.0	8.9	27.7	63.7	2.3
SC	11	57.0	54.0	9.8	33.4	56.8	1.7

Acknowledgement

It is very important to mention that this work is a review of a comprehensive research project on wind erodibility (WE) was implemented, in several states in Sudan, by postgraduate students as complimentary research in partial fulfilment of their M.Sc. degrees, in the Desertification and Desert Institute, University of Khartoum. Furthermore, my deep thanks extended to postgraduate students and Desertification and Desert Institute (DADCSI), University of Khartoum.

References

Abdelgadir, I. A., Mustafa, M. A., and Ganawa, E. S. 2013. Assessment and mapping of wind erodibility of soils of southwestern kassala state in Sudan. Sudan Journal of Desertification Research 5:19-33.

Abdelgadir, I. E. 2007. Assessment of wind erodibility of soil using GIS techniques: Kassala State, Sudan. M.Sc. (Desertification) Thesis, University of Khartoum, Sudan

Abdelwahab, M.H. 2005. Wind Erodibility of Soils from the Northern State. M.Sc. (Desertification), U.of K.

Abdelwahab, M.H., Mustafa, M. A. and Ganawa, E.S. 2009. Spatial variation of wind erodibility of soils from the Northern State, Sudan. Sudan Journal of Desertification Research 1 (1): 56-70.

Black, C.A., Evans, D.D., White, J. L., Ensminger, L.E., and Clark, F.E. 1965. Methods of Soil Analysis (Part I). Agronomy Monograph No. 9 American Society of Agronomy, Inc., Publisher, Madison, Wisconsin, U.S.A

Chapman, H.D., and Pratt, P.E. 1961. Method of Analysis of Soils, Plant and Water. The University of California, Division of Agriculture Science, California, USA.

Chepil, W.S., and Woodruff, N.P. 1959. Estimation of wind erodibility of farm fields. USDA Production Research Report No. 25, 21p.

Ibrahim, I.S. 1991. Laboratory Test of Soil Fertility. University of Omar El Mukhatar, El Baida, Libya

Mustafa, M. A. (2007). Desertification Processes. Khartoum University Printing Press.230 pp

Skidmore, E.L. and Woodruff, N.P. 1968. Wind erosion forces in the United States and their use in predicting soil loss. USDA Handbook No. 346, 42 pp, Washington DC

Black, J.M.W. and Chanasyk, D.S. 1989. The wind erodibility of some Alberta soils after seeding: aggregation in addition to field parameter. Canadian Journal of Soil Science 69: 835-875.

Chepil, W.S. 1953. Factors that influence clod structure and erodibility of soil by wind. I. Soil texture. Soil Science 75: 473-483.

Chepil, W.S. 1962. Stubble mulching to control erosion Proceedings of the Great Plains Workshop on Stubble Mulch Farming, Linkon, Nebraska

Dregne, H. Kassas, M. and Rosanov, B. 1991. Anew assessment of the world status of desertification. Desertification Control

Emerson, W.W. 1959. The Structure of Soil Crumbs - Journal of Soil Science 10: 232-244.

Harrison W.A, and Jackson J.K. 1958. Ecological Classification of the Vegetation of the Sudan; Forests Bulletin No. 2. Agric. Publications, Khartoum

Harris, R.F., Chesters, G. and Allen, O.A.1966. Soil Aggregation. Advances in Agronomy 18: 107-169.

Hassan, A.A. and Mustafa, M. A. 2011. Assessment and mapping of wind erodibility of Aridisols and Entisols in the Nile State, Sudan. Sudan Journal of Desertification Research 3 (1): 49-61.

Hayes, W.A. 1965. Wind erosion equation useful in designing North Eastern Crop production. J. of Soil and Water Conservation 20: 153-155.

Kheir El Seid, A. M. R. 1998. Wind Erosion Study in North Kordufan, El-Obeid. Ph.D. University of Khartoum

Lyles, L. and Tatarko, J. 1986. Wind erosion effects on soil texture and organic matter. Journal of Soil and Water Conservation 41: 191-194.

Medani, G. H. 2001. Wind Erodibilibilty of Soils from Khartoum and North Darfur States. M.Sc. (Agric.) Thesis, University of Khartoum, Sudan

Medani, G.H., and Mustafa, M.A. 2003. Wind erodibility of Soil from North Darfur State. U. of K. J. Agriculture Science 11: 369-387.

Mohammed, M.A.E. 2008. Assessment and Mapping of Wind Erodibility of Soils from the Red Sea State Using GIS Techniques. M.Sc. (Desertification), University of Khartoum, Sudan.

Mohammed, M.A.E. and Mustafa, M.A. 2011. Assessment and mapping of wind erodibility of Aridisols and Entisols in the Red Sea State, Sudan. University of Khartoum Journal of Agricultural Science 2 (1): 128-144.

Mustafa, M.A., and Medani, G.H. 2003.Wind erodibility of soils from Khartoum State. U.of K. Journal of Agriculture Science 11: 149 - 164.

Rehan, S. A. and Mustafa, M.A. 2005. Wind erodibility of soils from the Gezira State, Sudan. In the proceeding of the Regional Workshop “Scientific Research and National Research Plans of Action for Combating Desertification.” Tuesday 22-Thursday 24 November 2005, Al Sharga Hall, University of Khartoum

Rehan, S.A. 2004. Wind Erodibility of Soils from the Gezira State. M.Sc. (Desertification) Thesis, University of Khartoum, Sudan

Romken, M.J.M., Roth, C.B., and Nelson, D.W.1977. Erodibility of selected clay soils in relation to physical and chemical properties. Soil Science Society of America Proceedings 41: 954-960.

Wishmeier, W.H., and Mannering, J.V.1969. Relation of soil properties to it is erodibility. Soil Science Society of America Proceedings 23: 131-137.

Woodruff, N.P., and Siddoway,F.H. 1965. A wind erosion equation, Soil Science Society of America Proceedings 19: 602-608

Young, R.A., and Muchler, C.K.1977. Erodibility of some Minesota Soils. Journal of Soil and Water Conservation 32: 180-182.

المملكة الأردنية الهاشمية

صندوق دعم البحث العلمي

الجامعة الهاشمية

المجلة الأردنية لعلوم الأرض والبيئة

JJEES

مجلة علمية عالمية محكمة

المجلد (١٢) العدد (٤)

http:// jjees.hu.edu.jo/

ISSN 1995-6681

المجلة الأردنية لعلوم الأرض والبيئة

مجلة علمية عالمية محكمة

المجلة الأردنية لعلوم الأرض والبيئة : مجلة علمية عالمية محكمة ومفهرسة ومصنفة، تصدر عن عمادة البحث العلمي في الجامعة الهاشمية وبدعم من صندوق البحث العلمي - وزارة التعليم العالي والبحث العلمي، الأردن.

ترسل البحوث إلكترونيا إلى البريد الإلكتروني التالي:

رئيس تحرير المجلة الأردنية لعلوم الأرض والبيئة

jjees@hu.edu.jo

لمزيد من المعلومات والأعداد السابقة يرجى زيارة موقع المجلة على شبكة الانترنت على الرابط التالي:

www.jjees.hu.edu.jo

المملكة الأردنية الهاشمية صندوق دعم البحث العلمي الجامعة الهاشمية

JJEES

المجلة الأردنية لعلوم الأرض والبيئة

Indexed by Scopus

ELSEVIER

المجلد (١٢) العدد (٤)

مجلة علمية عالمية محكمة تصدر بدعم من صندوق دعم البحث العلمي

ISSN 1995-6681 jjees.hu.edu.jo كانون أول ٢٠٢١